Ec-108

ORNL-5128

GAS-COOLED REACTOR PROGRAMS

THORIUM UTILIZATION PROGRAM PROGRESS REPORT

January 1, 1974 - June 30, 1975

A. L. Lotts

P. R. Kasten

BLANK PAGE

Printed in the United States of America. Available from
National Technical Information Service
U.S. Department of Commerce
5285 Port Royal Road, Springfield, Virginia 22161
Price: Printed Copy $3.50; Microfiche $2.25

ORNL-5128
UC-77 – Gas-Cooled
Reactor Technology

Contract No. W-7405-eng-25

GAS-COOLED REACTOR PROGRAMS

THORIUM UTILIZATION PROGRAM PROGRESS REPORT FOR JANUARY 1, 1974, THROUGH JUNE 30, 1975

A. L. Lotts, Program Manager

P. R. Kasten, Program Director

MAY 1976

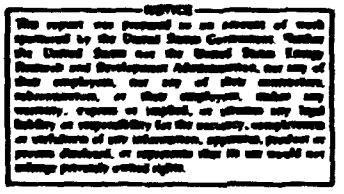

OAK RIDGE NATIONAL LABORATORY
Oak Ridge, Tennessee 37830
operated by
UNION CARBIDE CORPORATION
for the
ENERGY RESEARCH AND DEVELOPMENT ADMINISTRATION

ACKNOWLEDGMENT

This report was edited by Sigfred Peterson of the Metals and Ceramics Division. Typing and composition were by the Metals and Ceramics Reports Office under the leadership of Meredith R. Hill.

CONTENTS

SUMMARY

1. HTGR REPROCESSING DEVELOPMENT (SUBTASK 110)

Overall HTGR fuel recycle involves shipment and storage, reprocessing, refabrication, and waste disposal. Reprocessing deals with the chemical reprocessing of spent fuel to recover useful fuel values — both residual ^{235}U and ^{233}U converted from ^{232}Th — and also to isolate and convert the fission products and other wastes into forms suitable for disposal. These chemical processing steps are conveniently grouped into four areas: head end, solvent extraction, off-gas cleanup, and waste processing and isolation. For HTGR recycle, the product is in the form of uranyl nitrate solution, which will be the feed for a refabrication plant. Reprocessing development is divided into these work units:

General Development (Work Unit 1100)
Head End Development (Work Unit 1101)
Solvent Extraction Development (Work Unit 1102)
Off-Gas Cleanup Development (Work Unit 1103)
Product Preparation (Work Unit 1104)
Waste Processing and Isolation (Work Unit 1105)

In general, reprocessing development in the Thorium Utilization Program proceeds through successive, although frequently overlapping, stages of: cold laboratory development, hot laboratory development, cold engineering development, hot engineering development, and cold prototype development. During the period reported herein, the program objective was to supply the technology required to design, build, and operate a reprocessing pilot plant (Subtask 120). This progress report describes those activities conducted at ORNL. Work was also carried out at Idaho National Engineering Laboratory by Allied Chemical Company and by the General Atomic Company at San Diego.

General Development (Work Unit 1100)

Experimental plans were prepared, program coordination was carried on, and review-and-comment services were provided to other participants and to Subtask 120.

Head End Development (Work Unit 1101)

Work was done in three major areas: small-scale hot cell tests, vapor transport studies, and an alternate burner concept. The hot cell tests characterized the off-gases and fission product distributions resulting from the burning of three different irradiated fuel specimens: a Triso-Biso carbide, a Biso-Biso oxide, and a Triso-Triso carbide.

BLANK PAGE

Storage tests were also conducted in-cell. Tracer-type work on the vapor-phase transport of semi-volatile fission products was initiated. Both experimentally and theoretically, we studied a whole-block burner concept, which uses gas recycle for heat removal and rate control.

Solvent Extraction Development (Work Unit 1102)

In addition to providing review and consulting services to the pilot plant design subtask, we initiated hot cell studies and upgraded a computer model. The fuel ash residues generated under work unit 1101 were dissolved and will be used for tests of feed adjustment and batch shakeout equilibrations. The SEPHIS code was modified and improved for the Purex system and then adapted to the Thorex system with existing data.

Off-Gas Cleanup Development (Work Unit 1103)

Development of the KALC process continued. Laboratory equilibrium data on the Xe-CO_2 system were obtained, work was started on absorption from liquid CO_2, and the chemistry of the CO_2-H_2O-I_2 system was studied. Engineering-scale development of the KALC process included two campaigns in the experimental engineering facility, two campaigns in the K-25 pilot plant, development of an in-line ^{85}Kr (beta) detector, and significant improvements in the mathematical model for the KALC system. In other areas, a paper study on ^{220}Rn holdup was done, and the feasibility of using the Iodox process (for I_2 removal) in a CO_2 atmosphere was demonstrated.

Product Preparation (Work Unit 1104)

No development activity was scheduled under this work unit, but calculations on radioactivity control by sparging and ion exchange were done in support of Subtask 120.

Waste Processing and Isolation (Work Unit 1105)

Two reviews were conducted: one on reprocessing wastes in general, and one on the fixation of ^{14}C as calcium carbonate. The general review identified and characterized reprocessing wastes in terms of source, form, quantity, and radioactivity. The ^{14}C study evaluated two processes for the carbonate conversion reaction, various methods of packaging the product, and the preferred location of the fixation step in relation to krypton removal.

2. HTGR REPROCESSING PILOT PLANT (SUBTASK 120)

The HTGR Reprocessing Pilot Plant, planned for construction at INEL, was conceptually designed to demonstrate the technology required for the design of a commercial-scale facility. The pilot plant was designed for 12 Fort St. Vrain fuel elements per day, expandable to 24 elements per day. The first phase of this design activity was the preparation of System Design Descriptions (SDDs), which parallel the Work Units under Subtask 110. The Subtask 120 Work Units and the specific SDDs were:

Work Unit	SDD No.	Title
1200	1.0	Overall Plant Design Description
	1.5.1	Fuel Transfer and Handling System
	1.5.2	Instrumentation and Control System
	1.5.3	Waste Handling System
	1.5.4	Utilities System
	1.5.5	Fire Protection System
	1.5.6	Ventilation and Vessel Off-Gas Systems
	1.5.7	Decontamination System
	1.5.8	Remote Handling and Maintenance System
	1.5.9	Sampling System and Analytical Laboratory
	1.5.10	Building and Associated Systems
1201	1.1	Headend Processing System
1202	1.2	Solvent Extraction Processing System
1203	1.3	Off-Gas Cleanup System
1204	1.4	Liquid Product Loadout and Shipping
1205		(see 1.5.3 above)

The overall design responsibility was carried by ACC, with ORNL performing the lead role on the Off-Gas SDD. In addition, ORNL reviewed and commented on all SDDs and performed supporting studies for SDD1.4.

Off-Gas SDD (Work Unit 1203)

This SDD was written to meet these functional and design requirements: (1) to provide a decontamination factor (DF) of at least 100 for tritium, krypton, and radon and a DF of at least 1000 for iodine; (2) to accept off-gases at rates varying from 0 to 0.24 std m^3/sec (500 scfm), corresponding to up to 36 Fort St. Vrain fuel elements per day; and (3) to isolate the wastes from these removal systems in a form suitable for subsequent disposal. The direct processes to accomplish the required decontaminations were: (1) iodine sorption on zeolites, (2) tritium sorption on molecular sieve, (3) radon holdup (and decay) on molecular sieve, and (4) krypton concentration by the KALC process. Two other direct processes were also required: conversion of NO_x to N_2 and H_2O (via NH_3 and a catalyst bed) and oxidation of CO (and any molecular tritium) to CO_2 (and tritiated water). The wastes requiring final

disposal included iodine-loaded zeolites, spent molecular sieves and catalysts, concentrated tritiated water (fixed in concrete or some other suitably stable form), and krypton isolated in pressurized bottles.

Liquid Product Loadout and Shipping (Work Unit 1204)

A design report was issued on a cask suitable for shipping uranyl nitrate (^{233}U + about 500 ppm ^{232}U). A series of studies was done on the depression of alpha and/or gamma activities in this uranyl nitrate solution by sparging (to remove ^{220}Rn from the decay chain) or by ion exchange (to remove thorium and other decay products from the chain). Ion exchange is an effective way to minimize the gamma activity, but the alpha dose, which derives from the ^{233}U chain as well as the ^{232}U chain, cannot be greatly decreased for uranium solutions of the isotopic compositions of interest.

3. HTGR REFABRICATION PROCESS DEVELOPMENT (SUBTASK 210)

Refabrication is the step in the HTGR fuel cycle that begins with the receipt of nitrate solution containing reprocessed ^{233}U and ends with it refabricated into fuel elements for use in an HTGR. The basic steps in refabrication are very similar to fresh fuel manufacture except that the recycle fuel must be fabricated remotely in hot cell facilities; therefore, the refabrication development program is directed toward the development of processes and equipment for remote application. Its ultimate goal is to develop technology needed to design and operate the refabrication portion of an ERDA-supported HTGR Recycle Demonstration Facility (HRDF). The development program will be accomplished in five phases: (1) cold laboratory development, (2) hot laboratory development, (3) cold engineering development, (4) hot engineering development, and (5) cold prototype development. Work during this report period has primarily been in cold engineering development. Expanded work in waste and scrap handling was initiated during this report period. The work is reported in sections parallel to the major system of the refabrication portion of the HRDF.

General Development (Work Unit 2100)

This area is involved in the coordination and review of all functions of the subtask and technical interfacing with Subtasks 220, 310, and 320. A summary work plan for this subtask was prepared and contributions were made to the conceptual design of the HTGR-FRPP (Fuel Refabrication Pilot Plant). An environmental statement was issued for the FRPP along with reports assessing the radiological safety requirements and the assay and accountability requirements for an HTGR Fuel Refabrication Plant.

Uranium Feed Preparation (Work Unit 2101)

(No activity was scheduled)

Resin Loading (Work Unit 2102)

The initial stage of an engineering-scale resin loading system was completed and operated with natural uranium. About 235 kg of resin loaded with natural uranium (110 kg U) and 20 kg loaded with enriched uranium (10 kg U, 93% enriched) were prepared for refabrication development studies. Alternate methods for resin loading were investigated, and loading of resin in the acid form was selected as the reference process. Resin was loaded successfully with highly active ^{233}U containing 250 ppm ^{232}U. Equilibrium constants for resin loading in the acid form were measured. Solvent extraction of nitric acid by a 0.3 *M* secondary amine in a hydrocarbon diluent was demonstrated for obtaining the required acid deficiency in the uranium feed for loading uranium on acid-form resin. In resin feed preparation, two acceptable commercial carboxylic acid cation exchange resins were identified. The cost of feed resin is about $0.05 to $0.09 per gram of uranium.

Resin Carbonization (Work Unit 2103)

Extensive progress was made in scaling the resin carbonization and conversion processes to engineering-size equipment. We made 134 carbonization and 82 conversion runs using 0.10- and 0.31-m-diam (4 and 5-in.) furnaces. A 0.23-m-diam (9-in.) carbonization furnace was designed, fabricated, and installed. Three resin batches loaded with 93%-enriched ^{235}U were prepared for subsequent coating and irradiation testing. Carbonized resin kernels had high strength, as measured by a crushing test. Converted kernels are weaker, having strengths that decrease from about 8.9 N (2 lb) for particles having 15% of the oxide converted to carbide to about 4.4 N (1 lb) for 75% conversion.

Microsphere Coating (Work Unit 2104)

The 0.13-m-diam (5-in.) coating furnace was improved by several modifications made to the frit-type gas distributor and by the addition of instrumentation and inert-atmosphere particle handling equipment to allow carbonization, conversion, and Triso coating of uranium-loaded resin kernels. The design of equipment to permit remote loading and unloading of the coating furnace as well as remote sampling and weighing of the coating batch was completed and fabrication begun. Considerable experimentation has defined the process variables that control broken and permeable LTI coatings. Several factors affecting the amount of uranium dispersion in the buffer have been determined. Silicon carbide coatings have been more completely characterized as regards both their microstructure and crushing strength. Pneumatic transfer of particle batches was extensively investigated. Three batches of Triso-coated 93%-enriched-uranium-loaded resin were fabricated in the 0.13-m-diam (5-in.) coater for irradiation testing.

Fuel Rod Fabrication (Work Unit 2105)

The principal activities were development of fuel rod molding and inspection. Improved methods for fabrication and analysis of fuel rod matrix slugs were developed. The sources of fuel particle failure during fuel refabrication were investigated, and methods of improving the failed particle fraction were identified. A remotely operable and maintainable commercial-scale machine for molding of fuel rods was conceptually designed. This machine will dispense and blend fuel particles, mold the rods by the slug injection process, and inspect the fuel rod lengths at a rate of 40,000 rods/day. The feasibility of a number of nondestructive inspection methods for fuel rod homogeneity was demonstrated. A laboratory instrument for nondestructive uranium assay of HTGR fuel rods has been fabricated and is currently being installed in the TURF hot cells. The assay instrument interrogates the fuel rods with thermal neutrons from a ^{252}Cf source. These neutrons induce fissions in the uranium, and the resulting prompt fission neutrons are detected as a measure of uranium content.

Fuel Element Assembly (Work Unit 2106)

The principal development activity in fuel element assembly has been carbonization and annealing of HTGR fuel elements. The feasibility of the in-block carbonizization and annealing (cure-in-place) process was demonstrated in 1/6-segments of fuel element blocks. Cure-in-place process conditions were determined to attain acceptable fuel rod microstructures. Samples in which in-block carbonization will be studied were fabricated for irradiation experiments HT-26, HT-27, and OF-2. A remotely operable engineering-scale furnace for in-block carbonization and heat treatment has been designed. The continuously operated vertical furnace has a capacity of 16 fuel elements per day. A detailed, computer-assisted heat transfer study has confirmed the design of the furnace.

Sample Inspection (Work Unit 2107)

Development work on the particle size analyzer has been completed, and the device is currently operating routinely in support of process development. The PSA measures and counts coated fuel particles at rates up to 1500/min with an accuracy of ±1 μm. The feasibility of vacuum transferring small samples of fuel particles and encapsulated fuel rod samples was established. Design of a sample subdivider capable of obtaining ten representative subsamples from a 1-to-10-g initial sample is nearing completion. We routinely use a gaseous chlorine leach technique for the determination of particle failure fraction in both loose particle samples and fuel rods.

Plant Management (Work Unit 2108)

A programmable logic controller (PLC) has been installed on the laboratory fuel rod machine to replace the relay control system. The installation and operation of the PLC on the laboratory fuel rod machine has demonstrated the versatility and value of this computer-based controller for the operation and maintenance of remote refabrication equipment. A development minicomputer has been installed to support development work in nondestructive assay and the fuel rod storage magazine loader-unloader equipment.

Waste and Scrap Handling (Work Unit 2109)

Development started in two areas of waste handling and scrap recovery that are peculiar to the HTGR fuel cycle. These are reclamation of the perchloroethylene furnace scrubber solutions and recycle of reject fuel material. We completed bench-scale demonstration of feasibility of distilling dirty perchloroethylene and burning the still bottoms. Several techniques for reclamation of high-uranium-content reject scrap material are under investigation. These include a grind-burn-leach cycle and a molten salt incineration technique developed by Atomics International.

Material Handling (Work Unit 2110)

The TURF material handling system was studied in detail and was found to be of adequate mechanical configuration (i.e., crane hoist and manipulator designs) but extremely deficient in control functional capability and level of automation. Current research and development associated with remote handling and commercial suppliers of remote handling equipment were surveyed. We contacted 14 research organizations and 14 commercial suppliers associated with robots, manipulators, and TV viewing systems. An automated material handling system concept using electromechanical manipulators, which is consistent with HTGR fuel recycle requirements, was developed.

4. REFABRICATION PILOT PLANT (SUBTASK 220)

The HTGR Fuel Refabrication Pilot Plant was conceptually designed to demonstrate the technology required for a commercial fuel refabrication plant that can produce recycle fuel elements for High-Temperature Gas-Cooled Reactors using ^{233}U, with radioactivity equivalent to material containing 500 ppm ^{232}U and aged for up to 90 days. Such a plant must

must be safe, reliable, licensable, and economic. The technology must be available on a timely basis and ensure that any risks are comparable with those of a first-of-a-kind radiochemical plant.

This pilot plant, as conceptually designed, will produce about 150 recycle fuel elements for the Fort St. Vrain Reactor using ^{233}U and will demonstrate the following:

1. effective process and equipment designs for all fuel refabrication operations, including scalability to commercial plant capacities;

2. control of radiation hazards associated with the ^{232}U content of recycled ^{233}U fuel so that operating, maintenance, sampling, and analytical activities can be conducted safely;

3. feasibility of remote maintenance for all in-cell equipment through loading of the fuel elements;

4. practical methods for assay, quality control, and quality assurance for intermediates and the completed reactor grade fuel elements.

The refabrication pilot plant will be scaled to handle a heavy metal throughput of 25 kg of uranium and thorium per day, or 2.5 fuel elements per day on an intermittent basis. The design is broken down into ten separate functions:

Uranium Feed Preparation
Resin Fuel Kernel Preparation
Resin Carbonization
Microsphere Coating
Fuel Rod Fabrication
Fuel Element Assembly
Sample Inspection
Plant Management
Waste Handling
Materials Handling

5. RECYCLE FUEL IRRADIATIONS (SUBTASK 230)

The reorganization of the HTGR Fuel Development Program, which occurred at the end of the reporting period, is described. Only two areas of activity remain under Subtask 230 of the Thorium Utilization Program – those associated with Work Units 2302 (Peach Bottom Irradiations)

and 2303 (Large Scale Recycle Element Irradiations). The postirradiation examination of the Peach Bottom Recycle Test Elements (RTE) is reported, and the Fort St. Vrain Reactor (FSVR) test element program is briefly described. The test element program does not begin until the first FSVR reload, currently scheduled for Spring 1977.

6. ENGINEERING AND ECONOMIC STUDIES

Subtask 310 utilizes the work done in other subtasks to provide the liason between the development efforts and the design of a commercial recycle plant. During the reporting period, the following activities were under way in Subtask 310: (1) economic analysis of HTGR fuel recycle, (2) analysis of receiving and storage of HTGR fuel, (3) characterization of effluents from a commercial HTGR fuel refabrication plant, (4) survey of safeguards problems associated with the HTGR fuel cycle, and (5) analysis of the environmental impact of ^{14}C releases from an HTGR fuel reprocessing plant.

7. CONCEPTUAL DESIGN OF A COMMERCIAL RECYCLE PLANT (SUBTASK 320)

A major part of the current plans for developing HTGR recycle technology is the design and construction of an ERDA-supported HTGR Recycle Demonstration Facility (HRDF).

The objective of this subtask is to assist in the conceptual design of the HRDF. During this report period, a preconceptual layout study of an HRDF capable of reprocessing 20,000 elements per year and refabricating 10,000 elements per year was completed (i.e., 20/10). This 20/10 HRDF is estimated to require about 46,000 m^2 (500,000 ft^2) floor space for process operation and utility service. The design study also includes sections on design philosophy and terminology generally applicable to the design of an HRDF.

1. HTGR REPROCESSING DEVELOPMENT (SUBTASK 110)

K. J. Notz

1.1 INTRODUCTION

Reprocessing development is divided into five work units, which parallel the major systems for which design descriptions were prepared for a planned pilot plant. Four of these systems – head-end, solvent extraction, off-gas cleanup, and waste processing and isolation – are counterparts to systems that would exist in a commercial reprocessing plant, and are the subjects of ongoing development activity at ORNL as well as at General Atomic Co. (GAC) and Allied Chemical Co. (ACC). The other system – product preparation – is for the solidification of recovered uranyl nitrate for shipment to a planned refabrication pilot plant at another location, and is not a counterpart to a commercial plant, where reprocessing and refabrication would be back-to-back on the same site.

1.2 GENERAL DEVELOPMENT (WORK UNIT 1100) – K. J. Notz

Assistance was furnished to GAC and ACC in all areas of reprocessing, by providing review-and-comment and consulting services. General overall guidance was provided in all areas of reprocessing development, and detailed experimental plans were prepared for all work units under this subtask (except 1104, for which no development activity is scheduled).

All development activities were related directly to the reference flowsheet except some work on an alternate burner concept. The whole-block burner work had been started earlier, and was terminated during this period; these results are summarized in Sect. 1.3.

1.3 HEAD-END DEVELOPMENT (WORK UNIT 1101) – V.C.A. Vaughen

Our primary effort in this work unit is in small-scale hot cell studies related to burning, using individual irradiated fuel sticks. These results provide data and information needed for the design of the

BLANK PAGE

head-end subsystems. This work is described in Sect. 1.3.1. The hot cell facilities were also used to prepare some ^{233}U-loaded resin.

Vapor transport of selected fission products and actinides is being studied out-of-cell by a tracer technique. This work is just beginning, and will provide data relevant to the condensation of slightly volatile components. This work is described in Sect. 1.3.2.

An alternate burner concept, a whole-block burner, was considered. A limited amount of experimental work was done, and two study reports were issued, one of which introduced the concept of "adiabatic burning," which may also be applicable to fluid bed burning. This work is reported in Sect. 1.3.3.

1.3.1 Hot Cell Studies

1.3.1.1 Burner Off-Gas Studies with RTE-2-3 — C. L. Fitzgerald and V.C.A. Vaughen

Design information on the burner off-gas was needed by ACC. Specifically, the information desired was the amounts and kinds of fission products that reported to the burner off-gas from an 875°C fluidized bed at a gas velocity of 0.3 m/sec (1 fps); that plated out on the sintered metal primary filters held at 500, 150, and 75°C; that passed through these filters; that deposited downstream on lines; and that were trapped on absolute filters downstream. Determination of these values required three complete head-end experiments, one at each sintered metal filter temperature.

Fuel for these experiments was taken from individual channels (2, 5, and 6) of RTE-2-3, a Triso UC_2-Biso ThC_2 (type f) fuel irradiated as a blended bed of coated particles at 1320 to 1360°C (estimated maximum end-of-life temperature). Each channel contained approximately 3.4 g U and 16.3 g Th.

The postirradiation examination data for RTE-2 are reported elsewhere.[1] Initial gamma scans of the irradiated fuels indicated a small concentration (≈5%) of the maximum activity level of ^{137}Cs and ^{95}Zr at the fuel hole ends. A failure rate of 2.5 to 5.4% (95% confidence interval) was found for the SiC-coated UC$_2$ (fissile) particles; the performance

limits of the SiC layers of this batch of Triso-coated UC_2 particles in this RTE element were exceeded.

1.3.1.1.1 Equipment. The equipment layout diagram for the experiments is shown in Fig. 1.1. A standard conical-body miniburner [19 mm ID at the base, 38 mm ID at the top, and 254 mm high (3/4 × 1.5 × 10 in.) was used for the three runs. The normal burner top filter was perforated with 1.6-mm (1/16-in.) holes to more closely simulate the dusty gas loading on the test 5-μm sintered metal filter that would be experienced in the reprocessing plant. The burner was held in a cylindrical electric heater at 875°C during burning.

The 5-μm sintered nickel filter disks (grade HN) were made by the Pall Trinity Company. These disks were mounted in a flange holder and connected to the top of the burner by 6-mm (1/4-in.) stainless steel tubing and Swagelok (TM) fittings. The outlet stainless steel tubing was bent tightly twice to bring it back down the outside of the filter holder and to allow a second electric furnace to fit down over the assembly from the top for temperature control. The temperature of this furnace was regulated so that the filter was held at 500°C (in Run 1)

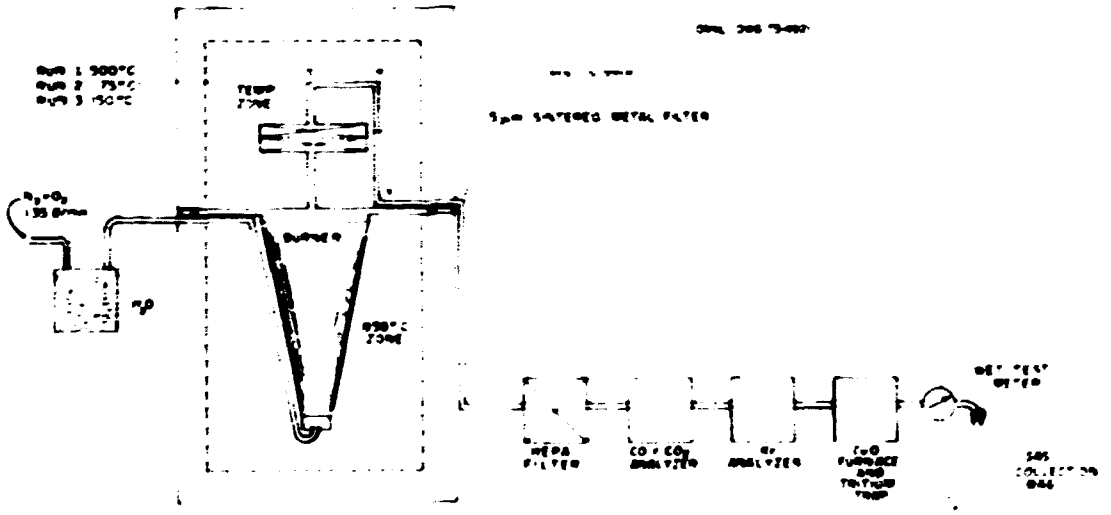

Fig. 1.1. Equipment Flowsheet for Burner Off-Gas Studies on Fuel from RTE-2.

and 150°C (in Run 3). It was removed for the 75°C test (ambient temperature, Run 2). The HEPA filter (COMFO Type "H" ultrafilter made by Mine Safety Appliances, Pittsburgh, Pa.) was mounted and specially wrapped before being inserted into the hot cell so that the unit could be unwrapped, removed, and disassembled in a clean hood. The filtered burner off-gas was subsequently passed through the normal off-gas train — that is, successively through CO_2 and CO detectors, a ^{85}Kr counter, a CuO oxidizer (500°C), two beds of Linde Molecular Sieves (Type 4A), and a wet-test meter and was finally routed to the gas collection bag.

1.3.1.1.2 Procedures. Each sample of the fuel was weighed, sieved to remove the graphite flour (about 6 g), reweighed, and charged to the small fluidized-bed burner. A small purge of N_2 (100 cm^3/min) was initiated while the burner and filter were being heated to operating temperatures. The gas flow (N_2 + O_2) was maintained at 1.4 std liters/min. This corresponds to 0.3 m/sec (1 fps) at 875°C on the 1.9-mm-ID (0.75-in.) bottom frit. Oxygen flow was started when the burner temperature reached 650°C. Immediate combustion was obvious from the CO_2 content of the off-gas and also from the increased heating rate inside the burner. The temperature within the burner was adjusted to 875°C with an "on-off" temperature controller on the furnace and by changing the O_2 flow rate. A CO spike, noted at the beginning of combustion, disappeared within 3 to 5 min. The CO_2 concentration in the off-gas averaged about 15%. These particular conditions give a ΔT across the burner of about 25°C.

All burner gases were collected in inflatable bags. The higher volume flow rates made it necessary to sample and change bags at about 30-min intervals during burning. This fast pace may not have allowed time to homogenize the gas bag contents before sampling. These samples were analyzed for CO_2, O_2, Ar, (N_2 + CO), ^{14}C, and ^{85}Kr. After completion of burning (defined as zero CO_2 concentration), the burner was held at temperature for about 1 hr with a 300-cm^3/min purge to ensure that all the ^{85}Kr and ^{14}C had been collected and allowed to cool overnight.

The ash was removed from the burner, weighed, and sieved to separate the fertile and fissile fractions. Each fraction was weighed to account for sieve losses (~0.1%). On disassembly (manual) of the 5-μm filter holder in the hot cell, a relatively large amount (1.5 to 3 g) of dust was observed on the inlet side of the filter. This dust, which came from the coated particles, was collected, weighed, and analyzed separately from the fertile and fissile fractions. The absolute filter (HEPA) holder was disassembled in the clean hood to minimize cross-contamination. The off-gas line was cut into approximately equal lengths in the cave. All samples were submitted for gamma scans; heavy-metal analyses were requested for the powders.

1.3.1.1.3 Results. The weights of the materials recovered in the various steps are presented in Table 1.1. The input weights were between 98.9 and 99.8% of the reported value of 63.954 g. Taking only the burner

Table 1.1. Material Balance Data for Burner Runs on RTE-2 Samples

Run	Filter Temperature (°C)	Input Measured[a] (g)	Output Measured, g			Material Balance[b] (%)
			+80 Mesh	−80 Mesh	Filter Dust	
		Combined ThO_2 and SiC-Coated Particles				
1	500	63.233	30.102	7.782	3.399	94.6
3	150	63.656	32.168	6.836	1.568	97.4
2	75	63.815	30.479	8.390	2.537	97.1
		ThO_2 Distribution[c]				
1	500		8.59	7.78	~0.2[d]	~89
3	150		10.66	6.84	~0.8[d]	~98
2	75		8.97	8.39	~0.6[d]	~97

[a]The input is reported by R. P. Morisette et al., *Recycle Test Element Program Design, Fabrication, and Assembly*, GA-10109 (September 1971), to be 63.954 g, corresponding to a calculated total output of 40.044 g.

[b](Burner product output/calculated output) × 100. Filter dust is not included.

[c]Obtained by assuming that none of the SiC-coated (fissile) particles are broken, so the entire 21.51 g is in the + 80 mesh fraction.

[d]Estimated from gamma-scan contributions (as originating from fuel ash). The remainder would be burnable carbon.

contents as ash product, the recoveries were between 94.6 and 97.4% of the theoretical output for combined ThO_2 and SiC-coated particles. Because the data are incomplete, we roughly estimated the ThO_2 material balance by assuming that no SiC-coated particles were broken and that the filter dust contained less than 1 g of fine burner ash (as determined from the average of the gamma scans as compared with the gamma scan of −80 mesh burner ash). The resulting ThO_2 material balance values range from 89 to 98%. These are reasonable recoveries.

Table 1.2 lists the total quantities of gamma emitters found in each unit on completion of the runs. The values in the burner column are based on the gamma scans of "grab" samples of −80 mesh ash solids and scaled to the theoretical amount of ThO_2 weight (18.535 g) plus the amounts (usually less than 1%) of fission products found on the perforated plate inside the burner. Contributions of ^{95}Zr and ^{144}Ce to these totals appear high.

1.3.1.1.4 Conclusions. A detailed analysis of the above results leads to a number of tentative conclusions, which follow.

1. Releases of certain fission products through a 5-μm sintered nickel frit were usually ≤0.1% and always ≤1.0% of the inventory.

2. Experiments at three filter temperatures (500, 150, and 75°C) yielded less than one order of magnitude variation in release of fission products through the sintered nickel frit.

3. The dust trapped by the sintered nickel frit contained most of the fission products (and burner ash fines) that left the burner. Recycle of this dust to the primary burner will return this material to the circuit. To avoid an accumulation, some sort of a purge mechanism must be provided.

4. The primary burner product from a Biso ThC_2-Triso UC_2 fuel (potential 1100-MWe reactor fuel) was not separable into fissile and fertile fractions by sieving.

5. These runs do not provide information pertaining to long-term plateout effects on the various surfaces.

6. Some 150°C filter results are inconsistent.

Table 1.2. Gamma Activity Found After Burning Coated Particles from RTE-2, Body 3

Gamma Emitter	Activity, dis/min				
	Burner[a]	Dust[b]	5-μm Filter	Off-Gas Lines	Absolute Filter
	Run 1, 63.233 g Particles from Hole 5, 5-μm Filter at 500°C				
^{95}Zr	1.46×10^{10}	9.86×10^{9}	2.95×10^{9}	2.64×10^{6}	1.40×10^{4}
^{95}Nb	7.11×10^{11}	1.84×10^{10}	5.74×10^{9}	7.78×10^{6}	2.97×10^{4}
^{106}Ru	4.15×10^{11}	3.47×10^{10}	3.30×10^{9}	2.88×10^{6}	2.06×10^{4}
^{125}Sb	1.27×10^{11}	5.91×10^{9}	8.70×10^{8}	9.27×10^{5}	5.18×10^{4}
^{134}Cs	9.03×10^{11}	5.17×10^{10}	3.13×10^{9}	3.38×10^{6}	1.24×10^{4}
^{137}Cs	1.50×10^{12}	8.94×10^{10}	5.28×10^{9}	6.27×10^{6}	2.07×10^{4}
^{144}Ce	3.79×10^{10}	5.17×10^{9}	2.59×10^{10}	2.66×10^{7}	1.72×10^{6}
	Run 3, 63.656 g Particles from Hole 2, 5-μm Filter at 150°C				
^{95}Zr	6.08×10^{10}	2.34×10^{9}	8.62×10^{7}	5.99×10^{6}	1.20×10^{4}
^{95}Nb	7.89×10^{11}	6.27×10^{10}	1.85×10^{8}	1.54×10^{7}	1.04×10^{4}
^{106}Ru	1.48×10^{12}	1.01×10^{11}	1.50×10^{8}	5.64×10^{6}	5.38×10^{4}
^{125}Sb	1.81×10^{11}	1.28×10^{10}	7.40×10^{7}	1.39×10^{7}	1.58×10^{7}
^{134}Cs	8.69×10^{11}	6.01×10^{10}	3.22×10^{8}	6.97×10^{6}	4.74×10^{3}
^{137}Cs	1.44×10^{12}	1.05×10^{11}	5.78×10^{8}	1.15×10^{7}	6.65×10^{3}
^{144}Ce	1.28×10^{11}	3.04×10^{9}	4.94×10^{9}	6.25×10^{7}	4.55×10^{4}
	Run 2, 63.815 g Particles from Hole 6, 5-μm Filter at 75°C				
^{95}Zr	5.64×10^{10}	2.09×10^{9}	7.48×10^{9}	2.04×10^{6}	7.05×10^{3}
^{95}Nb	8.29×10^{11}	8.73×10^{10}	1.04×10^{10}	4.17×10^{6}	8.44×10^{3}
^{106}Ru	2.10×10^{12}	8.30×10^{10}	7.20×10^{9}	2.22×10^{6}	5.74×10^{4}
^{125}Sb	1.98×10^{11}	1.53×10^{10}	1.78×10^{9}	3.53×10^{5}	4.56×10^{5}
^{134}Cs	8.15×10^{11}	7.61×10^{10}	5.67×10^{9}	1.55×10^{6}	1.41×10^{4}
^{137}Cs	1.37×10^{12}	1.30×10^{11}	9.82×10^{9}	3.26×10^{6}	1.86×10^{4}
^{144}Ce	2.67×10^{11}	4.08×10^{9}	9.84×10^{10}	1.38×10^{7}	7.34×10^{5}

[a]Includes ThO_2 ash and material from perforated plate inside burner. Material inside SiC-coated UC_2 particles is not included.

[b]Dust trapped on inlet side of 5-μm filter.

1.3.1.2 Release of ^{14}C During Primary Burning of RTE-2-3 — C. L. Fitzgerald and V.C.A. Vaughen

The off-gases for the three burning runs described in the previous section were analyzed for ^{14}C and CO_2. Although the 30-min interval between gas collection bag changes did not allow adequate time to homogenize the contents before sampling, the in-line CO_2 and CO monitors did indicate that approximately correct amounts of carbon were burned. However, the material balance on carbon yielded only about 50% of the calculated amount in the gas bags. Thus one can state with some assurance that the ^{14}C recovery is also incomplete. However, it is unlikely that the ^{14}C-to-CO_2 ratio is greatly affected by the probable nonrepresentative sampling, and the ratio may shed some light on the release pattern for ^{14}C even though the total amount is uncertain. In addition, a comparison of the three runs should indicate any trends.

The fuel, Triso UC_2-Biso ThC_2, should burn to SiC-coated UC_2 and bare ThO_2 ash. Thus the burnable carbon is the outer pyrolytic coatings of both fissile and fertile particles plus the inner pyrolytic carbon coatings and carbon from the ThC_2 kernels of the fertile particles. Any broken fissile particles would also release their ^{14}C.

Six gas bags were sampled, each about 40 to 60 liters, on about 30-min intervals. The results are presented in Table 1.3. The most interesting feature seen in this table is the apparent peaking of ^{14}C concentration (in two cases by a factor >10) near the midpoint of the runs. The carbon content varied only within a factor of 2 during the central four samples.

One concludes from these data that the ^{14}C is not uniformly distributed within the coated particles; however, no clear evidence points to the location or the region of highest content, except that it is probably not within the outer pyrolytic carbon coatings.

Each experiment had about 20 g heavy metals (U + Th). The measured ^{14}C releases range from 15 to 19 Ci/metric ton.

1.3.1.3 Analysis of Individual Fissile Particles from RTE-2-3 — V.C.A. Vaughen, F. F. Dyer, and T. B. Lindemer

The release of fission products from HTGR fuels is currently the subject of study in the HTGR Base and Thorium Utilization Programs. In

Table 1.3. Release of ^{14}C from HTE-2-3 During Primary Burning

Sample[a]	Run 1 (500°C)		Run 2 (75°C)		Run 3 (150°C)	
	C[b], g	^{14}C, μCi/g C	C, g	^{14}C, μCi/g C	C, g	^{14}C, μCi/g C
1	0.67	10.2	1.44	3.8	1.03	7.2
2	1.72	27.3	2.58	42.6	2.00	43.1
3	1.87	36.0	3.11[c]	51.4[c]	2.25	73.0
4	1.66	46.8	2.69	14.6	2.18	
5	3.32	21.6	2.53	7.4	2.29	7.5
6	2.36	11.4	0.45	11.0	2.04	5.8
Totals	11.59	25.7[d]	12.81	26.4[d]	12.15[e]	~31[d,f]

[a]Samples taken nominally about 30 min apart at nominal volumes of about 50 liters of off-gas.

[b]Carbon calculated from gas laws and CO_2 analyses.

[c]CO_2 concentration taken as the average of samples 2 and 4.

[d]Total ^{14}C found/total C found.

[e]A seventh sample had 0.36 g C but was not analyzed for ^{14}C.

[f]Samples 4 and 7 were omitted.

both these programs fractional and relative releases of fission products are the desired data, and starting inventories are required to normalize the data. While the total amounts of materials formed in the reactor core and present in typical discharged fuel at various decay times can be calculated from burnup estimates, reactor operating parameters, and decay times, e.g., by the ORIGEN code,[2] these results seldom agree well for the small samples used in these studies since the small samples typically do not see "average" conditions in the reactor.

To alleviate this shortcoming, we examined individual coated particles and fuel sticks nondestructively by gamma-scan analysis. This provides a measurement of the gamma-emitting isotopes for each coated particle. With dimensional data and with suitable calculations, inventories of fission products and estimates of burnup can be made for each coated particle or fuel stick. Estimates determined in this way also serve as an independent measurement for postirradiation examination of irradiation

test elements. The postirradiation examination of F. F. Dyer and T. B. Lindemer is reported elsewhere.[1]

Seven of the SiC-coated particles were separated from the burner ash and submitted for gamma-scan analysis and fission gas release. A summary of the data is presented here. The fissile particles had average measurements[3,4] as follows: kernel, 99 μm diam, density 10.44 g/cm^3; buffer, 51 μm thick, 1.30 g/cm^3; inner PyC, 21 μm thick, 1.81 g/cm^3; SiC, 20 μm thick, 3.21 g/cm^3. We calculate an average kernel uranium content of about 4.81×10^{-6} g before irradiation.

Table 1.4 lists the activity in disintegrations per second measured for the SiC-coated particles on the day of measurement. Counting times were 1000 sec; decay time, 4.277×10^7 sec. Table 1.5 lists the activity present at reactor shutdown, back-calculated from the data in Table 1.4. Table 1.6 gives estimated burnups calculated from the fission yield data. Although the average diameter was listed as 99 μm, actual kernel diameters were measured directly by radiography. The apparent low burnup values calculated from ^{95}Zr measurements are not significant, since its activity approaches saturation during irradiation and thus does not measure burnup. The low apparent burnup values estimated from the ^{144}Ce values are at present unexplained.

1.3.1.4 Long-Term Storage Experiment with RTE-2-5 Biso $(4Th,U)O_2$-Biso ThC_2 — C. L. Fitzgerald and V.C.A. Vaughen

The release of radioactive materials during storage of HTGR fuel elements is of interest to the designer of the reprocessing plant storage facility. The impact of releases on the requirements for cleanup of the cooling gas and the cost of specification storage containers prompted a request by GAC for some hot cell studies. The requested study was to measure the releases of ^{85}Kr, ^{3}H, and other isotopes from a stored fuel element and determine the release patterns at several temperatures.

Fuel body RTE-2-5 was available for these tests. It consists of a cylindrical graphite body about 76 mm diam by 0.38 m long (3 by 15 in.) containing a central hole and eight smaller holes arranged like a telephone dial. Seven of the holes still have the original loading of loose

Table 1.4. Analysis of Seven Individual SiC-Coated Fissile Particles from RTE-2-3. Nuclide contents at time of analysis (January 22, 1975) (4.277×10^7 sec decay)

Fission Product	Activity, dis/sec, per Particle in each Sample						
	1	2[a]	3	4	5	6	Average
^{95}Zr	4.377×10^4	4.833×10^4	3.785×10^4	2.856×10^4	1.993×10^4	4.857×10^4	3.243×10^4
^{106}Ru	1.706×10^5	1.989×10^5	1.535×10^5	1.192×10^5	8.688×10^4	2.101×10^5	1.342×10^5
^{125}Sb	b	1.394×10^4	b	b	b	b	
^{134}Cs	4.664×10^5	4.982×10^5	3.772×10^5	2.929×10^5	2.178×10^5	5.202×10^5	3.390×10^5
^{137}Cs	4.907×10^5	5.318×10^5	3.973×10^5	3.066×10^5	2.271×10^5	5.412×10^5	3.564×10^5
^{144}Ce	1.654×10^6	1.793×10^6	1.312×10^6	9.940×10^5	7.299×10^5	1.684×10^6	1.167×10^6

[a] Two particles in this sample.

[b] Not determined.

Table 1.5. Nuclide Contents of Individual SiC-Coated Fissile Particles from RTE-2-3 at Reactor Shutdown (September 14, 1973)[a]

Fission Product	Activity, μCi per Coated Particle, in each Sample					
	1	2[b]	3	4	5	6
^{95}Zr	222	246	192	146	101	247
^{106}Ru	11.7	13.6	10.5	8.18	5.96	14.4
^{125}Sb	c	0.54	c	c	c	c
^{134}Cs	19.9	21.2	16.1	12.5	9.29	22.2
^{137}Cs	13.7	14.8	11.1	8.54	6.32	15.1
^{144}Ce	149	161	118	89.3	65.6	151

[a]Variations in fission product content from particle to particle are attributed to variations in kernel diameters among the particles.

[b]Two particles.

[c]Not determined.

Table 1.6. Burnup Calculated from Fission Product Contents Found in Analysis of Individual Fissile Particles from RTE-2-3

Sample	Kernel Diameter (μm)	Burnup, % FIMA, Calculated from Activity of			
		^{95}Zr	^{106}Ru	^{137}Cs	^{144}Ce
1	124	33.3	42.8	42.7	30.1
2	100,118[a]	26.5	31.7	33.3	23.6
3	125	28.0	32.2	33.6	23.9
4	115	27.1	31.0	33.4	22.2
5	100	29.0	38.3	37.7	26.0
6	135	28.6	35.3	36.5	26.4

[a]Two particles in this sample.

Biso-coated (4Th,U)O_2 and Biso ThC_2 (type a) fuel. The fuel in the other hole has been removed for postirradiation examination. Experimental work described here began on January 27, 1975, and is continuing.

Postirradiation examination of coated particles from the maximum temperature region of fuel body 5 revealed no unusual microstructural features, no evidence of migration in either type of kernel, and no indication of failure or potential failure of the coatings. A more comprehensive description of results for RTE-2 is reported elsewhere.[1]

The amount of ^{85}Kr in RTE-2-5 has been estimated by analogy to RTE-2-3 with the ORIGEN code. About 0.38 Ci ^{85}Kr per fuel channel was predicted for RTE-2-3. We measured 0.30 Ci ^{85}Kr (about 80% of the calculated amount) in the experiment with fuel channel RTE-2-3-2. The flux at RTE-2-5 was 75% of the flux at RTE-2-3. Also, RTE-2-5 has seven fuel channels filled with fuel, and it contained more uranium and thorium than RTE-2-3. By adjusting the ORIGEN yield of ^{85}Kr for RTE-2-3 by simple factors, we have estimated an inventory of 2.6 Ci ^{85}Kr in RTE-2-5.

The fueled body was placed into a closed system as shown in Fig. 1.2. The element was purged with moist air, continuously at first. After the daily release rates fell to levels approaching the analytical limits, the system was sealed and purged weekly. The filtering units were added after the ambient temperature run was finished.

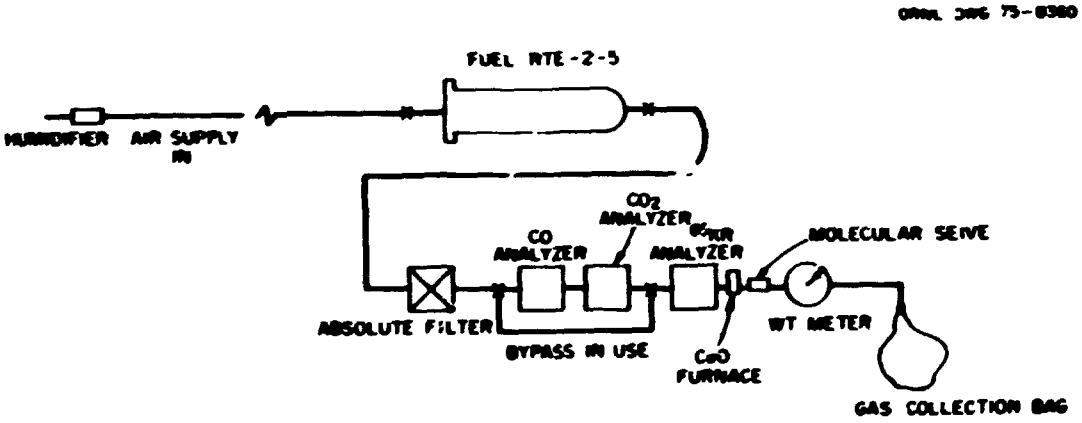

Fig. 1.2. Equipment Flowsheet for the Long-Term Fuel Element Storage Experiment.

The releases of ^{85}Kr in this experiment are shown in Table 1.7. Almost any change resulted in an increased release rate temporarily. The integrated amounts released, the initial release rates, and the final release rates are given in the table. The total release (in the stabilized release rate region for 150°C) was 184 mCi, or about 7% of the total calculated inventory. The release rate of 200 to 400 μCi/day corresponds to less than about 0.02% per day.

Table 1.7. Release of ^{85}Kr from RTE-2-5 in Storage

Temperature (°C)	Exposure (days)	Total Release at Temperature (mCi)	Rate, μCi/day	
			Initial	Final
25 ± 5[a]	71	13.7	9190	94
100	78	131.1	6530	55
150	110	39	1171	302

Tritium release rates are listed in Table 1.8. By analogy to RTE-2-3 and use of the same overall factor (75%) as for ^{85}Kr, the total ^{3}H inventory in RTE-2-5 was estimated to be 56 mCi. Approximately 0.2% of the calculated total ^{3}H has been released.

Table 1.8. Release of ^{3}H from RTE-2-5 in Storage

Temperature (°C)	Total Release at Temperature (μCi)	Rate, μCi/day	
		Initial	Final
Ambient	6.6	2.98	0.021[a]
100	9.0	0.24	0.014[a]
150	~90	~0.2[b]	~1[b]

[a]Average value.

[b]Being reevaluated.

1.3.1.5 Head-End Studies with H Capsules - C. L. Fitzgerald

Head-end reprocessing studies constitute a necessary step in the evaluation of the various fuel combinations being considered for use in commercial HTGRs. The "H" capsules were designed to provide performance data on Biso UO_2, Biso $(2Th,U)O_2$, and Biso $(4Th,U)O_2$ fissile particles and Biso ThO_2 fertile particles at several temperatures and burnups. In addition, several fuel sticks about 13 mm diam by 50 mm long (0.5 by 2 in.) were included for hot cell head-end studies.

These head-end studies were designed to follow the behavior of the many species of interest throughout the various stages of processing. Particular emphasis was given to considerations of fission product gas release patterns and determination of the extent and manner of fission product transport in the off-gases during the burning operations. The materials also provided some information on selective leaching.

1.3.1.5.1 Irradiation History and Description of Fuel. Two irradiation test capsules, H-1 and H-2, were designed to provide performance data on candidate HTGR recycle fuels and provide fuel for head-end reprocessing studies. Complete details of the fabrication and performance data are reported elsewhere.[5] The test capsules were irradiated in the ETR for four reactor cycles from May 1971 to May 1972. Capsule H-2 was removed for part of one cycle and both were removed for most of one cycle such that capsule H-1 was irradiated for 136.4 EFPD and H-2 for 124.9 EFPD total, with 29.3 EFPD in an inverted position. The capsule had been accidentally inverted for the fourth cycle. The inverted position resulted in about half the samples operating at significantly higher temperatures in the final cycle. Some severe degradation was experienced. The samples selected for our studies were the second, third, and fourth fuel rods in H-2. The fuel rods were made at ORNL by an intrusion-bonding technique with 35 wt % Poco AXZ graphite filler in 15 V pitch binder. All three were fabricated to be about 13 mm in diameter by 53 mm long (0.5 by 2.1 in.). Coated particle measurements are given in Table 1.9.

Table 1.9. Coated Particle Characteristics

Rod	Fuel Material	Dimensions, μm			Density, g/cm³		
		Kernel Diam	Buffer Thickness	Outer PyC Thickness	Kernel	Buffer	Outer PyC
HZ-2-2	UO_2	114	53	70			1.89–1.95
HZ-2-3	$(2Th,U)O_2$	355	77	134	10.18	1.1	1.9
HZ-2-4	$(4Th,U)O_2$	355	77	134	10.10	1.1	1.9
All	ThO_2	440	46.5	73.3	10.10	1.10	1.9

Estimated burnups in the fissile particles for rods HZ-2, -3, -4 were 31, 11, and 7.5% FIMA, respectively; calculated maximum center-line temperatures were 1200, 1350, and 1430°C, respectively. The shipping containers were not identified, and some question remains as to which sample was which fuel rod. The identification of the specimens was inferred by their behavior during the various stages of processing.

The general flowsheet was Burn-Leach since all test specimens were Biso-coated fuel combinations. Emphasis during burning was concentrated on (1) recovery and characterization of volatile and entrained materials in the off-gases and (2) reduction-oxidation cycling intended to force tritium release. Fission gas release data (^{85}Kr) were collected at each stage of the processing. A simple size separation (e.g., by sieving) cannot be depended on to separate the fertile and fissile fractions since the oxide fissile kernels may not be reduced to a fine powder during the burning process. Therefore, each sieve fraction was tested for selective dissolution of the uranium-bearing fissile fraction by use of boiling concentrated nitric acid before complete dissolution in Thorex reagent (13 M HNO_3–0.1 Al–0.05 F^-). Specific procedures for each operation are described below.

1.3.1.5.2 Primary Burning. The off-gas system is shown schematically in Fig. 1.3. It consists of a graded filter system, cascade impactor, water-cooled condenser, molecular sieve traps for ^3H retention, instrumentation, and an inflatable bag to collect all burner gases for

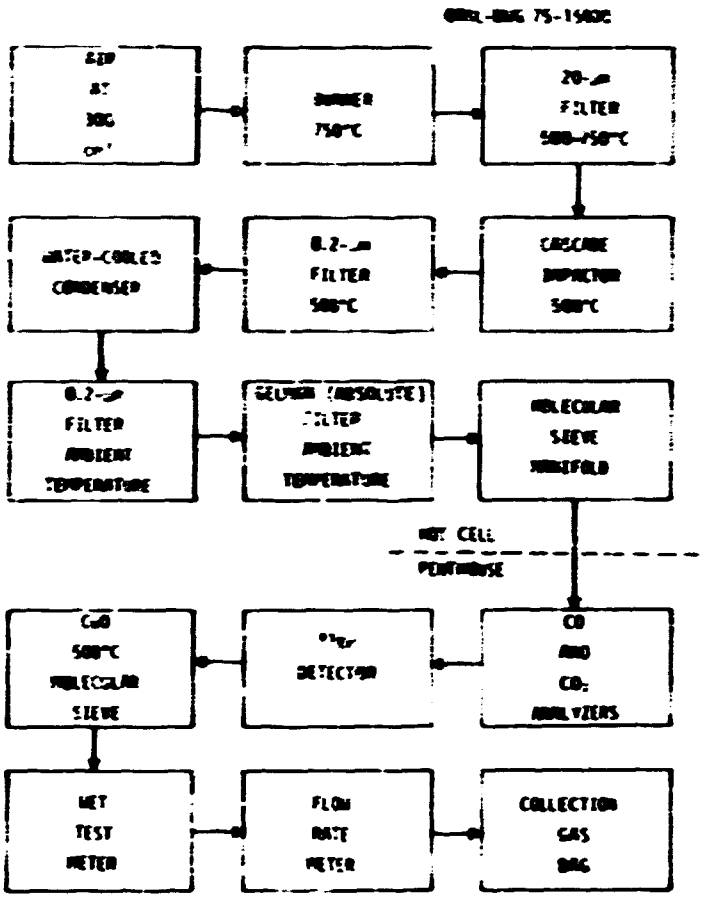

Fig. 1.3. Flow Diagram for H-Capsule Hot Cell Experiment.

subsequent analysis. To accomplish the oxidation-reduction cycling, the burning operation was broken down into six stages:

1. hold at 850°C for 1 hr in Ar-4% H_2 before burning (100 cm^3/min),
2. burn with wall temperature at 750°C in saturated air for the time required (300 cm^3/min),
3. hold at 850°C for 2 hr in saturated air (100 cm^3/min),
4. hold at 850°C for 8 hr in saturated air (100 cm^3/min),
5. reduction cycle in Ar-4% H_2 for 6 hr at 850°C (100 cm^3/min),
6. oxidation cycle in saturated O_2 for 2 hr at 850°C (100 cm^3/min).

The presence of hydrogen or water vapor at each stage was to provide isotopic dilution for ^3H. A manifold with molecular sieve traps for ^3H recovery was provided so that these could be changed at each

stage. Additionally, the inflatable gas collection bag was changed at the end of each stage and sampled for ^{85}Kr analysis.

After completion of the burning and oxidation-reduction cycling, the equipment was allowed to cool overnight and then disassembled. The cascade impactor, condenser, and all filter holders were decontaminated before disassembly to minimize cross-contamination. These samples were bagged out of the facility and submitted for analysis. The 20-μm sintered metal filter was taken to the analytical laboratory in a shielded carrier to minimize exposure to operating personnel. The burner ash was removed from the burner, weighed, and sieved to obtain +40 (420 μm) and +50 (297 μm) mesh fractions as well as a fines (−50 mesh) fraction. Each fraction was weighed by the procedures described under dissolution. The two sieve products are shown in Fig. 1.4.

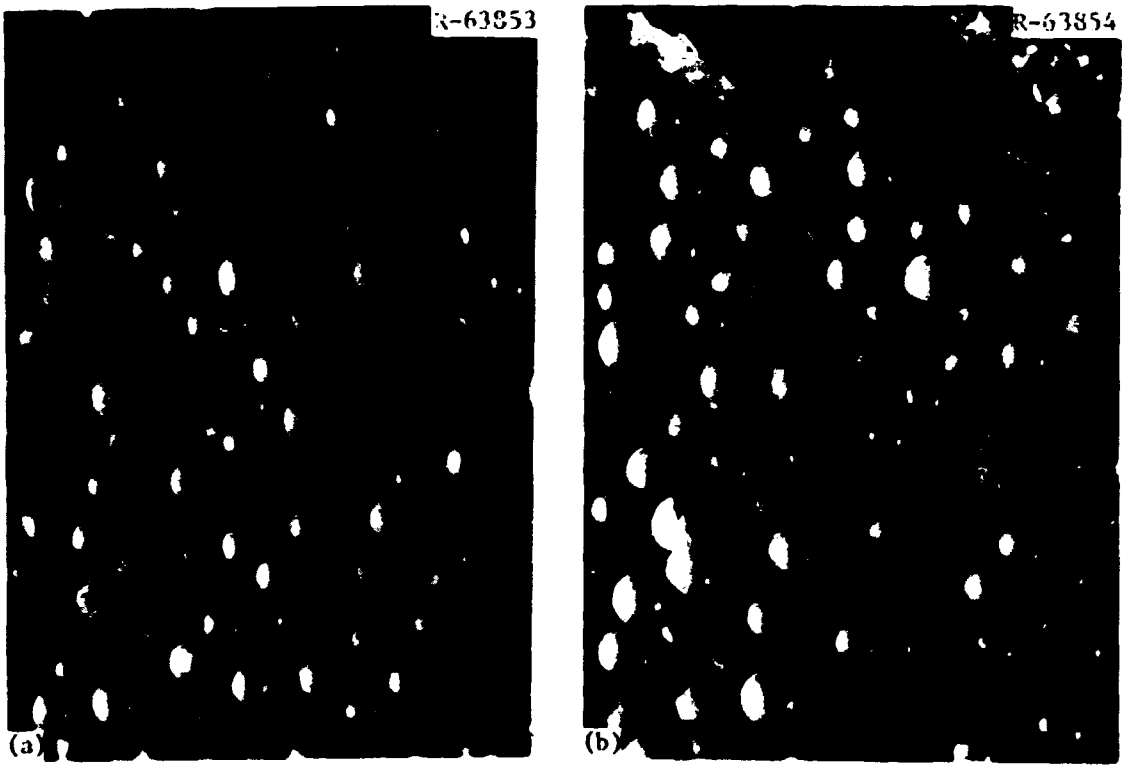

Fig. 1.4. Fractions from H-2-4 Burner Product. (a) +50 mesh fissile particles, $(4Th,U)O_2$. (b) +40 mesh fertile particles, ThO_2.

1.3.1.5.3 Dissolution. The dissolution procedure was designed to determine if the uranium-containing fissile fraction could be selectively dissolved from the thoria fertile fraction. The equipment consisted of a 100-ml glass dissolver fitted with a side-arm (for purge gas) and reflux condenser. The dissolver was purged with air at 100 cm^3/min; all gases were collected for ^{85}Kr analyses. The leaching time was 2 hr in each case. This was not long enough for complete recovery of heavy metals from the burner ash.

Each of the three fractions was first tested for selective dissolution of the uranium with boiling 15.7 *M* HNO_3 before two Thorex leaches. The fertile and fines fractions were leached once and the fissile fraction twice with nitric acid. The residue and filter paper from each leach served as feed for the next leach. The final filter paper was analyzed as residue when the leaching sequence was completed. All liquid and solid samples were analyzed for heavy metals and principal fission products.

The detailed analysis of the burner material balances and leaching results are omitted here, for brevity. Suffice it to say that the two selective leaches (each 2 hr) with 15.7 *M* HNO_3 dissolved about 30% of the ^{235}U in the $(4Th,U)O_2$ sample and about 7% of the ^{233}U. More of the ^{235}U and ^{233}U was dissolved in the other tests with the $(2Th,U)O_2$ and UO_2 samples. One concludes that leaching for 4 hr in 15.7 *M* HNO_3 is not selective enough to separate the ^{235}U and ^{233}U isotopes. A more dilute acid may be more effective.

1.3.1.5.4 Burner Off-Gas Contaminants and Fission Gas Release. Two primary purposes of these experiments were to determine ^{85}Kr and ^{3}H release patterns, and to characterize the burner off-gas contaminants. The burning operations (described earlier) were done without interruption thorugh the 8-hr postburn holding period; the reduction-oxidation operations were done the following day. A molecular sieve manifold was close-coupled to the filter assembly to collect the ^{3}H from each operation; the off-gases for each operation were collected in inflatable bags and sampled for ^{85}Kr analyses. The cascade impactor and filter holders were

disassembled in a shielded cave located above the hot-cell, and special precautions were taken to minimize cross-contamination. The filter holders and impactor were decontaminated between experiments. All connecting lines were replaced with new tubing before each experiment.

The fission gas releases are shown in Table 1.10. The results show that recovered tritium values agree within a factor of 3, and ^{85}Kr within a factor of 6. The condition of the samples indicates that the initial contents may have been nonrepresentative.

Results from experiments H-2-2 (UO_2) and H-2-4 [$(4Th,U)O_2$] show that all the high-temperature operations were required to effect about 99% ^{3}H removal, while the additional 2-hr postburn holding period was all that was required to accomplish the same effect in H-2-3 [$(2Th,U)O_2$]. This is one area that continues to raise doubts as to the identity of the samples. The UO_2 particle was expected to release the ^{3}H easily. The $(2Th,U)O_2$ and $(4Th,U)O_2$ samples were expected to have nonporous kernels and thus have slow diffusion processes. Perhaps the high surface area with the urania fissile particle may have led to chemisorption of the tritium.

The bulk of the ^{85}Kr associated with H-2-2 (≈80%) was released during the burning operation, while only about 50% of the ^{85}Kr was released from the mixed Th-U kernels. Although the first 2-hr soak released up to 10% more, the bulk of the residual ^{85}Kr was released during dissolution. This type of behavior is to be expected with oxide fuels, and similar behavior has been observed in Germany.[6]

All filters and the condenser were scanned directly without pretreatment. The amount of each nuclide found on each component was summed and divided by the total gas volume to give an average concentration in the off-gas stream for the burning operations. These results are presented in Tables 1.11 and 1.12. The concentrations found in the off-gases agree between runs within 35% for ^{106}Ru, and within about 20% for other nuclides. This is excellent agreement. Generally, more than 95% of the contaminants were found upstream from the cascade impactor, so the bulk of the deposition occurred between about 850 and 500°C. The two exceptions were ^{95}Zr and ^{144}Ce in experiment H-2-4, and we feel

Table 1.10. Fission Gas Releases for Experiments H-2-2, -3, and -4

	^{85}Kr Released, %			^{3}H Released, %		
	H-2-2	H-2-3	H-2-4	H-2-2	H-2-3	H-2-4
Percent of total released in each operation						
Pre-burn soak (Ar–4% H_2)	0.04	0.03	0.83	3.16	7.04	31.01
Burn (air)	77.71	49.22	59.82	67.92	64.49	47.28
2-hr soak (air)	1.92	8.57	1.52	5.34	25.94	3.10
8-hr soak (air)	0.37	0.79	0.86	11.66	1.68	7.53
Reduction cycle (Ar–4% H_2)	0.15	0.19	0.33	8.18	0.40	8.86
Oxidation cycle (O_2)	0.16	0.09	0.07	1.52	0.09	0.53
Fines						
L-1 (HNO_3)	0.20	Not done	0.03	1.36	Not done	0.15
L-2 (Thorex)	0.17	0.79	1.30	0.82	0.002	1.10
L-3 (Thorex)	0.07		0.06			0.26
Fertile						
L-1 (HNO_3)	3.29	0.21	0.04	0.01	0.12	0.06
L-2 (Thorex)	6.33	18.32	16.39	0.01	0.08	0.03
L-3 (Thorex)	0.82	0.22	0.07		0.03	<0.01
Fissile						
L-1 (HNO_3)	0.15	11.16	0.10	0.01	0.03	<0.01
L-2 (HNO_3)	0.11	0.17	0.09	0.01	0.05	0.01
L-3 (Thorex)	7.05	9.61	18.42	<0.01	0.04	0.06
L-4 (Thorex)	1.45	0.35	0.08		0.01	<0.01
	Total Activity in Specimens, dis/min					
	1.36×10^{11}	8.03×10^{10}	1.62×10^{11}	1.87×10^{9}	2.57×10^{9}	9.09×10^{8}

Table 1.11. Fission Product Concentrations in Burner Off-Gas in H-2 Experiments

Experiment	Total Volume (liters)	Concentration, μCi/liter, for each Isotope				
		^{95}Zr	^{106}Ru	^{134}Cs	^{137}Cs	^{144}Ce
H-2-2	136	0.73	150.8	121.4	567	9.2
H-2-3	133	0.93	122	98	441	10.7
H-2-4	148	0.71	190	97.2	454	14.0

Table 1.12. Fission Product Distribution in Burner Off-Gas in H-2 Experiments

Component	Temperature (°C)	Activity Retained, %, for each Isotope				
		^{95}Zr	^{106}Ru	^{134}Cs	^{137}Cs	^{144}Ce
		Experiment H-2-2				
Stainless steel frit	<750	99.91	99.41	75.723	74.504	99.133
Hot off-gas line	500			23.732	24.621	
Impactor	500		0.059	0.23	0.24	0.375
Hot Ag filter	500	0.044	0.061	0.005	0.005	0.028
Condenser	20	0.011	0.001	0.002	0.0002	0.020
Cold Ag filter	Room	0.036	0.014	0.004	0.004	0.020
Gelman filter	Room	0.012	0.001	0.0001	0.0001	0.054
Cold off-gas line	Room		0.460	0.301	0.651	
		Experiment H-2-3				
Stainless steel frit	<750	89.21	80.96	84.96	85.22	79.56
Hot off-gas line	500	10.04	18.89	14.85	14.59	16.67
Impactor	500	0.02	0.02	0.14	0.13	0.05
Hot Ag filter	500	0.004	0.001	<0.001	<0.001	0.008
Condenser	20	0.004	0.001	0.001	0.001	0.007
Cold Ag filter	Room	0.004	0.001	<0.001	<0.001	0.008
Gelman filter	Room	0.006	0.002	<0.001	<0.001	0.010
Cold off-gas line	Room	0.68	0.12	0.06	0.06	0.69
		Experiment H-2-4				
Stainless steel frit	<750	83.97	98.58	97.15	97.13	64.89
Hot off-gas line	500	7.71	1.06	2.29	2.32	7.58
Impactor	500	0.25	0.18	0.49	0.47	0.09
Hot Ag filter	500	0.006	<0.001	0.001	0.001	0.01
Condenser	20	0.005	<0.001	<0.001	<0.001	0.01
Cold Ag filter	Room	0.007	<0.001	<0.001	<0.001	0.01
Gelman filter	Room	0.01	<0.001	<0.001	<0.001	0.02
Cold off-gas line	Room	8.05(?)	0.19	0.17	0.08	27.44(?)

that these results are due to cross-contamination of the cold off-gas line. Relatively larger amounts of contaminants were found in the ambient temperature off-gas lines. One concludes that either the Gelman absolute filter disk was ineffective or the lines were cross-contaminated. The possibility of external surface contamination of these lines cannot be eliminated since the cell is contaminated.

The cascade impactor (Fig. 1.5) was a five-stage unit, Model B, purchased from EnviroChem Systems Inc. It was modified to provide improved sealing surfaces between stages at our operating temperature (500°C). Gold foil gaskets were used, and the inner surfaces and collection plates were gold plated before use in the hot cell. Deposited particulate matter should have the characteristics shown in Fig. 1.6. As an example, the trapped diameters range from 7.75 to 1.04 μm at an average density of 5.0 g/cm^3 and a flow of 300 cm^3/min at 500°C. Typical deposited particles are shown in Fig. 1.7. The larger spherical particles on Plate 4 are unidentified; they must be low-density particles. We were unable to determine whether they represent trapped aerosol particles or were trapped and then grew to this size.

The compositions of principal contaminants for the three impactor experiments are shown in Fig. 1.8. For experiments H-2-2 and H-2-3, the percentages found on the collection plates decreased with decreasing particle size. In experiment H-2-4, the concentrations reached a minimum on Plate 2 (4.57 μm with the conditions stated previously), and then increased with decreasing particle size. The reason for the difference is not understood, but the same trend is obvious with all principal contaminants in this particular experiment. This behavior needs further investigation since concentration increases on the smaller particle sizes could affect the type and/or efficiency of off-gas filtration systems.

1.3.1.6 Studies with RTE-7 – C. L. Fitzgerald, V.C.A. Vaughen, K. J. Notz, and R. S. Lowrie

Two complete experiments were performed with RTE-7 specimens,[7] which contained Triso UC_2 and Triso ThC_2 in a rod matrix; only two rods

Photo 0858-71

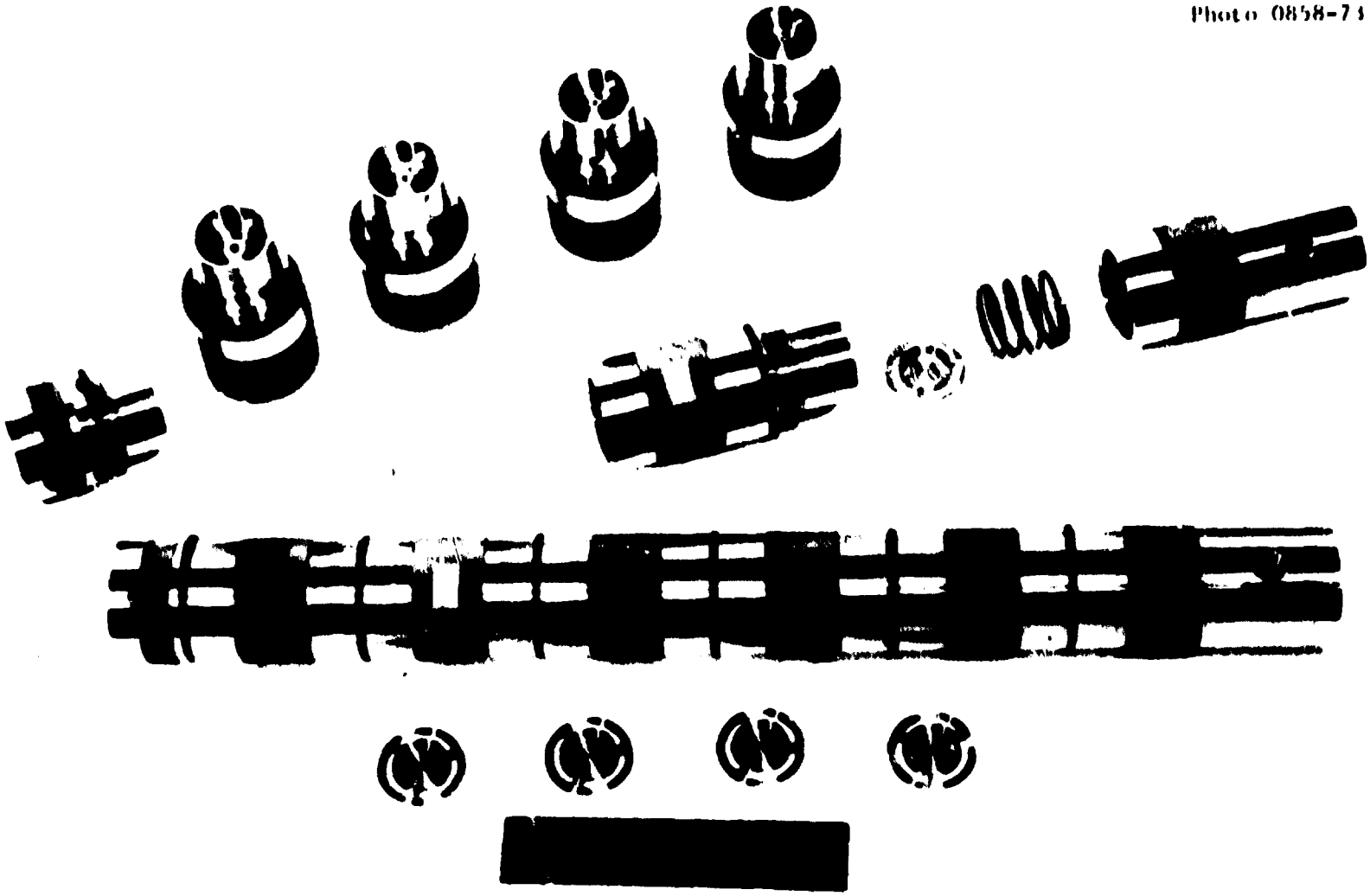

Fig. 1.5. Cascade Impactor. The scale shown is numbered in inches; total length is 0.10 m.

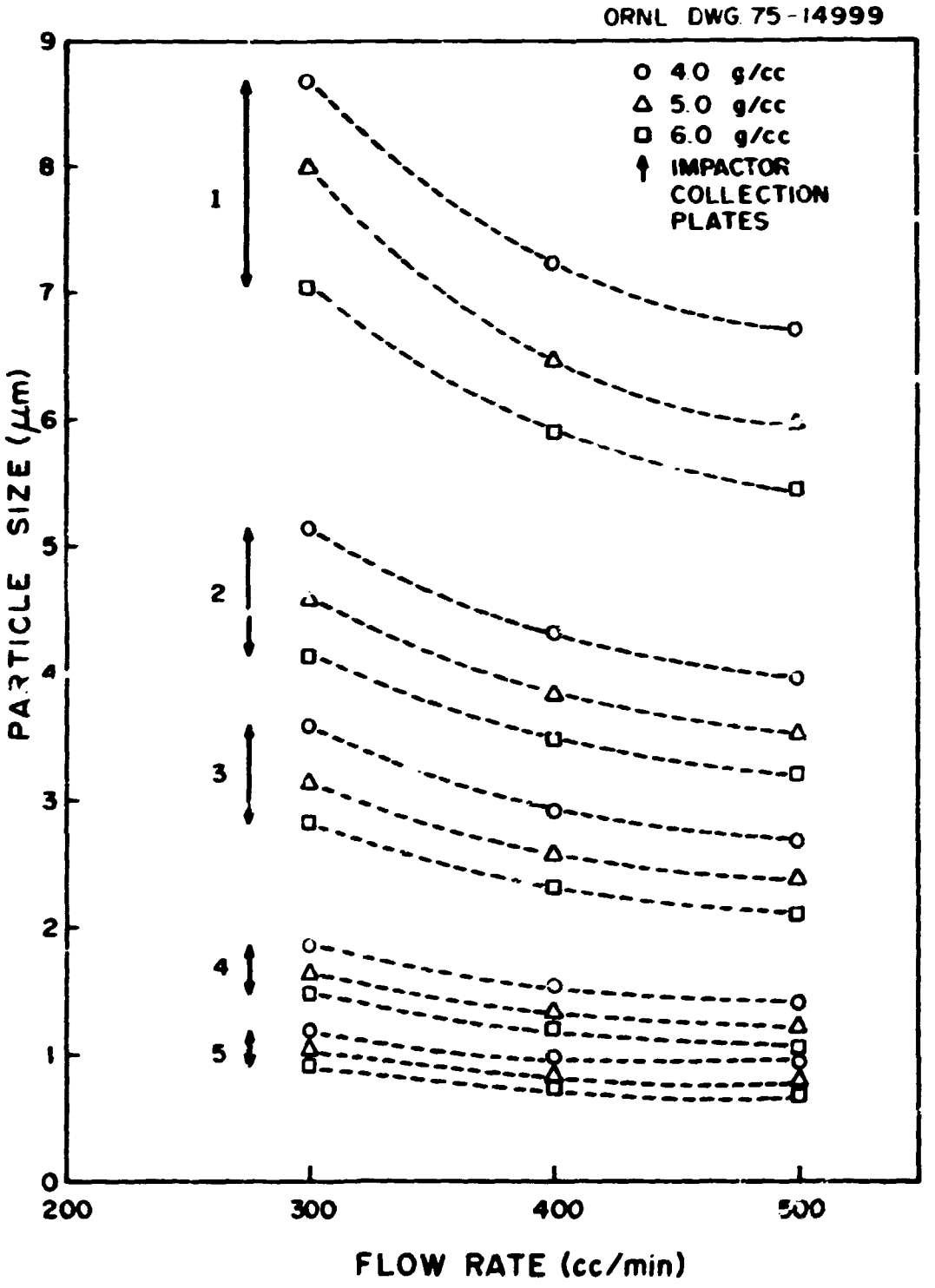

Fig. 1.6. Particle Size as a Function of Flow Rate for Cascade Impactor Used in H-Capsule Experiments.

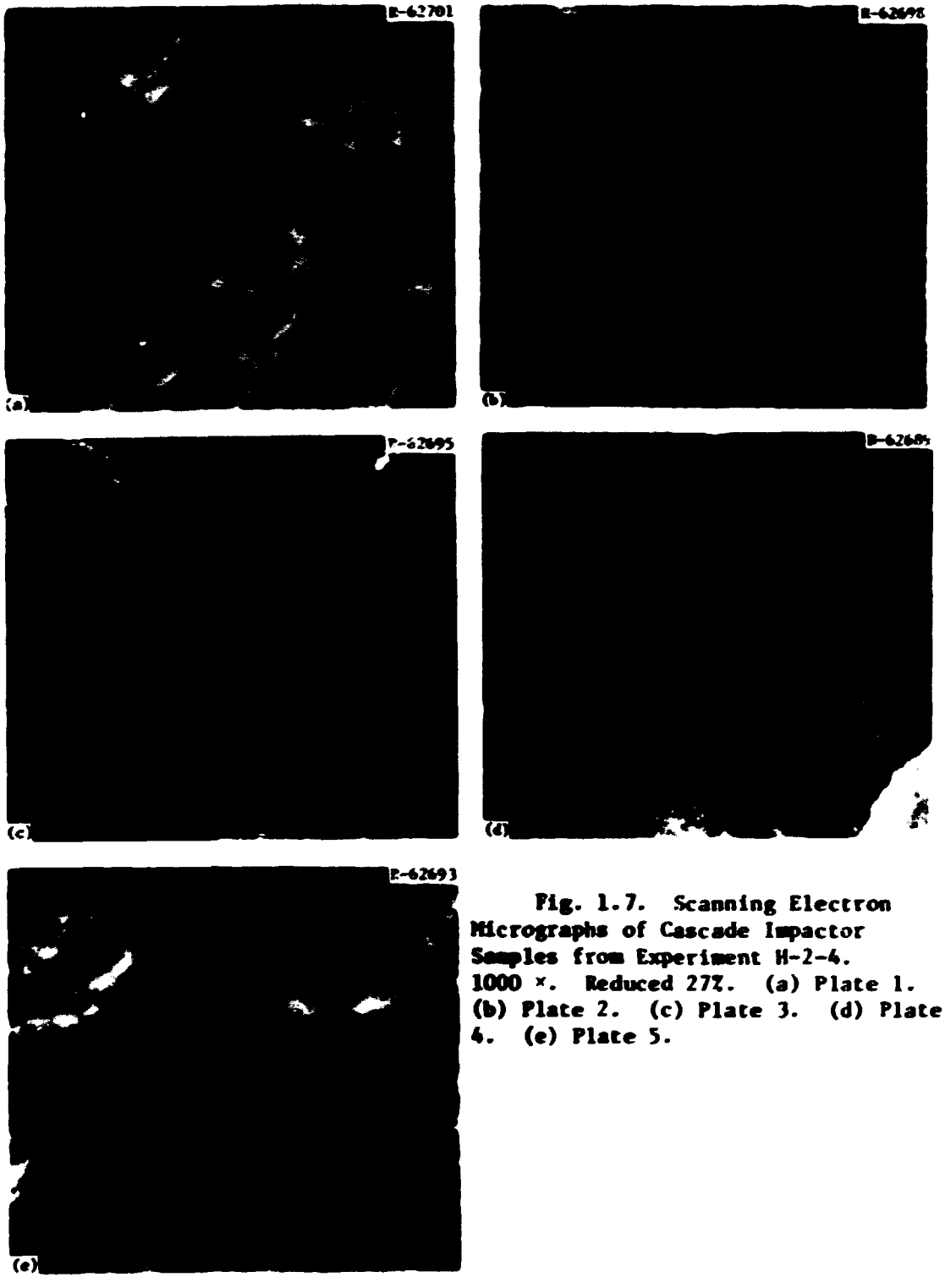

Fig. 1.7. Scanning Electron Micrographs of Cascade Impactor Samples from Experiment H-2-4. 1000 ×. Reduced 27%. (a) Plate 1. (b) Plate 2. (c) Plate 3. (d) Plate 4. (e) Plate 5.

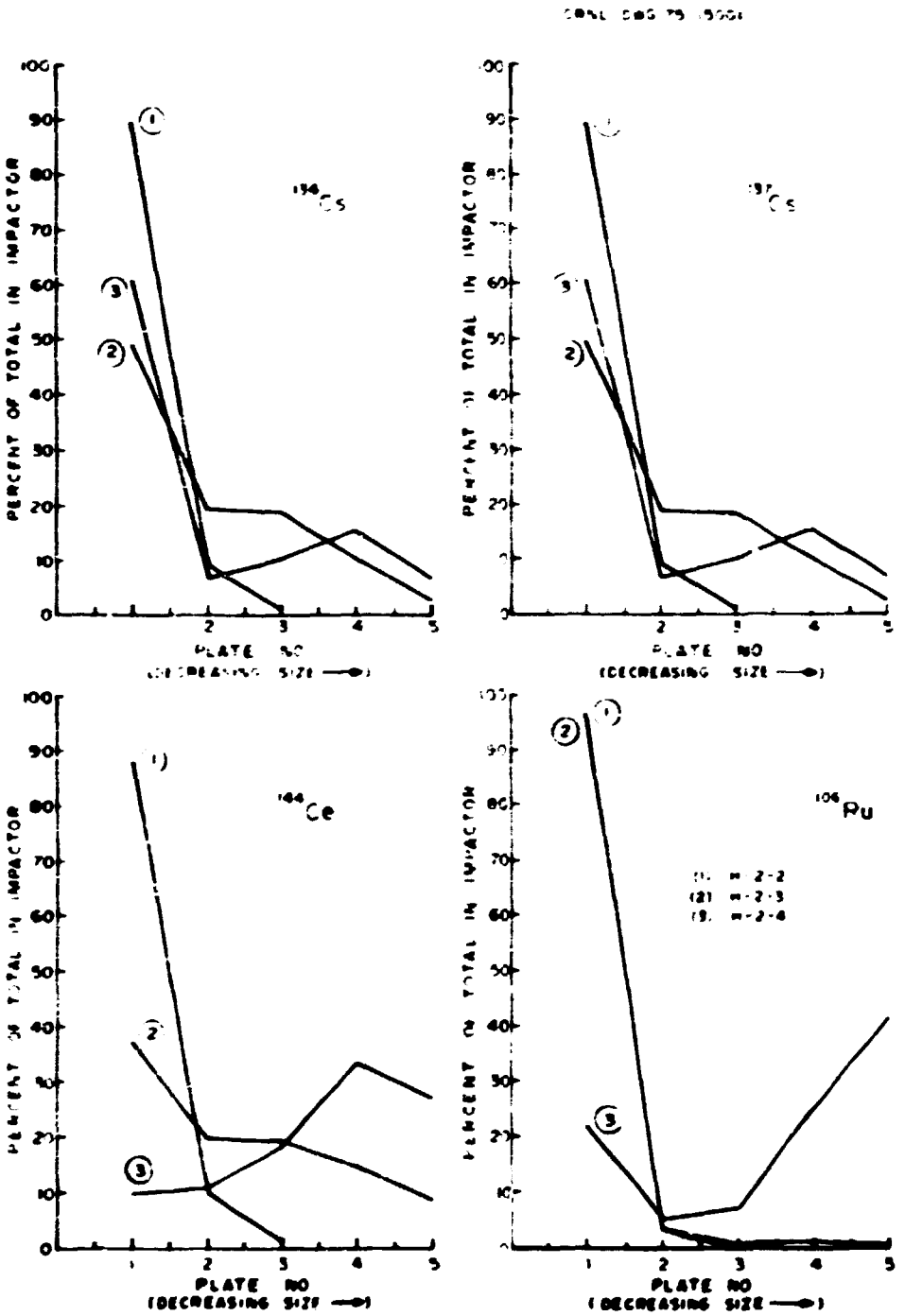

Fig. 1.8. Distribution of Fission Product Contaminants in a Cascade Impactor for Experiments H-2-2, -3, and -4.

were available. Figure 1.9 shows the burner and metallic filter assembly, and Figs. 1.10 and 1.11 are the equipment flowsheets used for the two fuel sticks.

Results of the second experiment are presented here. In general, the first and second experiments agreed, but where they did not the second is considered to be the more reliable since it incorporated improvements in both equipment and technique designed to minimize uncontrolled hydrolysis, gas losses, etc. This fuel had a thorium-to-uranium ratio of about 4, was exposed to a fast neutron fluence of about $1.6 \cdot 10^{21}$ n/cm^2 and a thermal neutron fluence of about $1.2 \cdot 10^{21}$ n/cm^2. The burnup (FIMA) was calculated to be 20% for the fissile particles and 0.23% for the fertile particles.

Table 1.13 shows the distribution of various nuclides between the off-gas train, the leaches, and the insoluble residues for all three burnings (primary, secondary-fissile, and secondary-fertile). Obviously, most of the activity was associated with the fissile particles. Of these nuclides, significant quantities of Ru (25%), Cs (6%), Sb (2%), and Nb-Zr (0.5–0.9%) were found in the off-gas train. Generally, the bulk of this activity in the off-gas train was retained on the sintered metal filters for the fissile fraction, with significant quantities being deposited downstream in the cold portion of the line (Table 1.14). For the primary and secondary-fertile burnings, almost all the off-gas activity plated out on the cold line (Table 1.14). Returning to Table 1.13, for the primary burn there is more activity found in the residues than in the leacher, while the reverse is true for both secondary burnings. Table 1.14 also shows ^{75}Se exclusively in the primary burning, trapped on the metal frit. This nuclide is an activation product, and the quantity found is equivalent to about 3 ppm natural Se in the fuel rod matrix.

Table 1.15 shows ^3H_2O and ^{85}Kr releases. The krypton release is largely as expected: a small release during primary burning, indicating a small fraction of broken particles; a much larger release from the fissile than from the fertile fraction; and significant release when the particles were crushed. The tritium release deviates from this pattern in several respects: 26% release during primary burning, indicating

ORNL DWG 72-8203R3

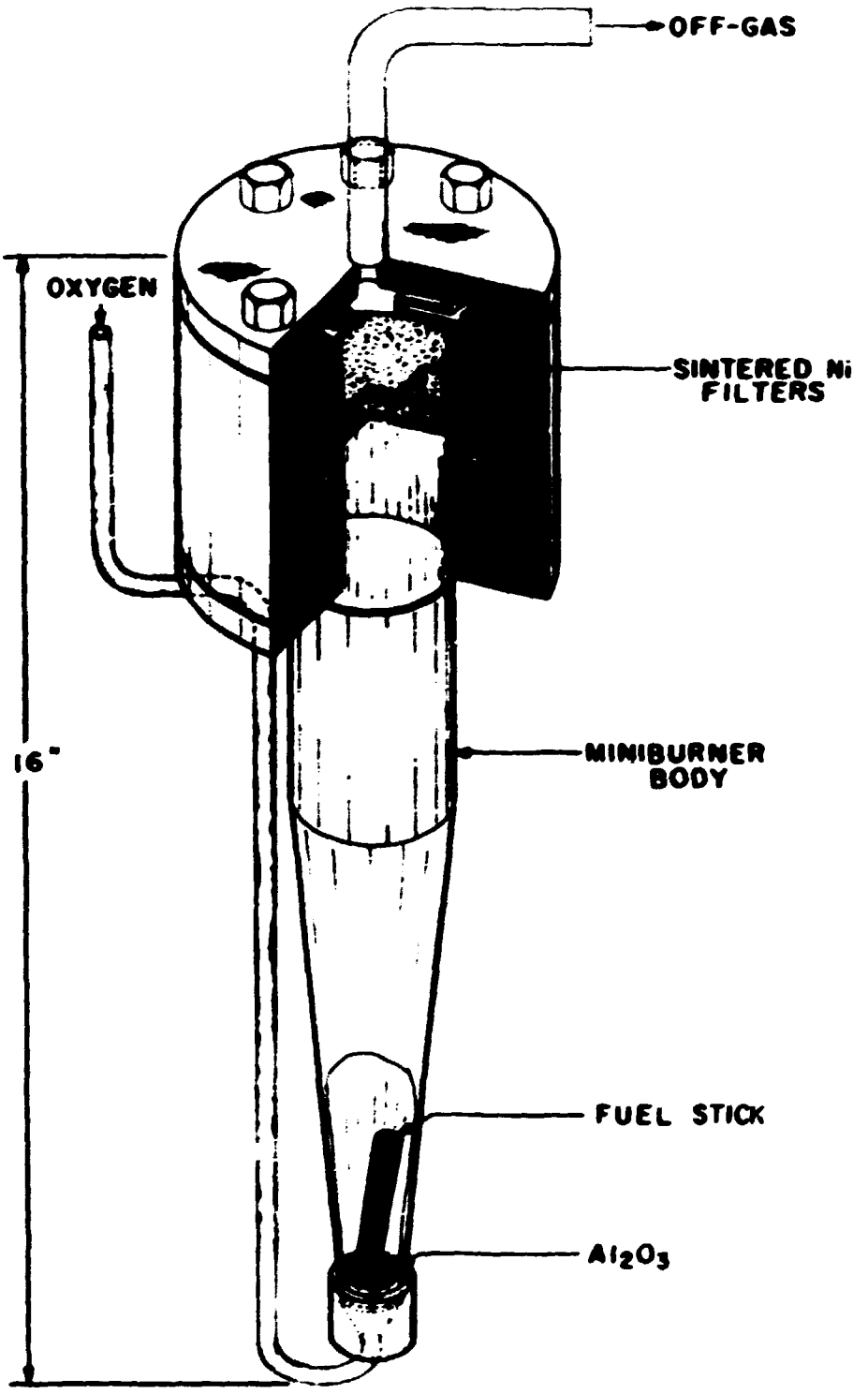

Fig. 1.9. Miniburner-Filter Assembly. Height is 0.4 m (16 in.).

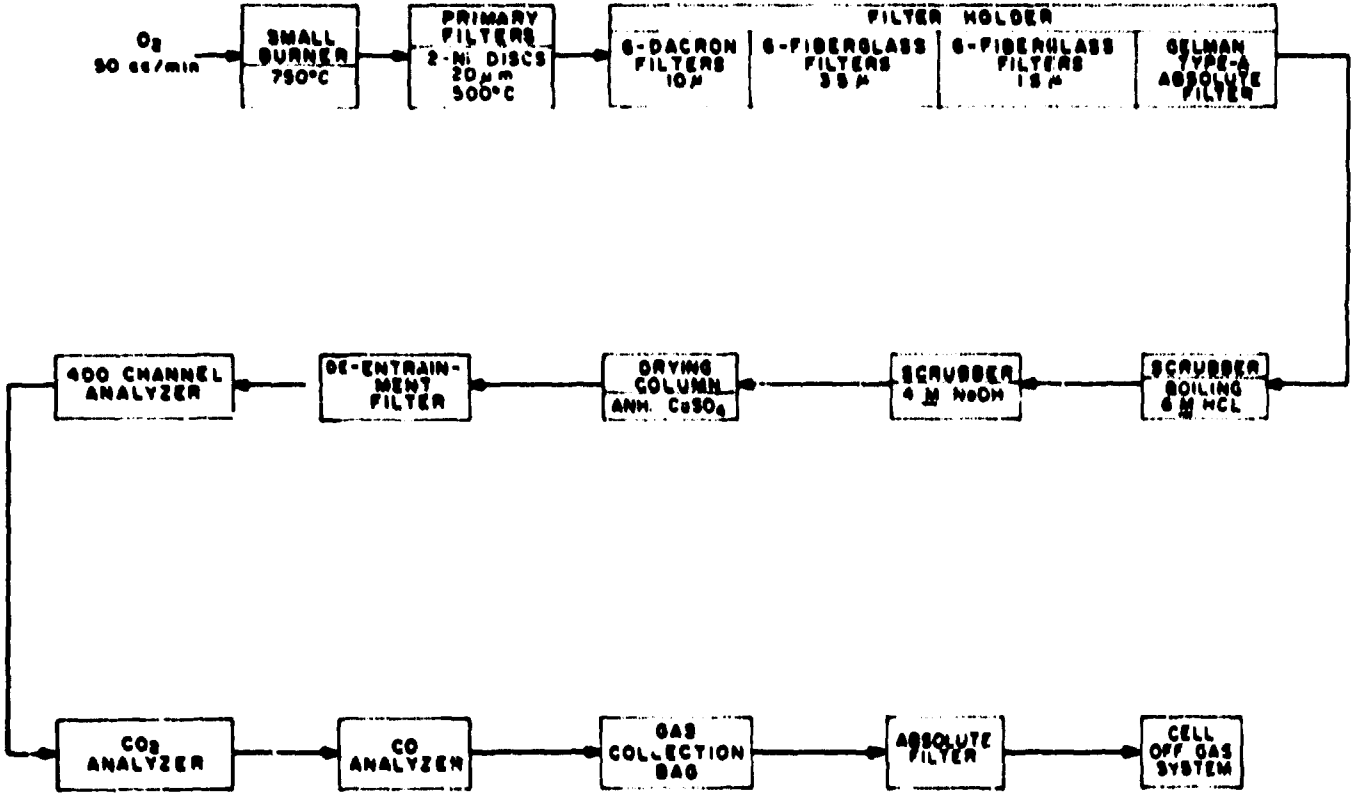

Fig. 1.10. Off-Gas Train Used for RTE-7-3-8-4 Burning (Triso UC_2-Triso ThC_2).

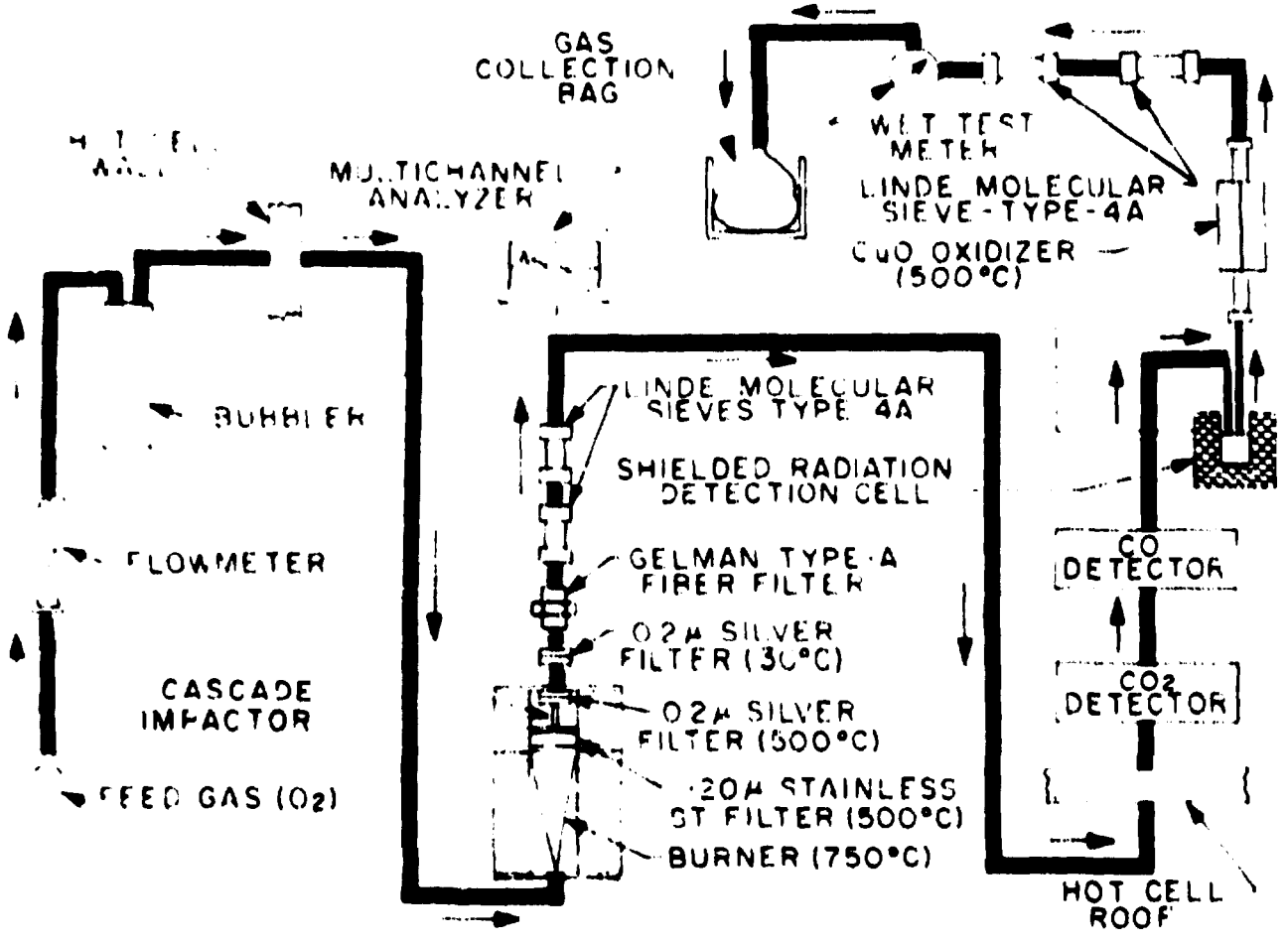

Fig. 1.11. Off-Gas Train Used for RTE-7-3-7-2 Burning (Triso UC_2-Triso ThC_2).

Table 1.13. Fission Product Recoveries and Main Stream Distribution for Second RTE-7 Experiment

	^{95}Zr	^{95}Nb	^{106}Ru	^{125}Sb	^{134}Cs	^{137}Cs	^{144}Ce
Grand total, dpm	1.532×10^{9}	2.129×10^{10}	1.266×10^{11}	4.635×10^{10}	1.983×10^{11}	5.954×10^{11}	3.800×10^{12}
Distribution (as found), %							
Off-gas trains							
Primary burner	0.03	<0.01	0.01	<0.01	<0.01	0.01	0.01
Fertile burner	0.02	0.05	0.41	0.02	0.02	0.02	0.01
Fissile burner	0.89	0.42	25.23	2.08	6.01	6.06	0.02
TOTAL	0.94	0.47	25.65	2.10	6.04	6.09	0.04
Leaches							
Primary burner fines[a,b]	0.06	0.07	0.02	0.04	0.04	0.04	0.03
Fertile particle ash[b]	4.58	6.73	4.96	4.77	1.81	3.58	2.28
Fissile particle ash[b]	75.92	70.91	26.64	69.21	73.29	71.82	87.03
TOTAL	80.56	77.71	31.62	74.02	75.14	75.44	89.34
Residues							
Primary burner fines[a,b]	0.39	1.27	0.41	0.51	0.43	0.44	0.22
Fertile particle ash[b]	0.16	0.54	0.53	0.50	0.13	0.25	0.04
Fissile particle ash[b]	17.96	20.00	41.78	22.87	18.25	17.79	10.36
TOTAL	18.51	21.81	42.72	23.88	18.81	18.48	10.62

[a] Broken particles.

[b] Includes Al_2O_3 bed.

Table 1.14. Plateout and Trapping of Fission Products in Downstream Off-Gas Equipment for Second RTE-7 Experiment[a]

	^{95}Nb	^{95}Zr	^{106}Ru	^{125}Sb	^{134}Cs	^{137}Cs	^{144}Ce	^{154}Eu
Total found in off-gas train, dpm	1.004×10^{9}	1.446×10^{9}	1.250×10^{10}	9.708×10^{8}	1.197×10^{10}	1.627×10^{10}	1.589×10^{9}	9.738×10^{5}
Percent of grand total	0.47	0.94	25.65	2.10	6.04	6.09	0.062	100
Distribution within fractions								
Initial burn,[b] µCi/liter	0.02	0.10	0.41	--	0.25	1.2	10.5(?)	0.02
SS frit No. 1, %	–	–	–	–	1.21	0.48	–	99.1
Hot Ag filter, %	–	–	–	–	–	–	–	0.9
Line leach, %	100	100	91.96	–	98.79	99.34	100	–
Cold Ag filter, %	No detectable gamma activity							
Gelman absolute filter, %	No detectable gamma activity							
Fertile burn,[c] µCi/liter	0.16	0.04	7.8	0.13	0.47	1.4	2.4	–
SS frit No. 1, %	–	<3.74	5.10	–	0.90	1.48	7.76	–
SS frit No. 2, %	–	<0.75	1.28	–	0.06	0.06	1.17	–
Hot Ag filter, %	0.08	0.08	<0.01	--	0.01	0.01	0.02	–
Line leach, %	99.92	<95.43	93.61	100	99.03	98.45	90.91	–
Cold Ag filter, %	No detectable gamma activity							
Gelman absolute filter, %	No detectable gamma activity							
Fissile burn[d] and soak, µCi/liter	0.85	1.3	306	9.2	114	345	8.8	–
SS frit No. 1, %	67.65	80.35	54.46	93.52	98.91	98.84	87.27	–
SS frit No. 2, %	26.86	17.24	35.68	4.88	0.99	1.05	7.57	–
Hot Ag filter, %	0.07	<0.22	0.53	0.03	<0.01	<0.01	<0.33	–
Line leach, %	5.43	2.19	9.33	1.56	0.11	0.12	4.83	–
Cold Ag filter, %	Trace of 0.24 MeV gamma activity							
Gelman absolute filter, %	Trace of 0.24 MeV gamma activity							

[a]Sought – not found (where dashes are shown).

[b]Volume = 21.925 liters

[c]Volume = 47.04 liters (with soak).

[d]Volume = 10.0 liters (with soak).

Table 1.15. Fission Gas Release to the Burner Off-Gas During Processing of Second RTE-7 Experiment

	^{3}H		^{85}Kr	
	(dpm)	(%)	(dpm)	(%)
Total	1.746×10^{9}	100	1.525×10^{11}	100
Initial burn		26.0		0.129
Fines leach		0.06		≤0.010
Fertile fraction (+45)				
Grind		0.06		0.221
Burn		13.23		3.220[a]
Soak (2 hr)		0.21		
Leach		0.02		<0.020[b]
Total		13.52		3.461
Fissile fraction (+80)				
Grind		0.01		19.016
Burn		56.47		77.377
Soaks (2 hr)		2.24		b
Soak (8 hr)		1.66		b
Leach		0.04		0.125
Total		60.42		96.518

[a]Value is known to be low because of a leak in the CuO unit, which occurred.

[b]Sought, not found.

formation by activation (e.g., of Li) since ^{3}H from ternary fission should be retained within the Triso coatings; a relatively large fraction from the fertile particles (note, however, that the ^{85}Kr result for the fertile particles may be low); and the delayed release of some of the tritium during prolonged thermal "soak" at temperature. Overall, including the thermal soak, 0.12% of the ^{3}H appeared in the leaches for an overall decontamination factor from burning of 830.

1.3.2 Vapor Transport of Fission Products – E. E. McCombs and J. H. Shaffer

An experimental program was initiated to examine the vapor transport of fission products and actinides from the burner off-gas during the head-end reprocessing of spent HTGR fuel elements. In this head-end process, fuel blocks, graphite matrix, and particle coating materials will be burned with oxygen, and the residual ash processed by solvent extraction for the recovery of fissile and fertile materials. The gas effluent from the graphite burner will likely contain prohibitive quantities of radionuclides and must, therefore, be processed to achieve suitable decontamination for its discharge into the atmosphere. Expected contamination consists of known gaseous fission products – xenon, krypton, tritium, and iodine – and certain other semi-volatile and particulate fission products and actinides, which may be entrained as aerosols in the burner effluent stream. Effective separations processes for these materials are currently under development. In addition to the anticipated types of contamination, some fission products and actinides may have sufficient volatility under burner conditions to require means to prevent their direct discharge with this process effluent into the atmosphere. This proposed experimental program will examine the vapor transport of elements and compounds selected from this group at temperatures in the range from 750 to 1300°C under conditions that will be applicable to burner technology.

Relevant literature has been examined, and various experimental techniques have been assessed for measuring very low vapor pressures [10^{-5} Pa (10^{-6} torr) and below] in the temperature range of interest in this program. A transpiration method by which burner environmental conditions can be simultated has been designed and is depicted in Fig. 1.12.

The heating unit is a horizontally mounted resistor tube furnace internally wound with Pt-40% Rh wire and is designed to operate at temperatures up to 1540°C. Centered in the furnace is a mullite combustion tube with an alumina boat containing the material under investigation. Two Pt vs Pt-10% Rh thermocouples are located within the mullite tube: one, centered in the tube above the sample, measures the temperature of the saturated vapor, and the other, above one end of the sample boat,

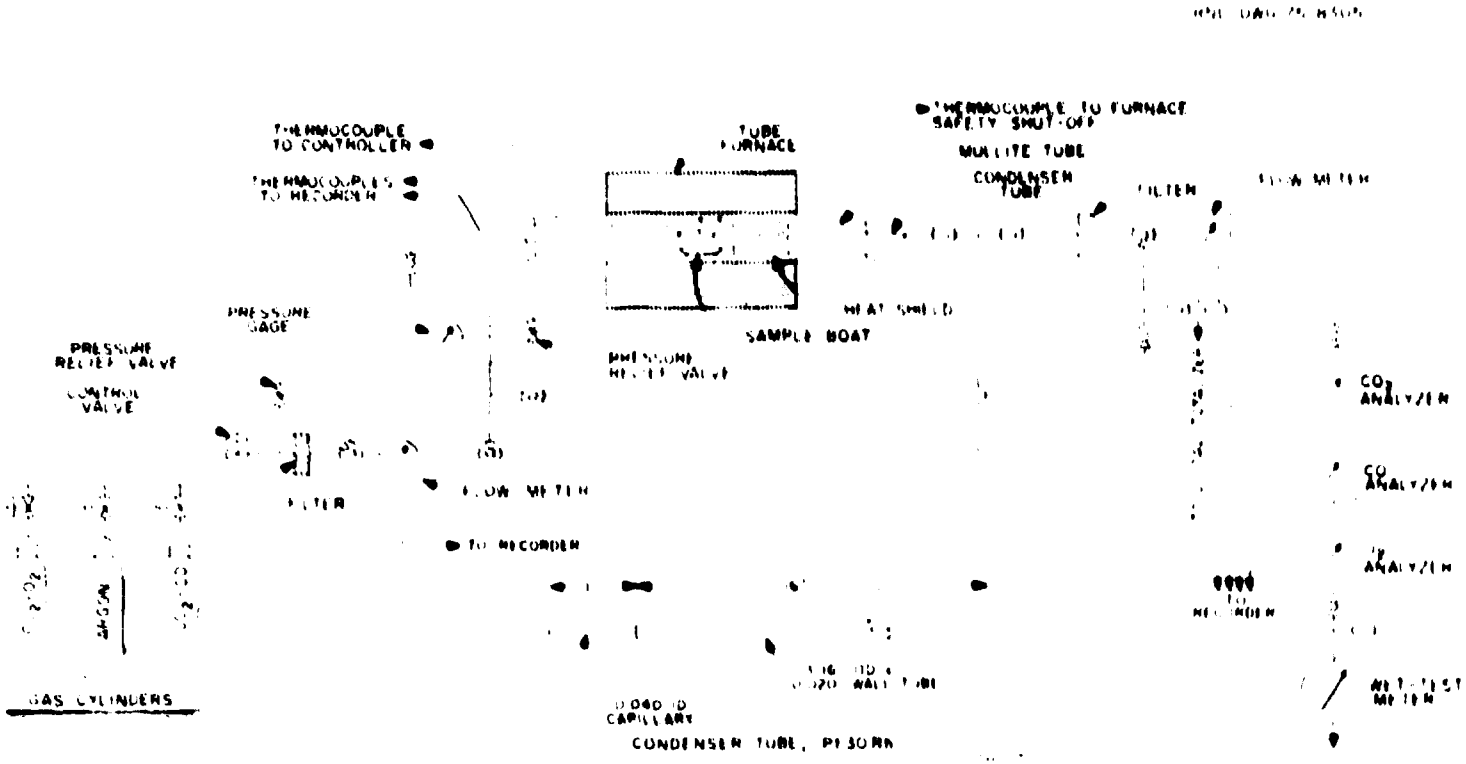

Fig. 1.12. Schematic Diagram of Transpiration Apparatus. Dimensions on the Pt-30% Rh condenser tube are in inches; multiply by 25.4 to convert to millimeters.

determines the longitudinal uniformity of temperature. Located above the sample boat and exiting from one end of the mullite tube is a Pt-30% Rh condenser tube. Leading into and out of the mullite tube are valves and tubing that permit the introduction of various atmospheres as well as reverse flow and bypass operation. Mass flow meters are used to measure the volumetric flow rate in both upstream and downstream lines. The concentrations of CO_2, CO, and O_2 are determined by in-line gas analyzers.

A compound (usually the oxide) of the element under investigation will be loaded into the sample boat exposing as much surface area as possible. During the heatup cycle, the system will be purged by reverse flow of the desired carrier gas. When the run temperature has been reached and stabilized, the gas flow will be directed over the specimen and out the condenser tube for the duration of the experiment, followed by reverse flow for the cooling cycle.

After each transpiration experiment, the condenser tube will be removed and the contents analyzed. Since nanogram and subnanogram amounts of condensed vapor species are anticipated, an isotope dilution technique followed by thermal emission mass assay analysis was selected as being the most sensitive. In this method, the element recovered from the condenser tube, being of normal assay, will be spiked by a known amount of an enhanced isotope of the same element. The quantity of vaporized element is then a function of the assay of the mixture, and is calculated thus:

$$W_v = \frac{W_s (A_{x/m} - A_{x/s})}{A_{x/v} - A_{x/m}} ,$$

where

W_v = weight of element in the condensed vapor,
W_s = weight of element in the spike,
$A_{x/m}$ = assay of isotope X in the mixture,
$A_{x/s}$ = assay of isotope X in the spike,
$A_{x/v}$ = assay of isotope X in the condensed vapor.

Initially, the volatility of Eu_2O_3 will be measured, with normal europium (assay: 47.82% ^{151}Eu, 52.18% ^{153}Eu) used as the vapor species and enhanced ^{153}Eu (assay: 1.24% ^{151}Eu, 98.76% ^{153}Eu) as the spike. Assuming a spike of 100 ng, the following table presents the calculated weights of europium in the condensed vapor corresponding to various assays.

Eu in Condensed Vapor, ng	0.00	0.13	0.34	0.56	0.78
^{151}Eu in Europium, %	1.24	1.30	1.40	1.50	1.60

Note: Mass assay analyses are accurate to ±1% of the minor constituent.

The above values attest to the excellent sensitivity and accuracy of the isotope dilution technique. The method has the additional advantage that, after the spike has been added and equilibrated, losses of euorpium during transfer, drying, etc. have no effect on the final determination. Except in the investigation of the actinides, radioactive material will not be encountered when isotope dilution is used.

Unfortunately, this superior analytical technique cannot be used in the investigation of some of the fission product and actinide elements, namely: (1) the mononuclides and (2) those whose mass assay cannot be determined by the very sensitive thermal emission method. Alternative methods of analysis include neutron activation, radioactive spiking, atomic absorption, and spark source mass spectrometry.

1.3.3 Whole-Block Burner Studies – P. A. Haas, J. W. Snider, H. Barnert-Wiemer,* and D. C. Watkin

An experimental program demonstrated the physical feasibility of the whole-block approach to burning. These results have been reported as an appendix to an evaluation study.[8] The burner employed for the experimental study used one-sixth of a Fort St. Vrain fuel block, and is shown schematically in Fig. 1.13. Two partially burned segments are shown with an unburned piece in Fig. 1.14. The abstract of the evaluation study[8] is repeated below. A suggested layout for a whole-block burner is shown in Fig. 1.15.

---

*Guest scientist from KFA Jülich.

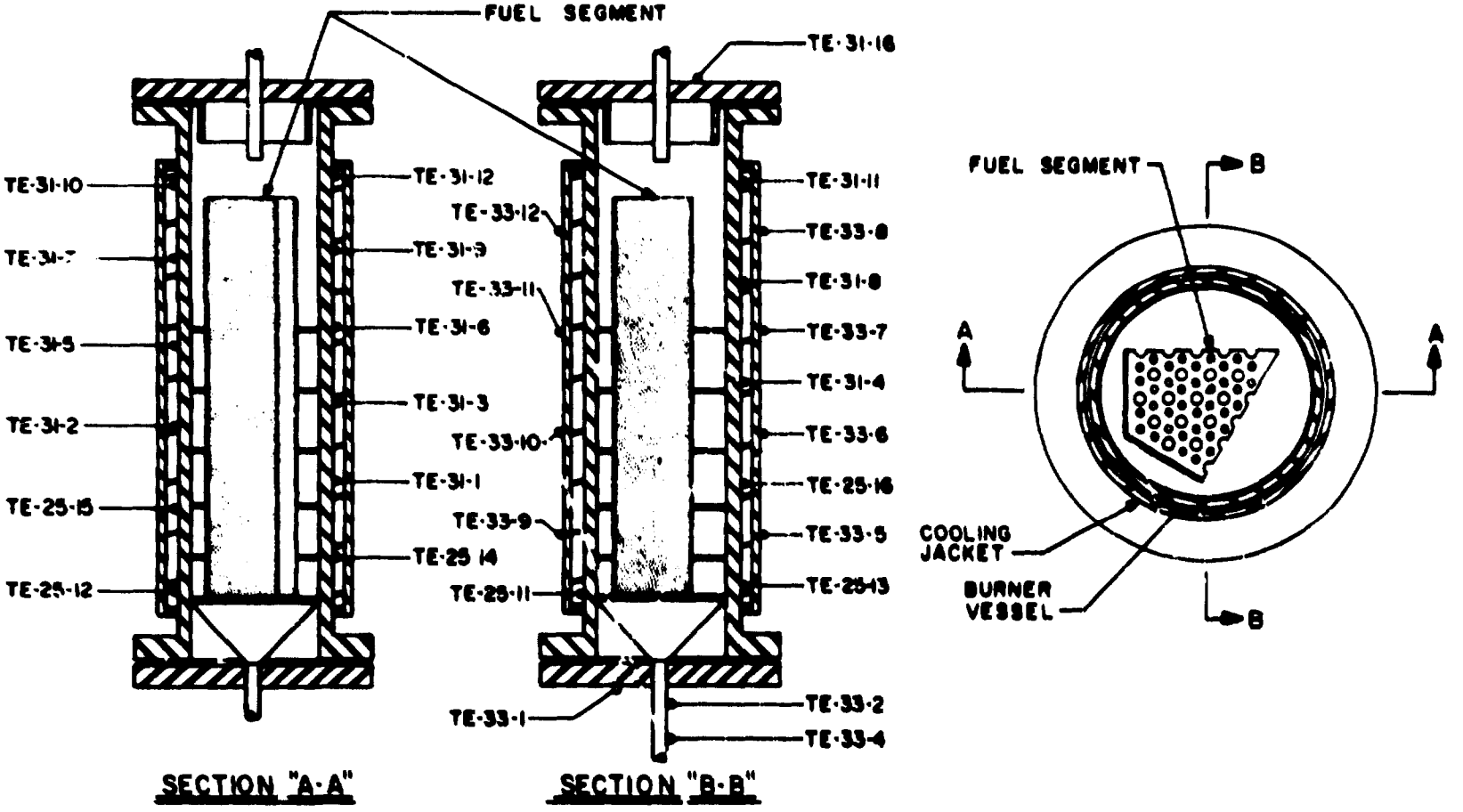

Fig. 1.13. Experimental Whole-Block Burner, Showing Thermocouple Locations.

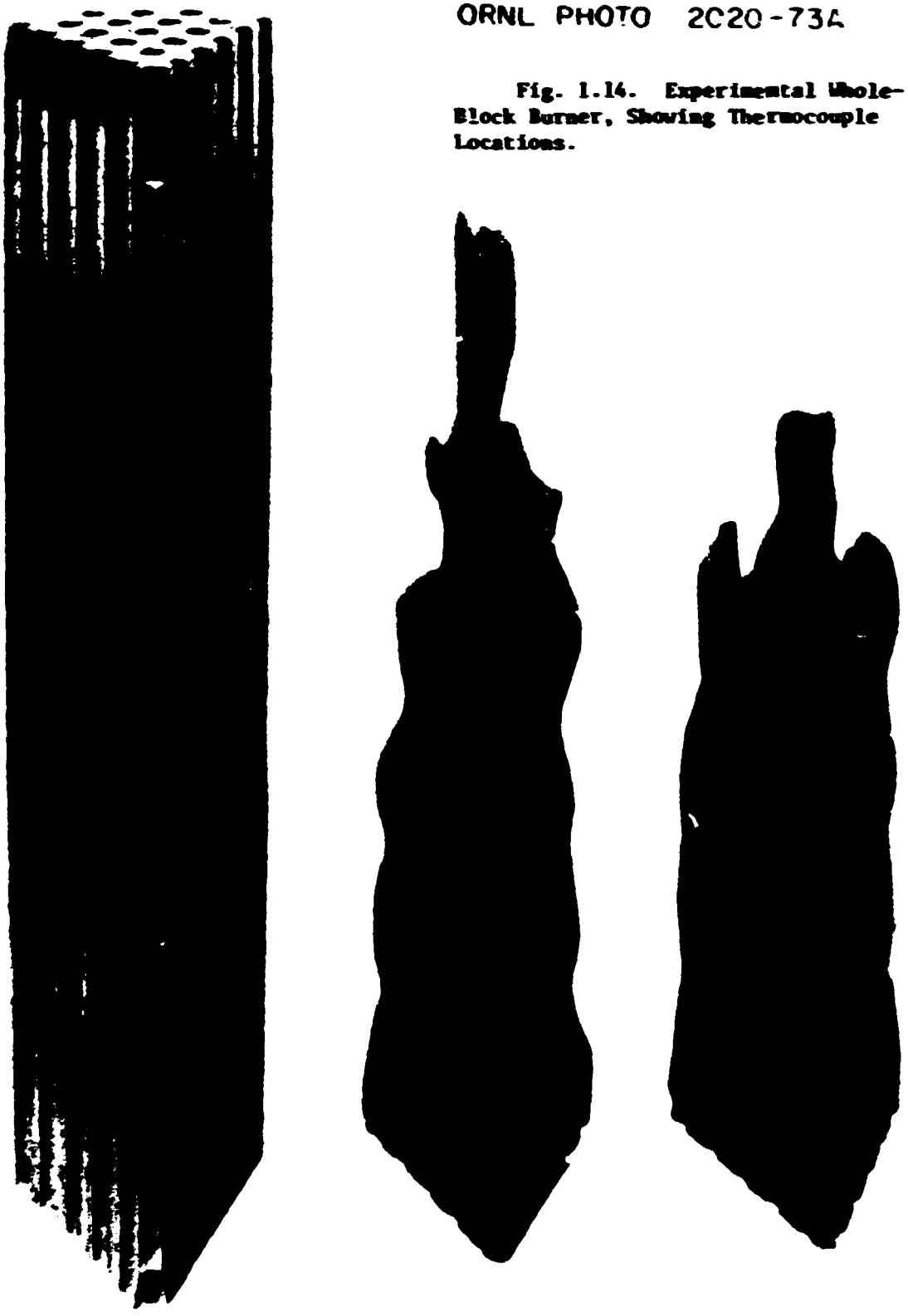

ORNL PHOTO 2020-73A

Fig. 1.14. Experimental Whole-Block Burner, Showing Thermocouple Locations.

ORNL DWG 73-11883R2

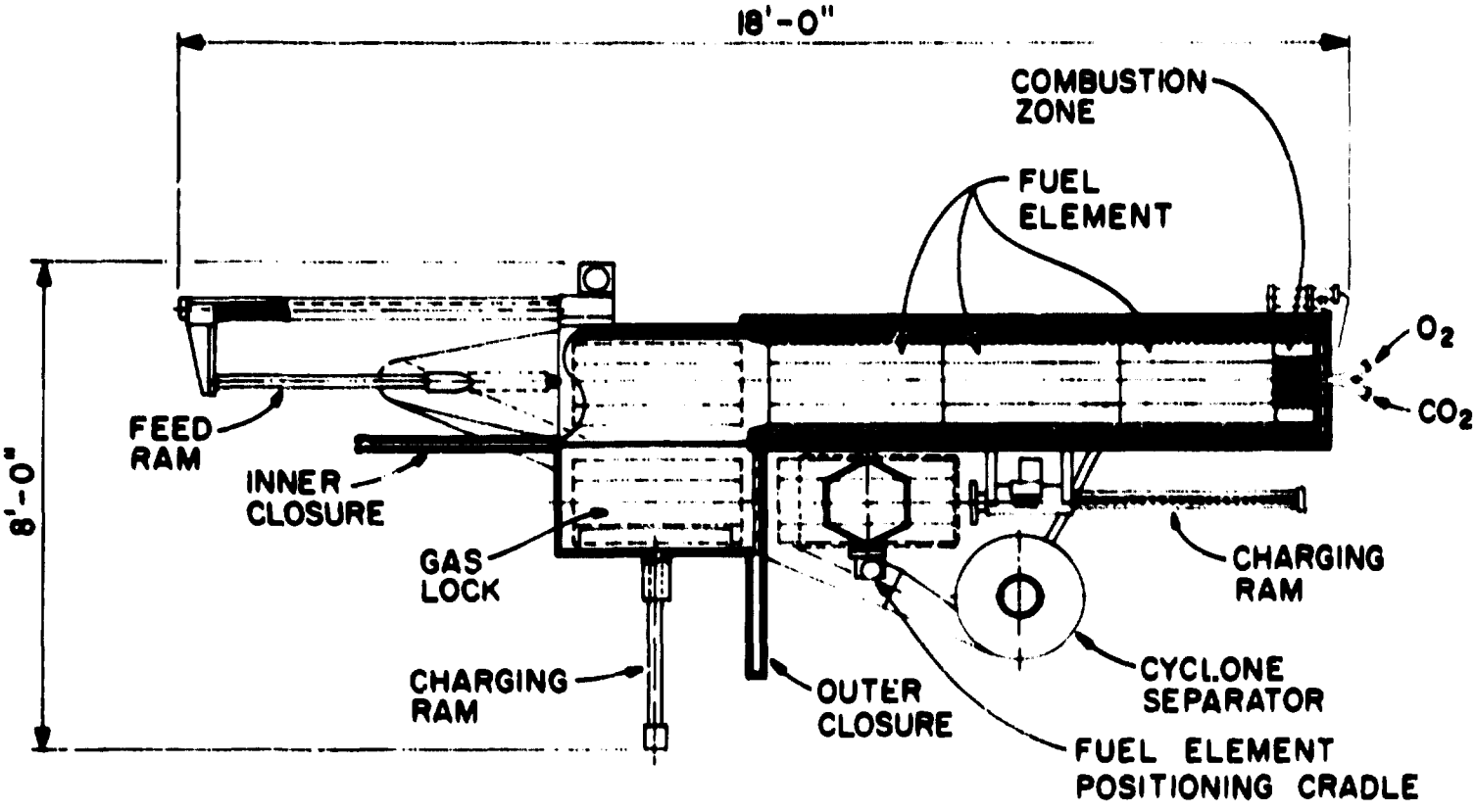

Fig. 1.15. Conceptual Plan View of a Whole-Block Burner. Overall size is 2.44 by 5.5 m (8.0 by 18.0 ft).

"An economic and technical comparative study was made of the reference method, fluidized-bed burning, and an alternative method, whole-block burning, for performing the primary burning step in HTGR fuel reprocessing. For each method, considerations were made of the ancillary equipment for heat removal and the fuel and ash handling; crushing was also included in the case of fluidized-bed burning. The scale of primary burning was that of a reprocessing plant handling the spent fuel from ~50,000-MW(e) HTGR generating capacity. Preliminary designs were prepared for the major equipment components and/or modules in canyons equipped with the necessary remote maintenance features. Cost estimates were prepared for the equipment items using a fractional cost factor for multiple modules. The cost of the building associated with the primary burning step was estimated using the volume of concrete in the heavily shielded canyons and the area of the operating corridors adjacent to or above the canyons. The cost of primary burning is guesstimated to be about $100 million, with no significant difference between fluidized-bed and whole-block burning. The layout of the various canyons suggests that a modular head-end plant with add-on capability is more easily obtainable with the whole-block burner than with the fluidized-bed burner. The development of a fluidized-bed burner with a low length/diameter ratio should be a developmental goal.

"A report of studies made by Dr. H. Barnert-Wiemer with a one-sixth whole-block burner is included as an appendix."

A theoretical study was made of the so-called "adiabatic" burner, wherein heat is removed from the system downstream of the burner via a separate heat exchanger.[9] Burner conditions are controlled by appropriate recycle of burner off-gas, utilizing the endothermic reaction, $CO_2 + C \rightarrow 2CO$, and high gas velocities. Figure 1.16 plots the calculated conditions for a gas exit temperature of 1000°C and presents a schematic equipment layout to accomplish adiabatic burning. The abstract of this study follows:

"Burning of whole fuel blocks (hexagonal prisms about 14 in. across the flats and 31 in. long) is being investigated as one

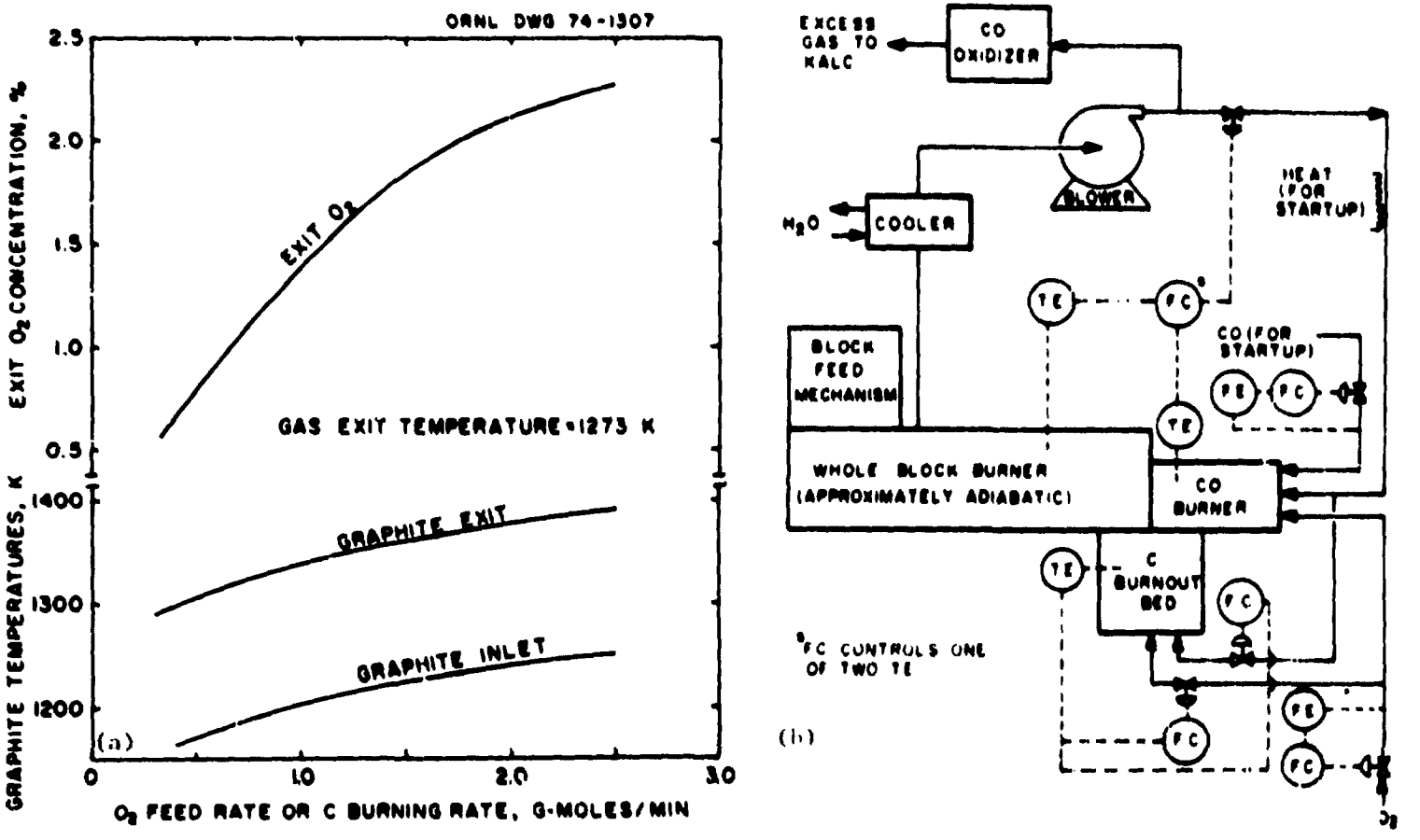

Fig. 1.16. Adiabatic Whole-Block Burner. (a) Calculated behavior with recycle of CO_2-O_2 and a gas exit temperature of 1000°C. (b) Flowsheet showing accessory concepts.

head-end treatment for reprocessing the General Atomic Company type of HTGR fuel. Experimental results with a one-sixth block burner have shown practical burning rates and good utilization of O_2. This report describes and presents analyses for a whole-block burner with recycle of cooled gas to provide temperature control and heat removal. A simplified model was selected and computer programs were written to calculate gas compositions and temperatures throughout the burner. Complete utilization of O_2 or low concentrations of O_2 in the exit gas depend on graphite temperatures that are sufficiently high to produce CO, which reacts with O_2 in the bulk gas. It does not appear practical to operate under conditions that promote both high utilization of O_2 and low CO concentration in the exit gas. Instead, the burner conditions should be chosen to clearly favor moderate concentrations of either O_2 or CO in the exit gas. Moderate concentrations of O_2 in the exit gas would allow lower graphite temperatures and would probably give the desired burning rates for three axially aligned blocks. Moderate concentrations of CO in the exit gas would ensure high burner capacities but would result in higher temperatures and more complex burner control behavior. An experimental burner is recommended to verify the calculated results."

Currently, experimental work on the adiabatic concept is being carried out under funding by the Division of Physical Research. This work focuses on control modes and recycle of off-gas, and is being reported elsewhere.[10]

1.4 SOLVENT EXTRACTION (WORK UNIT 1102) — R. H. Rainey

Three major activites were conducted under this work unit: consulting with GAC and ACC on their development work, upgrading and expanding the SEPHIS code, and preparing for in-cell tests of feed adjustment and solvent extraction.

1.4.1 Solvent Extraction Processing — R. H. Rainey

The System Design Description for the HTGR Fuel Reprocessing Facility for the Solvent Extraction Processing System at Idaho was

critiqued, and the feed adjustment and pulse-column experiments at General Atomics were reviewed. The SEPHIS-Thorex computer calculations were used to help evaluate the solvent extraction flowsheets at both of these sites. A tentative solvent extraction flowsheet for reprocessing engineering hot cell tests was prepared.

1.4.2 Computer Code for Simulating the Acid Thorex Solvent Extraction System — R. H. Rainey and S. B. Watson*

The Solvent Extraction Processes Having Interacting Solutes (SEPHIS) computer program, which was originally written to simulate the Purex solvent extraction system, is being modified to simulate the Acid Thorex system. The SEPHIS program calculates the concentration of the principal soluble components (i.e., thorium, uranium, and nitric acid) in both phases of each stage of a countercurrent system throughout the transient from start-up to steady-state operation. The use of this program can therefore greatly simplify the design of the flowsheet, the design of the contactor equipment, the determination of operating conditions, the safety evaluations, etc.

As a result of this program, the basic SEPHIS-Purex code structure and the mathematical model were modified so that the computer core storage was reduced by about 100K and the calculational time was reduced. The program was further modified so that when convergence times became long the program accepts a lower quality value for printout so as to guide future flowsheet trials.[11]

The SEPHIS program was then modified to calculate the Acid Thorex flowsheet. Empirical equations were fit to calculate the distribution coefficients of thorium-uranium-nitric acid system in 30% TBP in a manner similar to that used for the SEPHIS-Purex system. In order to obtain satisfactory fits of this data it was necessary to use a $Th(NO_3)_4 \cdot 3TBP$ complex for the thorium extraction instead of the 2TBP complex usually reported in the literature. Also in contrast with the Purex system, which uses molal concentrations, a better fit was obtained

---

*Computer Sciences Division.

in the Thorex system when molar concentrations were used. The computer code using these empirical equations resulted in a good fit to laboratory countercurrent batch extraction data (Table 1.16). Copies of the preliminary SEPHIS-Thorex computer program were sent to engineers at GAC at La Jolla and ACC at Idaho Falls. The program was used at those sites to evaluate the proposed solvent extraction flowsheets and to calculate the height equivalent to a theoretical stage of the experimental pulse columns.

The calculations using equations from the fit of the distribution coefficients failed to converge when the concentration of salts in the organic phase approached saturation. A new approach is being tried in which the concentrations of thorium, uranium, and nitric acid in the organic phase are calculated instead of the distribution coefficient. This procedure enables including an estimate of the error of the data in the least squares fitting. So far only the thorium extraction equations have been derived by this system. An improved statistical fit of the data to the derived equation was obtained.

Other parameters in the calculation of the Acid Thorex extraction system that have not been completed include TBP concentration and temperature.

1.4.3 Feed Adjustment and Solvent Extraction Development — R. H. Rainey

Hot cell experiments are being planned in which highly irradiated fertile fuel particles will be dissolved, adjusted to acid deficient solvent extraction feed conditions, and then batch solvent extracted. The purpose of the experiments will be to determine the path of the fission products and gather other data to be used to develop chemical flowsheets. A principal problem in these experiments is the small amount of fuel available. At the point of maximum concentration in the feed adjustment, the solution occupies about 5 ml. Feed adjustment equipment has been developed and demonstrated in cold tests and is being installed in the hot cell.

The adjusted feed solution will be used for batch shakeouts. This equipment and procedure must also be developed, since only small amounts of feed will be available.

Table 1.16. Comparison of Experimental and Calculated Results of Acid Thorex Solvent Extraction System

Flowsheet Conditions

Feed: 278 g/liter Th, 17.6 g/liter U, 0.21 *M* AD, 1 volume.
Scrub 1: H_2O, 0.8 volume at stage 6S.
Scrub 2: 5 *M* HNO_3, 0.2 volume at stage 3S.
Salting acid: 13 *M* HNO_3, 0.5 volume at stage 4E.
Solvent: 30% TBP-NDD, 7 volumes at stage 5E.

Stage	Heavy Metal Concentrations, g/liter								Acid, *M*			
	Aqueous Th		Organic Th		Aqueous U		Organic U		Aqueous		Organic	
	Exptl	Calcd	Exptl	Calcd	Exptl	Calcd	Exptl	Calcd	Exptl	Calcd	Exptl	Calcd
6S	85.9	86.0	40.2	39.5	0.31	0.32	2.64	2.51	0.42	0.46	0.07	0.08
5S		95.7		49.3		0.30		2.57		0.88		0.13
4S	103	90.9	50.4	50.5	0.28	0.28	2.69	2.55	1.26	1.31	0.19	0.18
3S		85.4		49.8		0.26		2.53		1.81		0.23
2S	90.6	96.9	52.6	51.6	0.28	0.27	2.74	2.55	1.60	1.60	0.23	0.19
1S		109		53.2		0.28		2.55		1.38		0.16
1E	126	117	55.8	55.1	0.30	0.29	2.54	2.55	1.03	1.10	0.13	0.13
2E		40.9		33.2		0.016		0.08		1.85		0.28
3E	11.6	8.2	11.6	11.6	0.0001	0.0016	0.002	0.004	2.36	2.65	0.50	0.49
4E		0.50		2.3		2×10^{-5}		0.0005		4.40		0.72
5E	0.27	0.09	0.27	0.15	<0.0001	3×10^{-6}	0.0005	7×10^{-6}	1.85	2.71	0.47	0.60

1.5 OFF-GAS CLEANUP (WORK UNIT 1103) – A. D. Ryon

Laboratory development under this work unit was directed mainly at support for the KALC process: solubilities in the CO_2-Kr and CO_2-Xe systems, removal of H_2O and I_2 from liquid CO_2, and interactions in the CO_2-H_2O-I_2 system. Other work included a test of the Iodox process and paper studies of ^{220}Rn removal.

Engineering development was involved only with the KALC process, and included mathematical modeling and analysis and experimental work in two facilities: the Experimental Engineering Facility, and the ORGDP Pilot Plant.

1.5.1 Laboratory Development

1.5.1.1 The Systems Kr-CO_2 and Xe-CO_2 -- R. D. Ackley and J. H. Shaffer

The Krypton Absorption in Liquid CO_2 (KALC) process is being developed for removing ^{85}Kr from the burner off-gas generated in the head-end reprocessing of HTGR fuel. To provide data for process design calculations, the distribution of krypton and of xenon between gaseous and liquid CO_2 has been investigated in the laboratory as reported previously.[12,13] The results were expressed in terms of a distribution ratio, Y_{KR}/X_{Kr} or Y_{Xe}/X_{Xe}, which is the ratio of the mole fraction of krypton or xenon in the gaseous phase to that in the liquid phase.

Experimentally, these distribution ratios were obtained by *in situ* gamma counting of ^{85}Kr or ^{133}Xe in the saturated vapor and in the liquid phase, in a vertical cylinder that contained CO_2 and either ^{85}Kr-labeled krypton or ^{133}Xe-labeled xenon at low concentrations. For each determination, the cylinder was maintained at constant temperature, and the liquid level was maintained near the midpoint of the cylinder.

During the latter stages of this experimental work, some concern developed over the possibility that these separation factors as determined might be biased high because of one or both of the following postulated situations: (1) a significantly thick condensed film of CO_2 on the wall of the cylinder above the liquid level and (2) an appreciable

amount of mist in the vapor. In view of this concern, an additional group of Xe-CO_2 distribution ratio measurements was performed in which a portion of the vapor phase maintained at a temperature some 10°C higher than that of the liquid phase was gamma counted. Any film or mist that might have been present previously should have been virtually eliminated by this modification in technique. Xenon, being more soluble than krypton, provides the more sensitive test.

The results obtained are presented in Table 1.17, which also includes separation factor values taken from a smoothed curve through the earlier Xe-CO_2 results. As may be noted, the two sets of results are in good agreement, thus indicating rather definitely that the previously reported Xe-CO_2 and Kr-CO_2 separation factor data were not significantly affected by film and/or mist effects.

Table 1.17. Distribution Ratios for the Xe-CO_2 System

Temperature, °C		Approach to Target Temperature	Separation Factor (Y_{Xe}/X_{Xe})	
Liquid[a]	Vapor[b]		Later Results	Earlier Results
−20.6	−12.5	From below	3.30	3.35
−20.7	−12.9		3.35	3.36
−20.5	−12.6		3.27	3.34
−21.0	−8.9		3.19	3.38
−30.5	−21.1		4.02	4.08
−39.7	−28.1		5.08	5.05
−20.6	−12.9	From above	3.39	3.35
−20.5	−11.3		3.33	3.34

[a]The temperature of principal interest with respect to the corresponding separation factor value.

[b]For the zone used in gamma counting. The vapor adjoining the liquid was at the liquid temperature.

1.5.1.2 Sorption of Tritiated Water and Elemental Iodine from Flowing Liquid CO_2 — R. D. Ackley, J. H. Shaffer, and D. C. Watkin

The burner off-gas generated in the head-end reprocessing of HTGR fuel will contain CO_2 as the major component and Kr, Xe, Rn, ^3H (as H_2O), and I_2 as low-concentration contaminants. As presently planned, the Rn, ^3H, and I_2 are to be removed from the off-gas (while in the gaseous state) by solid sorbents. Then, further downstream and following compression and liquefaction of the CO_2, the Kr (and possibly the Xe) are to be removed by using the KALC process. However, should it prove feasible to trap H_2O and/or I_2 from liquid CO_2, the additional removal of one or both of these contaminants from the liquid would provide protection of the KALC equipment against freeze-up or corrosion and would also provide supplemental capability for off-gas decontamination. Accordingly, an investigation to determine the feasibility of removing H_2O and I_2 from flowing liquid CO_2 has begun.

A laboratory system for this investigation has been designed, and the various components and special equipment that will be needed for assembly of the system have been ordered. Liquid CO_2 containing either ^3H-labeled H_2O or ^{131}I-labeled I_2 will be passed through beds of the sorbent(s) under test in series. Further downstream, the CO_2 will be vaporized, depressurized, and then passed through backup sorbent beds capable of quantitative removal of any ^3H or ^{131}I penetrating the test beds. Subsequently, the exposed sorbent beds will be analyzed by well established techniques.

The planned experimental work may be divided into four phases in chronological order: (1) survey testing of possible sorbents for H_2O removal, (2) the same for I_2, (3) detailed investigation of H_2O removal by sorbents found most effective (if degree of effectiveness warrants doing so), and (4) the same for I_2. Thus, the feasibility of this approach to trapping H_2O and/or I_2 from burner off-gas will first be ascertained. Then, if indications are favorable, the data needed for optimization of sorbent bed design and operation will subsequently be acquired.

1.5.1.3 Removal of ^{220}Rn from HTGR Fuel Reprocessing and Refabrication Off-Gas Streams by Adsorption — R. D. Ackley and W. L. Carter

Off-gas streams from ^{233}U reprocessing and refabrication operations will be contaminated with ^{220}Rn, and, as a consequence, some effective means for its removal will be required. In view of its short half-life and relatively favorable volatility, a method based on adsorptive holdup and decay should be feasible for coping with this decontamination problem.

As a means of obtaining further information regarding radon adsorption behavior, a literature search was made, and subsequently a report presenting available theory and data considered relevant to the removal of ^{220}Rn from off-gas streams by adsorption was issued.[14] An experimental program outline was also prepared,[15] but never carried out at ORNL because ACC assumed this responsibility. The proposed experimental arrangement is shown in Fig. 1.17.

The treatment of dynamic adsorption theory that was included for possible use in data analysis and adsorber design is based on the assumption of a linear adsorption isotherm. This treatment yields an equation relating decontamination factor with a holdup coefficient, the mass of sorbent, the volumetric flow rate of the carrier gas, the number of theoretical plates, and the decay constant. The holdup coefficient is, in turn, related to the adsorption coefficient and the sorbent temperature.

The data that were considered include equilibrium adsorption coefficients for radon on activated carbon (charcoal) and silica gel in the presence of air and other gases, and for radon on molecular sieve Type 5A in the presence of air. Also included were a few dynamic adsorption data (adsorption coefficients and values for the number of theoretical plates per foot) for radon on charcoal, with air as the carrier gas. These various data, which were obtained mainly at or near 25°C, are actually for ^{222}Rn; however, they should also be applicable to ^{220}Rn, provided the conditions are the same. Based on the available information, the radon adsorption coefficients decrease in the expected order: charcoal, moelcular sieve Type 5A, and silica gel. Thus, charcoal should be the most effective of these sorbents for ^{220}Rn removal; however, its use for

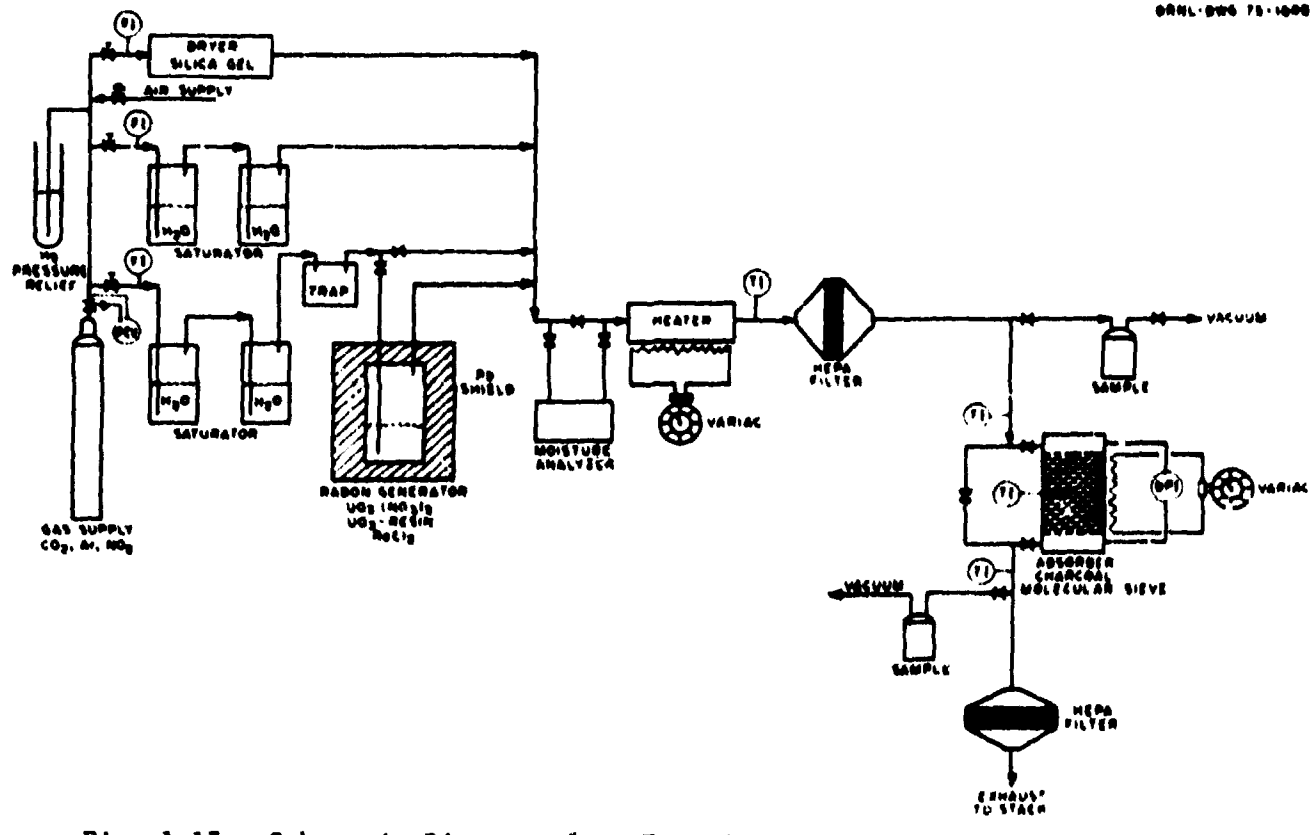

Fig. 1.17. Schematic Diagram of an Experiment to Demonstrate Removal of Radon from Carrier Gases.

this application cannot be recommended until the associated fire and explosion hazards, particularly those with regard to interaction with ozone, are resolved.

Sorbent poisoning and particle penetration due to alpha recoil were briefly treated. Adsorber design was discussed. Existing information appears adequate for sizing, albeit crudely, the sorbent bed for a ^{220}Rn-charcoal-air [1-atm (0.1 MPa), <10% relative humidity] system, and a suggested approach for doing this was outlined.

1.5.1.4 Iodine Removal via Iodox Process — B. A. Hannaford

The Iodox process[16] for iodine decontamination from air by nitric acid scrubbing is being developed for LMFBR application. For HTGR reprocessing, the iodine will be in a predominantly CO_2 atmosphere, and a series of tests was conducted to test the Iodox process in such an atmosphere.

Tests were run with a CO_2-CH_3I mixture and with a CO_2-CO-I_2 mixture to simulate HTGR off-gas. In both tests, some air was also added to simulate to O_2 and N_2 contents of HTGR off-gas. A control test was also run, using air-CH_3I. The results, summarized in Table 1.18, show that

Table 1.18. Iodine Removal from Simulated HTGR Off-Gas[a]

Stage of Apparatus	Decontamination Factor		
	CH_3I in Air (control)	CH_3I in CO_2-Air (7% air, 93% CO_2)	I_2 in CO_2-Air-CO (7% air, 1% CO, 92% CO_2)
Plate 1	6.3	5.9	6.4
2	4.0	3.6	5.5
3	2.7	3.0	4.4
4	3.0	2.8	4.9
5	2.9	3.1	4.0
6	2.4	2.5	1.6[b]
7	3.1	3.3	6.5[b]
Average[c]	3.3	3.4	4.4
Whole column	4700	5000	33,000
Condenser	13	10	3
Overall	6×10^4	5×10^4	1×10^5

[a]Gas flow rate, 28 std liter/min; scrub solution, 20 *M* HNO_3.

[b]Reflecting poor ^{131}I counting statistics for plate 7.

[c]Geometric mean for all seven plates.

the Iodox process will work in a predominantly CO_2 atmosphere containing some CO and O_2, typical of HTGR off-gas.

1.5.1.5 Studies of the CO_2-I_2-H_2O System – J. T. Bell and L. M. Toth

Spectrophotometric studies of this system[17,18] were carried out under funding by the Division of Physical Research and are included here because of the applicability to ongoing HTGR work. These studies have indicated that corrosion attack by iodine on stainless steel is greatly enhanced when moisture is present.[18] Distribution coefficients for I_2 were determined in the absence of moisture (Table 1.19).

Table 1.19. Distribution Coefficients of I_2 Between CO_2 Liquid and Vapor

Temperature (°C)	$\mathcal{D}_I$ (±6%)[a]
29	2.2
25	5.2
19	10.0
15	14.5
10	27.5
5	54.0
0	80.0
−10	135
−20	260
−26	320

[a]Defined as: $\mathcal{D}_I = \left(\frac{\text{Specific Absorbance}_\ell}{\text{Specific Absorbance}_v}\right)\left(\frac{\rho_v}{\rho_\ell}\right)$

$$= \frac{\text{mole fraction in liquid}}{\text{mole fraction in vapor}}$$

where

$$\text{specific absorbance} = \frac{I_2 \text{ absorbance at 520 nm}}{\text{path length}}$$

and

$$\rho = \text{density } CO_2 \text{ .}$$

1.5.2 Engineering Development — H.W.R. Beaujean,* H. D. Cochran, Jr., V. L. Fowler, T. M. Gilliam, R. W. Glass, D. J. Inman, D. M. Levins,† J. C. Mullins,‡ A. D. Ryon, F. H. Wilson,§ and W. M. Woods

Reprocessing of HTGR fuel involves burning of the graphite-matrix elements to release the fuel for recovery. The resulting off-gas is primarily CO_2, with residual amounts of N_2, O_2, and CO, together with fission products. Trace quantities of ^{85}Kr must be recovered in a concentrated form from the gas stream, but processes commonly employed for rare gas removal and concentration are not suitable for use with off-gas from graphite burning. The KALC process employs liquid CO_2 as a volatile solvent for the krypton and is, therefore, uniquely suited to the task.

Engineering development of the KALC process[19] is currently under way using facilities at both the Oak Ridge National Laboratory (ORNL) and the Oak Ridge Gaseous Diffusion Plant (ORGDP). The ORNL system[20] is designed for close study of the individual separation operations involved in the KALC process, while the ORGDP system provides a complete pilot facility for demonstrating combined operations on a somewhat larger scale. Packed column performance and process control procedures have been of prime importance in the initial studies.

Computer programs have been prepared to analyze and model operational performance of the KALC studies, and special sampling and in-line monitoring systems have been developed for use in the experimental facilities.

1.5.2.1 Process Analysis

The monitoring, sampling, and analysis of various process streams[21] is extremely important in the quantification of KALC experimental operations. In the ORNL system ^{85}Kr concentrations in the most important gas streams are monitored continuously with beta-sensitive radiation

---

*Guest scientist from West Germany.

†Guest scientist from Australia.

‡Research participant from Clemson University.

§Student from Georgia Institute of Technology.

detectors using a CaF_2 (Eu) scintillation disc. These detectors (see Fig. 1.18) were designed specifically for use with corrosive fluids at high pressures. In addition, representative samples of gas and liquid are withdrawn from 14 process streams via a semiautomatic sampling system; these samples are then analyzed for ^{85}Kr with a beta detector and for other constituents by mass spectrometry.

The in-line monitors have operated satisfactorily for several months without requiring maintenance. They perform four main functions:

1. They furnish a permanent record of the radioactivity in the main process streams throughout an experiment.

2. They monitor the approach of the system to steady-state conditions. Before samples are withdrawn for analysis, it is essential to establish that ^{85}Kr concentrations are, within acceptable limits, not varying with time. A particularly good indicator of overall plant performance is the ^{85}Kr off-gas concentration, which is very sensitive to changes in the liquid-to-vapor ratio in the absorber column or to periodic fluctuations due to cycling of the refrigeration systems.

3. They provide a first estimate of the decontamination and concentration factors at any given time.

4. They enable transient effects resulting from changes in operating conditions to be investigated.

Another important analysis aspect in the development of the KALC process and one to which considerable attention has been given is the computer modeling of operational and equilibrium processes of concern. In 1973, Whatley[22] correlated data available into a model of the KALC system. This model described the multicomponent system adequately to provide a basis to assess the feasibility of the process. More recently, an empirical equilibrium model for the CO_2-O_2-Kr-Xe system[23] has been developed to provide rapid but accurate information for data analysis and experimental planning. Figure 1.19 presents some of the more important results of this empirical model. At the present time an advanced equilibrium stage model[24] is in use for multicomponent, multicolumn calculations. This program represents thermodynamic properties of the CO_2-O_2-N_2-CO-Kr-Xe system accurately over the entire temperature,

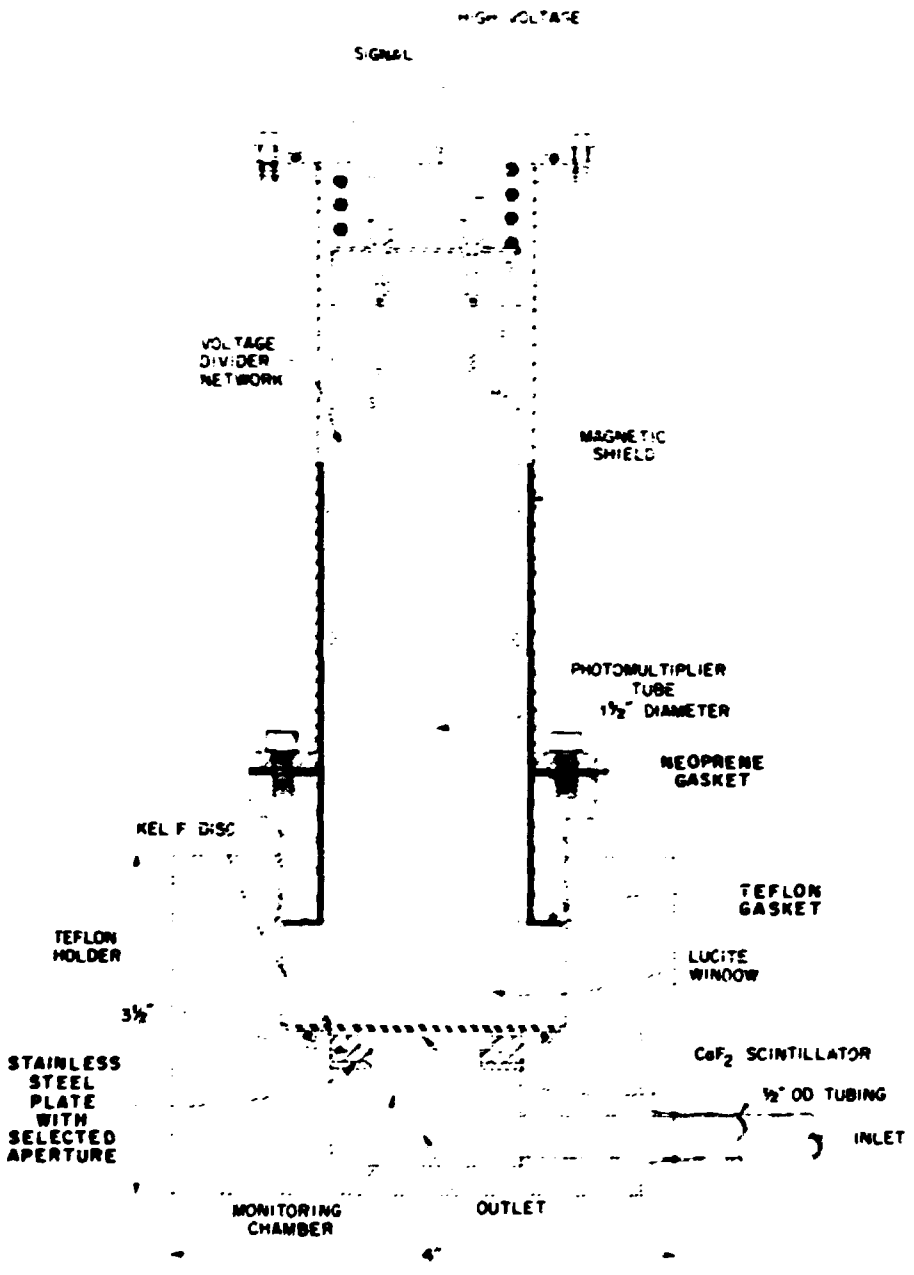

Fig. 1.18. High-Pressure Beta Scintillation Detector with Flow Cell. Dimensions shown are in inches; to convert to millimeters multiply by 25.4.

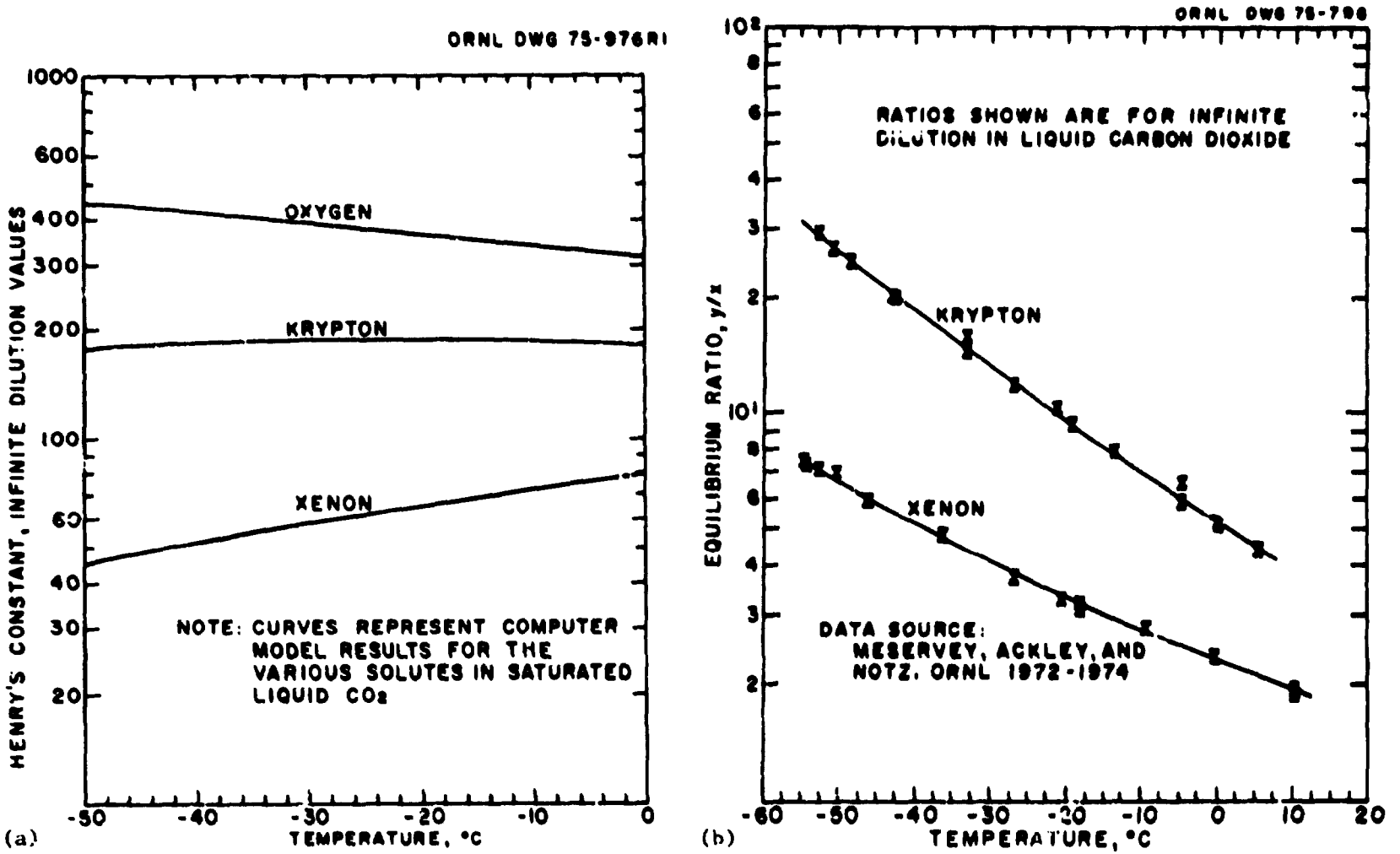

Fig. 1.19. Results from Empirical Model of CO_2-O_2-Kr-Xe System. (a) Henry's law constants. (b) Equilibrium ratios.

pressure, and concentration range of interest. Matrix algebra techniques are used to solve selected equilibrium stage configurations.

1.5.2.2 Experimental Engineering Facility

The ORNL experimental KALC system is described completely elsewhere,[20] but a simple equipment flowsheet is presented as Fig. 1.20. The system consists of two packed columns for gas-liquid contacting and associated support items, including gas compressors, solvent pumps, condensers, heaters, and complete sampling and monitoring capabilities. Process cooling is achieved by means of two conventional evaporative refrigeration units.

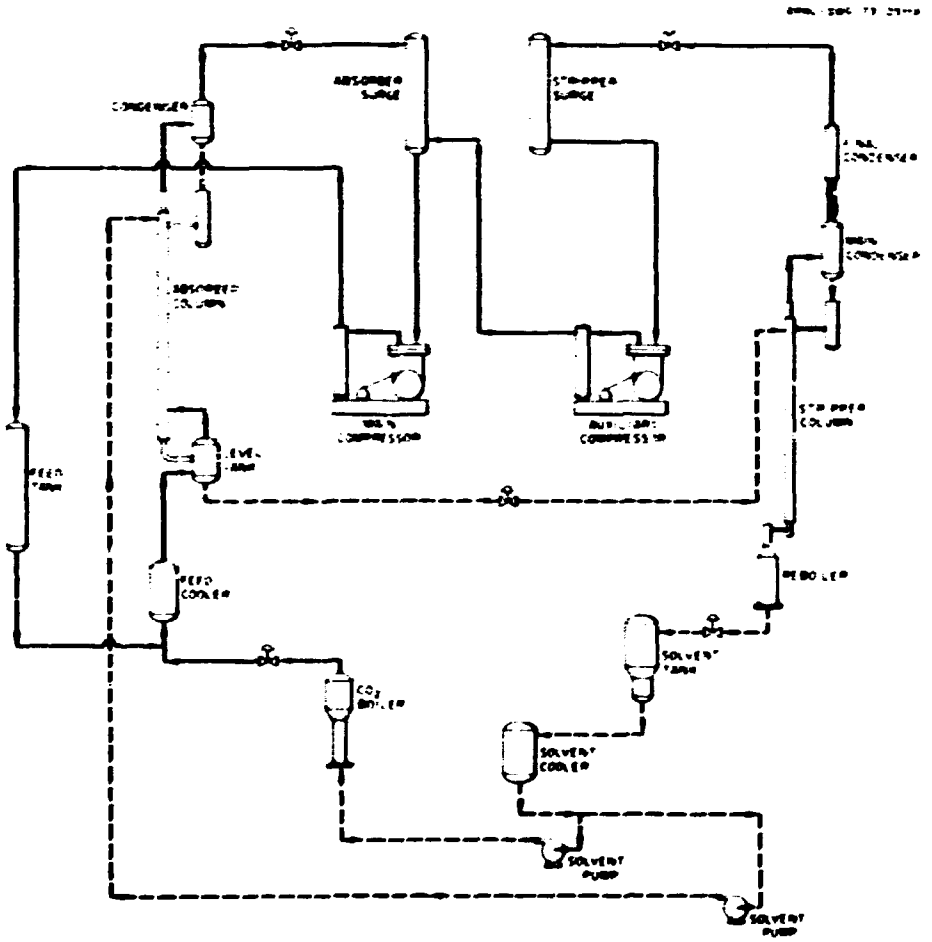

Fig. 1.20. Equipment Flowsheet for the ORNL Experimental KALC System.

Preliminary operation of the system began in March 1974, and since that time two experimental KALC campaigns have been completed. The first campaign was preliminary and was completed in October 1974. A primary goal for that campaign in addition to shakedown was to obtain column packing fluid dynamics. The flooding curve resulting from these and subsequent studies is presented as Fig. 1.21. The packing material used in these experiments is of the woven wire mesh cannister type.*

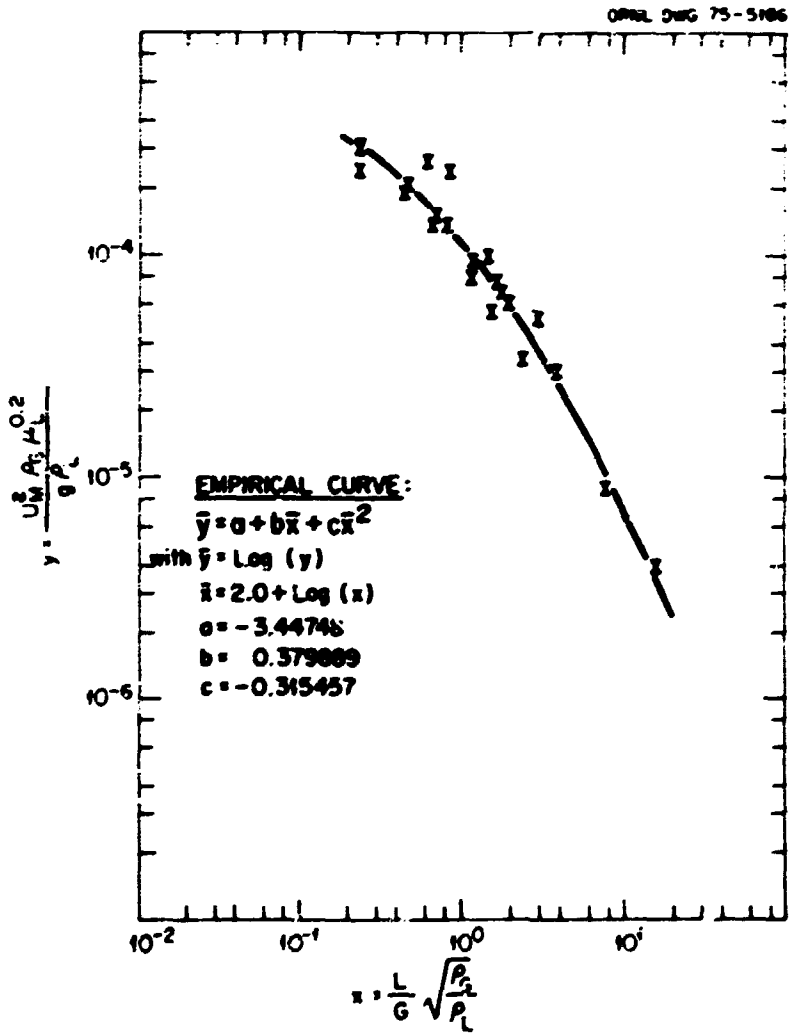

Fig. 1.21. Generalized Flooding Curve for the Experimental KALC Columns.

*Goodloe packing; Packed Column Company; a division of Metex Corp., Edison, New Jersey.

The second KALC campaign[25] in the ORNL system primarily concerned the mass transfer (absorption) of krypton into the liquid CO_2 phase. Some 30 experiments were conducted at 1.72 to 2.83 MPa gage (250–410 psig) and −28° to −11°C. For column krypton decontamination factors of 100 to 10,000 a theoretical transfer unit height of about 0.12 m (0.4 ft) was observed [see Fig. 1.22(a)]. Absorber column krypton decontamination factor as a function of the combined ratio of absorber liquid-to-vapor rates (L/V) and process krypton separation factor (K) is shown in Fig. 1.22(b).

1.5.2.3 Experiments in the ORGDP Pilot Plant

The KALC system was tested in the ORGDP Pilot Plant[26] in May and June 1974 and in a four-month campaign started in May 1975. The first campaign[27] served mainly as a shakedown of the equipment and the determination of flooding rate of a packed column. The primary objective of the second campaign was to demonstrate simultaneous decontamination of a gas stream consisting of CO_2–O_2 with respect to ^{85}Kr and concentration of the ^{85}Kr in the waste stream.

The results of the first campaign showed that generally satisfactory performance of the equipment was attained at the end of the campaign except for difficulty with the gas compressor and the refrigeration units. The shakedown tests also showed that additional instrumentation would be required to improve flow control and flexibility of operation. Equipment for recycle of superheated refrigerant would provide better control of heat exchangers and condensers. Flooding test data for the fractionator agreed very well with data obtained on the same diameter column in the ORNL facility (see Sect. 1.5.2.2), but the capacity was only about 50% of that predicted by the packing manufacturer.

The results of the second campaign through June 1975 show that operation is significantly improved with new instrumentation. However, failure of refrigeration units has caused interrupted operation. The system control modes were adjusted to reduce flow oscillations, and runs were made with tracer ^{85}Kr. Preliminary results show that decontamination factors greater than 200 were obtained in the absorber. Data obtained during the four-month campaign will be reported later.

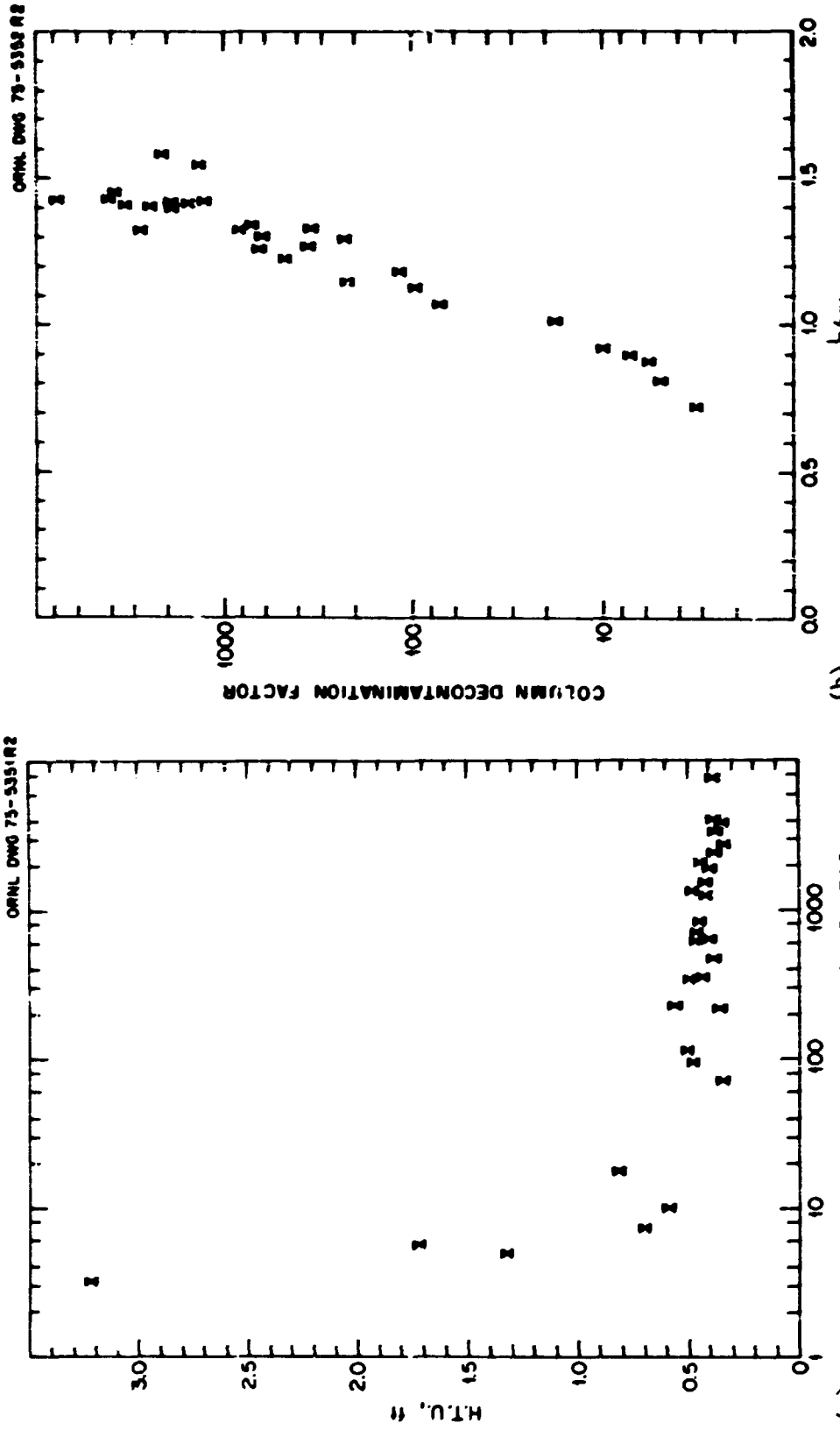

Fig. 1.22. Relationship of Column Decontamination Factor to (a) Height of a Transfer Unit (1 ft = 0.305 m) and (b) Column Absorption Factor.

1.6 PRODUCT PREPARATION (WORK UNIT 1104)

This work unit deals with the conversion of recovered uranyl nitrate to a form suitable for shipping. Although no development activity was scheduled, calculations and paper studies related to radioactivity control (by sparging to remove ^{220}Rn and by ion exchange to remove ^{232}U decay products) were carried out.

1.6.1 Radioactivity Control — W. L. Carter

Handling $UO_2(NO_3)_2$ product during shipping and resin loading operations can be troublesome because of radiation from ^{232}U decay products. A typical HTGR fuel after six years irradiation may contain about 350 ppm ^{232}U (total U basis), and, even though solvent extraction gives rather high decontamination factors for ^{232}U decay products, the activity soon rebuilds to levels that require remote handling of the solutions. Studies were made to assess the benefits of treating product solutions by sparging to remove ^{220}Rn or ion exchange to remove decay products, in particular ^{228}Th. Both these treatments reduce the activity of the ^{232}U decay chain, as the curves of Figs. 1.23 and 1.24 show. (The ordinates of these figures are normalized to a metric ton of heavy metal charged to the reactor. The activity is for the ^{232}U decay products that have significant gamma emissions.) In the case of sparging (Fig. 1.23), activity decrease, as shown by the bottom envelope curve, is controlled by the 10.58-hr half-life of ^{212}Pb, but the buildup of activity to the value that would have obtained without sparging (curve A) is quite rapid. This occurs because the ^{220}Rn parents, ^{224}Ra and ^{228}Th, continue to increase in the solution during sparging and very quickly replenish the short-lived ^{220}Rn when the inert-gas flow is stopped. The dwell-time of a sparged $^{233}UO_2(NO_3)_2$ solution at its lowest activity is only a few hours, making sparging a somewhat impractical way of decontamination.

Figure 1.24 shows that ion exchange, which removes ^{228}Th, is a considerably more effective treatment. A demonstrated treatment is shown by curve A, which depicts a period of minimum activity at two to three days after ion exchange. During this period the product could be handled with minimal shielding. Curve B is included to show the ideal

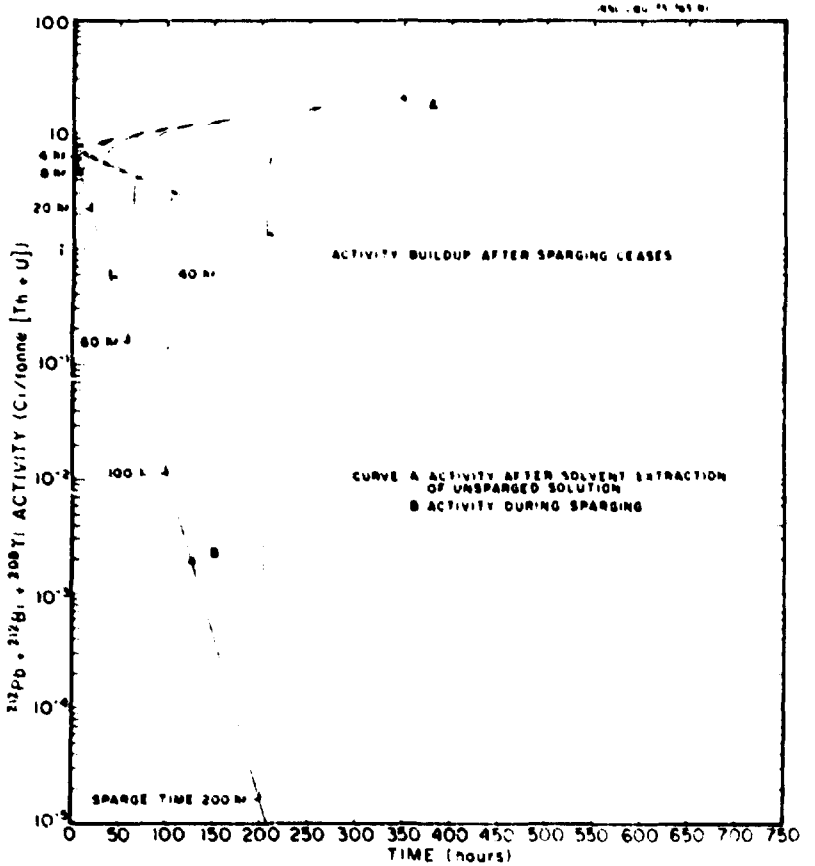

Fig. 1.23. Effect of Sparging $UO_2(NO_3)_2$ Solution to Reduce Activity of the ^{232}U Decay Chain.

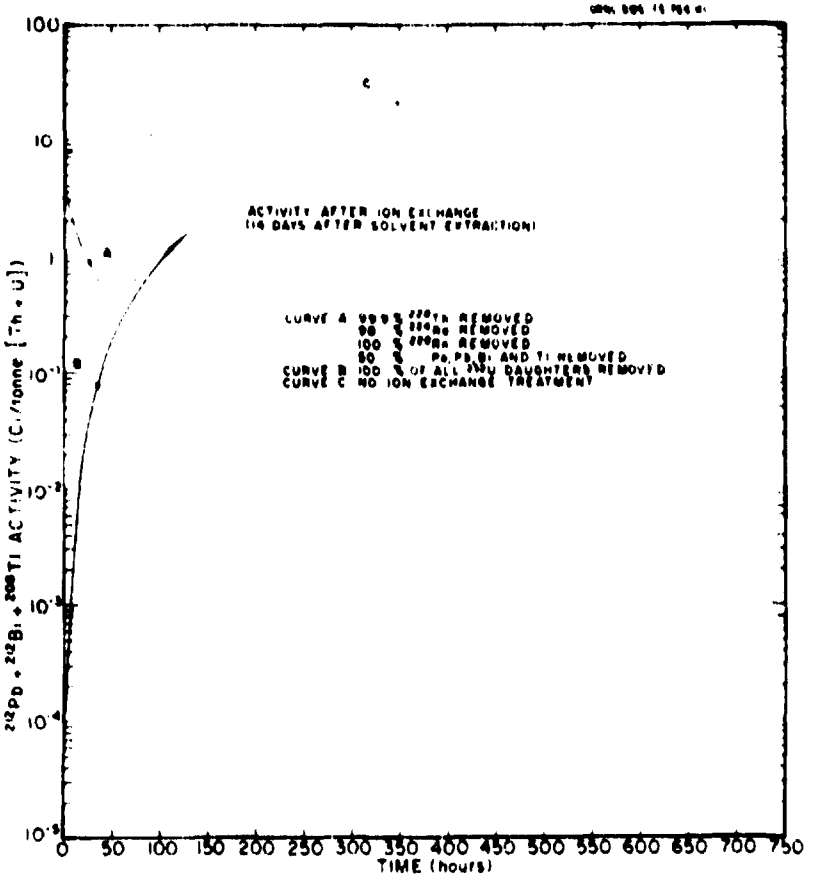

Fig. 1.24. Reduction in Activity of ^{232}U Decay Products by Ion Exchange Cleanup of $UO_2(NO_3)_2$ Solution.

case where 100% decontamination is achieved, and curve C shows the normal activity-versus-time relationship of $^{233}UO_2(NO_3)_2$ solution that has not been treated by ion exchange.

The study was extended to determine the benefit of an ion exchange treatment for lowering radiolysis due to ^{232}U in $^{233}UO_2(NO_3)_2$ solutions during shipment. Only a nominal benefit of about 7% is achieved (Fig. 1.25). Solvent extraction rather completely removed ^{232}U decay products, so that the dose received by the solution is initially about 94% from ^{232}U, hence an ion exchange treatment to remove the few remaining decay products causes little reduction in the dose. These calculations did not include ^{233}U; activity from the much larger amount of ^{233}U could make this isotope a more significant contributor to the overall dose.

These studies point out the importance of close-coupling an ion exchange cleanup step with fuel refabrication. Uranyl nitrate solution can be loaded on resin during the first four to five days after ion exchange to take advantage of the 10- to 20-fold lowering of gamma activity and a corresponding reduction in ^{220}Rn release during carbonization and conversion.

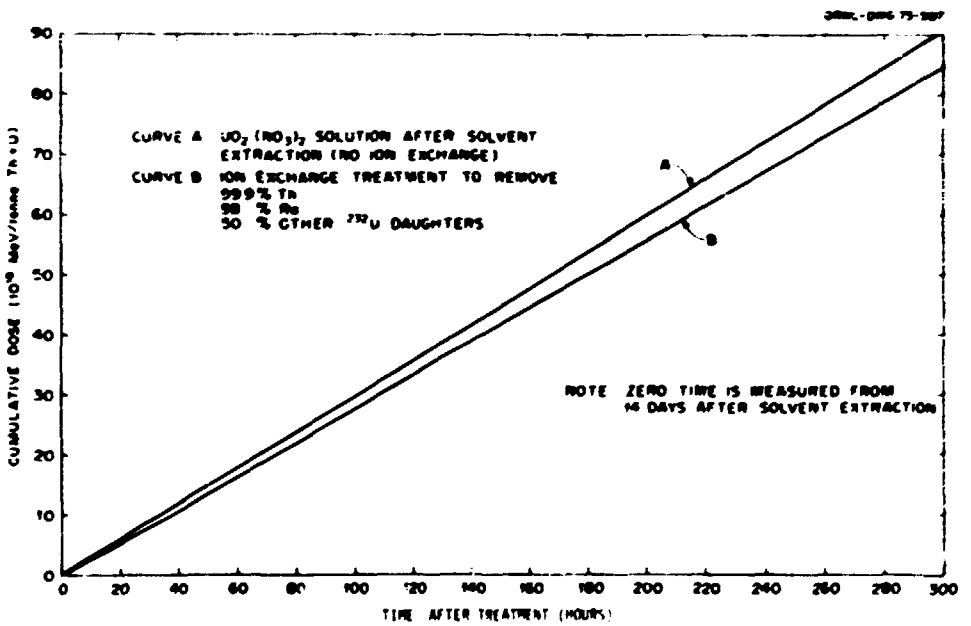

Fig. 1.25. Total Dose Received by Uranyl Nitrate Solution of HTGR Fuel from the ^{232}U Decay Chain.

1.7 WASTE PROCESSING AND ISOLATION (WORK UNIT 1105) — K. H. Lin

Waste streams of various forms are produced at different process steps in fuel reprocessing. The major sources of these wastes may be grouped into four areas — head-end processing, solvent extraction, off-gas cleanup, and miscellaneous sources. The overall objectives of the studies pertaining to waste processing and isolation are (1) to define radioactive waste streams from an HTGR fuel reprocessing plant, (2) to identify requirements for isolation and disposal of individual waste streams, (3) to evaluate various potential techniques for processing and isolation, and (4) to carry out development work on processing techniques for selected waste streams to acquire design data for a waste processing facility.

1.7.1 Identification and Characterization of Waste Streams — K. H. Lin

Various key process steps in HTGR fuel reprocessing have been reviewed in detail to identify important waste streams that require further processing before disposal or long-term storage.[28] Essentially all the waste streams resulting from head-end processing are in solid forms, while those discharged from the solvent extraction system are practically all liquids. Solid, liquid, and gaseous wastes are produced in the off-gas cleanup operation.

Most of the waste streams are unique to HTGR fuel reprocessing, although those from the solvent extraction system and from the plant facilities are not very much different from wastes discharged from an LWR fuel reprocessing plant. The liquid high-level waste, however, is somewhat different from the corresponding waste in LWR fuel reprocessing in that it contains fluorides that were introduced to facilitate dissolution of thoria. Thus, an additional processing step would be required to convert fluorides into a stable form before solidification of the wastes at high temperatures.

Solid waste streams from the head-end system are unique to HTGR fuel reprocessing. This is especially true of waste fissile particles (from 25W fuel elements), SiC hulls, and clinkers. Selection of specific

processing methods (e.g., whether to separate actinides from fission products or not) for these wastes will be governed largely by future Federal regulations and other noneconomic features. Also unique is the ^{14}C-containing waste stream, which may have to be converted into a form acceptable for isolation.

Table 1.20 summarizes pertinent characteristics of waste streams from an HTGR fuel reprocessing plant in regard to their sources, forms, and approximate quantities. Also shown are radionuclides that may be present in detectable quantities in individual waste streams and estimated amounts of radionuclides. The result of the study presented in the table is based on the following assumptions:

1. The fuel cycle has reached steady-state condition (≈8–10 years after the start).

2. Three different types of spent commercial fuel elements (25R, 23R, and 25W; see Table 1.21 for definition) are reprocessed.

3. The fuel contains Triso-coated fissile particles and Biso-coated fertile particles (Table 1.21).

Assumptions regarding the rate of fuel reprocessing and heavy metal (U and Th) contents of the initial and spent fuel elements are also summarized in Table 1.21.

1.7.2 Overall Process Evaluation – K. H. Lin

This phase of the HTGR waste studies is concerned with critical review and evaluation of available information related to processing and isolation of waste streams from the HTGR fuel reprocessing plant. Waste streams that require further processing before disposal or long-term storage, as identified in the study described in Sect. 1.7.1, are emphasized.

Evaluations are in progress of various alternatives for interim and final processing of different waste streams as shown in Fig. 1.26. Pertinent development work in progress and available technical data are being evaluated in the light of the requirements imposed by the current Federal regulations. We are also considering the proposed rule-making by ERDA and NRC, experiences of LWR fuel reprocessing plants, and other

Table 1.20. Sources and Estimated Flow Rates of Waste Streams from HTGR Fuel Reprocessing Plant [Basis: 20,000 Fuel Elements/Year; 58% 25R, 39% 23R, 3% 25W]

Stream	Source (Subsystem)	Waste Form	Estimated Quantities Per Year	
			Masses and Volumes	Probable Key Radionuclides
		Head-End Processing System		
H-1	Primary and secondary burners	Semi-volatile nuclides, particulates	110 kg, 10 MCi; particulates incl. in H-3	Fission products (e.g., Zr, Nb, Ru, Sb, Cs, Ce, etc.), actinides
H-2	Primary and secondary burners	Clinkers	0-6 MT[a]	Fission products, actinides
H-3	Crushers, hoppers, classifier	Particulates	12 MT	Fission products, actinides
H-4	Fissile particle canning station	Fissile particles (from 25W blocks)	4 MT	Actinides (U = 1.3 MT; 170 Ci); fission products (1 MT; 62 MCi)
H-5	Particle dissolver, centrifuge	SiC hulls, insol. residues (incl. noble metals)	20 MT	Actinides (5 kg, 4300 Ci); fission products (~1 MT; 70 MCi) (esp. noble metals)
		Solvent Extraction System		
S-1	Feed preparation	Stream stripper overhead	4200 m^3 (1,100,000 gal)[b]	I, Ru
S-6	Uranium salvage	Evaporator condensate	(solid content ≈0.5-1% wt)	I, Ru
S-7	First and second cycle extraction	Carbonate wash solution		Zr, Nb, Ru, Rh, I
S-2	Feed preparation	Insol. residue	1-3 MT	Zr, Nb
S-3	First and second cycle extraction	High-level liquid waste	760 m^3 (200,000 gal)[b]	Fission products (15 MT, 1400 MCi); actinides (2 MT, 95 MCi)
S-4	First and second cycle extraction	Thorium nitrate solution	190 m^3 (50,000 gal)[b]	Th (166 MT, 60 kCi) actinides; Zr, Nb, Ru, Rh (total F.P. ~2 MCi)
S-5	First and second cycle extraction	Kerosene scrub	21 m^3 (5500 gal)	Fission products, actinides
S-8	Solvent cleanup	Crud	~1 MT	Fission products (~2 kg, ~150 Ci), actinides (~170 kg, ~95 kCi)

Table 1.20. (Continued)

Stream	Source (Subsystem)	Waste Form	Estimated Quantities Per Year	
			Masses and Volumes	Probable Key Radionuclides
		Off-Gas Cleanup System		
O-1	NO_x decomposition, catalytic oxidation	Spent catalysts	4 m^3 (140 ft^3)	Fission products (esp., semi-volatile)
O-2	Iodine removal	Spent zeolite	Pb zeolite = 34 m^3 (1200 ft^3) Ag zeolite = 4.2 m^3 (150 ft^3)	Iodine isotopes (60 Ci, 35 kg)
O-3	Radon removal	Spent molecular sieve	12 m^3 (440 ft^3)	Rn decay products, traces of I and HTO
O-4	Tritium removal	Spent molecular sieve	4.2 m^3 (150 ft^3)	HTO
O-5	Tritium removal	Tritiated water	14 m^3 (3700 gal)	HTO (^3H = 277,000 Ci)
O-6	Krypton removal	Kr product stream	Kr: 460 kg	^{85}Kr (11 MCi)
O-7	Krypton removal	CO_2 gas	6680 MT	^{14}C (~1 kg $^{14}CO_2$), traces of ^{85}Kr
		Miscellaneous		
M-1	HTGR	Reflector blocks	160 m^3 (5600 ft^3) 350 MT	^{14}C, neutron-activation products
M-2	Facilities	Decontamination solution	4–8 × 10^3 m^3 (1–2 × 10^6 gal)	Variable
M-3	Facilities	Rags, spent filters, failed equipment and tools, etc.	2100 m^3 (74,000 ft^3)	Variable

[a] Assume ~5% of the fuel material formed clinkers. MT means metric ton.

[b] Unconcentrated solutions.

Table 1.21. Estimated Processing Rate and Characteristics of Individual Types of Fuel Elements[a]

Fuel Types[b]	Processing Rate (Fuel Elements Per Year)	Heavy Metal[c]	Average Contents of Heavy Metals (kg/Fuel Element)[d]			
			Initial Fuel		Spent Fuel	
			Fissile Particle	Fertile Particle	Fissile Particle	Fertile Particle
IM-25R	11,600	U	0.706	0	0.216	0.222
		Th	0	8.550	0	7.926
23R	7,800	U	0.742	0	0.226	0.222
		Th	0	8.830	0	7.926
25R-25W	600	U	3.250	0	2.24	0.19
		Th	0	7.000	0	5.60

[a]Based on a HTGR fuel reprocessing plant of 20,000 fuel elements per year.

[b]All fuel types contain Biso-coated (inner porous carbon and outer dense carbon) fertile particles and Triso-coated (porous carbon, dense carbon, SiC, and dense carbon) fissile particles. Fertile particles contain thorium, while fissile particles contain uranium of varying isotopic compositions depending upon the fuel type as follows:

IM: contains virgin uranium of ~93% ^{235}U, initially charged to HTGR
25R: contains recycle uranium of ~30% ^{235}U (refabricated from burned IM)
23R: contains recycle ^{233}U
25W: contains uranium of ~4–5% ^{235}U (burned 25R)

[c]Uranium is present as UC_2, and thorium as ThO_2.

[d]Adapted from General Atomic Co., *Conceptual Design Summary and Design Qualifications for HTGR Target Recycle Plant*, GA-A-13365, Vols. I and II (March 1975).

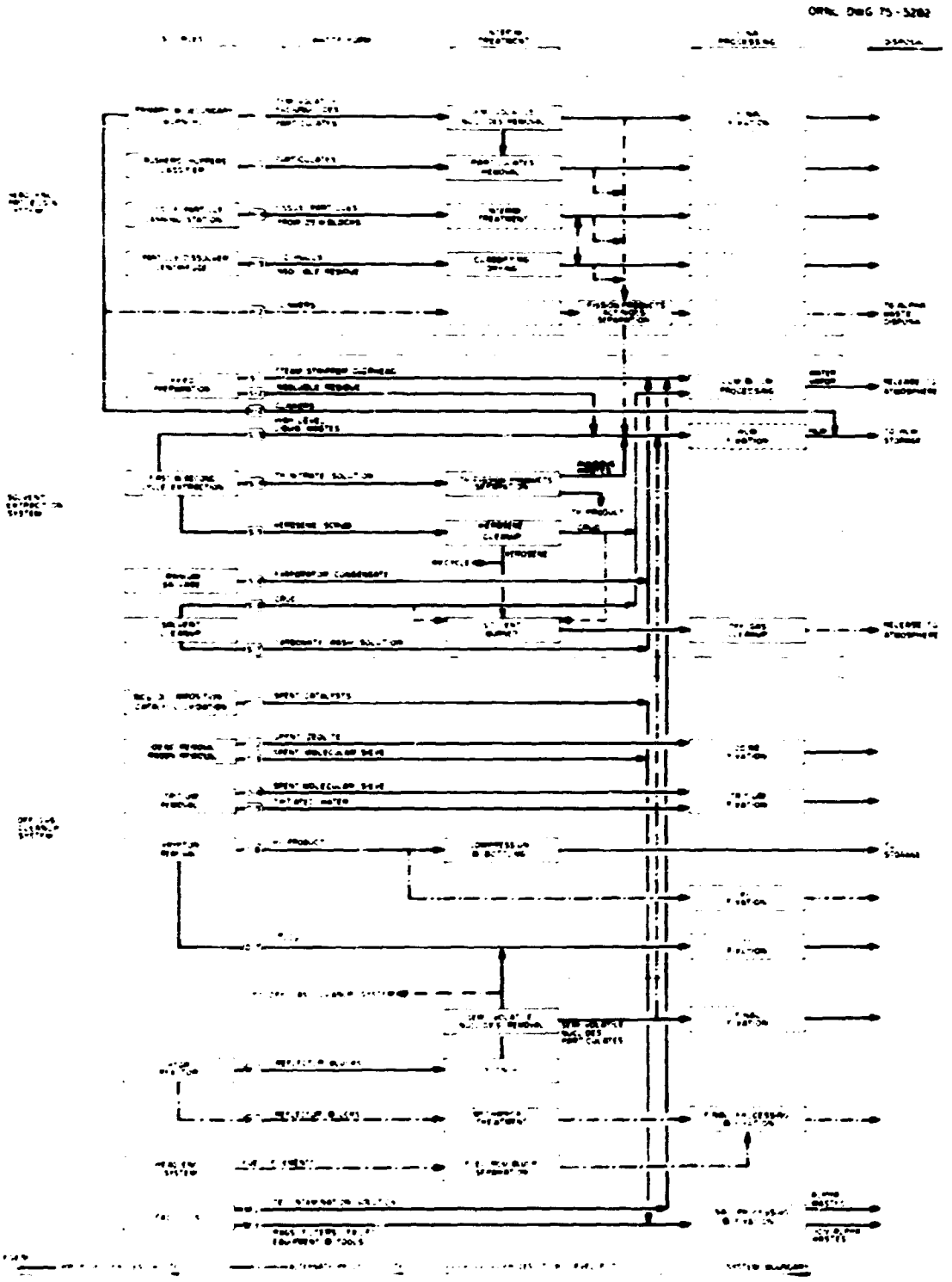

Fig. 1.26. Overall Schematic Flow Diagram for HTGR Fuel Reprocessing Wastes (Semi-Volatiles, Liquids, and Solids).

factors that might influence the requirements in the future. The estimated radiochemical compositions and flow rates of individual waste streams are used as part of the criteria in determining which of the available process alternatives should be employed.

Evaluation of waste processing alternatives has identified waste streams that require hot cell development programs to supply design data. The tentative scope of the recommended hot cell development work for these waste streams is outlined in Table 1.22. In addition to these waste streams, cold engineering development is required for $^{14}CO_2$ fixation, as described in Sect. 1.7.3.

1.7.3 Fixation and Disposal of $^{14}CO_2$ Waste Streams — A. G. Croff

A scoping study has been conducted to determine the best method for the fixation of ^{14}C-contaminated CO_2 as $CaCO_3$, and to evaluate the various options available for disposing of the $CaCO_3$ thus produced. The fixation and disposal options were evaluated on the basis of technical merit, economics, and regulatory acceptability.

The two CO_2 fixation processes considered were:

1. a direct process, wherein the CO_2 reacts directly with a slaked lime [$Ca(OH)_2$] slurry to form a $CaCO_3$ slurry; and
2. a double alkali process, wherein the CO_2 reacts with an NaOH solution to form Na_2CO_3; the Na_2CO_3 subsequently reacts with a slaked lime slurry to produce the $CaCO_3$ product and regenerate the NaOH solution.

The direct CO_2 fixation process appears to be superior to the double alkali process because of reduced complexity, reduced corrosiveness of the chemical reagents involved, and reduced cost. The two processes were judged to be equivalent with respect to the amount of solids handling required. The double alkali process has an advantage with respect to design data availability, since the $NaOH$-CO_2-H_2O system has been well characterized.

The $CaCO_3$ disposal options considered were as follows:

1. shallow land burial of
   (a) unpackaged, unconcreted $CaCO_3$,
   (b) packaged, unconcreted $CaCO_3$,

Table 1.22. HTGR Fuel Reprocessing Waste Streams that Require Hot-Cell Development Work

Waste Streams	Scope of Development Work	
	Characteristics	Process Alternatives[a]
Semi-volatile and entrained radionuclides	Criteria for replacement of cold traps and filters.	Mechanical volume reduction.[b]
	Types, chemical and physical forms, and relative amounts of radionuclides.	Separation of radionuclides from removal agents by chemical means.
	Loading on filters and cold traps at the time of replacement.	
SiC hulls	Types, chemical forms and concentrations of radionuclides, especially U concentration.	Fixation and disposal as HLW.
	Leachability of radionuclides.	Chemical separation of radionuclides, and recovery of uranium, if justified.
Retired fissile particles	Radiochemical composition of fuel kernels.	Fixation and disposal as HLW.
	Characteristics of SiC hulls as above.	Recovery of U and other useful actinides, and disposal of the residue as HLW.
Clinkers	Chemical and radiochemical composition.	Same as above.
High-level liquid wastes	Chemical and radiochemical composition, especially of fluorides.	Conversion of fluorides to nonvolatile compounds before high-temperature solidification process.
Krypton product	Chemical and radiochemical composition, especially ^{85}Kr, CO_2, and other impurities.	Storage in compressed gas cylinders; effect of radiolysis of CO_2, etc., by ^{85}Kr.
		Fixation in solids.
Reflector blocks	Types, forms, and concentrations of radionuclides	Fixation and disposal as HLW.
		Removal and fixation of radionuclides after burning.
Decontamination solution from head-end system	Chemical and radiochemical composition.	Concentrate and combine with liquid high-level wastes.[c]
		Recovery of U and other useful actinides, and disposal of the residue as HLW.[c]

[a] HLW = high-level waste.

[b] Processing of removal agents (e.g., cold surfaces and filters) contaminated with radionuclides.

[c] Requires a minimum modification of the existing techniques.

(c) unpackaged, concreted $CaCO_3$,

(d) packaged, concreted $CaCO_3$;

2. hydraulic fracturing (mixing a $CaCO_3$ slurry with cement and injecting it into deep geological strata);
3. deep sea disposal (concretion and dumping in the deep sea);
4. partial block burning;
5. emplacement in a geologic repository for material contaminated with alpha emitters.

Shallow land burial of the $CaCO_3$ appears to be the best disposal option available. The burial of unpackaged, unconcreted $CaCO_3$ [Option 1(a)] will probably not be acceptable. The future acceptability of burying packaged, unconcreted $CaCO_3$ [Option 1(b)] or unpackaged, concreted $CaCO_3$ [Option 1(c)] is not clear at the present time. The burial of packaged, concreted $CaCO_3$ [Option 1(d)] will probably be acceptable in the future. Thus, the potentially acceptable shallow land burial options, in decreasing order of economic preference, are:

Burial of packaged, unconcreted $CaCO_3$ ($18.47/kg heavy metal)

Burial of unpackaged, concreted $CaCO_3$ ($29.11/kg heavy metal)

Burial of packaged, concreted $CaCO_3$ ($55.54/kg heavy metal)

($43.33/kg heavy metal when concreted at burial site; $55.54 kg/heavy metal when concreted at reprocessing plant.)

The disposal of $CaCO_3$ by hydraulic fracturing does not appear to be attractive based on a combination of economic ($36.78/kg heavy metal), regulatory, and technical grounds. Dumping of the $CaCO_3$ in the deep sea does not appear to be attractive on both economic ($56.43/kg heavy metal) and regulatory acceptance grounds. Partial block burning is unattractive because the maximum volume reduction is only about 50% and the fission products sorbed on the unreprocessed blocks elevate the waste from low level to at least intermediate. The geologic repository burial of the $CaCO_3$ is economically unattractive ($281.39/kg heavy metal) and technically unjustifiable in view of the relatively low toxicity of ^{14}C.

The feasibility of placing the CO_2 fixation system before the krypton removal system to reduce or eliminate the gas volume that the krypton removal system must handle was also investigated. The process

complexity and increased cost resulting from this change indicate that putting the CO_2 fixation process after the krypton removal process would be more advantageous.

1.8 REFERENCES

1. F. J. Homan, "HTGR Fuel Qualification," *HTGR Base Program Progr. Rep. Jan. 1, 1974–June 30, 1975*, ORNL-5108, Chap. 6.
2. M. J. Bell, *ORIGEN – The ORNL Isotope Generation and Depletion Code*, ORNL-4628 (May 1973).
3. R. P. Morisette et al., *Recycle Test Element Program Design, Fabrication and Assembly*, GA-10109 (September 1971).
4. E. L. Long, Jr., R. B. Fitts, and F. J. Homan, *Fabrication of ORNL Fuel Irradiated in the Peach Bottom Reactor and Postirradiation Examination of Recycle Test Elements 7 and 4*, ORNL-TM-4477 (September 1974).
5. R. A. Olstad, A. R. Olsen, and R. B. Fitts, *An Irradiation Test of Candidate HTGR Recycle Fuels in the H-1 and H-2 Capsules*, ORNL-TM-4398 (July 1974).
6. R. S. Lowrie, C. L. Fitzgerald, and V.C.A. Vaughen, "Determination of the Radioactive Nuclides Present in the Off-Gas Streams Generated by the Head-End Steps in Reprocessing HTGR Type Fuels," pp. 528–39 in *Proceedings of the Twelfth Air Cleaning Conference Held in Oak Ridge, Tennessee, August 28–31, 1972*, CONF-720823, Vol. 2.
7. C. L. Fitzgerald, V.C.A. Vaughen, K. J. Notz, and R. S. Lowrie, *Head-End Reprocessing Studies with Irradiated HTGR-Type Fuels: III. Studies with RTE-7: Triso UC_2-Triso ThC_2*, ORNL-5090 (November 1975).
8. J. W. Snider, D. C. Watkin, and H. Barnert-Wiemer, *An Evaluation of HTGR Primary Burning*, ORNL-TM-4520 (November 1974).
9. P. A. Haas, *HTGR Fuel Reprocessing: A Whole-Block Burner with Recycle of Cooled Gas for Temperature Control*, ORNL-TM-4519 (August 1974).

10. R. M. Canon, "Adiabatic Combustion of Graphite," *Experimental Engineering Section Semiannu. Progr. Rep. (Excluding Reactor Programs) Sept. 1, 1974–Feb. 28, 1975*, ORNL-TM-4961, pp. 381-87.

11. S. B. Watson and R. H. Rainey, *Modifications of the SEPHIS Computer Code for Calculating the Purex Solvent Extraction System*, ORNL-TM-5123 (November 1975).

12. A. B. Meservey and K. J. Notz, "Krypton-CO_2 System," *Gas-Cooled Reactor Programs Annu. Progr. Rep. Dec. 31, 1972*, ORNL-4911, pp. 7–8.

13. R. D. Ackley, K. J. Notz, A. B. Meservey, J. T. Bell, and S. R. Buxton, "Laboratory Development," *Gas-Cooled Reactor Programs Annu. Progr. Rep. Dec. 31, 1973*, ORNL-4975, pp. 11–14.

14. R. D. Ackley, *Removal of Radon-220 from HTGR Fuel Reprocessing and Refabrication Off-Gas Streams by Adsorption (Based on a Literature Survey)*, ORNL-TM-4883 (April 1975).

15. W. L. Carter, internal memorandum.

16. W. S. Groenier and B. A. Hannaford, *An Engineering Evaluation of the Iodox Process: Part II: Removal of Iodine from Air Using a Nitric Acid Scrub in a Bubble Cap Column; Part III: Correlation of Mass Transfer Data; Part IV: Process Sensitivity of Impurities*, ORNL-TM-4701 (May 1975).

17. Work by J. T. Bell and L. M. Toth, reported in "Spectrophotometric Studies of I_2 and H_2O in Condensed Gases," *Chem. Tech. Div. Annu. Progr. Rep. Mar. 31, 1974*, ORNL-5966, pp. 49–51.

18. J. T. Bell, D. W. Fuller, S. R. Buxton, L. M. Toth, and H. A. Friedman, "Chemistry of Fission Products in Carbon Dioxide," *Chem. Div. Annu. Progr. Rep. Nov. 1, 1975*, ORNL-5111, p. 49.

19. R. W. Glass, H.W.R. Beaujean, H. D. Cochran, Jr., P. A. Haas, D. M. Levins, and W. M. Woods, "Development of the Krypton Absorption in Liquid Carbon Dioxide (KALC) Process for HTGR Off-Gas Reprocessing," pp. 232–45 in *Proceedings of the Thirteenth AEC Air Cleaning Conference, San Francisco, 12–15 August, 1974*, CONF-740807 (March 1975).

20. R. W. Glass, H. D. Cochran, Jr., D. M. Levins, J. W. Snider, D. C. Watkin, W. M. Woods, and M. E. Whatley, *System Features and Component Descriptions for the Unit Operations Off-Gas Decontamination Facility*, ORNL-TM-4596 (February 1975).

21. D. M. Levins, R. W. Glass, M. M. Chiles, and D. J. Inman, *Monitoring and Analysis of Process Streams in a Krypton-85 Off-Gas Decontamination System*, ORNL-TM-4923 (July 1975).

22. M. E. Whatley, *Calculations on the Performance of the KALC Process*, ORNL-4859 (April 1973).

23. R. W. Glass, T. M. Gilliam, and V. L. Fowler, *An Empirical Model for Calculating Vapor-Liquid Equilibrium and Associated Phase Enthalpy for the CO_2-O_2-Kr-Xe System for Application to the KALC Process*, ORNL-TM-4947 (January 1976).

24. J. C. Mullins and R. W. Glass, *An Equilibrium Stage Model of the KALC Process*, ORNL-TM-5099 (in preparation).

25. R. W. Glass, H.W.R. Beaujean, V. L. Fowler, T. M. Gilliam, D. J. Inman, and D. M. Levins, *Krypton Absorption in Liquid CO_2 (KALC): Campaign II in the Experimental Engineering Section Off-Gas Decontamination Facility*, ORNL-TM-5095 (February 1976).

26. M. J. Stephenson et al., *System Design Description of the ORGDP LMFBR-HTGR Fuel Reprocessing Off-Gas Decontamination Pilot Plant*, K-GD-873 (September 1973).

27. H. D. Cochran, Jr., and A. D. Ryon, internal memorandum.

28. K. H. Lin, *Characteristics of Radioactive Waste Streams Generated in HTGR Fuel Reprocessing*, ORNL-TM-5096 (January 1976).

2. REPROCESSING PROTOTYPE FACILITY (SUBTASK 120)

J. W. Snider

2.1 INTRODUCTION

A Reprocessing Prototype Facility to be fabricated by the Allied Chemical Company (ACC) at Idaho Falls, Idaho, was planned to demonstrate hot HTGR head-end reprocessing. Because of cost considerations and uncertainties in HTGR sales, this facility has been dropped from ERDA planning. However, during this report period ORNL was assigned the task of designing a liquid carrier for transport of the $^{233}UO_2(NO_3)_2$ product from this facility to ORNL and for preparation of the system design description (SDD), for the off-gas cleanup systems.

2.2 GENERAL PLANT REQUIREMENTS (WORK UNIT 1200)

Space and service requirements for the off-gas cleanup system (see Sect 2.5) for the HTGR Prototype Fuel Processing Facility was estimated for ACC. The amount of shielded space (concrete thickness to be determined) and the amount of contained space required for a 0.24 std m^3/sec (500 scfm) off-gas system are summarized on Table 2.1.

2.3 HEAD-END PROCESSING (WORK UNIT 1201)

The activity of this work unit consisted of participation in review meetings with ACC, General Atomic Company (GAC), and R. M. Parsons personnel. The major technical issue considered has been the interaction between the burners and the KALC process. This study resulted in the substitution of CO_2 for air in two applications: the mixture with oxygen and the purge of the crusher, hoppers, etc., which may release small quantities of krypton.

2.4 SOLVENT EXTRACTION PROCESSING (WORK UNIT 1202)

This work is reported under Sect. 1.4 (Work Unit 1102).

BLANK PAGE

Table 2.1. Estimated Space Requirements for the Off-Gas Cleanup System

Subsystem	Space Type Required	Width × Length × Height (m)	(ft)
NO_x decomposition	Shielded	1.52 × 1.52 × 2.4	5 × 5 × 8
Gas collection	Shielded	10.7 × 4.6 × 2.4	35 × 15 × 8
Off-gas oxidation Iodine removal and disposal Radon removal and disposal Tritium removal	Shielded	4.6 × 4.6 × 2.4	15 × 15 × 8
Tritium fixation and disposal	Contained	2.4 × 3.0 × 6.1	8 × 10 × 20
Gas compression	Shielded	9.1 × 4.6 × 2.4	30 × 15 × 8
Gas cooling Krypton absorption Krypton fractionation Krypton stripping	Contained	7.3 × 9.1 × 18.3	24 × 30 × 60
Krypton concentrating Krypton compressing and bottling	Shielded[a]	3.0 × 2.4 × 2.4	10 × 8 × 8
Liquid CO_2 storage and metering Liquid CO_2 evaporation and recycle	Contained	8.5 × 15.2 × 6.1	28 × 50 × 20
Refrigeration (two levels)	Contained	7.3 × 13.7 × 6.1	24 × 45 × 20
Chemical requirements	Contained	2.4 × 6.1 × 6.1	8 × 20 × 20

[a]Designed to earthquake Category II.

2.5 OFF-GAS CLEANUP (WORK UNIT 1203) — W. L. Carter, R. W. Glass, K. H. Lin, and J. W. Snider

The Off-Gas Cleanup System (OGCS) is being considered for the removal of the radioactive and volatile constituents from head-end operations for gaseous release to the environment. Specifically, separate processes are planned for the removal and separation of iodine, tritium, radon, and krypton. Solid absorbers (molecular sieves and zeolites) are being considered for the removal of iodine, tritium, and radon, and the KALC process is being considered for removal of the krypton.

The role of ORNL under a cooperative program with ACC was to provide technical assistance to ACC in the design of the OGCS for the HTGR Fuel Reprocessing Facility (HTGR-FRF) to be located in Idaho Falls. During the past year, the primary effort had been directed toward preparation of the system design description (SDD 1.3) for the OGCS, as depicted

in Fig. 2.1. The various gas streams that make up the wet head-end and dry head-end streams are shown in Fig. 2.2.

The SDD has been written to assure that the OGCS satisfies the following function and design requirements:

1. to demonstrate the capability of removing radioactive iodine, tritium, krypton, and radon from the head-end off-gas streams to predetermined levels (minimum decontamination factors: 10^3 for iodine and 10^2 for tritium, krypton, and radon);
2. to process the off-gas streams at rates ranging from 0 to 0.24 std m^3/sec (500 scfm), corresponding to a maximum of 36 fuel elements per day through the head-end system;
3. to isolate radioactive wastes from various removal systems, either as concentrated contaminants or as integral parts of spent removal agents for loading into individual approved containers for final disposal.

As shown in Fig. 2.1, the OGCS shall be designed to accomplish the following major functions:

1. Catalytically decompose NO_x in the off-gas from the particle dissolver into nitrogen and water vapor.

2. Provide a constant-subatmospheric-pressure vessel to accumulate and mix off-gas streams from various sources in the head-end system and a prime mover to transport the off-gas to other OGCS process steps.

3. Catalytically oxidize CO to CO_2 and tritium to tritiated water vapor, and if required convert excess O_2 to CO_2.

4. Remove iodine by adsorption on exchangeable-metal zeolites.

5. Remove radon by delay techniques using molecular seives.

6. Remove tritium by adsorption on molecular sieves.

7. Remove krypton by use of liquid CO_2 as solvent (KALC process) in three steps — namely, adsorption, fractionation, and stripping — followed by concentration.

8. Separate and isolate radioactive wastes from individual removal subsystems, and prepare them for storage and/or disposal. The wastes will be either concentrated radioactive contaminants (e.g., tritiated water in concrete, and krypton) or spent adsorbents containing contaminants (e.g., zeolites with iodine, and molecular sieves either with radon

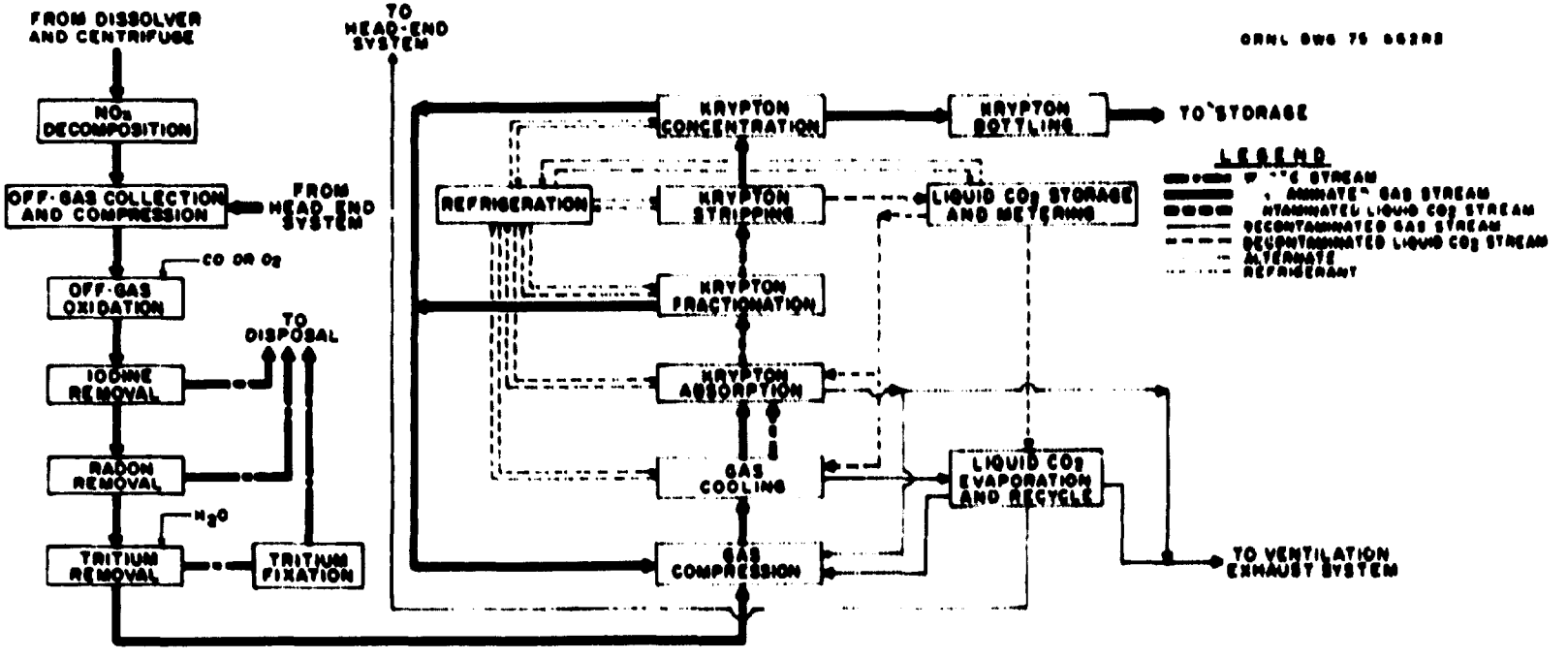

Fig. 2.1. Schematic Flow Diagram of the Off-Gas Cleanup System.

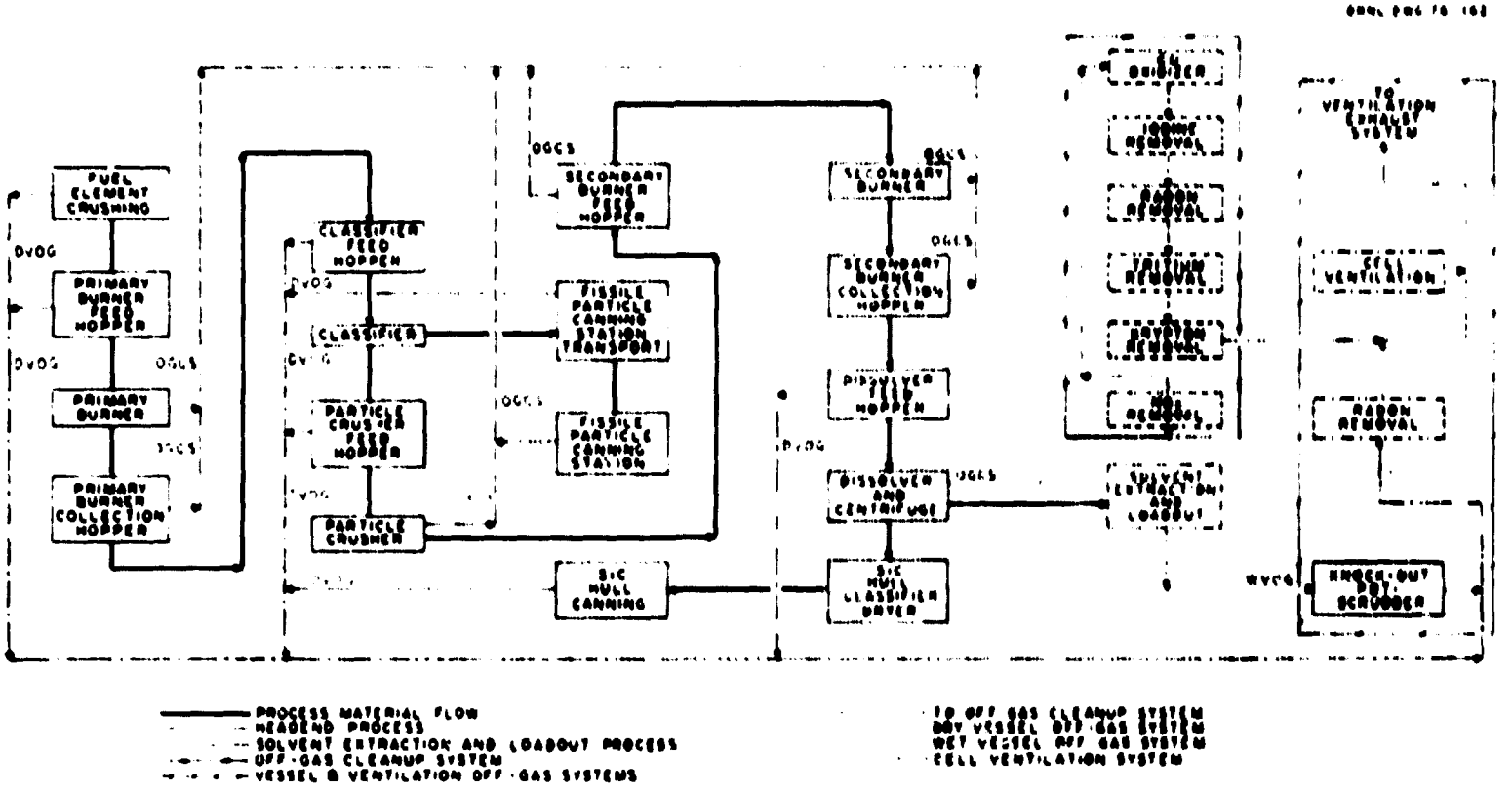

Fig. 2.2. A Flowsheet of the Various Off-Gas Streams Originating from HTGR Head-End Processing that are Treated by the Off-Gas Cleanup System and the Wet Vessel Off-Gas System.

and its decay products or with tritiated water).

9. Provide the required refrigeration for the KALC process.

Five modes of KALC operation were considered. They were as follows:

1. Normal Operating Mode. In this mode 0.19 std m^3/sec (400 scfm) of off-gas is being fed into the KALC process. This stream combines with 0.033 std m^3/sec (70 scfm) of fractionation recycle for a combined feed of 0.22 std m^3/sec (470 scfm) to the absorber. The absorber vents 0.080 std m^3/sec (170 scfm) into the ventilator exhaust system, and 0.11 std m^3/sec (230 scfm) of stripper CO_2 is either recycled to the head-end systems or discharged into the ventilation exhaust system. The stripper releases less than 0.5 std m^3/sec (1 scfm) of product for krypton concentration and bottling.

2. Reduced Feed Operation Mode. This mode of operation is encountered during periods in which some head-end processes are not operating. The absorber feed is held at 0.22 std m^3/sec (470 scfm) by recycling sufficient stripper CO_2 or absorber off-gas.

3. Maximum Feed Rate Mode. A 25% increase over normal flow from head-end for a 30-min period was considered. By increasing the feed gas rate to the KALC process by 10% while accumulating the remainder in a surge vessel this condition can be adequately handled.

4. Total Recycle Operating Mode. When no feed is being introduced to the KALC process the subsystem will operate on total recycle at a rate equivalent to the normal rate.

5. High and Low Light Gas Concentration Operating Modes. During periods in which high concentrations of light gases are entering from head-end the surge vessel will increase in pressure, and stripper CO_2 is recycled to limit the light gas concentration entering the absorber. During periods in which low concentrations of light gases are entering from head-end the surge vessel will decrease in pressure, and absorber off-gas is recycled to maintain light gas concentration entering the absorber.

We conceptually designed an automatic control mode that uses pressure and light gas composition in the surge vessel for biasing the control valves for automatic control. Thus the KALC process can automatically

switch to the various operating modes and accommodate flows from zero to the maximum design while accommodating various light gas compositions. Thus, the KALC process will not be required to handle the maximum instantaneous flow and composition perturbations from head-end, as these will be dampened by the use of a surge vessel.

The pertinent column data are shown on Table 2.2, and a preliminary layout for space allocation is shown in Figs. 2.3 and 2.4.

Table 2.2. Operating and Design Requirements for Krypton Removal (KALC) Columns

	Adsorber Column	Fractionator Column	Stripper Column
Normal Operating Conditions[a]			
Pressure, MPa (atm)	2.0 (20)	1.8 (18)	1.5 (15)
Temperature, °C, Reboiler	−35 (surge pot)	−22	−20
Upper column section	−30	−35	−30
Liquid Rate/Vapor Rate (mole/mole)	12	10	4
Design Data			
Diameter, m (in.)	0.33 (14)	0.46 (18)	0.61 (24)
Packing length, m (ft)	6.7 (22)	4.9 (16)	4.3 (14)
Reboiler load, kW		+73	+220
Btu/hr		+250,000	+750,000
Condenser load, kW		−73	−190
Btu/hr		−250,000	−650,000

[a]The maximum pressure drop in each column is 0.82 Pa/m packing (1 in. H_2O/ft packing).

2.6 PRODUCT PREPARATION (WORK UNIT 1204)

This work was performed to study the problems associated with shipping the $^{233}UO_2(NO_3)_2$ product from the proposed HTGR Head-End Processing Prototype Facility to be located at ACC in Idaho Falls, Idaho, to ORNL. Current plans do not call for this facility to be built, and this shipment will not be required. However, the handling of $^{233}UO_2(NO_3)_2$ solutions will be required in any HTGR Reprocessing and Refabrication operations.

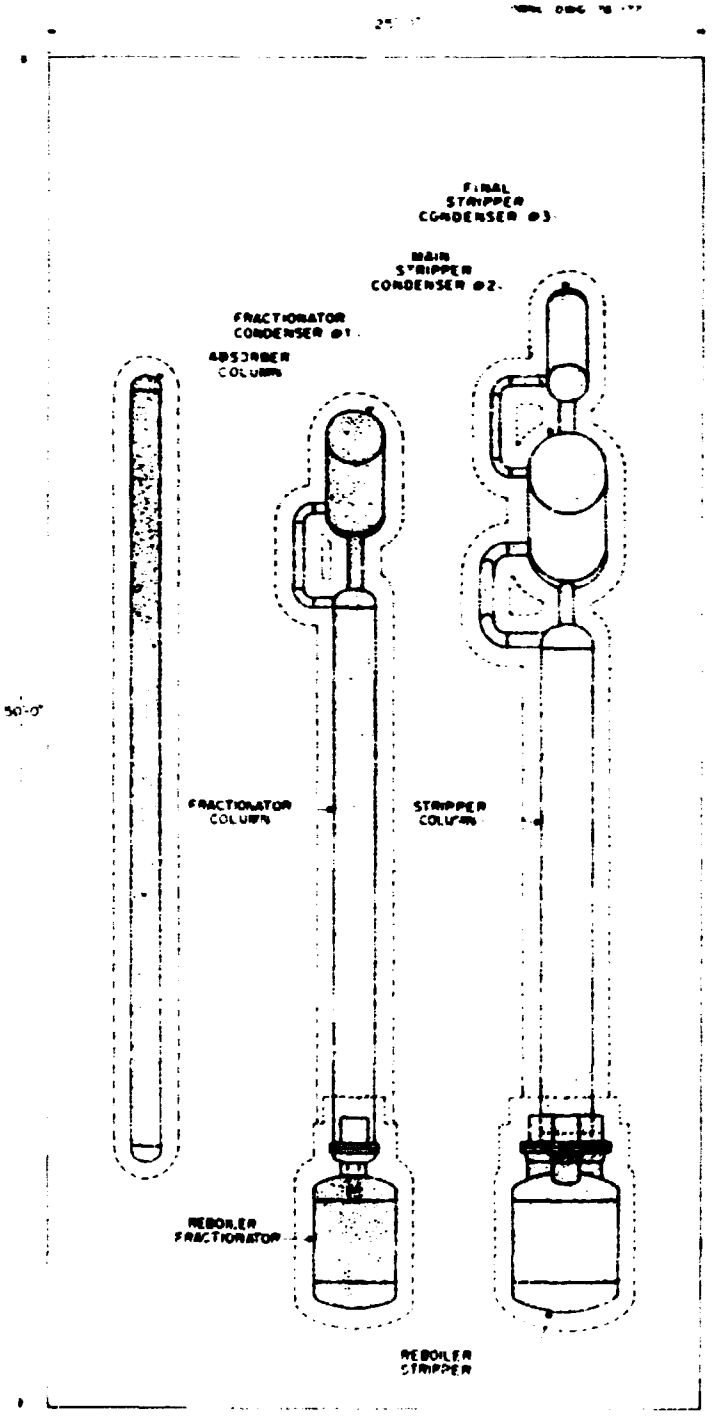

Fig. 2.3. Elevation View of the Space Requirements for the KALC Columns Capable of Handling 0.24 std m^3/sec (500 scfm). Overall dimensions shown are 7.62 by 15.24 m (25.0 by 50.0 ft).

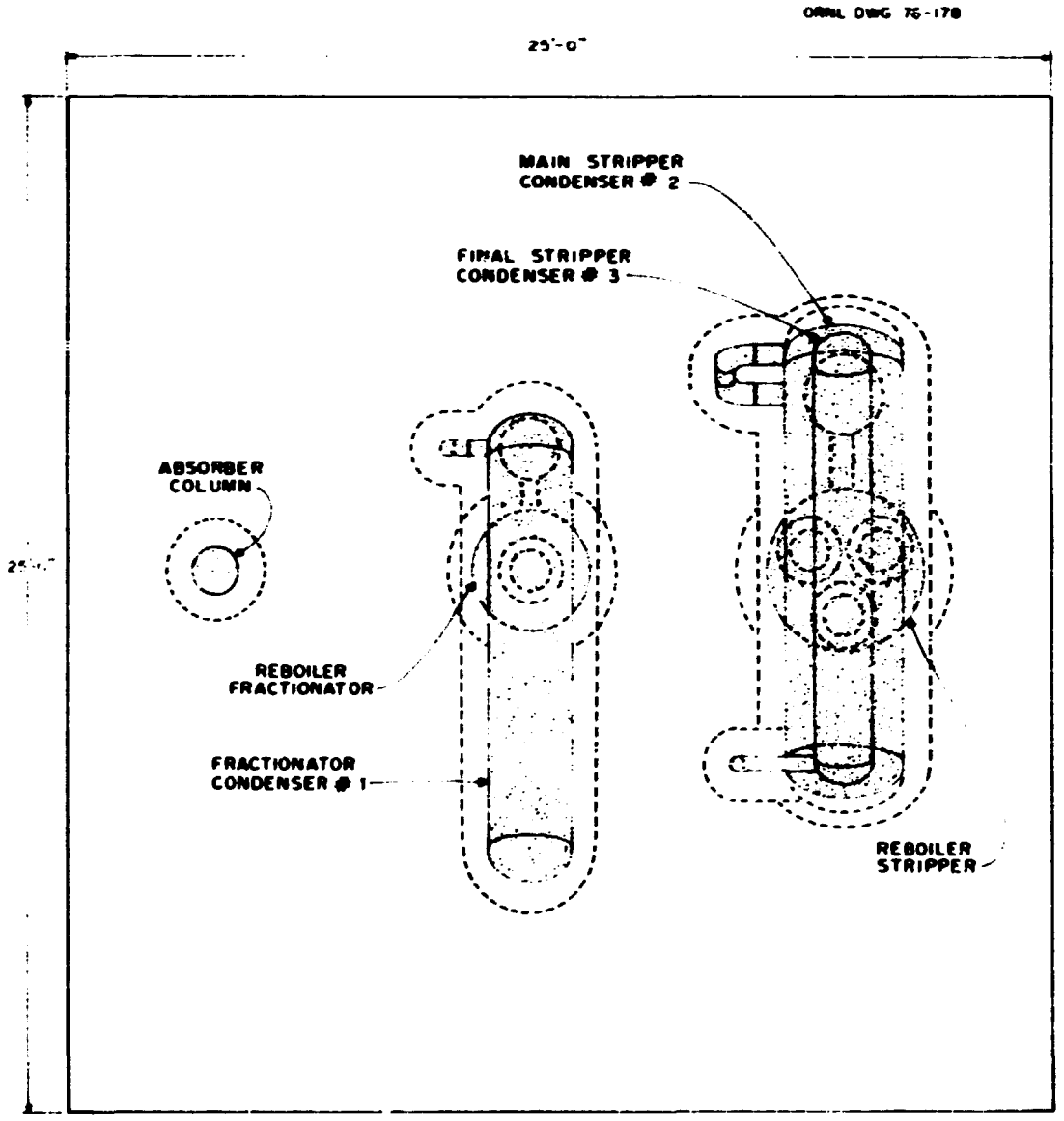

Fig. 2.4. Plan View of the Space Requirements for the KALC Columns Capable of Handling 0.24 std m^3/sec (500 scfm). Dimensions shown are 7.62 by 7.62 m (25.0 by 25.0 ft).

2.6.1 Product Shipping — L. B. Shappert and W. C. Ulrich

A report[1] describing the design features of a package for shipping liquid plutonium and uranyl nitrates was published. The abstract follows:

"Packages intended to be used for the shipment of aqueous nitrate solutions containing ^{239}Pu and ^{233}U must satisfy the same requirements as packages for shipping other forms of radioactive material, such as those related to heat transfer, shielding, and criticality; in addition, other factors which must be considered are potentially high generation rates of radiolytic gases with attendant pressure buildup and hydrogen-oxygen reaction possibilities, material compatibility, and operational requirements. This report discusses these problems in terms of their effects on the design of packages for shipping plutonium and uranyl nitrate solutions and describes a concept for an improved package capable for solving them."

2.6.2 Gamma Activity Depression in $^{233}UO_2(NO_3)_2$ Solutions — W. L. Carter

A study was made to determine the extent to which the gamma activity of a $^{233}UO_2(NO_3)_2$ solution could be depressed before shipment by sparging it to remove ^{220}Rn and by ion exchange to remove ^{232}U decay products.

The ORIGEN[2] program was used to compute the isotopic composition of HTGR fuel that had been irradiated six years and cooled 180 days before solvent extraction. It was assumed that solvent extraction partitioned thorium and uranium to give a $^{233}UO_2(NO_3)_2$ product having a Th/U ratio of 1.00×10^3 and that the solution was decontaminated from all other ^{232}U decay products (Ra, Rn, Po, Pb, Bi, Tl) by a factor of 10^6.

The $^{233}UO_2(NO_3)_2$ solution will probably be stored for a short period before loading into shipping casks, and during this time the quantities of ^{232}U decay products will increase. A storage time after solvent extraction of 14 days was assumed. After that time, the calculated quantities, normalized to one metric ton of heavy metal charged to the reactor, are shown in Table 2.3. The gamma activity of the ^{232}U decay products originates from three isotopes (^{212}Pb, ^{212}Bi, and ^{208}Tl).

Table 2.3. Quantities of ^{232}U Decay Products in Uranyl Nitrate Solution After 14 Days Storage

Nuclide	Quantity Corresponding to 1 Metric Ton Th + U Charged to Reactor	
	(g)	(Ci)
^{232}U	17.83[a]	
^{228}Th	6.44×10^{-3}	
^{224}Ra	2.16×10^{-5}	
^{220}Rn	3.76×10^{-9}	
^{216}Po	1.07×10^{-11}	
^{212}Pb	2.31×10^{-6}	3.23
^{212}Bi	2.19×10^{-7}	3.21
^{208}Tl	3.95×10^{-9}	1.15
^{212}Po	1.16×10^{-17}	
^{208}Pb	2.88×10^{-5}	

[a]Corresponds to 346 ppm ^{232}U in the uranium.

2.6.2.1 Effect of Sparging

A computer program was written to study the effect of gas sparging of $^{233}UO_2(NO_3)_2$ solution to reduce the gamma activity of the ^{232}U decay chain. The chain would be broken at ^{220}Rn, which was assumed to be instantaneously removed in the sparge gas; hence, there would be no further accumulation of radon decay products during the sparging cycle. However, when sparging ceases, accumulation of daughter products resumes. Obviously, ^{228}Th and ^{224}Ra are increasing during the entire cycle. This model was chosen for the computation to determine (1) the sparging time required to obtain significant reductions in acitivity and (2) the postsparging interim period of reduced activity during which the $^{233}UO_2(NO_3)_2$ solution might be handled with minimal or no shielding, for example, during transfer to shipping containers. The results of these calculations are shown in Fig. 2.5, and the gamma activity at the end of selected sparging cycles is given in Table 2.4.

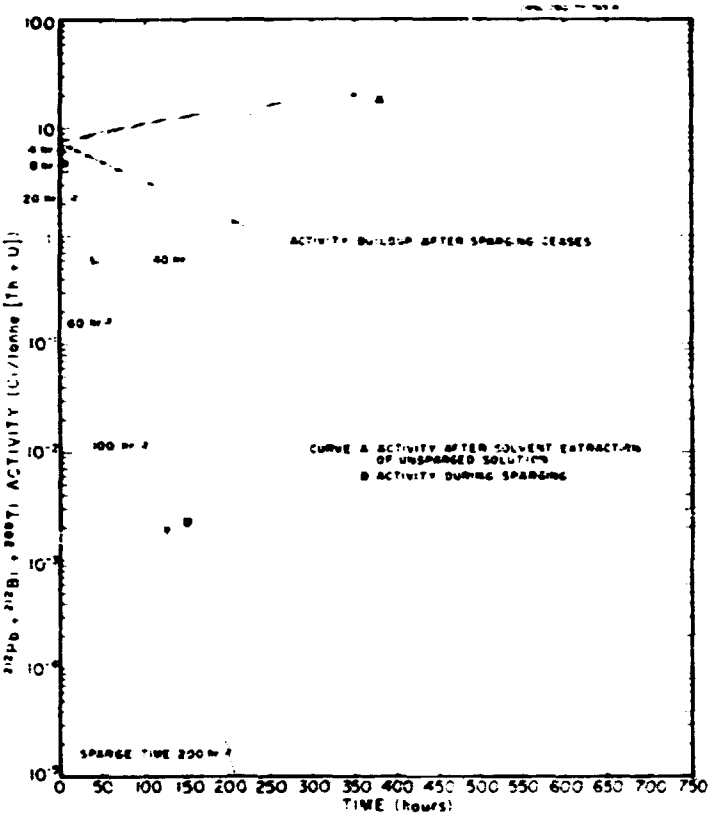

Fig. 2.5. The Effect of Sparging $UO_2(NO_3)_2$ Solutions to Reduce the Gamma Activity of the ^{232}U Decay Chain.

Table 2.4. Effect of Sparging on the Combined Activity of ^{212}Pb, ^{212}Bi, and ^{208}Tl in 14-Day-Stored Uranyl Nitrate Solution Corresponding to 1 Metric Ton Heavy Metal in Reactor

Sparging Time (hr)	Activity (Ci)	Sparging Time (hr)	Activity (Ci)
0	7.59	40	0.59
0.5	7.47	60	0.16
1	7.32	80	0.043
2	6.97	100	0.011
4	6.19	150	4.36×10^{-4}
8	4.79	200	1.65×10^{-5}
20	2.18	250	6.22×10^{-7}

The bottom envelope curve of Fig. 2.5 graphs the decay of ^{212}Pb, ^{212}Bi, and ^{208}Tl while sparging is in progress; the slope of the curve is determined by the decay of ^{212}Pb, whose 10.58-hr half-life controls the decay rate. This curve shows that $^{233}UO_2(NO_3)_2$ solution must be sparged for rather long periods to obtain substantial reductions in the gamma activity. At selected times, sparging was stopped and gamma activity buildup in the solution was calculated; these results are shown as the buildup curves on Fig. 2.5. It is interesting to note that the rate of recovery of gamma activity becomes increasingly faster as sparging time increases. This happens because the population of parent atoms (^{228}Th and ^{224}Ra) increases during the sparge period, and, since ^{220}Rn is in equilibrium with ^{228}Th and ^{224}Ra, the radon daughters increase rapidly when radon removal stops. Hence any operations that are to be carried out with the $^{233}UO_2(NO_3)_2$ at reduced activity must be started immediately after sparging and completed quickly. The buildup curves converge within about 60 hr into an upper envelope curve that represents the normal activity growth for the system without sparging.

An undesirable consequence of sparging is the necessity of treating large quantities of sparge gas for removal of radon and its decay products before the gas is released. Adsorption of radon for decay and hyperfiltration for removal of particulates would be required.

2.6.2.2 Effect of Ion Exchange

A more effective method of reducing the gamma activity of the ^{232}U decay chain (excluding isotopic separation of ^{233}U and ^{232}U) is to break the decay chain at thorium, leaving only the parent (^{232}U) having the longest half-life. A cation exchange process[3] was developed at ORNL for decontaminating uranyl nitrate solutions by separating thorium and uranium and has been demonstrated on a scale that produced kilogram quantities of uranium product. Rainey's work indicated that more than 99% of the thorium, about 98% of the radium, and about 50% of the lead could be easily retained on the resin. Data for other ^{232}U decay products were not obtained. The first uranium product to break through the resin is practically free of thorium and radium; hence, at lower throughputs extremely high decontamination factors can be obtained.

Two calculations were made to determine the activity-versus-time characteristics of $^{233}UO_2(NO_3)_2$ solutions that had been decontaminated by ion exchange. Curve A of Fig. 2.6 was computed for an ion exchange cleanup that removed ^{228}Th, ^{224}Ra, and ^{212}Pb to the extent indicated by Rainey's data; decontamination factors for decay products for which there were no ion exchange data were assumed to be the same as for lead. Ion exchange initially halves the gamma activity, and this is followed by a further decrease in activity as ^{212}Pb, ^{212}Bi, and ^{208}Tl decay faster than they are being produced. Approximately 55 hr after ion exchange the activity passes through a minimum, after which the daughter production from the parents exceeds decay and the curve rises.

Curve B of Fig. 2.6 shows the limiting case for 100% removal of all ^{232}U decay products. This curve rises rather steeply, and in five days the solution gamma activity approaches that of the cation-exchange-treated solution. The gamma activity of the treated solution gradually approaches that of the untreated solution (Curve C). At the end of one month the gamma activity of the treated solution is only two thirds that of untreated solutions.

2.6.3 Alpha and Beta Activity Depression in $^{233}UO_2(NO_3)_2$ Solutions — W. L. Carter

During the transport of uranyl nitrate solutions of recycle HTGR fuel, absorbed energy from decaying nuclides decomposes a portion of the aqueous medium into hydrogen and oxygen. This radiolysis causes a pressure increase in the shipping container and is a factor in shipping cask design and allowable transit time. The major source of radioactivity in recycle fuel is the ^{232}U decay chain, accounting for about 57% of the total activity immediately after solvent extraction. However, as the uranyl nitrate solution ages, the fraction of activity due to this decay chain increases toward 91%, which is attained at equilibrium. The remainder of the activity is primarily from other uranium isotopes; these isotopes have such long half-lives that their decay product activities are minor in comparison with ^{232}U decay product activities.

To reduce the alpha and beta activity, the same ion exchange method used in Section 2.6.2 was assumed to be used to treat the same feed

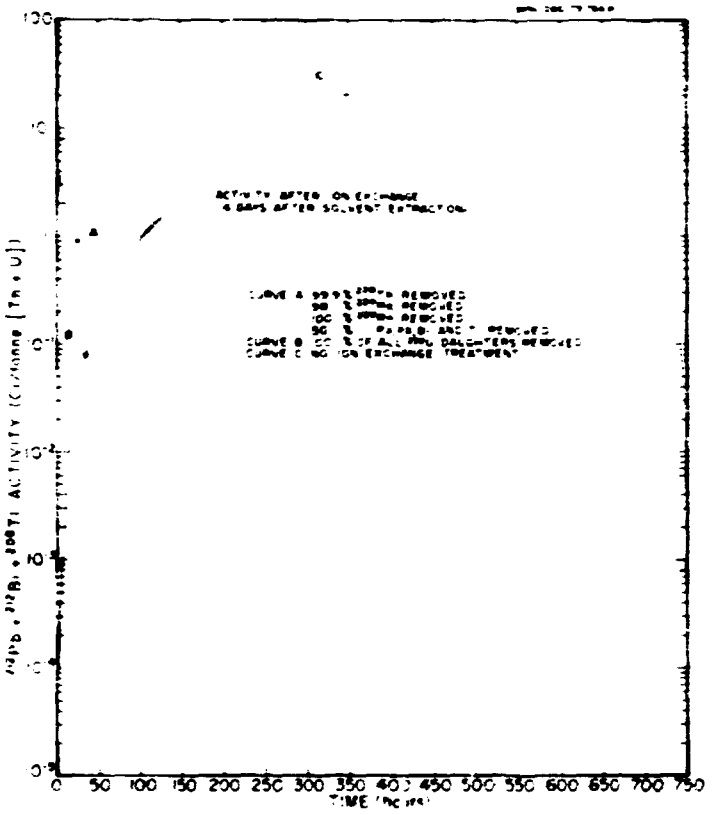

Fig. 2.6. The Effect of Ion Exchange Treatment on $UO_2(NO_3)_2$ Solutions to Reduce the Gamma Activity of the ^{233}U Decay Chain.

containing 346 ppm ^{232}U in total uranium. Fission product decontamination factors of 10^6 were also assumed; this large DF essentially removed fission products from consideration in dose calculations since their activity is only about 1.3% of total activity immediately after solvent extraction. Nuclear data used in the activity calculations are given in Table 2.5.

Total activity and cumulative dose for the entire ^{232}U decay chain in the uranyl nitrate solution are plotted in Figs. 2.7 and 2.8, respectively, as functions of time after ion exchange. Curve A on each figure shows the increase in activity (Fig. 2.7) or cumulative dose (Fig. 2.8) for $^{233}UO_2(NO_3)_2$ solution untreated by ion exchange. Curve B on each figure shows activity and dose for the $^{233}UO_2(NO_3)_2$ solution after ion exchange treatment. Ion exchange initially lowers the activity about 4%; however, the activity continues to decrease for about 50 hr as ^{232}U decay products decay faster than they are produced. When Curve B begins

Table 2.5. Data for the ^{232}U Decay Chain
(data from ORIGEN library)

Nuclide	Type of Decay	Half-Life	Total Decay Energy (MeV)	γ Energy Fraction
^{232}U	α	72 years	5.414	0
^{228}Th	α	1.91 years	5.525	0
^{224}Ra	α	3.64 days	5.771	0
^{220}Rn	α	55.88 sec	6.396	0
^{216}Po	α	0.15 sec	6.903	0
^{212}Pb	β	10.58 hr	0.242	0.51
^{212}Bi	36% α, 64% β	60.5 min	2.929	0.10
^{208}Tl	β	3.1 min	3.929	0.85
^{212}Po	α	0.3 μsec	8.940	0
^{208}Pb	stable			
			46.047	

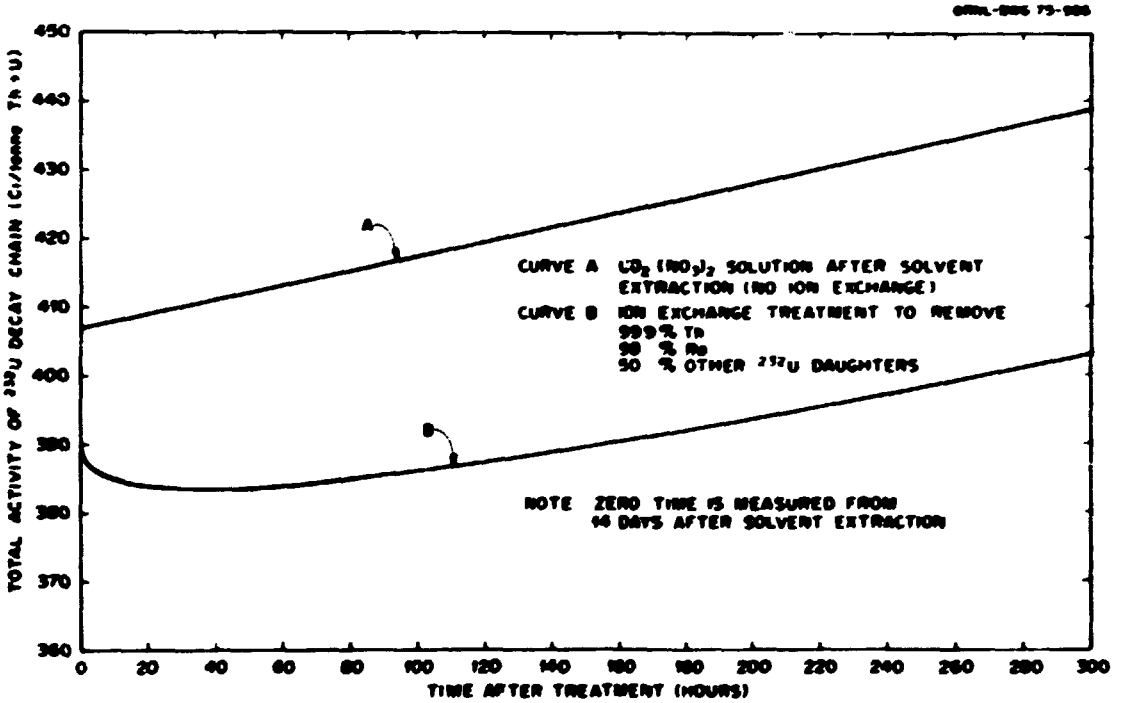

Fig. 2.7. Total Activity of the ^{232}U Decay Chain for Ion Exchange Treated and Untreated $UO_2(NO_3)_2$ Solutions.

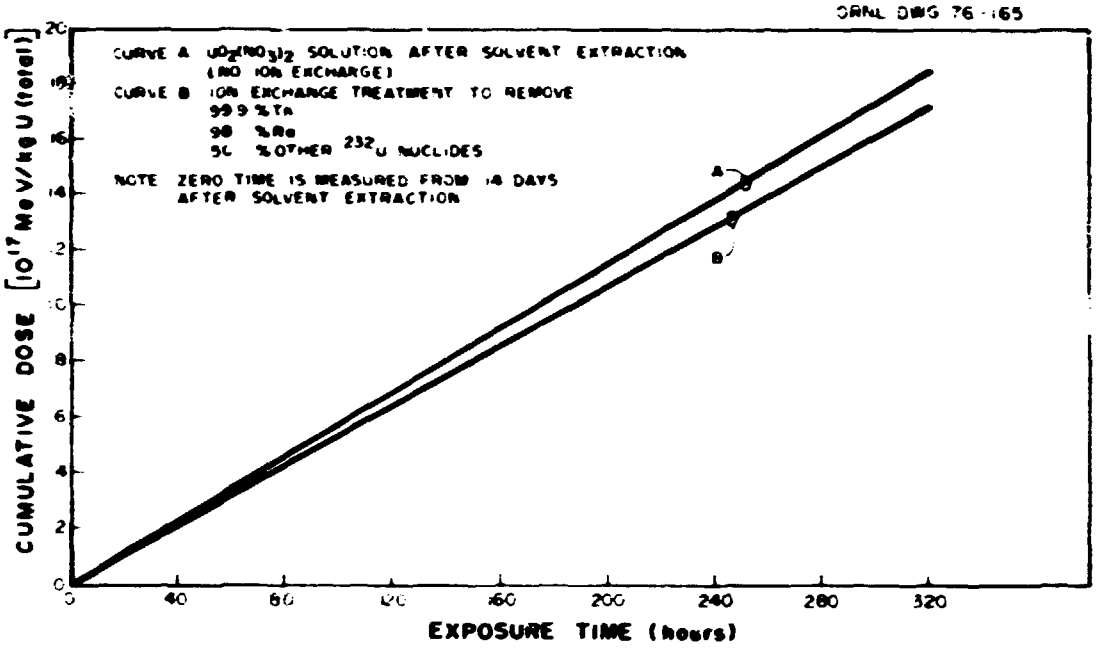

Fig. 2.8. Cumulative Dose of the ^{232}U Decay Chain for Ion Exchange Treated and Untreated $UO_2(NO_3)_2$ Solutions.

to rise (Fig. 2.7), the ion exchange solution is about 7.5% lower in activity than the solvent extraction product, and this difference holds over most of the time span of the graph. The cumulative dose (Fig. 2.8) is monotonically increasing for both untreated and ion exchange products; the ion-exchange-treated solution receives about 7% less dose.

The cumulative dose was calculated by assuming that all energy in the ^{232}U decay chain was deposited in the $^{233}UO_2(NO_3)_2$ solution. About 92% of total ^{232}U chain energy is alpha and beta energy (Table 2.5), so ignoring the small portion of the gamma energy that escapes introduces little error.

The reason that ion exchange cleanup decreases the radiation dose by only 7% is made clearer by examining the data in Table 2.6. These data show that solvent extraction partitions uranium and thorium rather completely and removes other ^{232}U decay products such that the ^{232}U activity is 90 to 94% of the activity of the entire decay chain during the first few days after solvent extraction. Hence the predominant dose to the solution is from ^{232}U, and ion exchange treatment to remove

Table 2.6. Comparison of ^{232}U Activity with Total Activity of ^{232}U Plus Decay Products in HTGR Fuel

Treatment of $UO_2(NO_3)_2$	Ratio: ^{232}U Activity/Total ^{232}U Chain Activity for each Time (days)						
	0[a]	7	30	60	300	1000	3000
No treatment	0.190	0.190	0.187	0.184	0.168	0.142	0.125 (equilibrium)
Solvent extraction 1000 ppm Th in product[b] DF = 10^4 for ^{232}U decay products	0.930	0.903	0.792	0.687			
Ion Exchange[c] 99.9% Th removed 90% Ra removed 50% other decay products removed	0.978	0.977	0.856	0.734			
Ion exchange[c] 100% all ^{232}U decay products removed	1.0	0.980	0.856	0.734			

[a] $UO_2(NO_3)_2$ solution was assumed to be stored 14 days after solvent extraction; zero time is measured at this point when $UO_2(NO_3)_2$ is treated by ion exchange.

[b] Ratio: Th(total)/U(total).

[c] Treatment applied to product from solvent extraction.

the remaining thorium and other decay products has only a small effect on the overall dose. The benefit from an ion exchange treatment would be more pronounced if carried out on $^{233}UO_2(NO_3)_2$ that had been stored much longer than the 14 days assumed for this study because, as equilbrium is approached, the fraction of ^{232}U activity drops to 12.5%. However, such long storage times would be impractical and uneconomic to any HTGR fuel recycle program.

For practical $^{233}UO_2(NO_3)_2$ storage times after solvent extraction, the radioactivity of the ^{233}U decay chain is neglible. However, since ^{233}U is present in such large amounts compared with ^{232}U, the amount of energy released in the decay of the parent ^{233}U nuclide makes a significant contribution to the dose that the solution receives. Calculated values of this dose are plotted in Fig. 2.9 for several concentrations of ^{233}U in the total fuel. The uppermost curve is typical of a fuel that is withdrawn from the HTGR after one year's irradiation; the other curves are for fuel that has been irradiated for succeedingly longer periods of time. Dose values from Fig. 2.9 may be added to those of Fig. 2.8 to obtain an estimate of the dose to uranyl nitrate solution for various concentrations of ^{233}U containing 346 ppm ^{232}U. Doses from

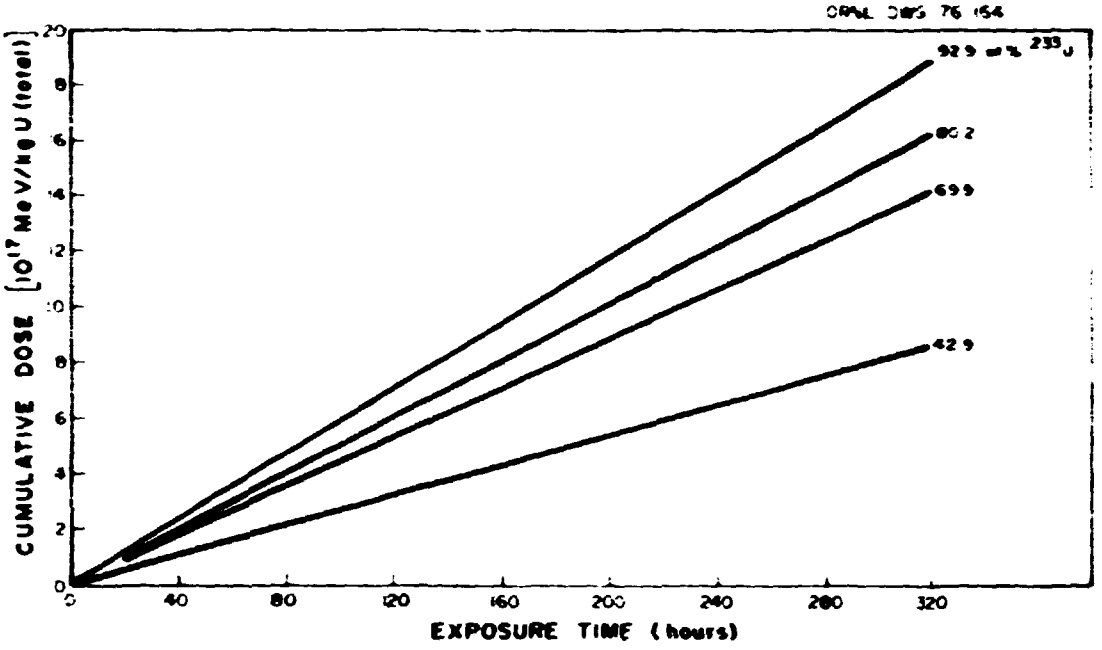

Fig. 2.9. Cumulative Dose from the ^{233}U in $UO_2(NO_3)_2$ Solutions as a Function of ^{233}U Enrichment.

the ^{234}U, ^{235}U, and ^{236}U decay chains were calculated for HTGR recycle fuels and found to be negligible in comparison with doses from ^{232}U and ^{233}U.

2.7 SUPPORT FACILITIES (WORK UNIT 1205)

The activity of this work unit consisted of participation in review meetings with ACC, GAC, and R. M. Parsons personnel.

2.8 REFERENCES

1. L. B. Shappert and W. C. Ulrich, *Conceptual Design of Packages for Shipping Solutions Containing ^{239}Pu and ^{233}U*, ORNL-TM-4720 (February 1975).
2. M. J. Bell, *ORIGEN — The ORNL Isotope Generation and Depletion Code*, ORNL-4628 (May 1973).
3. R. H. Rainey, *Laboratory Development of a Pressurized Cation Exchange Process for Removing the Daughters of ^{232}U and ^{233}U*, ORNL-4731 (December 1972).

3. HTGR REFABRICATION PROCESS DEVELOPMENT (SUBTASK 210)

J. D. Sease and K. J. Notz

3.1 INTRODUCTION

Refabrication is the step in the HTGR fuel cycle that begins with the receipt of nitrate solution containing recovered ^{233}U and refabricates this material into fuel elements for use in an HTGR. The basic steps in refabrication are similar to those in fresh fuel manufacture and consist of preparation of fuel kernels, application of multiple layers of pyrolytic carbon and SiC, preparation of fuel rods, and assembly of fuel rods into fuel elements. The major difference between the manufacture of fresh fuel and recycle fuel is that the recycle fuel must be fabricated remotely in hot-cell facilities. The HTGR fuel refabrication development program is therefore directed toward the development of processes and equipment for remote application.

At the start of this period, the overall HTGR fuel recycle program included a proposed Fuel Refabrication Pilot Plant (FRPP) at ORNL as well as a Fuel Reprocessing Pilot Plant to be located in Idaho. These pilot plants were in support of a commercial HTGR recycle plant proposed by General Atomic Company. Escalating costs and other programmatic considerations led to the preparation of an alternate plan. The alternate plan, prepared near the end of this reporting period, included the design and construction of an ERDA-supported HTGR Recycle Demonstration Facility (HRDF) as its ultimate goal. This change in programmatic direction tended to increase the scope of the refabrication development effort to include an expanded cold prototype development phase. Essentially all development work done in support of the FRPP is applicable to the alternate plan.

The current program is subdivided into five phases leading to the design, construction, and operation of the HRDF. These development phases are: (1) cold laboratory development, (2) hot laboratory development, (3) cold engineering development, (4) hot engineering development, and (5) cold prototype development. The objective of cold and hot

BLANK PAGE

laboratory development is to prove process feasibility. For cold and hot engineering development, the objectives are to establish the space envelope required for in-cell process equipment and to verify process feasibility. The objectives for cold prototype development are to establish in-cell equipment configuration and to develop process procedures. The term cold development refers to work not requiring the presence of radioactivity, while hot development requires the presence of radioactivity. The phases will not necessarily be accomplished sequentially. Work during this report period has primarily been in cold engineering development. Work in waste and scrap handling (Work Unit 2109) has been expanded over that required for the FRPP, and all the work in this area is in the cold laboratory development phase.

The work in refabrication development is subdivided into 11 work units parallel to the major systems of the refabrication portion of the HRDF. These are:

1. Work Unit 2100 — General Development,
2. Work Unit 2101 — Uranium Feed Preparation,
3. Work Unit 2102 — Resin Loading,
4. Work Unit 2103 — Resin Carbonization,
5. Work Unit 2104 — Microsphere Coating,
6. Work Unit 2105 - Fuel Rod Fabrication,
7. Work Unit 2106 — Fuel Element Assembly,
8. Work Unit 2107 — Sample Inspection
9. Work Unit 2108 — Plant Management,
10. Work Unit 2109 — Waste and Scrap Handling, and
11. Work Unit 2110 — Material Handling.

3.2 GENERAL DEVELOPMENT (WORK UNIT 2100) — A. R. Olsen and J. D. Sease

This area is involved in the coordination and review of all functions of this subtask, interfacing with Subtask 220, providing criteria and technical guidance for the refabrication process portions of Subtask 320, the preparation of recycle fuel specifications, development of the material accountability, nuclear materials safeguards

and criticality control programs, the assessment of safety considerations for development activities and the proposed operating plant, and coordination of work done in this subtask in support of recycle fuel irradiation testing.

3.2.1 General Coordination Activities — R. A. Bradley, A. R. Olsen, and J. D. Sease

In accordance with the objectives of this work unit, a Summary Work Plan and Schedule was prepared for Subtask 210. This document is the principal planning instrument on which detailed experimental programs for all the work units in Subtask 210 are based.

Significant effort was expended in assisting in the writing, reviewing, and editing of the overall plant design description and individual system design descriptions incorporated in the conceptual design report for the proposed HTGR Fuel Refabrication Pilot Plant.[1] With the evolution of a possible alternate program with the end objective of designing, constructing, and operating an HTGR Recycle Demonstration Facility (HRDF), a new phased generic development program outline directed at supporting the design and operation of the HRDF was drafted. This outline is expected to provide the basis for specific experimental program definition when the new overall HTGR recycle program has been established by ERDA.

Reviewing the proposed pilot plant concept and the HRDF study showed that increased emphasis was required on scrap processing and waste treatment for the refabrication portion of the recycle plant. Work in this area was increased (see Sect. 3.11).

The fabrication effort in producing materials for irradiation testing in experiments OF-2 and the planned Early Validation Test 1 was coordinated and monitored as were all schedules and funding of the work units within Subtask 210.

3.2.2 Environmental and Safety Considerations — R. A. Bradley and J. E. Till

A final Environmental Statement[2] for the proposed HTGR FRPP was issued by the USAEC. The conclusion of this study from the final summary

sheet was: "The environmental impacts and adverse effects from this project are expected to be minor. The gaseous and liquid effluents resulting from operation of the pilot plant will be discharged into existing waste handling and treatment systems. The subsequent concentrations of the radioactive and chemical discharges to the environment will be several orders of magnitude below the established limits and background radiation levels. The solid wastes resulting from pilot plant operation and decommissioning will be disposed of in existing solid waste storage facilities." Assessment of the source terms for a commercial scale plant is discussed in Sect. 6.3 of that report.

The radiological safety requirements associated with the refabrication of HTGR fuels depend in part on the radiological hazard associated with the ^{233}U. Therefore, the Environmental Sciences Division was asked to compare the relative radiological hazards of LMFBR plutonium fuel and recycle ^{233}U HTGR fuel. The results of this investigation have been reported,[3,4] including a brief review of the physical characteristics of uranium and plutonium isotopes in the fuels. Natural uranium and light-water-reactor uranium fuel are chemical toxicants; therefore, the chemical vs radiological toxicity of ^{233}U HTGR fuel and plutonium LMFBR fuel is discussed.

The recycle uranium is primarily ^{233}U, but it also contains up to 1200 ppm ^{232}U. The highly radiotoxic ^{232}U contributes from 50 to 90% of the internal dose to man from this recycle uranium. Four computer codes developed by the ORNL Environmental Hazards Study Group are used to predict potential hazards to man and biota from hypothetical exposure to recycle ^{233}U fuel and LMFBR plutonium fuel. Equal amounts (by weight) of each fuel are assumed to be released to the environment or ingested by man directly. All calculated doses are hypothetical and are not representative of actual insult to man from a nuclear facility handling ^{233}U or plutonium fuel. Instead, it is the relative magnitude of the doses from each type of fuel that is significant.

From a radiological impact standpoint, LMFBR plutonium fuel is approximately 500 times more radiotoxic than ^{233}U fuel when inhalation is the exposure pathway. In terms of doses to man via ingestion and

doses to biota the two fuels are comparable. It is concluded that if atmospheric release is the only source of effluent, LMFBR plutonium fuel is more hazardous than recycle ^{232}U fuel by a factor of approximately 500; however, if these fuels are predominantly present in the terrestrial environment, their radiological impact on man is similar.

As a result of this study, the conceptual design criteria for effluent treatment in the FRFP and HRDF have been based on existing criteria for plutonium, although we recognize that this may be ultra-conservative in some instances.

3.2.3 Recycle Fuel Specification — R. A. Bradley and J. M. Chandler

Although a number of feed material and intermediate product specifications within the total fuel recycle process must eventually be addressed, the primary specifications are those dealing with the uranium solution, which is the reprocessing product, and the recycle fuel product.

Interim I specifications for the $^{233}UO_2(NO_3)_2$ solution recovered from spent HTGR fuel by solvent extraction were prepared and forwarded to Allied Chemical Corporation for comments.

Interim I HTGR Recycle Fuel Product Specifications, based on General Atomic's fresh fuel draft specification, were prepared and issued for review by GAC and USAEC-RRD. Resolution of the comments is scheduled for early next year, and an Interim II version of the specifications will be issued then for use in developing refabrication processes and quality control techniques.

3.2.4 Material Accountability and Safeguards — S. R. McNeany

As conceived, the purpose of these studies was twofold. First, estimates of uranium and thorium average flow rates through a refabrication facility were required for equipment design. Secondly, these studies are to lead to an efficient design of a material accountability system.

A computer program called NOMUF was written to calculate time-averaged uranium and thorium flow rates through a semigeneralized model

of a refabrication facility. The program documentation is written up in an ORNL internal report, and a sample problem demonstrating its application to the proposed FRPP is published.[5]

The code output can be used during system development to study the sensitivity of calculated limits of error on materials unaccounted for (LEMUF)[6] on the precision and location of various measurement devices in the process line. This application is useful to optimize an assay system with respect to assay locations and required precision of the proposed assay devices.

Future plans call for the development of a real-time dynamic model of material flows through a refabrication facility. Such a model will have several uses. During plant operation, the program will estimate flow rates at various points in the process. If actual measurements differ significantly from these estimates, management will be notified since this might indicate a diversion of material from the process line. The model will also provide estimated quantities of materials located in nonmeasurement process areas and waste streams.

Thus, the real-time simulation model will be useful as a development tool in the optimization of an assay system, as a monitor for material diversion or errors in material transfer, and as an estimator of unmeasured material flows in an operating plant. Currently, a dynamic model has been developed to the point where uranium mass movement is simulated through 40% of the proposed FRPP.

3.2.5 Nondestructive Assay Techniques — J. E. Rushton, S. R. McNeany, and J. D. Jenkins

A conceptual design of the special nuclear material nondestructive assay and accountability system has been prepared.[5] The report uses the NOMUF model described in Sect. 3.2.4 to calculate typical fissile and fertile material flows and to identify necessary measurement points within the refabrication process. Measurement points that require or would benefit by the application of nondestructive assay measurements are described. The main body of the report addresses the selection of appropriate nondestructive assay methods.[7] The primary factors affecting

the selection of nondestructive assay techniques are the physical and nuclear characteristics of the fuel forms. A partial listing of the properties described in the report includes the gamma radiation levels, the uranium isotopic compositions, the spontaneous (α,n) neutron production rates, and the chemical and physical compositions of the fuel at each stage in the process. Based upon these material properties, specific assay techniques were identified for each of the measurement requirements. The following general conclusions are also derived from this analysis:

1. The high gamma activity of the recycled fuel precludes the application of many nondestructive assay techniques presently developed for light-water-reactor fuel or ^{235}U-Th HTGR fuel.

2. The recycled HTGR fuel does not spontaneously emit time-independent radiation that could be directly measured and correlated with fissile or total uranium content. The time-varying property of the gamma radiation limits the use of direct gamma-ray measurements for nondestructive assay.

3. Accurate nondestructive methods for recycled ^{233}U HTGR fuel can be based on active interrogation of the fuel by neutron or gamma radiation and subsequent detection of an induced signature radiation. Because of the high gamma level, the most suitable signature is induced fission neutrons.

The study concludes with an analysis of data flow and data handling requirements for a real-time accounting of special nuclear material within the proposed pilot plant. Although the report focuses on the pilot plant, the assay methods identified are applicable to demonstration or commercial-scale facilities.

The primary nondestructive assay requirement identified is for the in-line assay of molded uncarbonized fuel rods. The program to develop such a capability is described in Sect. 3.7 of this report.

3.2.6 Criticality Analysis — J. D. Jenkins and S. R. McNeany

Previously, all ^{233}U criticality calculations performed at ORNL in support of the HTGR fuel refabrication program utilized the 16-group

Hansen-Roach cross section set.[8] Recently, some calculations performed at Battelle Pacific Northwest Laboratory (BPNL)[9] pointed to discrepancies between ENDF/B-III-based results and Hansen-Roach results for highly enriched ^{233}U systems in simple geometries. These discrepancies prompted a further investigation of the cross section sets used at ORNL.

This investigation[10] compares criticality calculations performed with ENDF/B-IV cross sections and the 16-group Hansen-Roach library at ORNL. The area investigated is homogeneous systems of highly enriched ^{233}U in simple geometries. Calculations are compared with experimental data for a wide range of $H/^{233}U$ ratios. Results show that calculations made with the Hansen-Roach cross sections agree within 1.5% on k_{eff} for the experiments considered. Results derived from ENDF/B-IV gave good agreement for well thermalized systems, but discrepancies up to 7% in k_{eff} were observed in fast and epithermal systems. Figure 3.1 graphically presents the calculated results.

The conclusions of this investigation are threefold. First, the 16-energy group Hansen-Roach cross section set presently used at ORNL is adequate for criticality safety calculations on homogeneous pure ^{233}U systems (i.e., systems containing ^{233}U as the prime heavy metal constituent) with $H/^{233}U$ ratios from about 40 to 2000 and metal systems. Secondly, to the authors' knowledge, no experimental criticality data are available on highly enriched ^{233}U systems having $H/^{233}U$ ratios of 10 to 30. Hence, no cross section set was directly confirmed for these systems, which are characteristic of some fuel forms that may be present in an HTGR fuel refabrication facility. Interpolation of results between higher $H/^{233}U$ ratios and zero is not valid because the neutron energy spectrum changes drastically between these bounds. Finally, calculation discrepancies between ENDF/B and Hansen-Roach cross sections for highly enriched ^{233}U systems were confirmed. However, a comparison of ENDF/B calculational results with experimental data for highly enriched ^{233}U systems indicates significant problems with ENDF/B results on systems having $H/^{233}U$ ratios less than 400.

In light of the fact that experimental criticality data are not available for some ^{233}U and ^{233}U-^{232}Th systems that will be encountered during

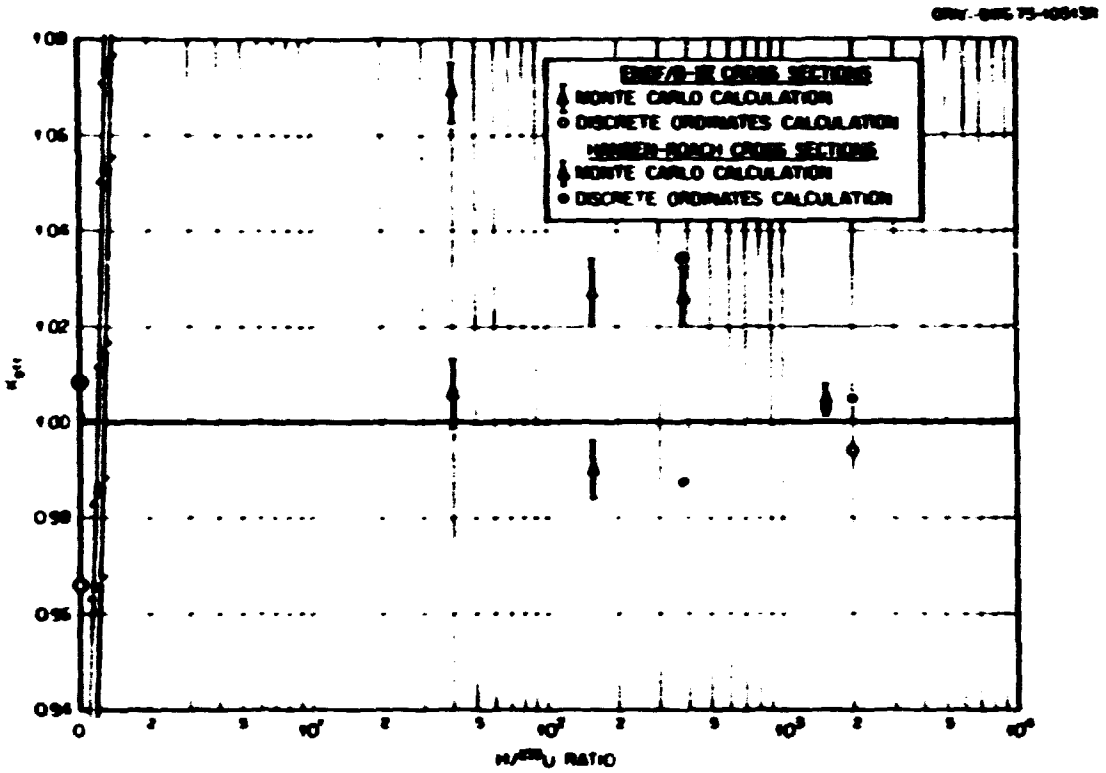

Fig. 3.1. Comparison Between ENDF-B-IV and Hansen-Roach Cross Sections for ^{233}U Criticality Calculations.

recycle of HTGR fuel, a recommendation has been made to ERDA that an experimental program be undertaken. The proposed program would be conducted at BPNL as a subcontract effort under the ORNL Thorium Utilization Program. Data collected from these experiments would be quite useful in the design of process equipment to ensure criticality safety, to allow optimization of process equipment size, and to facilitate plant licensing.

3.2.7 Gamma-Ray Dose Rates Associated with Small Samples of Recycled ^{233}U Fuel — J. E. Rushton

The gamma radiation associated with ^{233}U is due primarily to the decay products of ^{232}U. The radiation requires remote handling of bulk quantities of the fuel. It was desired to determine whether small samples of ^{233}U fuel could be handled in unshielded or lightly shielded glove boxes. The production of reactor fuel requires numerous quality

control and quality assurance measurements, and consequently there is a strong economic incentive to perform sample analysis outside of totally remote facilities. Gamma-ray dose rates were calculated at several distances from a 1-g quantity of ^{233}U with 500 ppm ^{232}U decayed 30, 60, 90, and 180 days since separation. The results of these calculations are listed in Table 3.1 for no shielding and for 5 cm of lead shielding. The dose rates were calculated under the following assumptions:

1. point source,
2. no self-absorption in ^{233}U,
3. only gamma rays above 100 keV included, and
4. shield adjacent to source.

These calculations demonstrated that unshielded 1-g samples of ^{233}U with 500 ppm ^{232}U cannot be routinely handled in glove boxes for the decay periods investigated. Thus, a time-window for operation of the proposed FRPP was developed and included in the conceptual design criteria. The time-window limits the FRPP to handling ^{233}U with no more than 500 ppm ^{232}U and within a period of less than 90 days since the uranium has been separated from the ^{232}U decay products. Glove boxes employing localized source shielding for some analyses in the sample inspection system proposed for the FRPP were considered adequate, provided a significant degree of automation was developed for the analytical processes. A high degree of automation and some fully shielded processes will be required for a commercial-scale plant, where the ^{232}U content may go as high as 1200 ppm and the time since decay product removal may be longer for practical considerations.

3.3 URANIUM FEED PREPARATION (WORK UNIT 2101)

No activity was scheduled during the report period.

Table 3.1. Dose Rates for a 1-g Source of ^{233}U With 500 ppm ^{232}U

Distance from Source Point to Dose Point (cm)	Dose Rate, mrem/hr, for Various Decay Periods			
	30 days	60 days	90 days	180 days
Without Shielding				
1	2203	4444	7407	14,605
2	551	1112	1854	3,655
5	88.3	178	297	585
10	22.1	44.5	74.2	146
20	5.52	11.1	18.6	36.6
35	1.80	3.64	6.06	12.0
50	0.88	1.78	2.97	5.86
100	0.22	0.45	0.74	1.47
Through 5 cm Pb				
5.2	7.41	14.9	24.9	49.1
10.0	2.00	4.04	6.73	13.3
20.0	0.50	1.01	1.68	3.32
35.0	0.164	0.33	0.55	1.08
50.0	0.080	0.162	0.27	0.53

3.4 RESIN LOADING (WORK UNIT 2102) — P. A. Haas and K. J. Notz

The reference kernels for recycle of ^{233}U to HTGRs are prepared by carbonization of carboxylic acid cation exchange resins loaded with uranium. The carbonized product kernels must meet specifications for composition, size, density, sphericity, microstructure, and uranium content per kernel. The resin loading process must produce uranium-loaded resin that can be carbonized to meet these specifications. A principal advantage of the resin-based preparation of kernels is that many of the critical product properties can be established and controlled for the feed resin before any radioactivity is present. Another advantage of the resin process is that the amount of material that must be processed

through resin loading, resin carbonization, and microsphere coating systems is one-fifth that of a $(4Th,U)O_2$ kernel.

Operations involved are: (1) preparation of resin feed to supply resin with properties adequate to meet product specifications, (2) conversion of the uranyl nitrate solution from a reprocessing plant into the acid-deficient feed required for the resin loading, (3) loading and drying resin to the form suitable for the carbonization furnace, and (4) preparation of materials as a service to subsequent development work units, including carbonization, coating, fabrication, and irradiation testing.

3.4.1 Resin Feed Preparation — J. P. Drago, P. A. Haas, K. J. Notz, and J. M. Shaffer

This includes both the procurement and evaluation of commercial ion exchange resins and processing them to meet specifications for size, shape, composition, and quality assurance. Amberlite IRC-72* is the reference weak-acid resin and is known to produce acceptable product kernels. A second source of resin supply is considered necessary to guard against process interruptions. The kernel size specification results in a limit on the size range of resin feed, and about 20% of the commercial Amberlite IRC-72 is usable for a size range of ±10% of the mean diameter. Wet screening of −20 +50 mesh Amberlite IRC-72 will be used as a short-term procedure, but some improved procedure is needed to meet long-term size specifications.

3.4.1.1 Purchase of Commercial Resin

Early studies[11] identified Amberlite IRC-72 as a commercial carboxylic acid cation exchange resin that could be processed to meet all requirements. Duolite C-464† has about equally suitable properties, but shows significant differences from the Amberlite IRC-72. The manufacturer of Duolite C-464 has delivered specially processed resin with

---

*Trademark of the Rohm and Haas Company.

†Trademark of Diamond Shamrock Chemical Company.

very large improvements in the size distribution and the fraction of off-shape resin as compared with the standard commercial resin. The cost of this specially prepared Duolite C-464, based on previous yields and the last price quotation, is $0.06/g U. The cost of standard commercial Amberlite IRC-72 with a 15% yield is $0.09/g U. The manufacturer has accepted an order to make a special batch to optimize the size yield with no increase in unit costs. The increased yield is expected to lower the Amberlite IRC-72 costs to $0.03 to 0.06/g U.

Scanning electron micrographs of uranium-loaded Amberlite IRC-72, Duolite C-464, and fines from Duolite have been made. Standard UO_3 batch loadings were used for both resins. Significant surface differences between the loaded Amberlite and Duolite are apparent at 10,000×. The Duolite has a coarse, agglomerated surface composed of subunits ranging from 0.5 to 1 μm in size. Circular areas approximating 25 μm in diameter where flaking had occurred were seen. Cracks approximately 0.5 μm wide by 50 μm long were also noted. The Amberlite has a very smooth surface at 10,000×. Gullies approximately 2 μm wide by 10 to 15 μm long were noted. The gullies were seen to be an infrequent defect, while the flaked areas on the Duolite were more characteristic of the sample viewed.

3.4.1.2 Size Classification by Wet Screening

Size classification of commercial −20 +50 mesh resins has been by wet screening with a large recycle of water through a 0.46-m-diam (18-in.) screen separator. The resin as received is like wet sand or sawdust and does not screen efficiently. Dried resin tends to blind screens badly. By using about 15 liters/min of water recycle and a coarser scalping screen to reduce the load on the first primary screen, the 0.46-m-diam separator can be operated with up to 14 liters (0.5 ft^3) of resin per hour.

We have seen detectable differences between the size distributions of different lots of Amberlite IRC-72. Typical yields are tabulated for standard resins (Table 3.2). Improvements would be expected if batches were optimized for our use. We have most commonly used a 710 ± 80 μm size range of sodium-form Amberlite IRC-72, which is a

Table 3.2. Size Fraction Yields for Commercial −20 +50 Mesh Resin

Resin and Manufacturer's Lot	Data from Wet Screening				Batch Volume	
	Mean Diam (μm)	Yield, Vol %, for Various Sizes			(liters)	(ft^3)
		−24 +32 750 μm ± 16%	−26 +32 710 μm ± 11%[a]	630 μm ± 8% 625 ± 50 μm[b]		
Amberlite IRC-72						
2-5612	820	24	14	10	560	20
2-5990[c]	660	30	20	18	140	5
2-5990[d]	680	24	16	11	225	8
2-6633	830	20	13	9	140	5
Duolite C-464						
05-03-4E	830	20	13	9	170	6

[a]710-μm Na^+-form resin loads 60×10^{-6} g U/kernel.

[b]625-μm Na^+-form resin loads 40×10^{-6} g U/kernel.

[c]Screened October 1974.

[d]Screened July 1975. Not combined with October 1974 screening because of different size classifications.

±11% range. The size distributions indicate about 20% yields in this range. Table 3.2 values are from straight lines drawn through the data points on a logarithmic probability chart. The quantities are approximate since the lots had only four size classifications (i.e., three data points). Duolite C-464 resin has been delivered as 700, 720, and 800 μm in diameter; these lots have been more than 90% within ±50 μm in diameter.

3.4.1.3 Drying and Shape Separation

Following the size classification by wet screening, the resin is dried, screened, and then shape separated to remove nonspherical beads. Shape separation requires that the resin be dried. Methods of drying that have been tested include: rotary drum, microwave, fixed bed, fluidized bed, and spouting bed.

Two batches, each 70 liters (2.5 ft^3), were dried at an industrial test laboratory in a jacketed, rotating cone-blender vacuum dryer. Heat transfer was very poor because a 6-mm-thick (1/4-in.) cake of porous dried resin formed on the heated surfaces. This cake was not due to heat transfer alone, as a similar undried layer also coated the unheated

flange. The overall result was unacceptable, both from the long drying time and excessive crusting or clustering of the dried product.

Drying tests using 2-liter batches of sodium-form resin in a 2-kW 2450-MHz microwave oven were conducted. Microwave drying was unacceptable because the resin continued to absorb the energy after it had become dry. Drying was not uniform and some resin charred.

Static bed drying with room-temperature and heated air was also investigated. The fixed-bed dryer permits the resin to form a large, lightly sintered mass according to the geometry of the vessel. Agitation of the clumped mass does not completely break the clusters into individual beads.

A small rental test unit was operated to evaluate fluidized-bed drying. The final product when the inlet air temperature was 80°C looked good for dry shape and size separations. The fluidization showed large variations as drying proceeded. The drained, wet resin showed a type of slugging fluidization with irregular gas bubbles. After drying was partially complete, this changed to a spouting bed with a fountain from a hollow core and downflow in an annulus around the spout. As drying continued, the resin beads became immobilized as one large porous cake. Finally, this cake suddenly broke up into individual dry resin particles that again showed a slugging fluidization.

A 0.46-m-ID (7-in.) spouting bed contactor was fabricated from Pyrex glass and tested. The resin beads become immobilized as a large cake with the spout as a hole in the middle. The fluidized bed unit is preferred over the spouting bed as the drying can be continued until the cake disintegrates and fluidization resumes. The dried resin is screened to remove any fines released during the drying and also to break up or remove any remaining clusters.

The shape separator used to remove the nonspherical beads is a flat-plate vibratory feeder. The polished plate is tilted slightly downward and parallel to the vibratory action and tilted also 90° to this direction. This type of shape separator has been used with coated particles.[12]

A five-nozzle feeder plate [0.18 × 0.76 m (7 × 30 in.)] has been fabricated and is being tested (Fig. 3.2). The spherical particles are

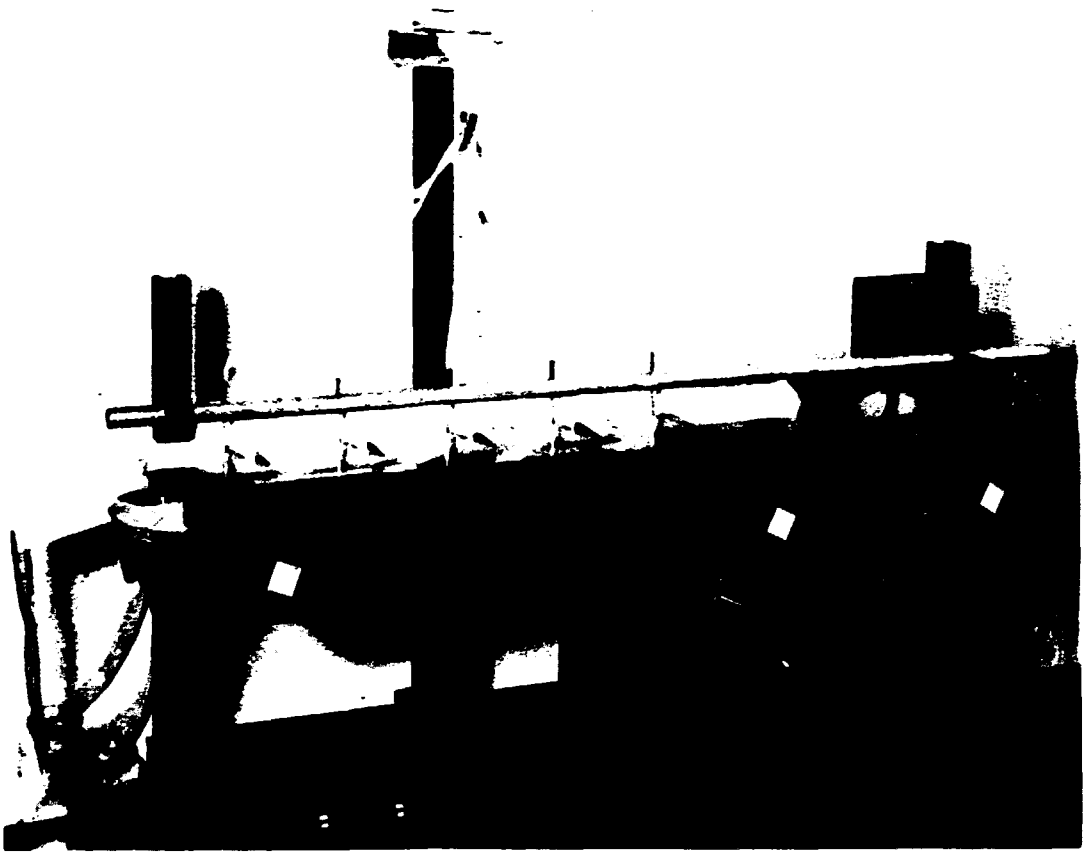

Fig. 3.2. A Prototype Five-Unit Shape Separator.

seen traveling diagonally across the plate. The vibratory action is parallel to the long axis of the plate. The vibration and slope move the nonspherical particles along the axis of vibration. The spherical particles roll according to the tilt; that is, downhill, with little effect from the vibration. A parametric study of tilt angles, magnitude of vibration, flow rate, and plate surface finish is under way.

Small-scale runs of shape-separated dried sodium-form resin before loading showed that the reject rate after loading and drying was on the order of 0.3 wt %. When no shape separation of the sodium-form resin was made, typical reject values of the loaded resin were 10 wt %, with values as low as 8 wt % and as high as 17 wt % for some batches.[13]

3.4.1.4 Resin Feed Preparation Facility

Procurement, fabrication, and installation are in progress for a resin feed preparation facility in Building 3503. The operations will be carried out as follows:

1. wet screening with a 0.76-m-diam (30-in.) screen separator to reject oversize and undersize resin particles,
2. drying of the sodium-form resin at about 80°C in air in a package fluidized bed dryer [82 liter (2.9 ft^3) maximum charge volume],
3. dry screening to reject large clusters and fines released during drying,
4. shape separation in multiple units (see Sect. 3.4.1.3),
5. complete conversion of rewetted resin to the hydrogen form with nitric acid, and
6. storing and metering of prepared resin to supply batches for uranium loading.

The minimum initial capacity required is to process 0.14 m^3 (5 ft^3) of resin per week and the final capacity for TURF operation may be an input of 0.7 m^3 (25 ft^3) of resin per week. The shape separation equipment will initially have the smaller capacity, with later addition of multiple units. The other components are sized for intermittent operation of oversized units, as this is more economical than more continuous operation of smaller units.

3.4.2 Resin Loading Flowsheet Development — J. H. Shaffer, P. A. Haas, J. P. Drago, R. H. Rainey, and D. A. Costanzo

The resin loading reaction is an exchange reaction, which can be written as follows, where R represents the carboxylic acid cation resin and the resin is in the hydrogen (HR) form:

$$2HR + UO_2^{2+} \rightleftharpoons UO_2R_2 + 2H^+ . \qquad (1)$$

Metal forms of the resin such as NaR or MgR_2 are not acceptable, as unexchanged metals remain as unacceptable impurities in the carbonized product. The ammonium form is a possible alternate, as any NH_4^+ in the loaded resin should be volatilized during carbonization. The exchange of UO_2^{2+} with the hydrogen form of the resin [Eq. (1)] reaches equilibrium

at low H^+ concentrations, and high loadings of uranium are possible only when the H^+ is removed by some other reaction. The initial development of loading flowsheets for the carboxylic acid resins was by addition of UO_3 to react with the H^+ and give acid-deficient uranyl nitrate solutions.[11,14] The continued development of resin loading flowsheets included determination of equilibrium and kinetic data for exchange reactions, correlation of the properties of acid-deficient uranyl nitrate solution, and evaluation of alternate loading flowsheets.

3.4.2.1 Equilibrium of Uranyl Nitrate Solutions with Carboxylic Acid Cation Exchange Resins

The HTGR Fuel Refabrication Pilot Plant will use batch loading of weak-acid resin particles from a flowing stream of acid-deficient uranyl nitrate solution. The effluent stream will be partially denitrated by solvent extraction and concentrated by evaporation for recycle with the feed solution. Measurements of equilibrium constants for the resin loading reactions are needed for engineering design and for establishing process parameters required for quality control of the product. Experimental results were obtained at a reaction temperature of 30°C on Amberlite IRC-72 and Duolite C-464 ion exchange resins as part of a systematic study of this process.

The various tests required for this study were conducted as small batch loading operations in which the uranyl ion concentration was varied with respect to fixed nitrate ion concentration and resin volume. Similar tests at different nitrate ion concentrations were conducted to examine the effect of nitrate ion concentration on the resin loading process. Experimental results were derived from chemical analysis on resin and solution samples, from pH measurements on the solution at reaction temperature, and from material balance data.

Resin loading with divalent uranyl ion was expressed as reaction (1). The equilibrium quotient, K_Q, was determined by linear regression analysis of the experimental data according to the equation

$$\ln [a^*_{H^+}]^2/[UO_2^{2+}] = \ln [HR]^2/[UO_2R_2] + \ln K_Q \ .$$

Concentration terms for the resin phase were arbitrarily expressed as moles of uranium and hydrogen ion per liter of wet resin in hydrogen form. Aqueous uranyl ion was expressed as molar concentrations, and approximate hydrogen ion activities were calculated from pH measurements using a Corning semimicro combination electrode standardized at pH = 2 with certified KCl-HCl buffer solution. Typical results obtained from these analyses for Amberlite IRC-72 resin are shown in Fig. 3.3. Equilibrium quotients obtained on this resin together with uncertainty limits at 95% confidence are shown in Table 3.3. Corresponding values obtained for Duolite C-464 resin are also shown in Table 3.3. The most probable error in these determinations was recognized as the actual capacity of the resin aliquot used in each test. Accordingly, this value was treated as an adjustable parameter in the least squares evaluation. The data presented in the table reflect resin loading capacities of 3.18 ± 0.07 equivalents per liter for Amberlite IRC-72 and 2.74 ± 0.14 equivalents per liter for Duolite C-464.

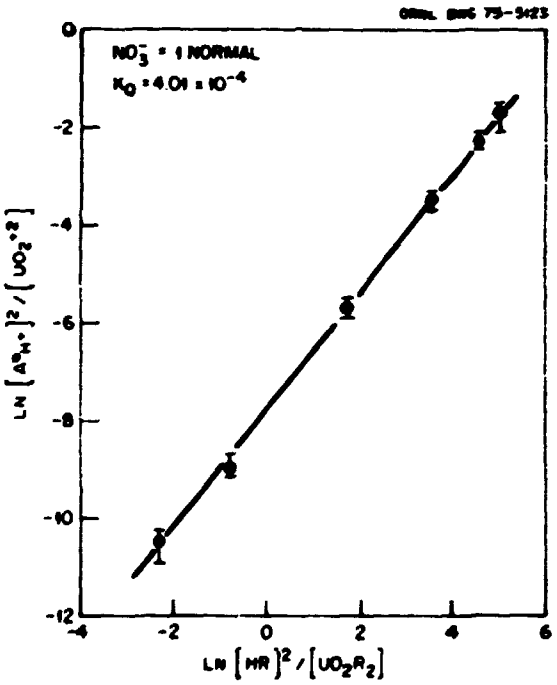

Fig. 3.3. Equilibrium Distribution of Reactants During Loading of Amberlite IRC-72 with Uranium From Uranyl Nitrate Solution at 30°C.

Table 3.3. Values for Equilibrium Quotients Calculated for the Uranium Loading of Carboxylic Resin from Uranyl Nitrate Solution at 30°C

Nitrate Ion (N)	K_Q	Limits on K_Q	
		Upper	Lower
	Amberlite IRC-72		
0.2	1.8×10^{-4}	3.0×10^{-4}	1.1×10^{-4}
0.6	2.6×10^{-4}	3.2×10^{-4}	2.0×10^{-4}
1.0	4.0×10^{-4}	5.0×10^{-4}	3.2×10^{-4}
1.6	1.4×10^{-3}	1.8×10^{-3}	1.0×10^{-3}
2.0	2.9×10^{-3}	4.6×10^{-3}	1.8×10^{-3}
2.5	8.7×10^{-3}	1.8×10^{-2}	4.2×10^{-3}
	Duolite C-464		
0.2	3.0×10^{-4}	4.8×10^{-4}	1.9×10^{-4}
0.6	5.6×10^{-4}	1.3×10^{-3}	2.5×10^{-4}
1.0	9.7×10^{-4}	2.0×10^{-3}	4.7×10^{-4}
1.6	2.7×10^{-3}	7.3×10^{-3}	9.8×10^{-4}
2.0	3.7×10^{-3}	6.2×10^{-3}	2.2×10^{-3}
2.5	1.2×10^{-2}	1.9×10^{-2}	7.2×10^{-3}

The similar chemical behavior of Amberlite IRC-72 and Duolite C-464 resins in the exchange reaction is illustrated in Fig. 3.4. The effects of nitrate ion concentration on values for the equilibrium quotients, as noted in Table 3.3, are also shown as a continuous function over the range 0.2 to 2.5 N NO_3^-. Although this behavior may be assigned to current concepts of hydrolysis in uranyl nitrate solutions, a quantitative evaluation could not be achieved. Further examination of these effects will be made as descriptions of the equilibria at higher temperatures are obtained. These experiments at 40 and 50°C are in progress.

3.4.2.2 Resin Loading Kinetics

Development of the resin loading process for the HTGR Fuel Refabrication Pilot Plant is based on batch contacting of commercially available weak-acid cation exchange resin (hydrogen form) with uranyl nitrate feed solution. Process control parameters will be based on measurements of

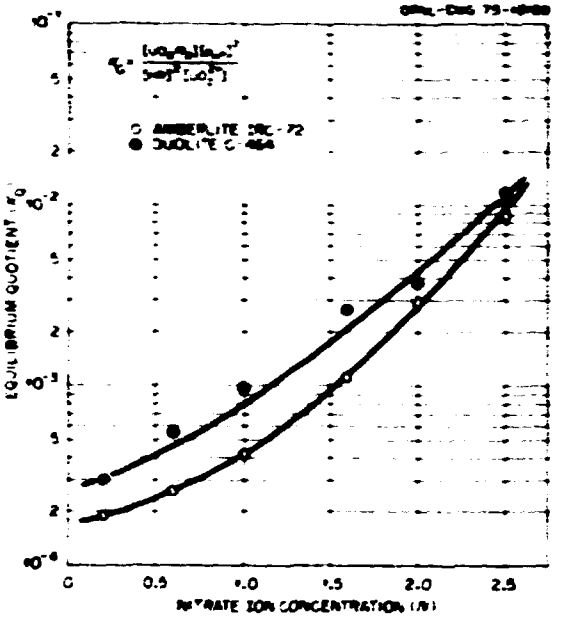

Fig. 3.4. Effect of Nitrate Ion Concentration on the Equilibrium Quotient for Loading Weak-Acid Resin from Uranyl Nitrate Solution at 30°C.

uranium content and solution acidity (pH) of the aqueous feed and effluent streams and related to the status of resin loading by comparison with data obtained from prior measurements of reaction equilibria. The contact period is planned to ensure uniform diffusion of uranium into the spherical resin beads. Since process parameters that affect the kinetics of the resin loading exchange reaction could have a direct effect on the time allotted for the loading cycle, an experimental program was started to evaluate relative reaction rates under simulated process conditions.

The reaction vessel, for experiments conducted thus far, was a small jacketed column constructed from a 250-ml glass buret that was fitted with a porous glass plate for retention of the resin. The column was loaded with selected volumes of sized Amberlite IRC-72 resin in its hydrogen form. Uranyl nitrate stock solutions were prepared at three concentrations (0.58, 1.15, 1.8 N NO_3^-) by saturation with solid UO_3 at room temperature. The feed solution for each test was filtered from the corresponding stock solution just before use and was sampled for chemical analysis of uranium and nitrate ion contents. For experimental expedience,

the feed solution was fed downflow through the resin bed at a controlled flow by means of a finger pump. The column effluent was continuously monitored for acidity by measurements of pH and was sampled at periodic intervals for chemical analysis of its uranium and nitrate ion contents. The reaction temperature was maintained constant at 30°C by recirculating water from a thermostatic bath through the outer annulus of the column and through a heat exchanger on the feed stream.

Although mathematical correlation of the data is incomplete, preliminary examination of the data show that the reaction rate depends strongly on the mass flow rate of uranium in the system. The existence of a concentration gradient of uranium through the bed during loading was recognized; however, this condition will also prevail in the engineering-scale process. Flow conditions were chosen to yield rapid breakthrough of uranium into the column effluent. The data were calculated as average bed concentrations, and the effect of bed depth was treated as a separate process parameter.

Expressions of the experimental data according to conventional rate equations indicate that the loading process follows a complex order. The reaction rate is initially controlled by the feed rate, followed by second-order concentration dependence and then by an apparent diffusion process. Since this latter process will regulate the uniform dispersion of uranium in the resin particle and, consequently, directly affect quality control of the product, a more refined experimental technique is under development to better characterize this phase of the resin loading process. This experimental technique will examine the loading characteristics as functions of uranyl nitrate concentration and particle diameter. The data should also provide a direct measure of uranium loading per resin particle rather than average batch concentrations.

3.4.2.3 Drying of Uranium-Loaded Resin

The uranium-loaded resin is dried to simplify handling and transfer and to meet the requirements for the carbonization feed. The uranium-loaded Asbetlite IRC-72 contains 25 to 30 wt % water when drained briefly on a filter or screen. Our drying results are expressed in loss on drying (LOD) in weight percent when resin is dried to approximate equilibrium

in ambient air at 110°C; that is, material already dried to 110°C in air has 0 wt % LOD. Some of the water is chemically bonded or absorbed, so that zero LOD does not mean zero water content.

The optimum water content for uranium-loaded Amberlite IRC-72 appears to be 10 to 15 wt % LOD. Above 20% LOD, resin particles stick together from the effects of moisture. Low LODs were initially preferred to minimize the introduction of water into the carbonization off-gas system. But uranium-loaded resin dried to less than 10% LOD shows detectable static charge effects, which were very troublesome for 0 to 2% LOD. The addition of graphite powder to coat the resin can alleviate the charge effects, but less complete drying to leave 10 to 15% LOD is preferred.

Uranium-loaded Amberlite IRC-72 in equilibrium with ambient air will generally show 11 to 13% LOD. Water present in the samples with LOD of greater than 13% is easily removed and probably fills large pores in the resin. The loaded resin dried to about zero LOD at 110 to 120°C will produce steam when added to water; this indicates water of hydration or chemical reaction.

3.4.2.4 Steam Stripping of Nitric Acid from Molten Uranyl Nitrate

Partial thermal denitration of uranyl nitrate, or a steam stripping of nitric acid from molten uranyl nitrate, was considered as an alternate process for producing the acid-deficient uranyl nitrate solution. Thermal denitration to UO_3 can be completed at 300°C. Excess nitric acid (for NO_3^-/U ratios greater than 2) can be distilled from boiling uranyl nitrate solutions. The proposed process at temperatures intermediate to the preceding operations would result in the following overall reaction:

$$2UO_2(NO_3)_2(aq) + H_2O \rightarrow 2UO_2(OH)_{0.5}(NO_3)_{1.5}(aq) + HNO_3\uparrow \quad . \qquad (2)$$

The steam denitration would have the following advantages over the other processes for providing acid-deficient solutions:

1. The flowsheet requires fewer or simpler equipment components than either solvent extraction of nitrate or the complete thermal denitration to UO_3.

2. It does not require in-cell use of a flammable solvent.

3. The uranium-free nitric acid is an optimum form of nitrate waste.

The steam denitration process was investigated in two types of test systems. Batch or semibatch laboratory studies were carried out in glass equipment. Then the process was tested in a stainless steel, natural convection evaporator loop operated with 20 to 100 ml/min uranyl nitrate solution feed and a continuous discharge of the product (Fig. 3.5).

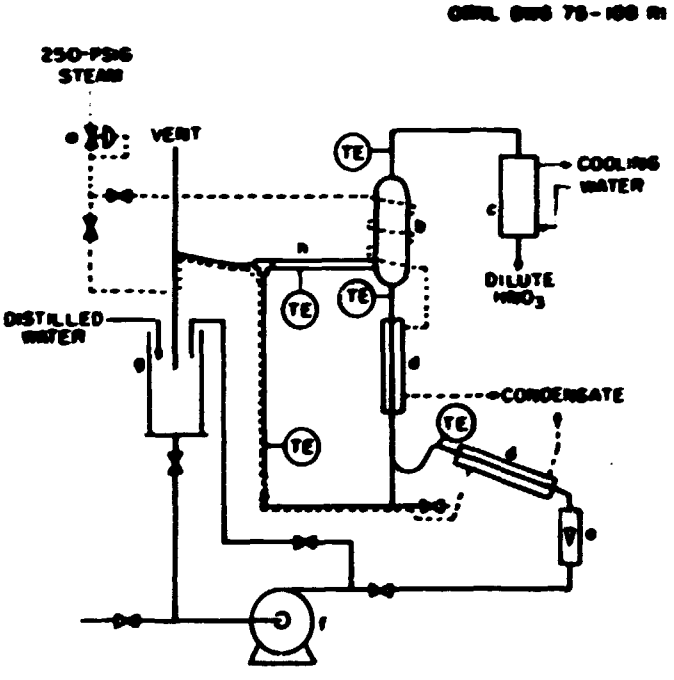

Fig. 3.5. Thermal Denitrator (Steam Stripping of HNO_3) for Uranyl Nitrate Solutions. Multiply dimensions by 25.4 to convert to millimeters.

The preparation of acid-deficient uranyl nitrate by a steam stripping or partial thermal denitration process is not as simple as had been hoped initially. High uranium concentrations and boiling points above 140°C are required to give useful acid deficiencies. As the NO_3^-/U ratio is reduced, UO_3 precipitates, and the process produces a slurry of UO_3 in uranyl nitrate. The conditions that result in precipitation are uncertain; however, no precipitation was observed for NO_3^-/U ratios of 2.0, but precipitate was present in solutions with NO_3^-/U ratios of 1.9 or slightly lower. Although the UO_3 dissolves easily when agitated in diluted uranyl nitrate solutions at 50 to 80°C, it can settle and be difficult to resuspend.

The nitric acid concentrations in the condensate decreased rapidly with decreases in the feed solution NO_3^-/U ratios; the condensate was 0.05 to 0.20 *N* HNO_3 for the most likely process conditions. Therefore, operation to produce lower NO_3^-/U ratios is more difficult as a result of slower removal of nitrate and more precipitation of uranium. When the feed solution had a NO_3^-/U ratio of 1.75, the exit solution had a higher ratio as a result of more removal (by precipitation) of uranium than removal of nitrate via the condensate.

The molten uranyl nitrate did not create any significant operating difficulty from freezing or during dilution after discharge. The steam trace line along the discharge line was to a feed preheater and was not used during most of the test operation. Insulation was removed from the vertical length of tubing below the overflow tee. The molten salt from this discharge dropped into the center of the uranyl nitrate solution tank and was cooled and diluted without any visible accumulations. Samples taken in glass bottles solidified slowly (30 min to 2 hr), apparently because of supercooling and slow crystallization. Circulation after shutoff of steam was effective for dilution, and there were no signs of plugging at the next startup when this shutdown procedure was followed.

A fine, opaque, orange-red slurry of iron precipitate appeared suddenly as the convection loop was operated at higher (148°C steam) temperatures and a lower (slightly below 2.0) NO_3^-/U ratio than for

previous operation that did not result in a precipitate. Filtration of the solution resulted in collection of more than 5 times as much iron as was in the initial feed solution. Apparently, corrosion occurred during operation with NO_3^-/U ratios of 3.3 to 2.1, and the iron precipitated during the next period of operation as a result of the higher temperature and/or the lower NO_3^-/U ratio. If this corrosion occurred over the whole loop, it would correspond to an average rate of about 0.2 in. (5 mm) per year. If corrosion occurred only in the heater, it would correspond to an average rate of about 1 in. (25 mm) per year. The conditions that might give excessive corrosion would necessitate additional investigation or a more corrosion-resistant construction material would be required if this process were used.

Measurements of the density and pH of the solution samples provided excellent process control for the solvent extraction process that was used for preparation of acid-deficient uranyl nitrate. These measurements were much less useful on diluted thermal denitration samples. The effects of uranium precipitation during the tests, followed by dissolution during circulation at the end of test operation, were noticeable as density increases and pH decreases. The pH of a freshly quenched and diluted sample was anomalous and indicated higher NO_3^-/U ratios than chemical analyses or measurements of aged samples. This probably resulted from slow hydrolysis reactions, which were incomplete in the short time required for cooling and diluting the molten uranyl nitrate.

The initial resin-loading flowsheets for the carboxylic acid cation exchange resins were batch flowsheets that used UO_3 to provide acid-deficient uranyl nitrate.[11,14] This type of batch operation could be used with partial thermal denitrations to prepare batches of UO_3 slurry from uranyl nitrate.

In summary, steam stripping of nitric acid or partial thermal denitration of uranyl nitrate produces a dilute (<0.2 %) nitric acid condensate and a slurry of UO_3 in molten, slightly acid-deficient uranyl nitrate. This UO_3 will redissolve in diluted uranyl nitrate at temperatures below 100°C to produce highly acid-deficient uranyl nitrate. No difficulties resulted either from freezing of the molten uranyl

nitrate or during dilution after discharge. Excessive corrosion of stainless steel occurred, but this might not be a problem if high NO_3^-/U ratios were avoided.

3.4.2.5 Loading from UO_2^{2+}-NH_4^+-NO_3^- Solutions

Our consideration of resin-loading flowsheets for ^{233}U recycle had been limited to loading solutions with uranyl and hydrogen as the only significant cations. The ammonium forms of the carboxylic acid resins appear to be the only attractive alternative to the hydrogen forms. The advantage to using the salt forms of the resins is the more favorable chemical equilibriums for exchange with uranyl salts. The reaction of the hydrogen form of the resin with a uranyl salt reaches equilibrium at low H^+ concentrations, and high loadings of uranium are possible only when the H^+ is removed by some other reaction. The equilibrium for ammonium or monovalent metals (Li, Na, K, etc.) allows much higher completion of the exchange reaction than does H^+; many divalent metals (e.g., Mg^{2+}) probably have more favorable equilibriums for loading than H^+. None of the metals are acceptable as impurities in the carbonized product nor do they volatilize out during carbonization. The flowsheets that would ensure low metal contents (other than uranium) in the loaded resin are inefficient, either from the viewpoint of complexity, incomplete utilization of uranium with a metal-uranium waste recycle solution, or an excessive sacrifice of uranium content in the loaded resin. Any NH_4^+ in the loaded resin should be volatilized during carbonization. One limit placed on NH_4^+ content is the amount that results in a significant reduction in uranium loading; should the formation of uranium nitrides occur, it would be objectionable.

The studies reported here were for a limited evaluation of flowsheets involving NH_4^+ for use with $^{233}UO_2(NO_3)_2$ in the recycle pilot plant. They were prompted by General Atomic reports of good results that were obtained by using the ammonium form of Duolite C-464 resin.[15] We had previously investigated the use of ammonium-form resins for loading from uranyl nitrate solutions.[16]

Acceptable loaded compositions using two carboxylic acid resins are possible with UO_2^{2+}, H^+, and NH_4^+ present as cations. The flowsheet conditions must be carefully selected and controlled to deal with two limitations. The loading of UO_2^{2+}, as compared with NH_4^+, is only moderately favorable; therefore, the loading process must be staged to give favorable (nigh) UO_2^{2+}/NH_4^+ ratios in equilibrium with the product resin. Significant decreases in uranium loadings occur for solution NH_4^+/UO_2^{2+} mole ratios greater than 0.5. The other limitation is that unacceptable precipitation of uranium occurs for conditions close to those necessary for good uranium recoveries and loadings. These two limitations control the conditions tested and the results observed.

The resins in the ammonium form (100% NH_4R, where R indicates the carboxylic acid cation resin) hydrolyze to give pH >10 in demineralized water; therefore, precipitation is very likely, and perhaps certain, when the feed resin is all in the ammonium form (100% NH_4R). For Amberlite IRC-72 resin, the hydrolysis of NH_4R proceeds faster than the loading of the UO_2^{2+}; this results in precipitation of uranium even though the final overall equilibrium would not give precipitated uranium. The two-stage flowsheet using Amberlite IRC-72 in the ammonium form, and $UO_2(NO_3)_2$-NH_4NO_3-NH_4OH solution as the feed, appears impractical. Precipitation of uranium in solution can be avoided for the same flowsheet using Duolite C-464. Radiographs of one product resin show density variations consistent with the presence of precipitated UO_3 inside the resin. This would be expected, since the pH must vary in some continuous manner from the solution pH below 3.0 to above 7.0 inside the resin sphere for resin of >90% NH_4R.

Analyses of dried resin products for NH_4^+ confirm that the loading of UO_2^{2+} in composition with NH_4^+ is not highly favorable. The mole ratios U/NH_4^+ for the four resin products were 4 to 8, and the ratio of $(U/NH_4^+)_{resin}/(U/NH_4)_{solution}$ is only about 10. The NH_4^+ analyses for the three-stage loadings with NH_4OH are in reasonable agreement with the difference between the expected capacity and the uranium loadings; that is $UO_2^{2+} + NH_4^+$, in millequivalents per milliliter, approximately equals the expected total capacities. For the runs with NH_4-form resin

feed, these totals are larger and are in agreement with the presence of precipitated uranium inside the resin particles. Samples of carbonized resin show about 200 ppm N, compared with about 30 ppm N for resin loaded without NH_4^+ in the uranyl nitrate solution.

Acceptable recoveries of UO_2^{2+} from NH_4NO_3 solutions occurred only for final solution pH values of 4.5 to 6, or for resins that were 20 to 40% in the ammonium form. For tests with Amberlite IRC-72, 19% and 10% NH_4R were present with uranium in the solution, while 34% and 21% NH_4R resulted in acceptable recoveries of uranium. For tests with Duolite C-464, the first-stage material balance indicates about 50% NH_4R in the product resin, but this may be more than the fraction required for good uranium recovery. At the preferred final pH values, the solubility of uranium is low, thus allowing good recovery of uranium.

The addition of NH_4OH to agitated resin-solution appears preferable to use of resin feed in the ammonium form. If the solution-resin reactions are reversible (approach equilibrium), either procedure can give the desired results, and the control of NH_4OH addition provides a more positive control of the end condition. The process is less controllable if irreversible reactions occur, and irreversible precipitation must be avoided. The use of the ammonium-form resin involves three adjustments of composition (washing resin to a reproducible ammonium content and two solution pH adjustments). The optimum solution pHs depend on the UO_2^{2+} and NH_4^+ concentrations and may be more difficult to determine than the optimum pHs for NH_4OH addition with the resin present. As compared with use of NH_4R, addition of NH_4OH to the solution-resin mixture allows better process control to avoid either precipitation of uranium or loss of soluble uranium.

The dried uranium-loaded product resins for the flowsheets involving NH_4^+ showed several differences from the products for reference flowsheets without NH_4^+. The two-stage loadings using NH_4R resin feed gave 0.95 to 0.98 of the reference uranium contents. The three-stage loadings using NH_4OH additions gave 0.93 or 0.95 of the reference uranium contents. The products from NH_4R-form resin feed showed some cracking, which did not occur in the reference products or in HR-form resin with NH_4OH additions.

Radiographs of products showed a high-density outer shell (outer 20% of radius) for Amberlite IRC-72 in the NH_4R form as resin feed. Other products did not show any density shell effects, but the technique used would not reveal gradual density variations.

3.4.2.6 Loading of Weak-Acid Ion Exchange Resin with ^{233}U

Fuel refabrication plants for HTGRs will use ^{233}U as the recycle fuel. Head-end reprocessing of the spent fuel elements will provide for the separation of ^{233}U from thorium and fission products and for its purification as a uranyl nitrate feed solution of a fuel refabrication plant. This ^{233}U will be radioactive, both from its own decay chain (mainly alpha) and from the decay chain of ^{232}U (alpha plus gamma). As part of the chemical development of the resin loading process, laboratory demonstrations with ^{233}U were desired to verify the application of techniques used for routine resin loadings with both normal uranium and with highly enriched ^{235}U. Initial loadings were conducted in a glove box with ^{233}U containing less than 10 ppm ^{232}U (to avoid high gamma-ray activities encountered with higher ^{232}U contents). With respect to radiation-induced degradation of the resin material and oxidation state of the uranium, these glove box tests provided an evaluation of the short-term effects of increased alpha activity on the resin loading process. A subsequent hot cell test was conducted to examine short-term effects of radiation using aged ^{233}U having a ^{232}U content of 250 ppm at equilibrium with decay products.

The experimental procedure used in all tests followed the method of UO_3 addition to a mixture of the resin (in hydrogen form) and dilute nitric acid.[11] The UO_3 addition was calculated to yield an acid-deficient uranyl nitrate solution in equilibrium with the fully loaded resin. Since ^{233}U (<10 ppm ^{232}U) was available as a nitrate solution plus free nitric acid, an initial preparation of solid UO_3 was necessary. The ^{233}U (250 ppm ^{232}U) was available as an impure oxide and also required precipitation from nitric acid solution for purification and preparation of UO_3. The resin was loaded at about 70°C to increase the dissolution rate of the solid UO_3. Ambient temperatures were used for prolonged

equilibration periods. Following the loading reaction, the supernatant was removed by filtration. The loaded resin product was washed free of excess uranyl nitrate with water and dried with forced air at 110°C to a free-flowing state.

In an earlier experiment with ^{233}U (<10 ppm ^{232}U), uranium [presumably as hydrous U(IV) oxide] precipitated during the resin loading reaction.[16] Since this effect was absent in preparations with both normal uranium and highly enriched ^{235}U, radiation-induced reduction of the hexavalent uranium ion was a possiblity. Consequently, these additional tests were conducted to determine resin loading conditions to preclude uranium reduction. The glove box experiments were designed to evaluate the effectiveness of an oxygen sparge in preventing the reduction of hexavalent uranium during the resin loading process. Saturation with oxygen was begun on an aqueous suspension of the Amberlite IRC-72 resin in its hydrogen form and continued during additions of nitric acid and solid UO_3 and until the exchange reaction was complete. No evidence of extraneous precipitation of uranium was observed. A repetition of this experiment with an air sparge in place of oxygen also failed to yield any evidence of uranium reduction. Additionally, the loaded resin remained quiescent in the aqueous exchange media without air sparge for three days without visible alteration or discoloration of the resin or the uranyl nitrate solution. A third experiment was conducted without gas sparge as a duplication of the original resin-loading operation. Again, there was no evidence of reduction of uranyl ion or any detectable evidence of extraneous precipitation. In each experiment, chemical analyses of the dried resin product showed typical values for full loading with uranium.

From these results, alpha activity associated with ^{233}U does not detectably introduce short-term degradation of either the ion exchange resin or the uranyl nitrate solution during the resin loading process. Observations of extraneous precipitation noted in the original experiment could not be reproduced following the established resin-loading procedure. Because of the difficulty in preparation of UO_3 by peroxide formation and thermal decomposition in the glove-box facility, the observed

irregularities of the original experiment were assigned to that operation – possibly to the production of U_3O_8 at localized high temperatures during the peroxide decomposition step.

To further substantiate this conclusion and to examine resin loading at higher radiation levels, an experimental loading was made with aged ^{233}U, which contained approximately 250 ppm ^{232}U in equilibrium with decay products. A hot-cell enclosure was required for the experiment with about 30 g of ^{233}U to attenuate gamma rays associated with the decay product ^{208}Tl. Operations were performed with master-slave manipulators. Inspection of the resin loading process used photographs taken through the cell periscope. As in the previous experiments, there was no detectable evidence of uranium precipitation nor of resin degradation, and the resin was loaded to its normal capacity.

Although ^{233}U having higher ^{232}U contents (about 500 ppm) is anticipated for the HTGR Fuel Refabrication Plant, gamma-ray intensities will be reduced by separation of decay products just before the resin loading operation. Thus, the results observed from this hot cell experiment probably do not require further verification. An experimental program will continue to investigate possible adverse radiation effects on the organic amine used for nitrate extraction in the reference process and to provide resin product for evaluation during carbonization and coating of the fuel kernels at elevated temperatures.

3.4.3 Resin Loading Equipment Development – J. P. Drago and P. A. Haas

The reference flowsheet for resin loading with amine extraction of nitrate can be integrated into an efficient system for conversion of purified $^{233}UO_2(NO_3)_2$ solution into loaded resin (Fig. 3.6). The nitrate extraction, amine regeneration, and resin loading steps of Fig. 3.6 were demonstrated with a system assembled from components of earlier process development programs.[17] A complete system for preparation of acid-deficient uranyl nitrate, loading of resin, and drying of resin must be operated before final design of hot pilot plant equipment can be accepted. This must provide information with respect to remote operation, control of criticality, material accountability, and interaction

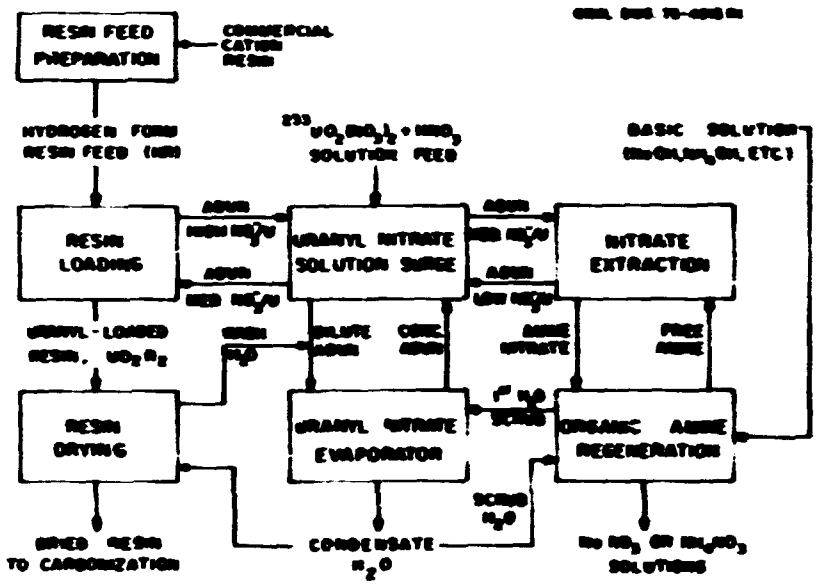

"ADUN" INDICATES ACID-DEFICIENT URANYL NITRATE ($NO_3/U<2$, MOLES/MOLE)

Fig. 3.6. Schematic Reference Flowsheet for Resin Loading.

of individual operations; such information is not available from the initial individual items used for flowsheet development. The equipment development studies include both the testing of individual components and the operation of part or all of the integrated system.

3.4.3.1 Demonstration of Amine Extraction

Acid-deficient uranyl nitrate solution can be produced by solvent extraction of the nitrate using liquid organic amines. Similar processes have been used for the preparation of oxide sols from thorium and uranium nitrate solutions.[18,19] The amine nitrate is contacted with basic solutions (Na_2CO_3, NaOH, or NH_4OH) to regenerate free amine for reuse, and the nitrate is discharged in the form of waste solutions containing $NaNO_3$ or NH_4NO_3. By adding an evaporator to remove water (Fig. 3.6) a highly efficient conversion of the purified $^{233}UO_2(NO_3)_2$ solution to loaded resin is possible.

The nitrate extraction, amine regeneration, and resin loading steps were demonstrated (Fig. 3.7) without provision for the removal of water

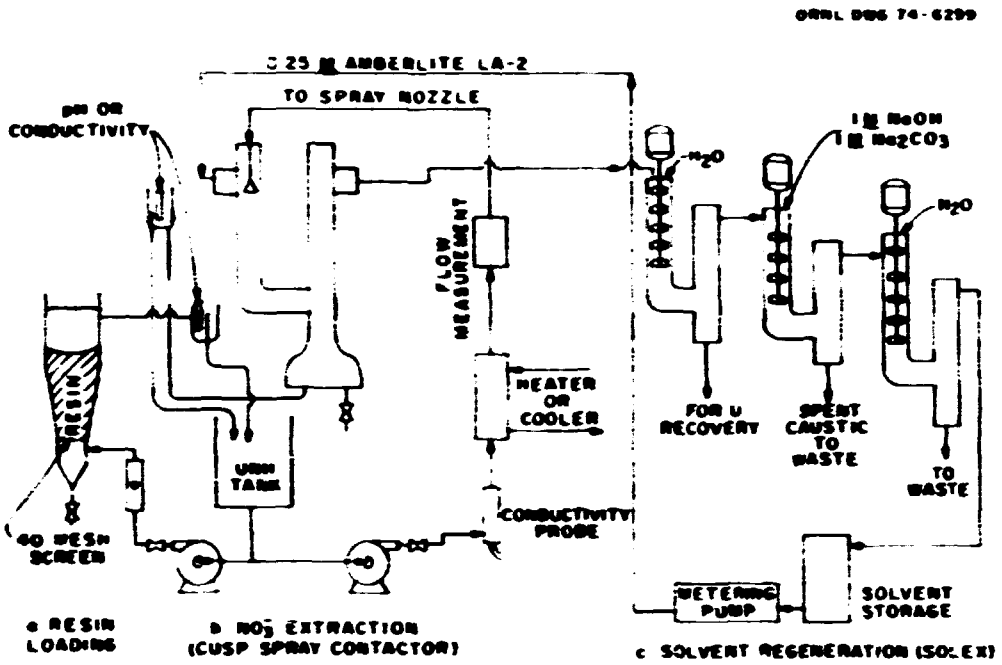

Fig. 3.7. Test System for Nitrate Extraction and Resin Loading.

by evaporation; thus the volume of uranyl nitrate solution increased as feed solution was added. The experimental studies[17] were made to obtain results for an integrated system with a minimum of equipment or chemical flowsheet development. Each of the equipment components had been operated for similar purposes in other flowsheets. The extraction of nitrate from uranyl nitrate had been studied previously in laboratory equipment.[20] The regeneration of Amberlite LA-2* secondary amine had been included as part of sol-gel demonstration runs.[18,19] The loading of resin with uranium from acid-deficient uranyl nitrate solutions that were 0.2 to 0.6 *M* in NO_3^- had been investigated in earlier studies.[11]

The conditions previously found to be satisfactory for the other flowsheets were applied to the resin loading demonstration without any systematic optimization of variables. The conclusions from this report[17] are as follows:

---

*Trademark of the Rohm and Haas Company.

A step in which nitrate is extracted by a liquid organic amine can be integrated into an attractive flowsheet for preparing resin based HTGR fissile kernels containing ^{233}U. This step provides acid-deficient uranyl nitrate for an optimum loading of uranium on a carboxylic acid cation-exchange resin. Water is removed as condensate from an evaporator, and the amine nitrate is regenerated to free amine by reaction with $NaOH-Na_2CO_3$ (or NH_4OH) solution to give wastes with low uranium losses.

The nitrate extraction, resin loading, and amine regeneration steps of the integrated flowsheet were demonstrated in 14 runs (Table 3.4) using components assembled from other developmental studies. All of the resin loading tests were completed as planned; no significant operating difficulties were encountered. Uranium that is extracted or entrained into the organic is easily recovered by a water scrub, which is returned to the uranyl nitrate solution tank. The process equipment components also demonstrated critically safe dimensions for the FRPP capacity of 4 kg of ^{233}U per batch.

The process is controlled via in-line pH measurements of inlet and exit solutions. The nitrate extraction is regulated so as to avoid NO_3^-/U mole ratios below 1.6 and thus prevent any precipitation of UO_3. The loading of resin is completed by maintaining favorable exit solution pH values for at least 1 hr. The dependability of in-line pH instrumentation needs to be demonstrated in a planned engineering-scale resin loading system.

Information was developed on pH values for uranyl nitrate solution vs NO_3^-/U mole ratios, resin loading kinetics, resin drying requirements, and other resin loading process information. It appears that 10 to 15 wt % water in the dried, uranium-loaded resin may be a preferred value since completely dried resin exhibits static charges which make handling and transfer more difficult. None of the other process information indicates any unexpected requirements or unusual difficulties.

3.4.3.2 Drying Uranium-Loaded Resin

Improved handling properties of uranium-loaded resin have been observed when the resin has a residual moisture content within the range 10 to 18 wt %. Methods of drying the loaded resin to a uniform and reproducible moisture content have been investigated. These methods are static bed, fluidized bed, and microwave dryers.

Uranium-loaded resin (approximately 8.5-liter batches) has been dried for routine product preparation in a dryer fabricated from a

Table 3.4. Loading of Natural Uranium on Amberlite IRC-72 Resin
Flowsheet: Reference via Amine Extraction of Nitrate

Run	Resin Feed		Loaded Resin			Final Solution			Loading Time (hr)
	Size (μm)	Volume (liters)	Weight (g)	U Content (wt %)	meq U / ml Resin	U Conc. (M)	pH	NO_3^-/U Mole Ratio	
RO1	Unsized	4.8	3,871	46.77	3.17	0.31	2.65	1.78	3.3
RO2	Unsized	7.05	5,392	46.26	2.97	0.32	2.60	1.81	2.5
RO3	Unsized	5.9	4,813	46.06	3.16	0.25	2.85	1.70	5.8
RO4	Unsized	6.7	5,430	46.03	3.13	0.17	3.05	1.67	4.7
RO5	590 ± 100	7.45	5,826	46.40	3.05	0.24	2.88	1.71	4.9
RO6	590 ± 100	7.35	5,954	46.87	3.19	0.23	2.94	1.70	5.8
RO7	590 ± 100	7.2	5,668	46.08	3.05	0.22	2.84	1.75	5.3
RO8	590 ± 100	8.1	6,335	47.83	3.17	0.21	2.90	1.70	4.5
RO9	590 ± 100	7.4	5,410	46.0	2.83	0.15	2.98	1.73	1.8
R10	590 ± 100	5.0	3,944	46.61	3.09	0.10	3.18	1.66	2.0
R11	560 ± 60	8.1	6,173	49.66, 49.96	3.18	0.22	2.88	1.74	3.7
R12	560 ± 60	8.5	6,394	49.57, 49.50	3.13	0.16	2.93	1.74	4.1
R13	560 ± 60	8.4	6,273	47.74	3.00	0.09	3.10	1.73	4.6
R14	560 ± 60	7.8	5,465	46.14	2.72	0.03	3.15	1.82	5.6

0.23-m-diam (9-in.) porous stainless steel filter frit. Both upflow and downflow of steam-heated air and downflow of room-temperature air have been tested.

For the initial requests for dry (LOD <5%) loaded resin, steam-heated air was the method of drying. Drying was approximately complete when the resin bed temperatures near the exit gas port approached the inlet gas temperature. The required gas flow per liter of uranium-loaded resin was about 10,000 liters. Times from 1 to 16 hr were observed, depending on the gas flow rate and the resin volume. The largest satisfactory upflow of air for the 0.23-m-diam dryer was 240 std liters/min. For higher flow rates, the air came through the bed as large gas bubbles, giving slugging fluidization. These bubbles carried resin particles out of the dryer, and the gas bubbles were probably not in equilibrium with the resin.

With respect to the residual moisture and uniformity requirements, this method of drying is unacceptable for the following reasons. The 0.23-m-diam dryer vessel is not critically safe for fissile fuel. The drying cycle time is too long. But most important, the drying of a large batch is not uniform, with almost complete drying near the gas inlet before the remainder of resin is dry enough to flow freely.

Fixed bed drying of loaded resin in this 0.23-m-diam vessel using downflow of room air at room temperature was also investigated. Samples of the dried, loaded resin at the top, middle, and bottom of an 8.6-liter batch showed LODs of 10.88, 11.04, and 10.98 wt %. Drying time was 48 to 72 hr. Although the uniformity is acceptable, the vessel geometry and drying cycle time are not. Fluidized bed drying was also rejected because of critically safe geometry restrictions, long drying cycle time, and poor fluidization.

Small-scale microwave drying of 2-liter batches of loaded resin using a commercial 2-kW, 2450-MHz oven has shown that the wet resin couples well with the energy. An initial drying rate of about 50 g water per min was observed, with decreasing water removal as the resin became dryer. Completely dry resin (LOD <1 wt %) does not overheat or char as the sodium-form resin does. Apparently mixing of the resin is essential

to uniformity at the desired water content (~15 wt % LOD), as samples showed from 12 to 17 wt % LOD depending on position in the batch. The initial preferential drying of the resin near the walls is later compensated for by preferential heating of the resin that contains more water.

From the results of these tests a microwave dryer system has been ordered from a commercial manufacturer. Since the engineering-scale resin loading equipment must demonstrate feasibility for hot-cell use, the microwave dryer system will also be demonstrated. Figure 3.8 shows the basic equipment components for drying ^{233}U-loaded resin. Wet uranium-loaded resin from the loading contactor will be introduced through the top flange of the 1.2-m-long (4-ft) 0.13-m-ID (5-in.) glass column located in the stainless steel microwave cavity. Transfer liquor will be drained by the screened bottom flange. If a 2.5-kW microwave power source is used, the estimated drying cycle for the reference 4 kg U on a 10.5-liter batch of resin is 1 hr. A program controller will adjust the forward power and also will receive the reflected power signal from the cavity. Since the resin absorbs less power as it becomes drier, we anticipate that the reflected power signal can be used to terminate the drying cycle at the desired resin moisture content. A carrier gas will be used to mix the resin bed and also to aid in steam removal. At the end of the drying cycle the resin will flow freely through the ball valve at the bottom of the column ready to be carbonized.

3.4.3.3 Engineering-Scale Resin Loading System

The initial stage of an engineering-scale resin loading system was completed (Fig. 3.9) and operated with natural uranium. Design, procurement, and fabrication of second-stage components are in progress. Four resin loading runs were completed; preliminary results indicate the following:

Mechanical operation was good, with greatly improved phase separation and interface control for the nitrate extraction contactor. A standard run appeared to duplicate the typical demonstration run results previously reported.[17]

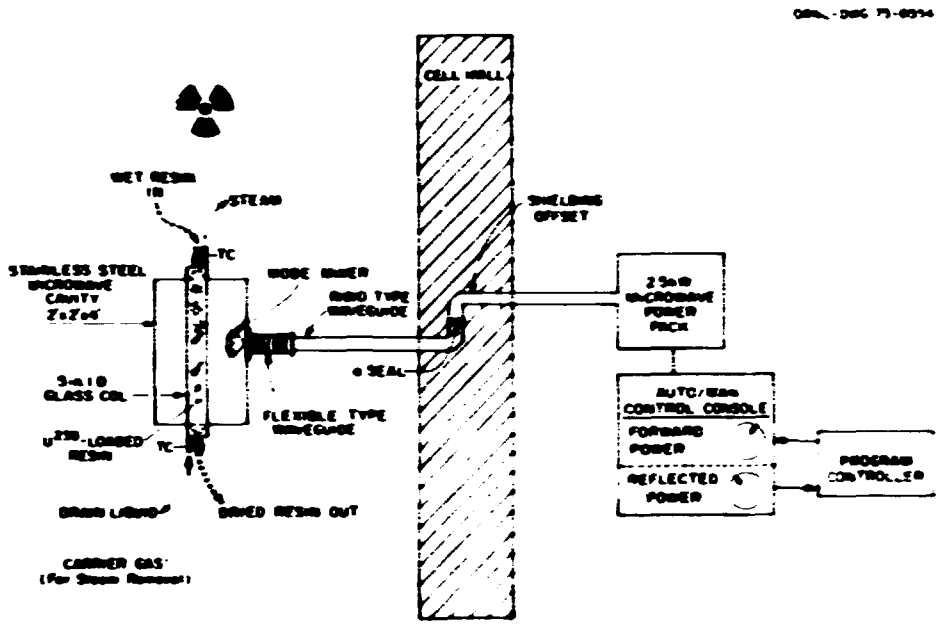

Fig. 3.8. Microwave Drying of ^{233}U-Loaded Resin. Cavity is 0.61 by 0.61 by 1.22 m (2 by 2 by 4 ft). Glass column is 0.13 m ID.

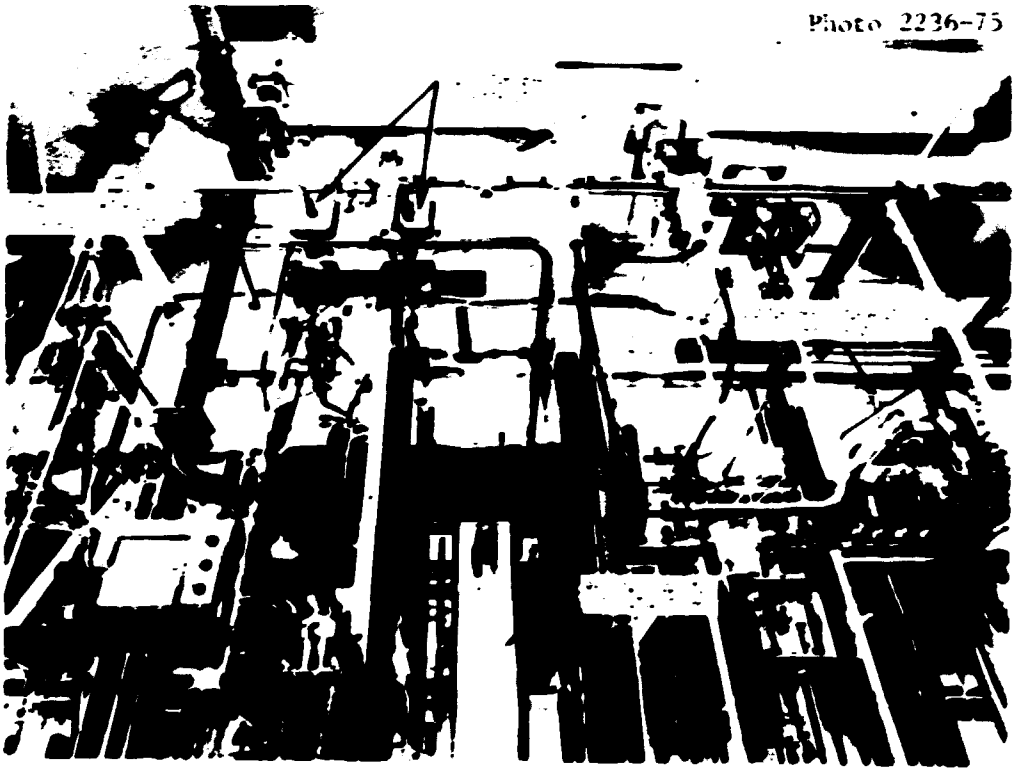

Fig. 3.9. Partial View of the Engineering-Scale Resin Loading Equipment Rack.

High uranium concentrations of 1 to 2 % give precipitation of UO_3 in the organic and float the fresh hydrogen-form resin in the loading contactor. One loading run was started with 1.5 % uranium and produced a normal loaded resin in spite of these difficulties. While the UO_3 is scrubbed from the organic in the first water scrub contactor for uranium recovery, the operation with less than 1 % uranium concentration is preferred.

Duolite C-464 was loaded by the same procedures as for Amberlite IRC-72. The loading of uranium was accomplished as expected with small differences from the lower capacity, lower density, and slightly different equilibrium for the Duolite resin.

Partial regeneration of amine using a NaOH/amine molar flow ratio of about 0.7 was demonstrated by one loading run. This should greatly reduce the waste volume since the Na/NO_3^- mole ratio for this mode of operation is 1.0 instead of the 1.7 ratio, which results when an excess of $NaOH-Na_2CO_3$ is used. This partial regeneration should also reduce the solubility of uranium in the waste and allow uranium recovery by filtration. Analyses to confirm this advantage are in progress.

The next improvement in the engineering-scale resin loading system will be installation of a 0.13-m-ID by 1.5-m-long (5-in. by 5-ft) resin loading contactor to replace the 0.10-m-ID (4-in.) column. This contactor has been fabricated and leak tested. The thermosyphon evaporator was designed, and detailed drawings are being prepared. Drawings were prepared for a slab-geometry phase separator for the nitrate extraction, but the unit will not be fabricated until the 0.15-m-diam (6-in.) pipe phase separator now in use is tested further.

3.4.4 Material Preparation — P. A. Haas and J. H. Shaffer

Irradiation test specimens generally require a few small batches (≤1 kg U) of resin loaded with ^{235}U or ^{233}U, while carbonization, conversion, coating, and fabrication development studies require many larger (1 to 10 kg U) batches of resin loaded with natural or depleted uranium. The irradiation test specimens and some initial batches with

depleted uranium were prepared by the initially developed loading process with addition of UO_3 to maintain acid-deficient uranyl nitrate.[11,14] Most recent requirements for depleted uranium have been supplied with resin loaded by the reference process with amine extraction of nitrate. The intended compositions of the solution and resin are identical for either nitrate extraction or UO_3 addition; but different impurities are possible.

3.4.4.1 Resin Feed

The resin used for materials preparation has been from 3.4 m^3 (120 ft^3) of commercial −20 +50 mesh Amberlite IRC-72 purchased from the Rohm and Haas Company or 0.57 m^3 (20 ft^3) of special sized Duolite C-464 from the Diamond Shamrock Company. Most of the Amberlite was sized by wet screening of sodium-form resin to separate −24 +32, −26 +32, and −32 +34 size fractions for use. The loaded Amberlite IRC-72 resin was from about 0.17 m^3 (6 ft^3) of unsized resin and about 0.4 m^3 (15 ft^3) of sized fractions within 24 and 34 mesh. The loaded Duolite C-464 resin was mostly from 700 ± 50 μm material as received in the sodium form.

3.4.4.2 Resin Loading with Fully Enriched ^{235}U for In-Reactor Tests

Chemical development of the resin loading process has included preparations with ^{235}U (93% enrichment) for in-reactor tests within the HTGR Program. During this report period approximately 20 kg of this product (9.63 kg of ^{235}U) was prepared in 28 batch operations. The dried resin was used for preparation of fueled carbide microspheres for the in-reactor test assemblies.

Since relatively small quantities of prepared resin were required for each test, small batch operations that yielded about 200 g ^{235}U per batch were initially used. This batch size was increased to approximately 650 g ^{235}U as the HTGR program needs increased. All operations required prior approval by nuclear safety review of the process equipment and production method.

The batch production method combined $^{235}UO_3$ and nitric acid with sized weak-acid resin (hydrogen form) in a stirred reaction vessel.

The quantities of reagents used in each batch operation were calculated to yield acid-deficient uranyl nitrate solution having the approximate stoichiometry $UO_2(OH)_{0.5}(NO_3)_{1.5}$ in equilibrium with the fully loaded resin. This solution was drained from the loaded resin and recycled to the successive batch loading for conservation of uranium. After a water wash to remove residual uranyl nitrate solution, the loaded resin was dried in flowing air at 110°C and packaged for shipment. The quality of each production batch was certified by chemical and spectrochemical analyses for uranium content, mass assay, and extraneous impurity elements. One production batch containing about 600 g of ^{235}U was prepared with Duolite C-464 resin; all others were prepared with Amberlite IRC-72 resin.

3.4.4.3 Resin Loading with Natural or Depleted Uranium

Over a one-year period, 235 kg of dried, loaded resin containing 110 kg of ^{238}U was delivered to the Metals and Ceramics Division. About 77 kg of this resin or 36 kg U was from the demonstration of the reference loading flowsheet via amine extraction of nitrate (Table 3.4). Delivery of resin loaded via this flowsheet in an engineering-scale system (see Sect. 3.4.3) was started at the end of the report period. The remainder of the loaded resin (160 kg total, 75 kg U) was prepared via the initially developed procedure[11,12] using UO_3. Results and conditions for the service preparations are given in Table 3.5.

The mechanical simplicity of the resin loading operation using UO_3 is illustrated by a system installed to process up to 0.23-m^3 (8-ft^3) batches of resin (Fig. 3.10). A cone-bottom 0.21-m^3 (55-gal) stainless steel drum is used as a spouting bed contactor. The fluidizing flow is always controlled or shut off by the valve at the bottom of the cone to keep all resin in the tank. A separate mixing tank is used for dilution of concentrated HNO_3 for the conversion from sodium to acid form and for mixing of the UO_3 with hot uranyl nitrate during loading. A 0.23-m-diam (9-in.) porous stainless steel filter on a movable dip leg is used for more complete removal of solutions during conversion with nitric acid and washing with H_2O. The loaded resin is transferred to a dryer by

Table 3.5. Loading of Natural or Depleted Uranium on Carboxylic Acid Cation Resins Using UO_3

Run	Resin Feed[a]		Loaded Resin			Final Solution			Loading Time (hr)
	Size (μm)	Volume (liters)	Weight (g)	U Content (wt %)	meq U / ml Resin	U Conc. (M)	pH	NO_3^-/U Mole Ratio	
	A. Loading of Amberlite IRC-72 in a large[b] conical-bottom, spouting-bed contactor								
B01	Unsized	62[c]	47,166	45.9	2.93	0.22	3.1	1.55	10
B02	560 • 60	33	25,570	48.2	3.14	0.22	3.0	1.65	7
B04	660 • 30	22	16,955	48.9	3.16	0.22	3.15	1.55	8
B05	560 • 60	38	28,780	48.0	3.07	0.22	3.1	1.6	7
	B. Loading of Duolite C-464 in a large[b] conical-bottom, spouting-bed contactor								
B03	700 • 50[d]	58[d]	25,425	46.4	1.71[d]	0.22	3.1	1.6	5
	C. Loading of Amberlite IRC-72 in baffled, agitated beakers								
58	Unsized	7.48	6,087	45.9	3.14	0.4	2.8	1.65	5
59	Unsized	7.31	6,100	46.2	3.24	0.4	2.8	1.65	2.5
62	Unsized	8.17	6,530	47.0	3.16	0.4	3.0	1.5	2.5
63	Unsized	8.34	6,721	46.35	3.14	0.4	3.1	1.5	3
	D. Loading of Duolite C-464 in baffled, agitated beakers								
72	800 • 50[d]	2.5[d]	1,083	46.1	1.68[d]	0.3	3.0	1.6	8
73	700 • 50[d]	2.7[d]	1,190	44.7	1.65[d]	0.25	3.1	1.5	5

[a]Resin sizes and volumes are given for the hydrogen form in water.

[b]0.21-m^3 (55-gal) drum.

[c]Inaccurate resin volume measurement resulted in low calculated loading.

[d]Duolite C-464 in sodium form for volume measurements.

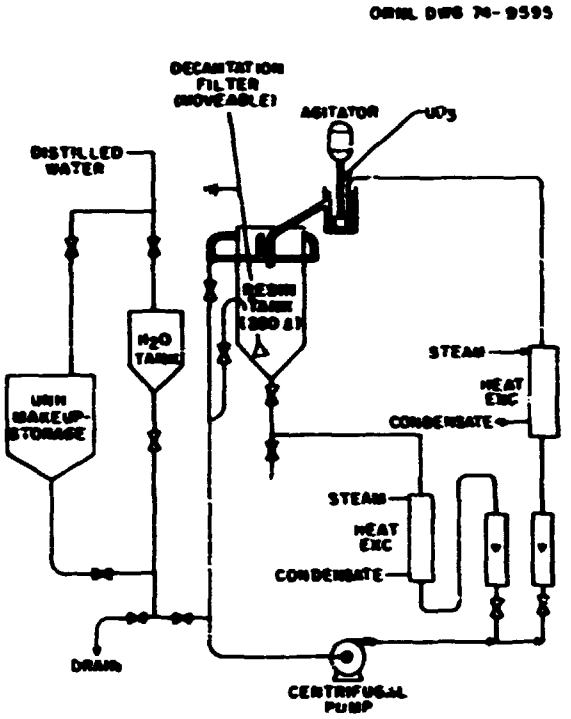

Fig. 3.10. Large-Batch Resin Loading or Conversion System.

gravity flow through the ball valves at the bottom of the drum. This system operated as intended without difficulty. The slow mixing of the large resin bed and the slow heatup to 60°C results in 8- to 16-hr loading times, as compared with one-fourth these times in small, well-agitated and heated vessels.

3.5 RESIN CARBONIZATION (WORK UNIT 2103) — W. J. Lackey

The objective of this work unit is to develop equipment and processes for carbonizing weak-acid resin microspheres. The carbonization process consists of controlled heating of the resin previously loaded with uranium. Such heating is performed in the absence of oxygen and causes evolution of volatile constituents. After heating to about 600°C, the carbonized microspheres consist of UO_2 finely dispersed in a carbon matrix. This material can then be heated to 1600 to 1800°C to convert the desired fraction of UO_2 to UC_2. This later operation is referred to as conversion. Both operations are conducted in fluidized beds using argon as the levitating gas.

3.5.1 Equipment Development – J. A. Carpenter, Jr., M. K. Preston, J. L. Heck, W. R. Hamel, J. E. Mack and D. R. Johnson

The effort toward development of equipment for resin carbonization has centered on three fluidized-bed furnaces. A 0.13-m-diam (5-in.) graphite muffle coating furnace was adapted for carbonization and conversion. A small, carbonization-only system employing a 0.10-m-diam (4-in.) Inconel muffle was constructed and used. A larger, engineering-scale system with a 0.23-m-diam (9-in.) Inconel muffle was designed and fabricated and is now ready for initial testing.

Initial carbonization runs were made by equipping the coating furnace system with thermocouples, a temperature programmer, and an inert-atmosphere unloading pot. A single-inlet graphite cone having an included angle of 30° was used for all carbonization runs made with the coating system. Conversion runs were made with either the same cone or with a porous-plate gas distributor described in Sect. 3.6. The perchloroethylene scrubber, used for removing soot from the off-gases of coating operations, was found adequate for removing the tars produced in resin carbonization. Perchloroethylene scrubbers were, therefore, provided in both the 0.10- and 0.23-m-diam (4- and 9-in.) systems discussed below.

To test concepts planned for the larger 0.23-m unit, a 0.10-m lab furnace was built. In the 0.10-m unit, the reaction chamber is an Inconel tube with a 60° single-inlet cone at one end. The capacity of the unit is 1.5 kg of dried loaded resin, representing about 0.75 kg of uranium. Temperature is measured by thermocouples, one in a well protruding directly into the fluidized bed of particles, the other located at the muffle wall between the muffle and the furnace heating element. A 200-μm stainless steel screen above the bed is provided to mechanically disentrain kernels from the fluidizing gas stream. Particles are fed from a hopper into the chamber by gravity flow through a line that penetrates the chamber wall just below the kernel retention screen. A bottom-loading scheme was tried but was not fail-safe and was, therefore, abandoned in favor of the gravity system. Sight ports were provided in the top of a flat muffle end and used to observe the action of the bed

during the early portions of carbonization runs. Buildup of tars on this type end forced its abandonment in favor of a smoother tapered end. It was also found necessary to insulate the crossover pipe from the muffle to the scrubber to avoid excessive tar buildup. A novel feature of this system is the incorporation of gas flow programmed via a digital function generator to decrease as the temperature increases. Also, pressure transducers have recently been installed in this system to determine if they are useful for monitoring the pressure drop across the bed.

The 0.10-m-diam furnace performed very well, and thus many of the features of it were incorporated in the design of the 0.23-m-diam system. This latter system is full commercial size and should allow carbonization of about 4 kg of uranium per batch. It will be loaded and unloaded pneumatically via a system of lines and hoppers, all under argon. The product will be fed to a large argon-atmosphere glove box for sampling and, if necessary, upgrading before conversion. The furnace had been fired and the system was nearing initial operation at the end of this report period.

3.5.2 Process Development — J. A. Carpenter, Jr., D. P. Stirton, and D. R. Johnson

Typically the carbonization processes consist of heating uranium-loaded weak-acid resin from room temperature to 600°C at a rate of 2°C/min followed by a hold at 600°C for 30 min. For conversion, the carbonized material is heated rapidly to about 1700°C and held for 10 to 30 min, depending upon the amount of UC_2 that one wishes to form via reaction with the carbon matrix of the kernel. With the 0.13-m-diam (5-in.) system the charge is typically 500 kg U, and the argon flow is usually 0.5 std liter/sec (1 scfm). Charges as large as 1.2 kg U have been successfully carbonized and converted in this system. Considering both the 0.1- and 0.13-m-diam (4- and 5-in.) systems, a total of 134 carbonization runs have been made. Of these, the resin source was Amberlite IRC-72 for 125 of the runs and Duolite C-464 for the remainder. We made 82 conversion runs, 76 with Amberlite resin

and 6 with Duolite. No significant problems were encountered during these runs, and both the carbonization and conversion processes appear commercially feasible.

The only problems encountered during carbonization and conversion were: (1) cracking of the kernels of one batch of resin during carbonization, and (2) sticking of kernels to one another and to the graphite muffle during conversion. The resin batch that cracked during carbonization differed in uranium content from numerous batches that did not crack. The inferior batch contained less than the desired uranium content. The central regions of the microspheres were much lower in uranium content than the outer regions. Thus, given properly loaded microspheres, which is the general case, cracking during carbonization will not be a problem. The second problem, kernel sticking during conversion, occurred whenever the heating rate during carbonization was greater than about 2°C/min. Higher heating rates cause more carbon to be evolved during carbonization, resulting in less carbon in the carbonized kernels. Kernels containing too little carbon have a high tendency to sinter and stick during conversion. The sticking can be minimized by using higher fluidizing gas flow rates during the conversion, stirring the fluidized bed more rapidly and efficiently. Similarly, the use of a cone having a 30° included angle appears preferable to one of 60°. With proper control of the heating rate during carbonization and given the preferred conversion process, sticking does not occur.

Besides the inter-particle variation in uranium loading, the intra-particle variation is also important. A technique based on neutron activation of individual resin particles was developed and used to show that the variation in the uranium loading between individual microspheres is typically much less than 1%. This work is described further in Sect. 3.7.3.

The properties of the carbonized and converted kernels — such as carbon content, density, diameter, percent conversion to carbide, and crushing strength — depend on process variables such as heating rate during carbonization, fluidizing gas flow rate, and conversion time and temperature. A statistically designed experiment employing these variables was conducted and reported.[21] These results can be summarized as follows:

1. Heating rate in the range 2 to 25°C/min during carbonization very strongly influences a number of other properties. Lower heating rates yield a product of kernels containing more carbon, having lower density, and tending less to sinter and stick to one another and to the furnace muffle during conversion.

2. Higher gas flow rates surprisingly lowered the conversion; this was perhaps a side effect caused by higher flows causing the particle bed to run cooler than the control point outside the furance muffle.

3. Kernel sphericity did not degrade during carbonization and conversion.

4. Uranium loss did not depend on time, temperature, or gas flow rate. This indicated that the observed loss of material, which averaged 1%, was due to physical carryover rather than evaporation or some other chemical means. That is, particle loss was the result of particles being blown out of the furance into the exhaust system. Of course, the particle retention screen on the prototypic carbonization furnace will eliminate such loss during carbonization, and a longer furnace should minimize loss during conversion.

The crushing strength of carbonized and converted resin-derived kernels was measured. Results for carbonized material are summarized graphically in Fig. 3.11. The data showed at the 99% level of confidence that crushing strength depended on both the uranium content and the precarbonization moisture content, as determined by drying at 110°C. Data for converted kernels are given in Fig. 3.12. Note that the crushing strength decreases for increasing conversion to the carbide.

A time-of-flight mass spectrometer was used on-line to study the off-gases from carbonization. The off-gases seen after the furnace but before the perchloroethylene scrubber are water vapor and CO_2 with lesser amounts of CO and H_2. Behind the scrubber, perchloroethylene and various derivatives of it are also present. Studies of the kinetics of the carbonization process are in progress. The results will hopefully allow minimization of the time required for the carbonization process.

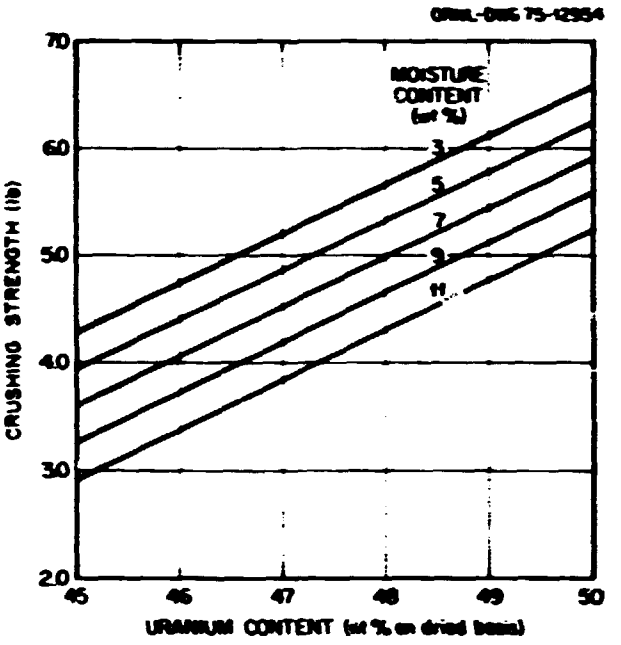

Fig. 3.11. Influence of Uranium and Moisture Contents on Strength of Carbonized Resin Kernels. To convert: 1 lb = 4.45 N.

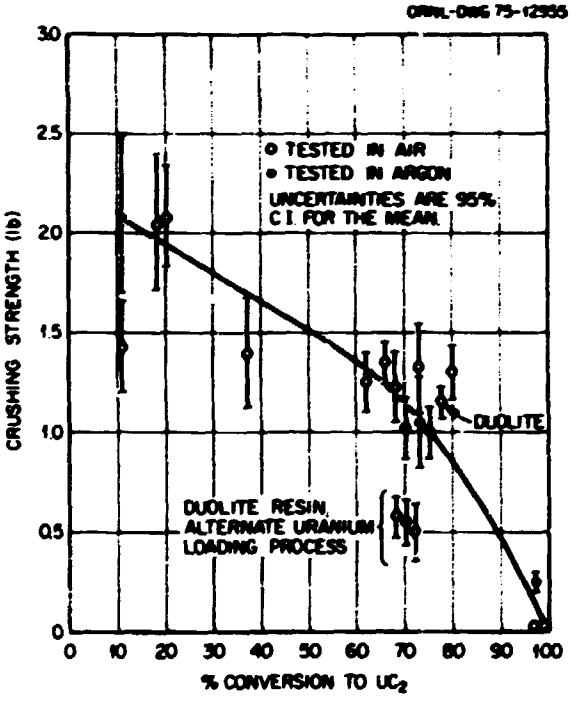

Fig. 3.12. Influence on Crushing Strength of the Extent to Which the UO_2 of Resin-Derived Kernels is Converted to UC_2. Data for Amberlite resin unless otherwise noted. To convert: 1 lb = 4.45 N.

Carbonized and converted kernels containing 93%-enriched ^{235}U were prepared for subsequent coating and irradiation testing. Three batches were prepared, two having nominally 75% conversion and one with 13% conversion. These particles are described further in Sect. 3.6.1.2.

3.5.3 Laboratory-Scale Resin Kernel Studies — G. W. Weber

The carbonization process can be optimized by defining critical reaction regions and appropriate control parameters. The differential thermal analysis (DTA) and thermogravimetric (TGA) behavior shown in Figs. 3.13 and 3.14, respectively, for two candidate resins, Duolite C-464 and Amberlite IRC-72, indicate the importance of the region from 200 to 500°C. Investigation of the weight loss, volume loss, and density at selected temperatures during this carbonization process produced property variations closely reflecting the TGA and DTA behavior, as shown in Fig. 3.15. A similar variation was found in particle size as shown in Fig. 3.16 and in mercury density.

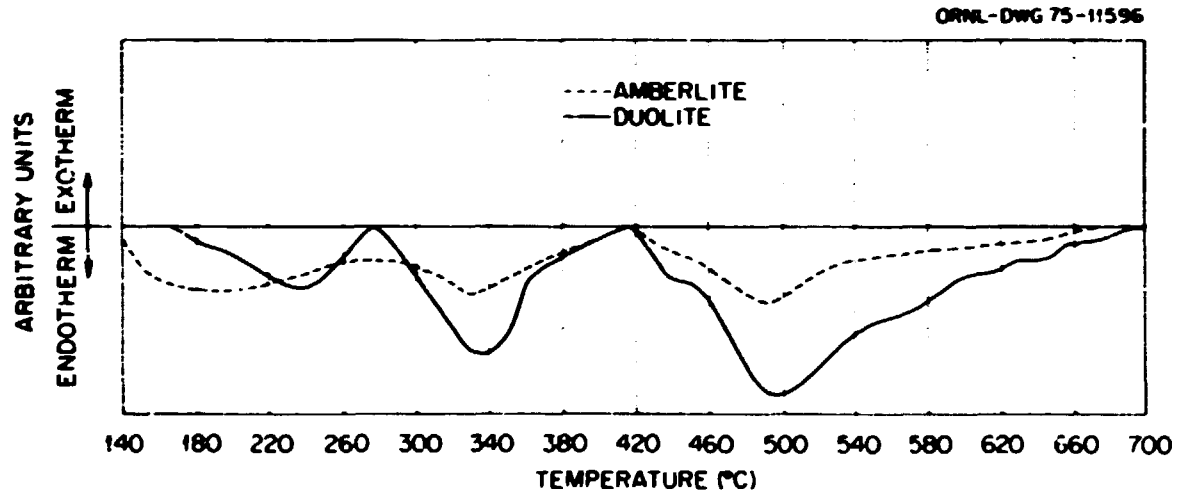

Fig. 3.13. Differential Thermal Analysis Behavior of Uranium-Loaded Duolite C-464 and Amberlite IRC-72 Weak-Acid Resins.

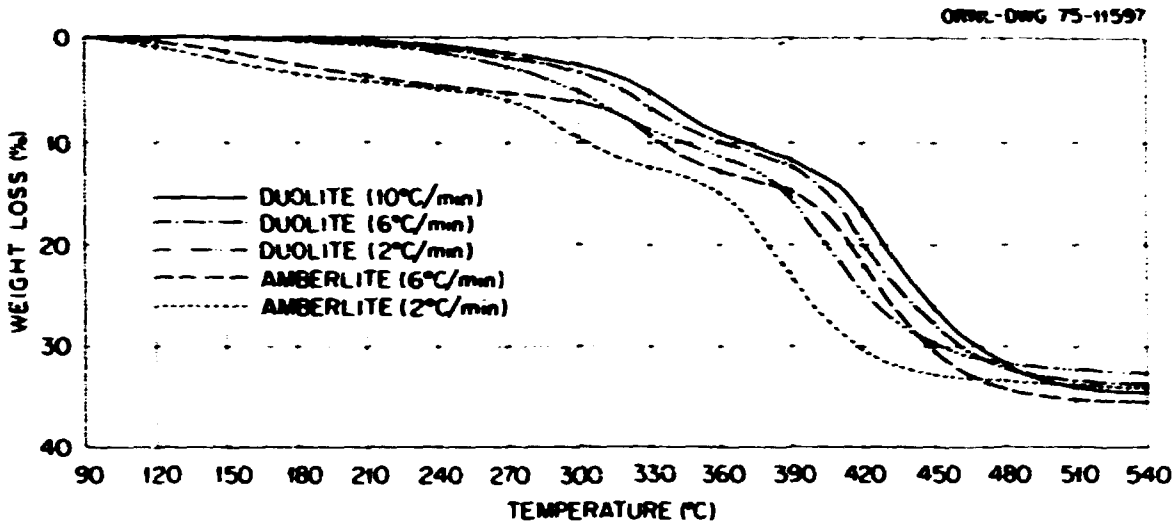

Fig. 3.14. Thermogravimetric Behavior of Uranium-Loaded Duolite C-464 and Amberlite IRC-72 Weak-Acid Resins from 90 to 540°C as a Function of Heating Rate.

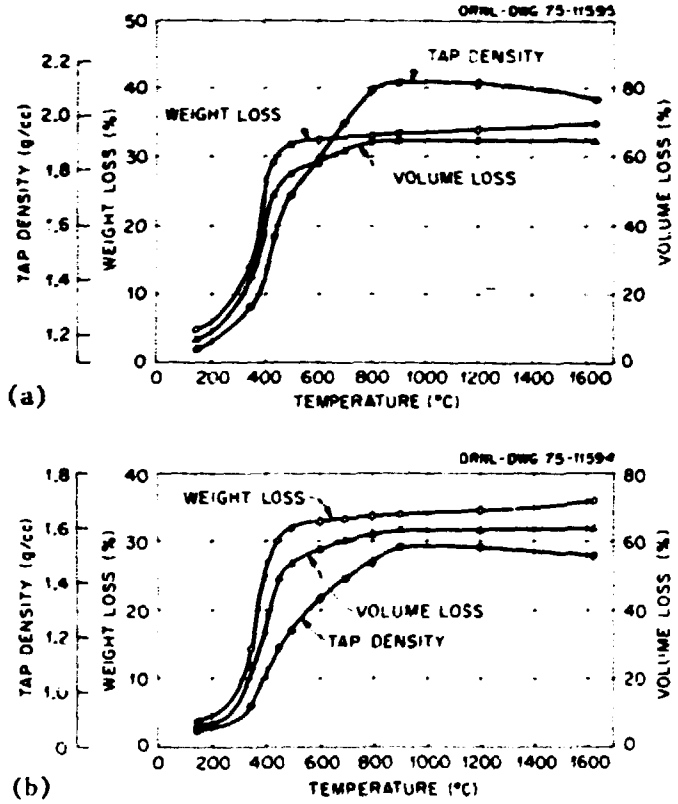

Fig. 3.15. Weight Loss, Volume Loss, and Tap Density Variation from 150 to 1625°C for Uranium-Loaded Weak-Acid Resin. (a) Amberlite IRC-72. (b) Duolite C-464.

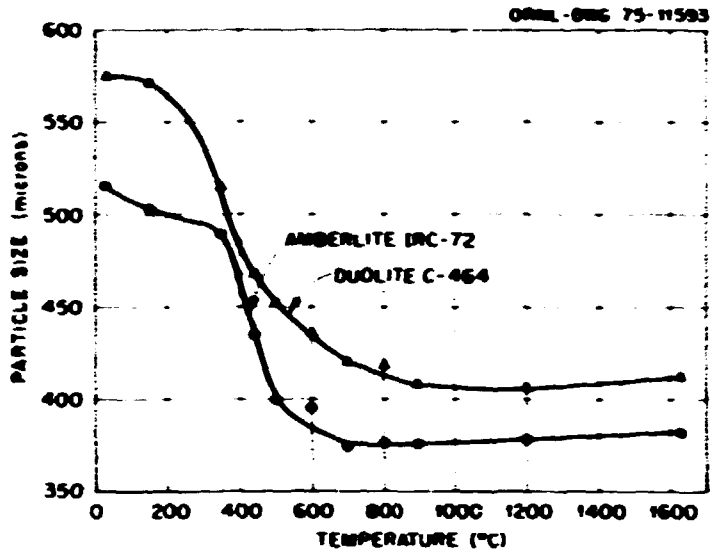

Fig. 3.16. Variation in Particle Size of Uranium-Loaded Duolite C-464 and Amberlite IRC-72 Weak-Acid Resins from 25 to 1625°C.

The heating rate through this critical carbonization region had a very strong effect on weight loss, volume loss, and carbon-to-uranium ratio. The final weight loss and volume loss for both resins are approximately linear with log heating rate for heating rates from 1 to 80°C/min through the critical process range, which was subsequently identified as 360 to 440°C for the Duolite resin. The variation of carbon-to-uranium ratio with carbonization rate behaved similarly for the two resins as shown in Fig. 3.17.

The carbon-to-uranium ratio is significant in defining the fluidization behavior of the material during the subsequent conversion step. An excess of carbon is required to successfully complete this step without agglomeration. Experiments have demonstrated that a carbon-to-uranium ratio greater than about 5.8 is necessary to prevent agglomeration during typical conversion operations. The Duolite C-464 material exhibited less tendency to agglomerate during conversion because of its slightly higher carbon-to-uranium ratio.

Partial conversion of the UO_2 to UC_2 at 1600 to 1700°C in accordance with the applicable reactions is controlled by the partial pressure of CO over the material. The high available surface area (BET $\approx$ 150 m^2/g)

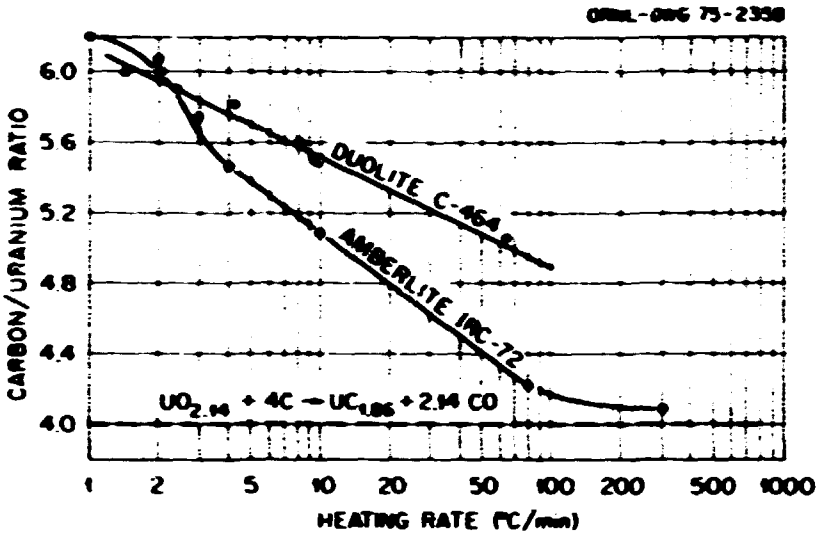

Fig. 3.17. Comparison of Carbon-to-Uranium Ratio of Carbonized (1200°C) Uranium-Loaded Weak-Acid Resins as a Function of Critical Range [Duolite (360–440°C), Amberlite (200–500°C)] Heating Rate.

and extensive interconnected porosity (0.01 μm diam for IRC 72 and 0.05 μm diam for C-464) of the carbonized kernels permit prediction of the rate of the UO_2 conversion to UC_2 under given conditions of specific gas flow rate and temperature. Debye-Scherrer examination of kernels processed to various conversion levels has shown that the partially converted material is a mixture of UO_2, UC_2, and UC_xO_{1-x}. The amount and proportion of the various phases can be controlled by temperature variation and by addition of hydrogen or carbon monoxide to the fluidizing gas stream.

The presence of these phases suggests the potential for uranium volatilization during conversion. However, measurements with a water-cooled collector have indicated that only about 0.035% U loss occurs during conversion under worst case circumstances. Although uranium loss during carbonization involves an aerosol that is difficult to collect, analysis has yielded a uranium loss of 0.02% during a very fast carbonization cycle under a worst case situation.

A further concern relating to processed fuel kernels is retained nitrogen, because of the transmutation to ^{14}C, which must be accommodated in fuel reprocessing. Thus the effect of the uranium loading method on

retained nitrogen is a factor in selecting the process flowsheet. Comparative data on kernels loaded by various schemes and carbonized in a similar manner have been analyzed by the Kjeldahl method. Amberlite (H^+ form) with acid neutralization by NH_4OH has shown 800 ppm retained nitrogen, while Duolite (NH_4^+ form) exhibited 1200 ppm N. These values are considered significant because of their high levels, although the Kjeldahl method is not sensitive to low nitrogen levels.

3.5.4 Resin Handling — J. A. Carpenter, Jr.

During this period it became clearer that size and shape classification of resin before loading with uranium was most advantageous. However, it was not clear whether further upgrading after loading might also be needed. Hence, some work along these lines continued.

Severe problems of handling the uranium-loaded resin microspheres, associated with electrostatic charge buildup, were encountered. The problem was found to be associated with lack of moisture in the resin. Blending small amounts of flake graphite minimized the problem when the resin was dried to about 3–4 wt % moisture as determined by loss-on-drying (LOD) at 110°C in air. Below 3–4% LOD, the static charging was so severe as to make the resin virtually unmanageable even with the graphite. Drying to 12–13% LOD eliminated the charging altogether. A commercial ionized-air static eliminator was adequate but slow. The solution adopted was to limit the resin moisture removal to 12–13% LOD.

Shape classification of loaded resin before carbonization was performed many times, and no problems were encountered, provided either graphite or moisture was present on the resin to eliminate static charging. Resin will likely be screened before loading with uranium, but further screening may be required. Attempts to screen loaded resin in anything other than laboratory-scale equipment have resulted in extensive screen blinding. Alternate approaches for full-scale screening are being investigated.

As an outgrowth of the above work aimed at solving the static charge problem by addition of water, we studied the swelling and density changes of the uranium-loaded resin associated with increasing moisture content.

For both types of weak-acid resins studied, Amberlite IRC-72 and Duolite C-464, the microsphere radius increased on increasing the moisture content up to about 5-10% LOD, above which it remained constant or even decreased somewhat. The density actually decreased somewhat up to water contents of between 10 and 20% LOD and then rose sharply to perhaps as much as 20% above its original value. At 30 to 35% LOD, the resin reached saturation and was no longer able to absorb any further water.

3.6 MICROSPHERE COATING (WORK UNIT 2104) - W. J. Lackey

The microsphere coating work unit has as its objective the development of equipment and processes necessary for the remote coating of HTGR fuel particles. We will obtain the performance data necessary to design and operate a commercial-scale coating system. Microsphere coating is separated into the following areas:

1. particle coating, which consists of the conversion of the desired fraction of the UO_2 in the kernel to UC_2 followed by the deposition of porous and dense carbon coatings as well as deposition of very high-density silicon carbide coatings;
2. effluent treatment, which renders the effluent from carbon and silicon carbide coating operations into forms suitable for disposal;
3. particle handling, which includes weighing, batching, transferring, classifying, sampling, and storing of kernels and coated particle batches.

3.6.1 Particle Coating

The equipment being developed to remotely coat recycled HTGR fuel includes a fluidized bed to deposit the carbon and silicon carbide coatings. The reference fissile particle coatings consist of buffer and dense (LTI) carbon layers, a layer of silicon carbide, and an outer LTI coating. The fissile kernel is obtained by loading uranium onto a resin bead (Sect. 3.4), carbonizing at about 600°C to remove volatiles (Sect. 3.5), and converting the desired fraction of UO_2 in the carbon matrix of the kernel to UC_2.

Conversion requires high temperatures (1600–1800°C), and therefore it is performed in the same furnace as that used for coating. However, since the carbonization and conversion operations are interrelated, the results of our conversion studies are presented in Sect. 3.5. Our 0.13-m-diam (5-in.) coating furnace used for conversion and coating has been described previously.[12,22] Major efforts during the year included modifying several components of the coating equipment, designing new equipment for remotely loading and unloading the furnace, developing a better understanding of the deposition of the carbon and silicon carbide layers, and preparing Triso-coated resin-derived microspheres for irradiation testing.

3.6.1.1 Equipment Development — M. K. Preston, J. L. Heck, D. P. Stinton, R. R. Suchomel, and W. R. Hamel

Two types of gas distributors can be used on the remote prototype coating furnace. The conical gas distributor has been used for many years and has operated satisfactorily. The porous plate[23] (frit) gas distributor is relatively new and has undergone several modifications. The problems that led to modification of the frit were the failure of the frit to seal properly to the gas distributor and the adherence of particles to horizontal or nearly horizontal portions of the frit. Sticking occurred during buffer coating runs in the regions between the blind holes and particularly in the central portion of the distributor where there was no hole. A new frit shown in Fig. 3.18 was designed to eliminate the sticking problem. A central blind hole was added, and the number of peripheral holes was increased from six to eight. Also the slope of the surfaces between the holes was increased to promote more rolling action of the particles. This frit has been evaluated for over six months; its performance is very satisfactory and considerably better than the previous design.

The problem of coating gas leaking around the frit was caused by the attempt to seal directly to the porous graphite. Gas leakage has been eliminated by cementing a solid graphite ring to the outside of the frit.

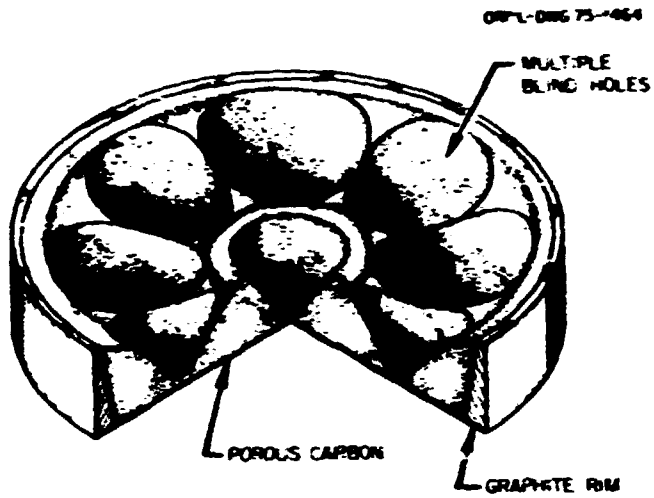

Fig. 3.18. Porous Plate or Frit Gas Distributor.

Several modifications were made to the furnace to allow its use for carbonization and conversion of resin particles. A "Trend Trak" temperature programmer was installed to permit heating the furnace at controlled rates. A glove box used for loading particles into the furnace was upgraded so that its atmosphere would be sufficiently inert to allow handling of carbonized and converted resin particles, which are pyrophoric.

A rigidized carbon felt heat shield has been evaluated and shown to be superior to the previously used molybdenum. The new heat shield provides better insulation and does not become brittle after heating.

The coating gas handling equipment was modified to allow mixing of acetylene and propylene to be used for deposition of mixed-gas LTI coatings. Laminar flow elements were also installed in the gas streams to replace the integral orifice flow measuring devices.

A time-of-flight mass spectrometer was connected to the coating furnace to monitor the gaseous effluent from carbon and silicon carbide coating operations. In addition to obtaining desired environmental data the mass spectrometer will be used to obtain information on coating process variables and their effect on product quality.

One area of major development is the so-called 0.13-m-diam (5-in.) coater loop. This equipment, which is required for automatically unloading particles from the coating furnace, consists of a number of components, as depicted in Fig. 3.19.

Because of the hot and often pyrophoric nature of coated particles an inert atmosphere must be maintained throughout the loop, and all components must be capable of handling particles as hot as 600°C. The requirements for remote operation of this loop necessitated redesign of the coating chamber and gas distributor as well as the furnace expansion chamber and seal support plate. These components have been fabricated.

The redesigned gas distributor will use perchloroethylene (C_2Cl_4) as the coolant in order to evaluate a nonhydrogenous coolant system. A heat transfer analysis of the gas distributor was performed to estimate the effects of substituting C_2Cl_4 for water as the coolant. Results indicate that the new coolant system will require flows of about 0.5 liter/sec (8 gpm) to accomplish equivalent cooling to that provided with about 80 ml/sec (1.3 gpm) water. Thus the heat exchanger, circulating pump, reservoir, piping, and valves have been sized and are being procured on this basis.

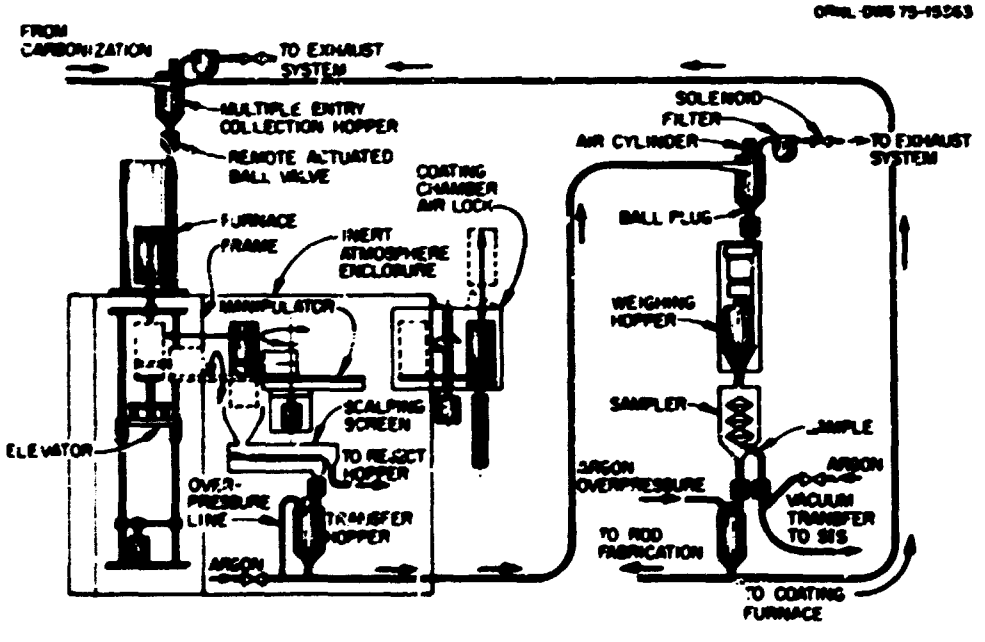

Fig. 3.19. Remote Coating Furnace Loop.

Redesign of the furnace stand was also required, as it must be compatible with the inert enclosure and unloading mechanism. The components within the enclosure have all been designed; the elevator and manipulator are being fabricated. A small programmable logic controller is being procured to operate all coater loop components. It will control the operations needed to pick the crucible off the lowered elevator, dump the particles from the crucible to the scalping screen, and scalp the particle batch to remove oversize agglomerates and soot balls. An air lock to the enclosure that will permit replacement of coater crucibles has also been designed and is awaiting fabrication.

Particles will be transferred from the enclosure to a series of column-mounted components, which will weigh, sample, and divert the batch. A precision weigher capable of weighing a batch with an accuracy of 0.1 wt % has been designed. Hopper designs have been completed.

Samplers of two different designs are to be tested as laboratory-scale equipment to determine the most satisfactory design. A ten-stage sampler built to yield a sample-to-input ratio of $1/2^{10}$ or 1/1024 is currently being tested. The second, a three-stage device designed for a ratio of 1/1000, is under fabrication. Initial testing of the ten-stage sample produced a sample-to-input ratio of about 1/500 rather than the anticipated 1/1024 and disclosed two major design faults. The long line-of-sight path from the top stage to the bottom plate resulted in an unacceptably large number of broken particles, and the bottom plate was so designed that particles in the main stream channel could bounce back into the lowest stages, accounting for the error in the sample ratio. Two particle containment systems were developed as modifications to the original sampler. One system uses a nine-layer turbine-blade-like deflector design. A second modification employs a ten-layer trough assembly to divert the main stream fraction from each stage. Both modifications yield the proper size sample and more importantly samples that are representative of the parent batch.

Other equipment development on the 0.13-m (5-in.) coating system is associated with the furnace-to-scrubber connecting pipe. A method is

being developed to eliminate the problem of soot buildup in this pipe. Fabrication is nearly complete on an auger assembly that can be periodically driven through the pipe to clean it.

3.6.1.2 Process Development — D. P. Stinton, W. J. Lackey, and D. R. Johnson

The first coating applied to both fertile and fissile particles is the buffer layer. Improvements in the buffer coating process have been described in the previous two progress reports.[23,24]

The second layer applied to both fissile and fertile particles is the low temperature isotropic (LTI) coating. The fraction of defective LTI coatings has been extensively studied in the past year.[25] Typical defects observed in as-coated particles are cracked or permeable LTI coatings. The particles used in this study were Biso-coated ThO_2. The LTI coatings were deposited from propylene in the 0.13-m-diam (5-in.) coating furnace using either the conical or frit gas distributor.

Defective particle fractions are given in Fig. 3.20, where each line is the result of a least squares fit involving from 10 to 50 different coating batches. The uppermost curve of Fig. 3.20 shows a very strong dependence of defective fraction on outer coating thickness. The defective particles in this case consisted of both cracked and permeable coatings. A decrease in the number of permeable coatings with increasing coating thickness is easily understood, but the reason for the correlation between number of cracked coatings and coating thickness was not obvious. We postulate that cracked outer coatings are the result of the combined action of two sources of stress; namely, stress built into the coating during the deposition process and stress appearing during cooling of the particles from the coating temperature. The cooldown stress results because the thermal expansion coefficient of the outer carbon layer is greater than that of the porous inner carbon. Stress analyses show that the tensile stress in the LTI layer can be as large as 103 MPa (15,000 psi). Further, the analyses show that the stress decreases with increasing LTI thickness, thus explaining the observed correlation of the number of cracked coatings with coating thickness. Thus, one should be able to

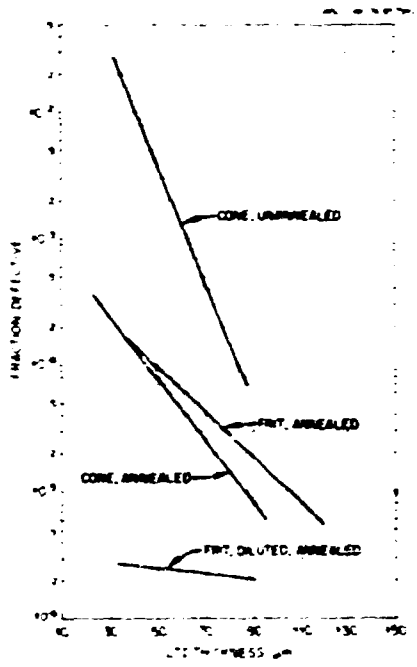

Fig. 3.20. Effect of LTI Coating Thickness, Annealing, and Dilution on Defective Particle Fraction for Biso-Coated ThO_2.

reduce the number of cracked coatings by annealing the coated particles before cooling from the coating temperature. Annealing removes the deposition stresses, and the coatings have to withstand only the cool-down stresses. The middle two lines of Fig. 3.20 show that annealing reduces the defective fraction by from one to two orders of magnitude. In fact, all the defective annealed particles had permeable rather than cracked coatings. The lower curve in the figure shows that the number of permeable coatings is significantly reduced if the propylene coating gas is diluted with helium. This effect may be associated with alteration of the coating pore structure.

These results show that the fraction of defective Biso-coated ThO_2 particles can be reduced to a very acceptable level. Annealing and mixing of an inert gas with the hydrocarbon coating gas reduced the occurrence of cracked and permeable coatings. Permeable coatings are more of a problem with the resin-derived fissile particles, and more work is required.

Considerable effort was devoted to measurement of the crushing strength of Biso- and Triso-coated particles. A report[26] describing this work was prepared. Briefly, the crushing strength of Biso-coated ThO_2 particles was increased by the following factors: (1) increasing the outer coating thickness by 10 μm increased strengths by 1.3 N (0.3 lb) for annealed particles and 2.2 N (0.5 lb) for unannealed particles, (2) an 1800°C postcoating anneal increased strengths by 4.4 N (1 lb) for particles with thick outer coatings and 9 N (2 lb) for particles having thin coatings, and (3) increasing the buffer coating density by 0.1 g/cm^3 increased strength by 2.6 N (0.6 lb). The crushing strength of Triso-coated fissile particles was proportional to the thickness of SiC coatings, and strength decreased on annealing by about 0.9 N (0.2 lb) when the frit was used to distribute the coating gas and by about 7 N (1.5 lb) when a conical gas distributor was used.

A large amount of work was done on the characterization of silicon carbide coatings. Several etching techniques were investigated, and three were satisfactory. One method uses a thermal grooving approach. Particles are mounted and polished metallographically. The particles are then removed from the mount and heated to 1550°C for 30 min. The material in grain boundaries is preferentially evaporated. The microstructure can be observed with a scanning electron microscope or by light microscopy.

The other two techniques are more conventional. One electrolytic etchant and one chemical etchant have been found that satisfactorily etch the silicon carbide. The electrolytic method uses a mixture of 500 cm^3 of H_3PO_4 and 20 g $K_2Cr_2O_7$ as the electrolyte. The polished sample is etched for 1.5 min at a current density of 4 to 5 A/cm^2. This method etches both large and small grained material very well. It also brings out any banding present in the silicon carbide coating layer. The chemical etch[27] is a mixture of NaOH and $K_3Fe(CN)_6$. Saturated water solutions of both chemicals are mixed in equal volume ratios. The mixture is then heated to its boiling point, and polished samples are dipped for 1 to 10 min. This method etches both large and small grained material. The microstructure of large grained material

is more distinct. This method does not show banding as clearly as the electrolytic method. Bands can be seen, but they are fewer and less pronounced. Figure 3.21 shows very good agreement between the thermal grooving method and the chemical etch.

The study of different etchants revealed two very different silicon carbide structures. A large grained material was seen when a coating was deposited at 1600°C and 0.17 μm/min. A highly banded material with a small grain size was seen when a coating was deposited at 1500°C and a deposition rate of 0.45 μm/min. These microstructures are seen in Fig. 3.21. Silicon carbide structures were examined further by looking at four coatings made with a conical gas distributor in the 0.13-m-diam (5-in.) coater. The deposition conditions and microstructures can be seen in Fig. 3.22. The coatings deposited at 0.1 μm/min were denser and coarser grained than coatings deposited at 0.2 μm/min. Changing the deposition temperature from 1600 to 1700°C did not result in a detectable change in structure.

The influence of annealing on the structure and strength of SiC-coated particles was investigated. The crushing strengths of these particles were examined because silicon-carbide-coated particles exhibit lower crushing strengths than any other step in the Triso coating cycle. Twelve particle batches processed through the silicon carbide layer were annealed at various conditions. The temperatures used varied between 1630 and 2000°C and the times varied from 12 to 420 min. The crushing strength of each particle batch clearly decreased on annealing. The SiC grain size increased only slightly during annealing.

Considerable time was spent preparing fuel for irradiation testing. Three batches of Triso-coated resin and ten batches of Biso-coated ThO_2 were prepared. This was the first time that resin-derived fuel had been prepared with the 0.13-m-diam (5-in.) coater. This fuel is shown in Fig. 3.23. It is apparent in the figure that the coated particles are more nearly spherical when the frit-type gas distributor was used rather than the conical distributor. This is a general observation and it is discussed further in a recent report[28] dealing with the influence of equipment and process variables on particle shape.

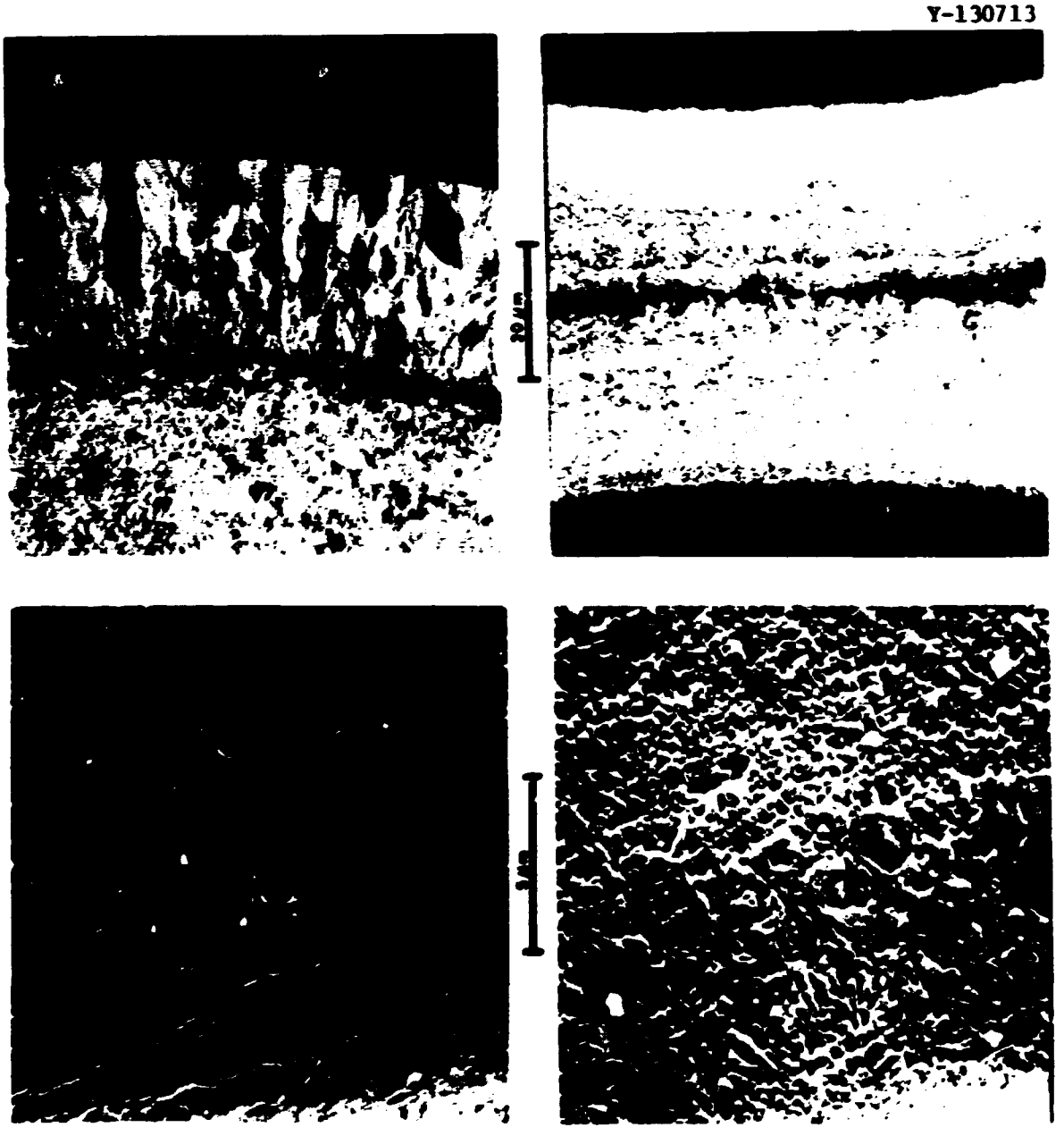

Fig. 3.21. Coarse and Fine Grained Silicon Carbide as Revealed by Chemical (top) and Thermal (bottom) Etching. On the left is material deposited at 0.7 µm/min at 1600°C having a crushing strength of 12.5 N (2.8 lb). On the right is material deposited at 0.45 µm/min at 1500°C having a crushing strength of 19.5 N (4.4 lb).

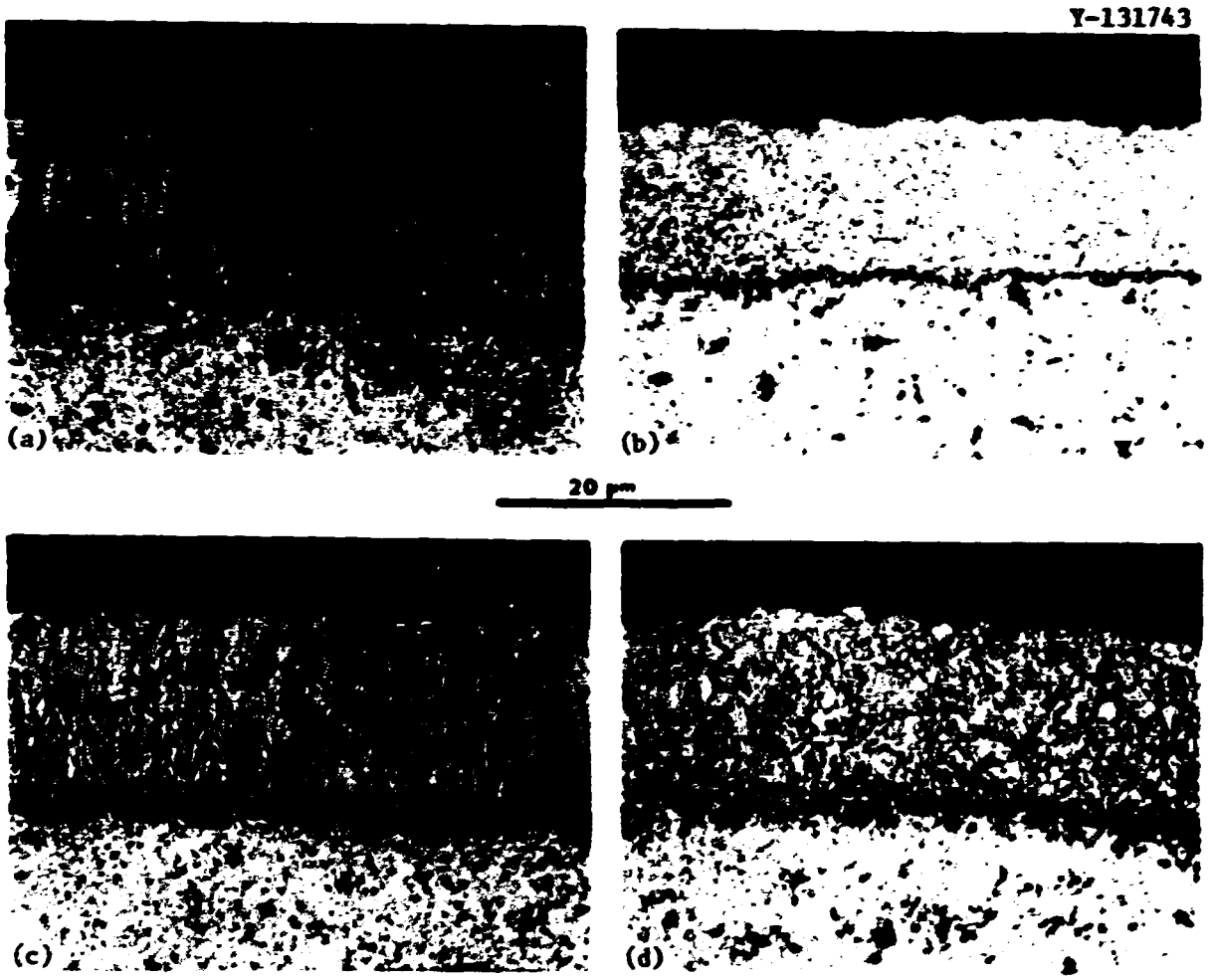

Fig. 3.22. Effect of Deposition Rate and Temperature on the Structure of Silicon Carbide. (a) 0.1 μm/min at 1700°C. (b) 0.2 μm/min at 1700°C. (c) 0.1 μm/min at 1600°C. (d) 0.2 μm/min at 1600°C.

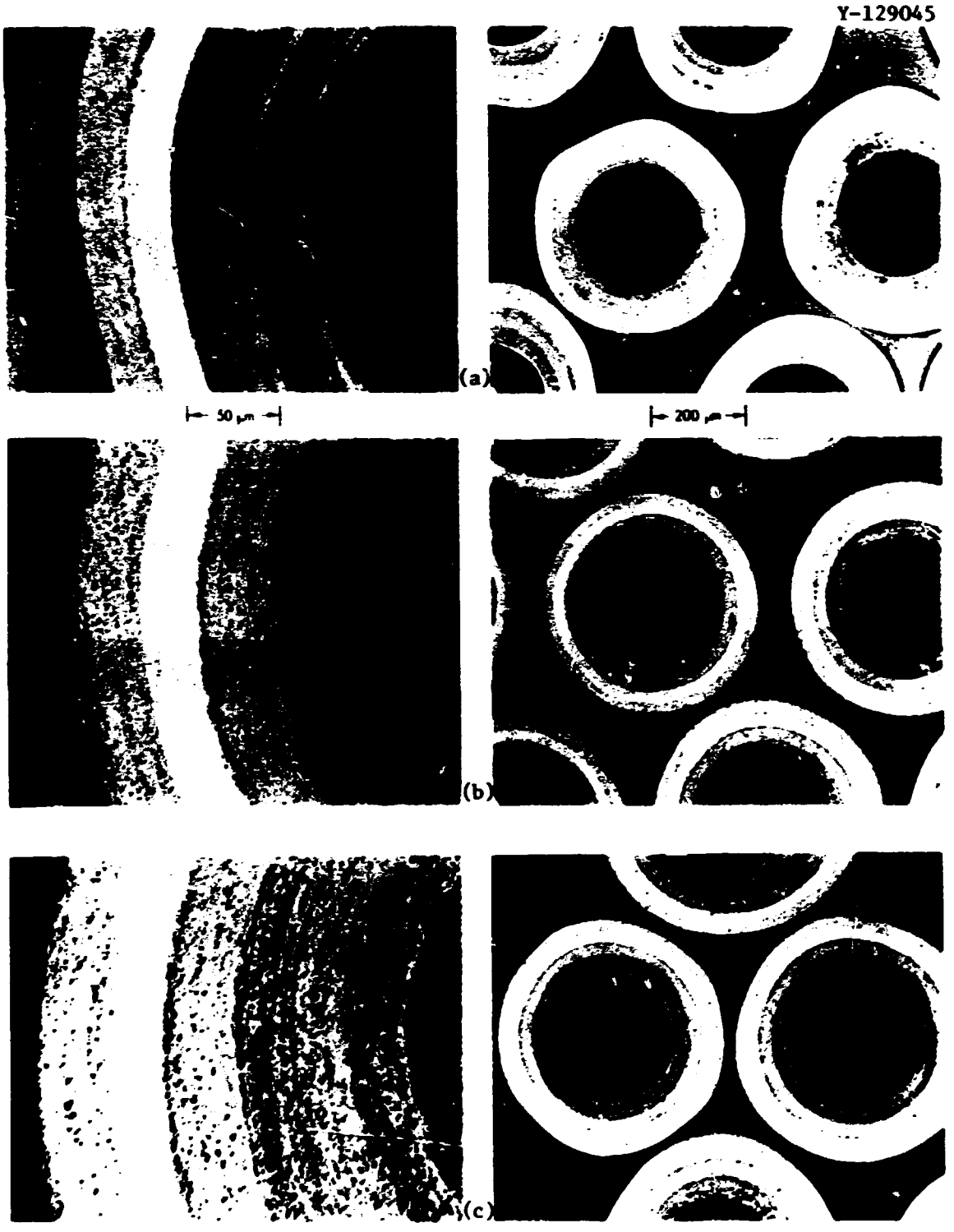

Fig. 3.23. Triso-Coated Resin Fuel Prepared in the 0.13-m-diam (5-in.) Furnace. (a) Cone distributor, 76.6 ± 2.6% converted. (b) Frit distributor, 12.6 ± 2.5% converted. (c) Frit distributor, 69.4 ± 2.1% converted.

Four of the batches of fertile particles prepared for testing in the OF-2 capsule are shown in Fig. 3.24. The variables being investigated here are C_3H_6 flow rate [0.94 vs 1.7 liters/sec (2 vs 3.6 scfm)] and diluent gas concentration (0 vs 50%). Each particle batch in Fig. 3.24 was coated by use of the 0.13-m-diam (5-in.) frit.

During fabrication of resin derived particles, uranium was found escaping from the kernels and being dispersed in the buffer layer. This occurred during annealing of inner LTI coated particles at 1800°C and also during SiC coating. X radiographs showing the extent of uranium dispersion for the particles prepared for irradiation testing appear in Fig. 3.25. About half the particles from the two batches having nominally 75% conversion show some dispersion. However, only an occasional particle from the batch having 12.6% conversion showed dispersion, and in these cases only a few small specks of uranium-bearing material were present in the buffer layer. Several factors that can cause uranium dispersion were identified. These factors were diffusion of HCl or Cl_2 present during the SiC coating through permeable LTI coatings and subsequent reaction with the kernel, reaction during the carbon coating operation of the kernel with C_2Cl_4 that had backstreamed from the scrubber into the coating furnace, and exposure of converted kernels to the atmosphere before coating. A report describing the fuel dispersion work in more detail is available.[29]

3.6.1.3 Laboratory-Scale SiC Coating — J. I. Federer

Most of the laboratory-scale SiC process development activities consisted of evaluating the effects of coating conditions on coating characteristics when methyltrichlorosilane (MTS) is used as the source for SiC. The principal variables of MTS flux, H_2/MTS ratio, and temperature were varied over wide ranges in search of trends: MTS flux was varied from 0.03 to 1.3 cm^2/min; H_2/MTS ratio was varied from 5 to 44; temperature was varied from 1225 to 1775°C. The results of this work may be summarized as follows:

1. Coating rate is affected by each of the principal variables; however, H_2/MTS ratio and temperature also affect density, whereas

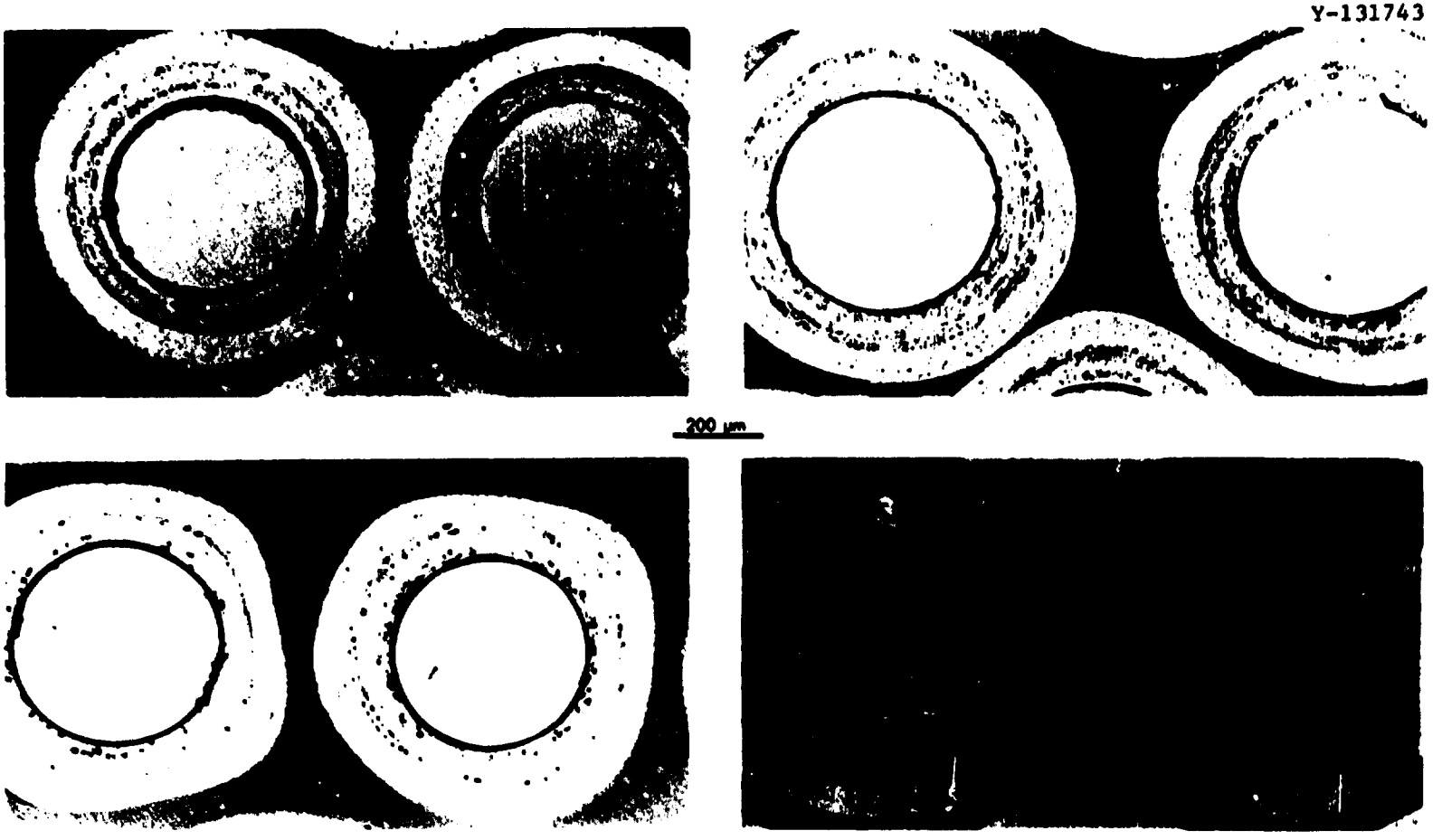

Fig. 3.24. Annealed Fertile Particles Prepared in the 0.13-m-diam (5-in.) Furnace. Top: C_3H_6 flow rate 0.94 liter/sec. Bottom: 1.7 liters/sec. Left: No helium diluent. Right: Helium flow equal to C_3H_6 flow.

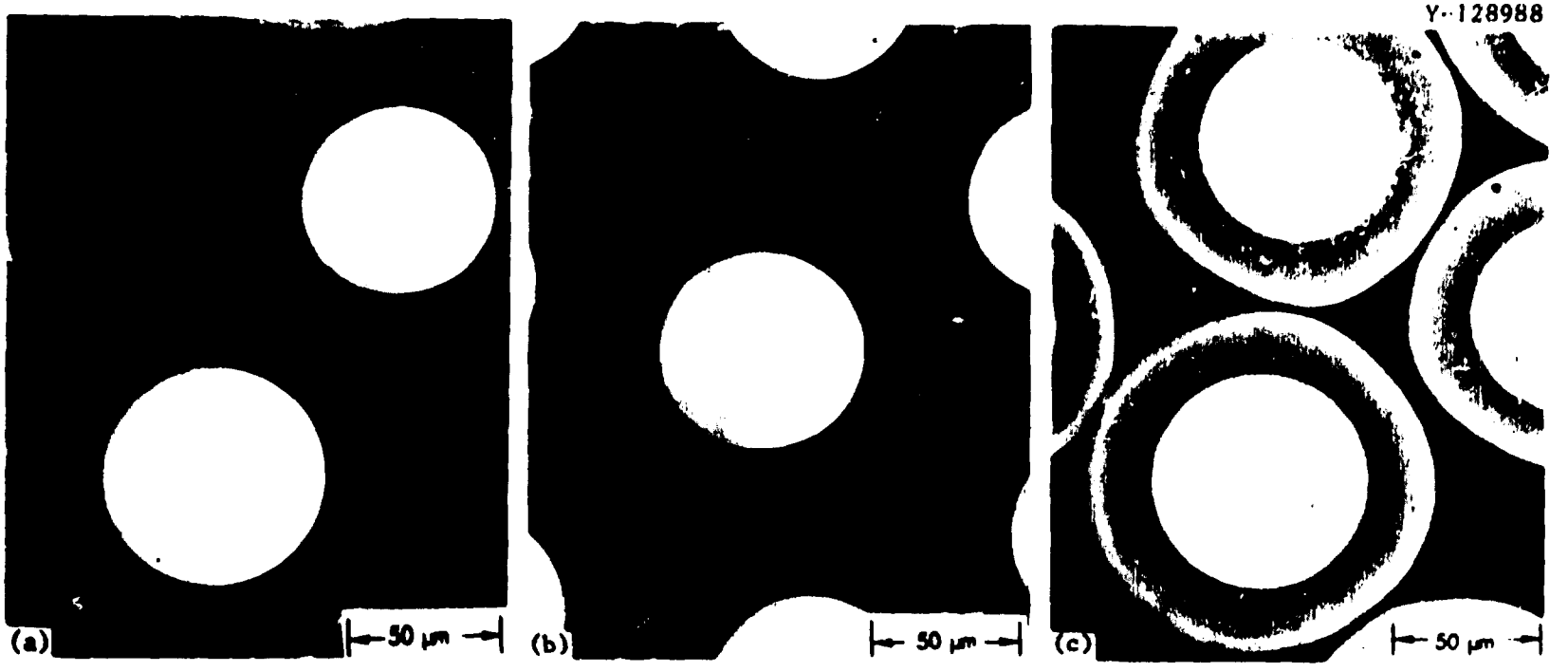

Fig. 3.25. X Radiographs of SiC-Coated Resin Showing Uranium in the Buffer Coating Layer of the Two Nominally 75%-Converted Batches. (a) Frit distributor, 69.4 ± 2.1% converted. (b) Frit distributor, 12.6 ± 2.5% converted. (c) Cone distributor, 76.6 ± 2.6% converted.

coating rate does not. A highly dense SiC coating can be obtained at optimum values of H_2/MTS ratio and temperature; the coating rate can then be conveniently varied by varying the MTS flux.

2. At optimum values of H_2/MTS ratio and temperature the coating rate is a linear function of MTS flux. Coating rates as high as 4 μm/min have been obtained.

3. Coating density is strongly affected by H_2/MTS ratio. Except for a few data points, the density appears to increase rapidly with increasing H_2/MTS ratio in the range 5 to 20, and is relatively insensitive to a further increase in H_2/MTS ratios. Coatings for irradiation testing were deposited at an H_2/MTS ratio of 30.

4. Since an H_2/MTS ratio of at least 20, and preferably higher, is needed for high density, the maximum coating rate is determined by the batch surface area and the coating tube size. The maximum coating rate occurs at the greatest MTS flux (and corresponding H_2/MTS ratio) that does not eject microspheres out of the coating tube. A coating rate of 1 μm/min appears to be practical in the small coating tubes used in this work. Significantly higher rates would likely require trade-offs among flow rates, batch surface area (batch size), and coating tube size.

5. The microstructure is also strongly affected by H_2/MTS ratio and temperature, but not by coating rate. Figure 3.26 shows that as the H_2/MTS ratio is varied from 5 to 25 the microstructure changes from a disorganized mass to a striated structure and finally to a grain structure. Although not evident in the microstructures, the amount of porosity decreases with increasing H_2/MTS ratio. Similarly, Fig. 3.27 shows that as temperature is increased from 1375 to 1775°C the microstructure changes from a striated structure (containing excess silicon) to a dense grain structure, and finally to a coarsely crystalline structure containing gross porosity.

6. Coating density is strongly affected by temperature. Figure 3.28 shows the results of the present study along with those of three other investigators.[30–32] Except for one case[31] the densities exhibited maximum values in the temperature range 1500 to 1650°C. Coatings deposited

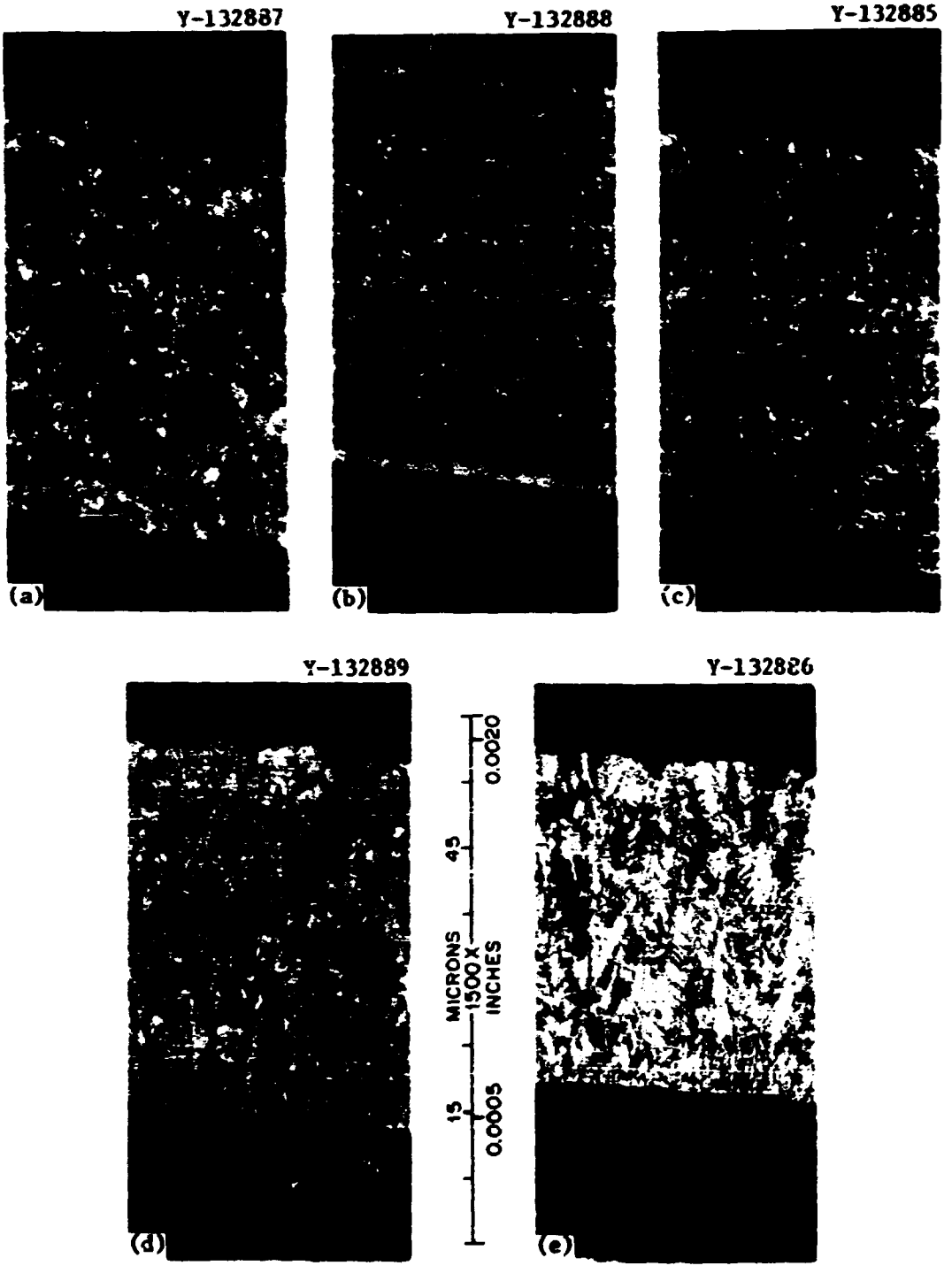

Fig. 3.26. Microstructures of Silicon Carbide Coatings Deposited at 1575°C at Various Ratios of Hydrogen to Methyltrichlorosilane. (a) 5. (b) 10. (c) 14. (d) 20. (e) 25.

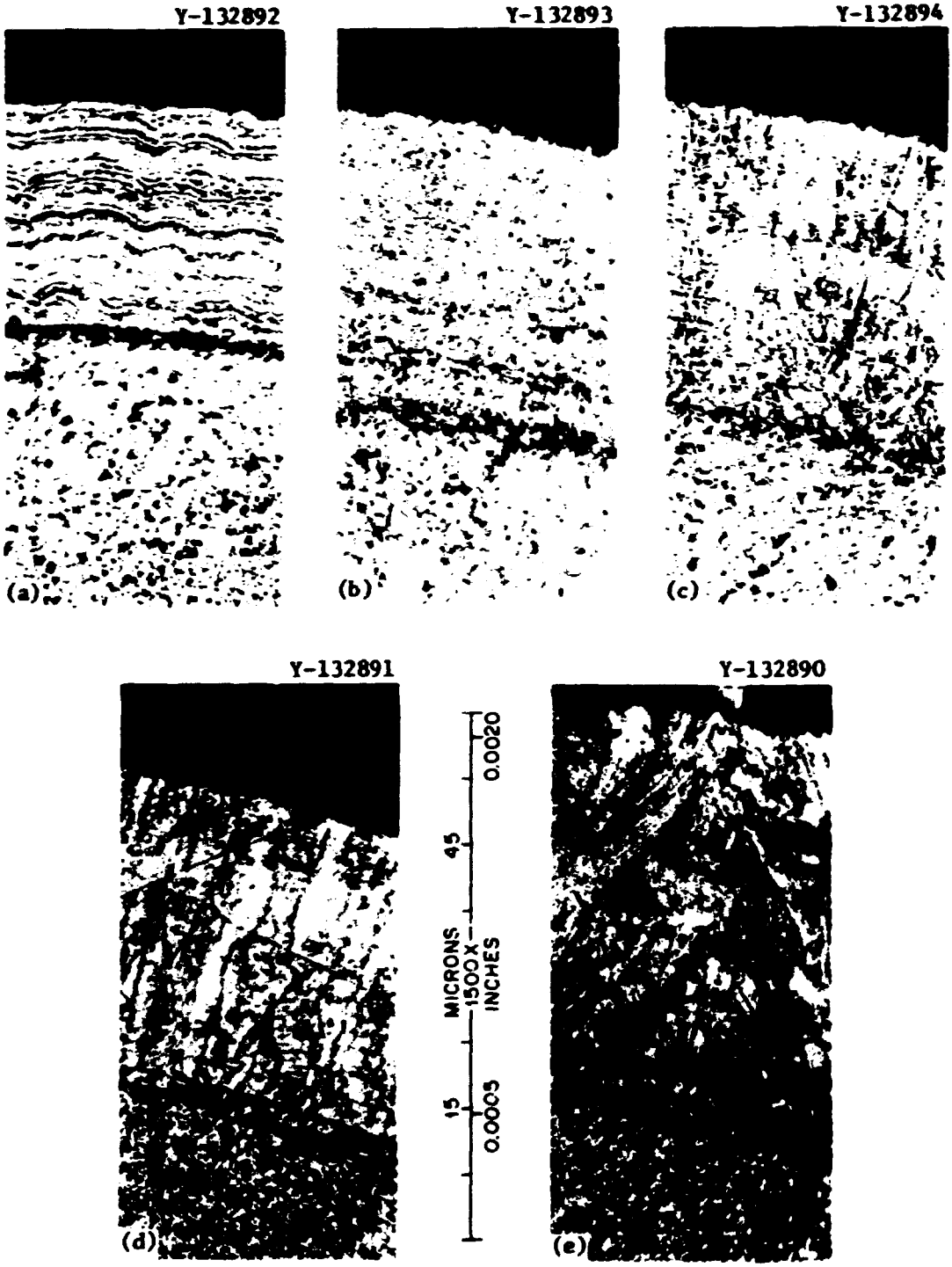

Fig. 3.27. Microstructures of Silicon Carbide Coatings Deposited at Various Temperatures and Hydrogen-to-Methyltrichlorosilane Ratio of 30. (a) 1375°C. (b) 1475°C. (c) 1575°C. (d) 1675°C. (e) 1775°C.

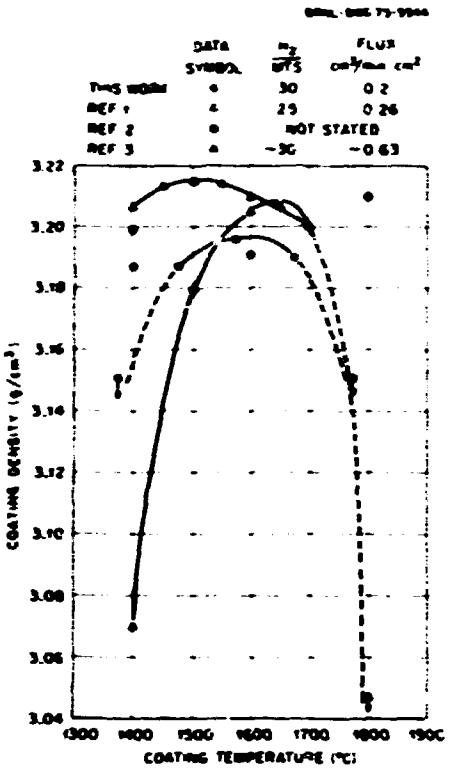

Fig. 3.28. Density of SiC Coatings as a Function of Coating Temperature. References cited are: E. Gyarmati and H. Nickel, JÜL-900-RW (ORNL-tr-2733); T. D. Gulden, GA-6275; and E. H. Voice and D. N. Lamb, DP-677.

below about 1400°C have low density due to the presence of excess silicon, while coatings deposited above 1700°C may have gross porosity, as shown in Fig. 3.27. Coatings for irradiation testing were deposited at 1575°C.

7. Heat treatment at 1900°C for 30 min, the standard treatment for consolidating coated microspheres into fuel sticks, does not significantly affect the microstructure of SiC coatings, regardless of the coating conditions or coating rate.

In summary, coatings have been deposited at rates up to 4 μm/min. A rate of about 1 μm/min appears to be practical for reasonable batch sizes. The effects of H_2/MTS ratio and temperature on density and microstructure have been determined. Highly dense polycrystalline coatings can be prepared at H_2/MTS ratios of 20 or more and at temperatures in the range 1475 to 1675°C. A more detailed discussion of these results will be published.[33]

3.6.2 Coater Effluent Treatment and Analysis

3.6.2.1 Perchloroethylene Scrubber — D. P. Stinton

A final area of equipment development is the perchloroethylene scrubber[34] used to remove soot and hydrocarbon vapors from the coater off gas. This scrubber has, in general, performed very satisfactorily since installation more than a year ago, but two minor problems required attention. These problems involved plugging of the demister filters and a large loss of C_2Cl_4 by evaporation. To eliminate these problems, a chilled-water heat exchanger was added just downstream of the scrubber to condense C_2Cl_4, and the plugging of the demisters has been significantly reduced but not completely eliminated by these modifications. Reclamation of used C_2Cl_4 is described in Sect. 3.11.

3.6.2.2 Effluent Analysis — D. A. Lee, W. T. Rainey, D. A. Canada, J. A. Carter, and D. A. Costanzo

A time-of-flight mass spectrometer* (TOFMS) has been purchased and installed onto the 0.13-m-diam (5-in.) coating furnace. The TOFMS will be used to monitor in-line the effluents from the various processes used in preparing HTGR fuel microspheres. The processes to be monitored are: carbonization and conversion of uranium-loaded resin, deposition of carbon and silicon coatings, and particle annealing. A heated sampling loop has been constructed to transfer effluents continuously to the TOFMS from any one of three sampling ports in the facility. The TOFMS may be operated in either the scanner or sequencer mode. Repeated spectral scans may be made for all masses, or five preselected masses may be monitored continously in sequence. The analysis of the effluents with respect to time and temperature will aid in determining reaction mechanism and optimum process parameters as well as assure occupational and environmental safety from hazardous pollutants.

---

*CVC Products, Inc. (formerly Bendix) type MA-3.

3.6.3 Bulk Particle Transfer — J. E. Mack and D. R. Johnson

A pneumatic system was chosen as the method to be used for transferring the fuel particles through the refabrication cycle. The system must have the capability of transferring a variety of particle types ranging from the bare loaded resin to the outer LTI coated particle with virtually no cross batch contamination and minimum particle wear and breakage. Handling of the particles after application of several coating layers is necessitated by the present sampling technique, which requires removing the entire batch from the furnace, weighing it, and passing it through a sampler before returning it to the furnace. As a result, the system will be handling material that is thermally as well as radioactively hot. The particles must also be handled in an oxygen-free atmosphere following carbonization and conversion, because of their pyrophoric nature. Since one line will carry different particle types at different times, all transfers will be made with argon and an argon atmosphere maintained in the lines and hoppers at all times.

To determine the requirements of such a system, two 30-m (100-ft) 13-mm-ID (0.5-in.) transfer lines were constructed, one in polyethylene to obtain extensive particle velocity data and one in stainless steel. A collection hopper was located above the transfer hopper, and a batch was recirculated by gravity feed through a diverter valve. An interchangeable 90° bend in both loops permitted data acquisition for bend radii from 0.15 to 1.8 m (6 in. to 6 ft). The system parameters measured were air velocity, particle velocity, and pressure drop. The system components tested were collection and feed hoppers and two types of gravity flow diverter valves.

Several particle types were transferred, providing data and operating experience with particles of 500 to 800 μm mean diameter over a density range of 1.5 to 4.4 g/cm^3. Flow through the transfer line for each of these particle types can be described as dilute phase conveying, wherein all the particles remain entrained in the gas stream, and the density of the gas-particle mixture is fairly low, about 8 to 16 kg/m^3 (1–2 lb/ft^3). Figure 3.29 illustrates particle slip — the difference between air velocity and particle velocity — for four different particle types. The particle

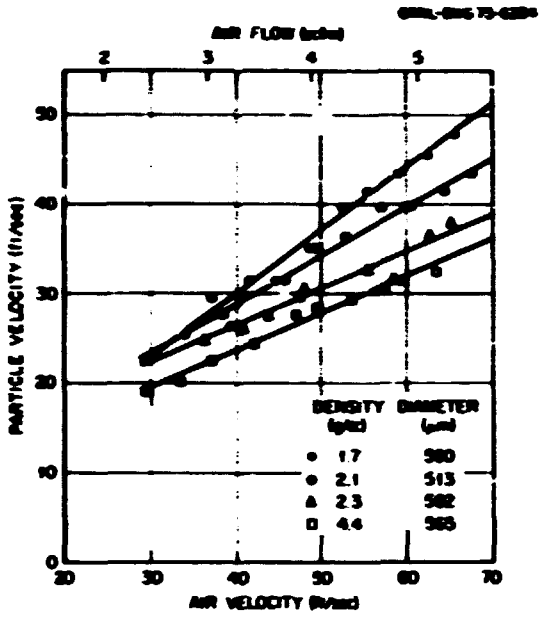

Fig. 3.29. Effect of Particle Density on Particle Slip During Pneumatic Transfer of Bare, Biso-Coated, and SiC-Coated Loaded Resin and Biso-Coated Thoria (in Order of Increasing Density) in 13-mm-ID (1/2-in.) Stainless Steel Tubing. To convert, 1 ft/sec = 0.30 m/sec; 1 scfm = 0.47 std liter/sec.

is moved along in the air stream by aerodynamic drag. The amount of slip a particle experiences depends primarily on the size, shape, and weight of the particle. As a result, particle velocity will be a function of the particle density and square of the diameter, as well as of air velocity. Multiple regression analysis is currently being used to determine the relative weights of each of these factors for use in predicting transfer characteristics of the pyrophoric material.

Figure 3.30 illustrates variation in the air-particle bed density with air velocity and particle type. As air velocity decreases, particle velocity decreases faster than the feed rate, and the air-particle density increases until saltation occurs. At saltation, the air velocity is insufficient to carry the particles along, and they become disentrained from the air stream, filling the horizontal sections and blocking the vertical sections. Tests show that this condition occurs when the driving pressure falls below 14 kPa gage (2 psig), indicating the minimum pressure drop for our system. Purge pressures below 69 kPa gage (10 psig) proved sufficient to reestablish the flow following a simulated loss-of-power shutdown.

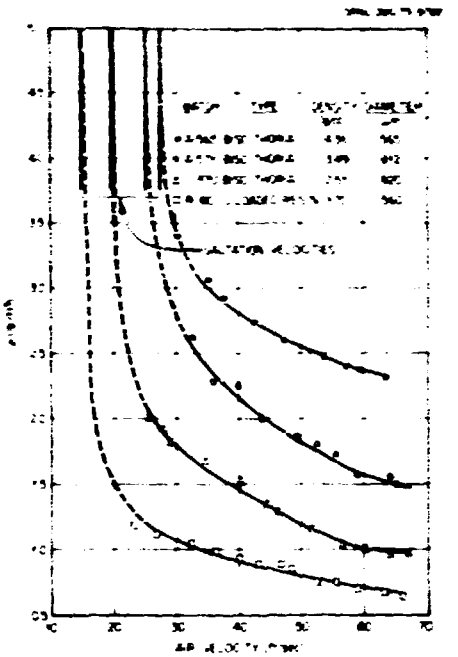

Fig. 3.30. Density of the Air-Particle Mixture Versus Air Velocity for Pneumatic Conveying in 13-mm-ID (1/2-in.) Stainless Steel Tubing. To convert, 1 lb/ft^3 = 16 kg/m^3; 1 ft/sec = 0.30 m/sec.

Pressure drops were measured over horizontal and vertical straight sections, across bends of different radii, and across the particle feed inlet for various transfer conditions and particle types. They ranged from 0.45 to 1.35 kPa/m (0.02–0.06 psi/ft) for horizontal conveying to 1.1 to 2.3 kPa/m (0.05–0.10 psi/ft) for vertical conveying. Pressure drops across the bends ranged from 0.45 to 2.3 kPa/m (0.02–0.10 psi/ft). Pressure drops across the inlet where the particles must be accelerated from rest ranged from 1.6 to 5.7 kPa/m (0.07–0.25 psi).

Particle wear and breakage were also evaluated. The particle types tested showed no measurable wear except the buffer-coated particle, whose mean diameter decreased 10 μm after 25 runs through the 30-m (100-ft) loop, averaging 0.4 μm per transfer. Particle breakage ranged from a failure fraction of 0.7×10^{-4} for the SiC-coated particle to 2×10^{-4} per transfer for a reference fissile design Biso thoria batch. The Biso thoria batch had an unusually low crushing strength of 6.2 N (1.4 lb) compared with 11 to 13 N (2.5–3.0 lb) for a normal batch. The failure

fraction for a buffer-coated thoria batch was 1.5×10^{-4} per transfer. No significant particle damage occurred in transferring bare loaded resin, other than the separation of smaller "satellite" spheres from their parent particles. We feel that most of the particle damage occurs in the collection hopper rather than in the transfer line, and current design effort is directed toward a collection hopper entry that minimizes abrupt particle-wall and particle-particle interactions. A report describing all the pneumatic particle transfer work is in preparation.

3.7 FUEL ROD FABRICATION (WORK UNIT 2105) — D. R. Johnson, P. Angelini, J. E. Rushton, S. R. McNeany, R. W. Knoll, R. A. Bradley, and R. M. DeLozier

The purpose of this work is to develop processes and equipment suitable for the remote refabrication of HTGR fuel rods. The fuel rods are 13 or 16 mm (1/2 or 5/8 in.) in diameter and 50 to 65 mm (2–2.5 in.) long and contain mixtures of fissile and fertile coated particles and graphite shim particles bonded by a matrix of pitch binder and graphite filler.

The principal activities in fuel rod fabrication are dispensing particles, blending them, and loading them into molds, injecting the matrix into the beds of particles to form fuel rods, and inspecting and assaying the rods.

3.7.1 Equipment Development

The conceptual design for a commercial-scale, remotely operable HTGR fuel rod molding machine has been prepared. It will form 40,000 rods per day by the slug injection process. The major steps of fuel particle dispensing and blending, mold loading, and fuel rod forming are performed by the machine.

A laboratory fuel rod molding machine was designed and built in 1972 to demonstrate the slug injection process.[35] This machine has met or exceeded all the design objectives and has produced over 30,000 HTGR fuel rods. The design and operating experience with the laboratory fuel rod machine provide the basis for the conceptual design of the commercial-scale machine.

The laboratory fuel rod machine comprises operating stations positioned around a rotary index table to which molds are permanently affixed. This type system is used extensively in automatic assembly operations in which the operating time for each station is about the same. The fabrication rate for this type of system is obviously controlled by the cyclic time of the longest operation.

The operation requiring the most time in fuel rod molding is injection of the matrix, which requires 20 to 30 sec. If a 20-sec cyclic time is assumed for this operation, the maximum fabrication rate obtainable with the laboratory fuel rod machine operated with single-station indexing is about 4000 rods per day. By using multiple matrix injection stations and a more complex indexing cycle, a maximum of about 10,000 rods per day could be achieved with this type of machine.

To achieve a fabrication rate greater than that obtainable with a machine employing molds affixed permanently to a rotary index table, the approach used in the conceptual design of the commercial fuel rod molding machine is similar to that used in the bottling and canning industry. In this concept, the molds are free members, which are transported from station to station via conveyor for processing as are bottles on a bottling machine. This system permits simultaneous multiple-rod injection while retaining the single-rod processing feature so important to interfacing with other operating stations, thereby providing a greater degree of flexibility than is obtainable with a fixed rotary system. The fabrication rate of the production machine depends only upon station multiplicity and the speed of the transfer system. A rate of one rod every 2 sec or about 40,000 rods per day was chosen as the design basis for the commercial-scale remote fuel rod molding machine.

The rod molding machine comprises four rotary tables on which the molds are carried through their sequence of operations and transferred from one table to the next at tangent points. The four tables are the mold-unload-load table, the mold heating table, the mold injection table, and the cooling table. The arrangement of these tables along with peripheral auxiliary equipment is illustrated in Fig. 3.31. The machine is to be constructed in modules designed for remote removal and installation. All service connections are to be quick disconnect types appropriate for manipulator operation.

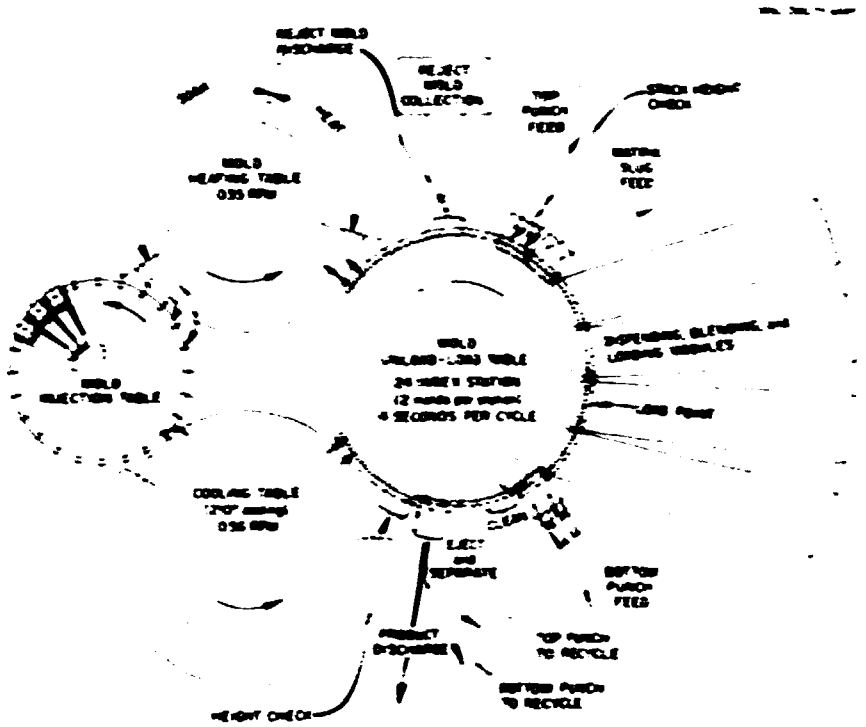

Fig. 3.31. Fuel Rod Molding Machine.

An HTGR fuel rod storage magazine and equipment for auxiliary loading, unloading, fuel rod stack height inspection, and reject stack handling have been designed. The basic element in the storage concept is the storage magazine, which provides surge capacity between fuel rod fabrication and fuel element assembly. The magazine is a rectangular array of 218 thin-wall stainless steel tubes, each of which holds 15 rods, thus giving the magazine a total capacity of 3270 rods. The geometry of the magazine is critically safe. The front of the magazine is made accessible for loading via a sliding door. The rods are retained by a rear faceplate, which is provided with properly aligned holes for an ejection plunger. The magazine is positioned for loading and unloading by an indexing device operating in the x and z planes. The magazine is designed for remote removal from the indexing device to an interim storage area. The magazine loading station interfaces with fuel rod inspection by means of an air levitation track. The magazine unloading device similarly interfaces with fuel element loading. Figure 3.32 illustrates the fuel element magazine and the unloading station.

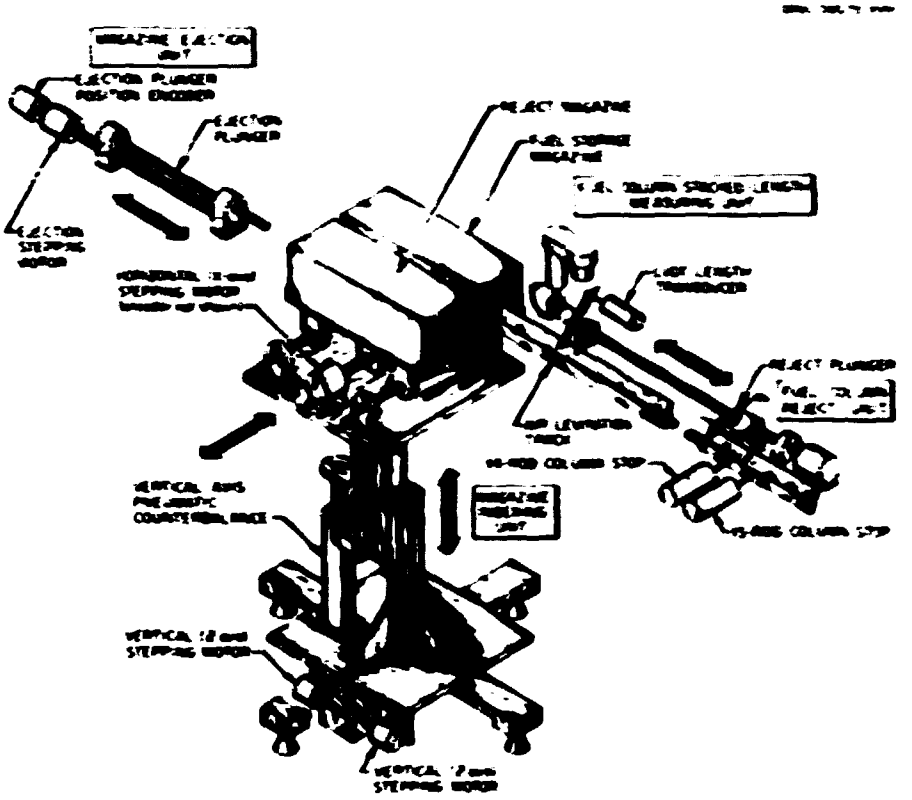

Fig. 3.32. Fuel Rod Storage Magazine Unloader Mockup Schematic.

3.7.2 Process and Materials Development

The slug injection process has been chosen for molding HTGR fuel rods. A preformed cylinder (slug) of matrix material is loaded into a mold containing the fuel particles, the mold is heated to soften the matrix, and the matrix is intruded into the bed of particles by a pneumatic ram. Many of the recent advantages in fuel rod fabrication development have centered around improvements in the characterization and fabrication of the matrix slugs.

The present reference matrix material is a mixture of petroleum pitch, graphite flour, a mold lubricant, and a low-coke-yield additive. The components are combined by melting the organics in a heated Helicone blender,* then adding the graphite, followed by high-shear mixing. The material is discharged from the blender and cooled as a solid mass. The cooled solid is then ground into a granular mix, <5 mm, and dry-pressed into the finished cylinders.

---

*Atlantic Research Corp., Alexandria, Virginia.

Procedures have been developed for chemical analysis of the matrix slugs. The relative proportions of pitch, graphite, mold lubricant, and low-coke-yield additive can be determined. Graphite content is measured gravimetrically once the organics have been dissolved. Gel permeation chromatography is used to analyze for the low-coke-yield additive as well as to qualitatively check the chemical composition of the pitch, while fluorine nuclear magnetic resonance is used to measure the concentration of mold lubricant.

The concentration of mold lubricant in the ground matrix material has been found to vary by as much as a factor of 3, indicating poor mixing of this component. Variation in the concentration of mold lubricant strongly influences the time required for matrix intrusion during fuel rod molding. As a result of these observations, the matrix blending step is presently being reevaluated.

The relatively coarse (<5 mm) ground matrix material normally used for dry pressing of matrix slugs frequently contains large gas bubbles within the granules. These pores are retained within the molded fuel rods and are thought to be a major source of gross macroporosity in fired fuel rods. The presence of large pores in the dry-pressed matrix slugs can be largely eliminated by grinding the hot-mixed matrix into finer granules, smaller than 300 μm. However, fine particles below 10 μm, may cause laminated matrix slugs; thus, the fine particles may be screened out and recycled. Figure 3.33 illustrates the effect of dry-press feed granule size on the porosity of dry-pressed matrix slugs. An experiment is in progress to demonstrate quantitatively that the porosity in fired fuel rods is related to the porosity in the matrix slugs.

Improved quantitative metallographic techniques have been developed for measurement of porosity in fuel rods. Two automatic quantitative metallographic instruments have been evaluated for the characterization of porosity in fuel rods from polished metallographic sections. One instrument uses a lineal analysis technique to measure the volume fraction of porosity and the distribution by volume of pore sizes; the other, a Quantimet P20 image analyzer uses areal analysis to determine the above

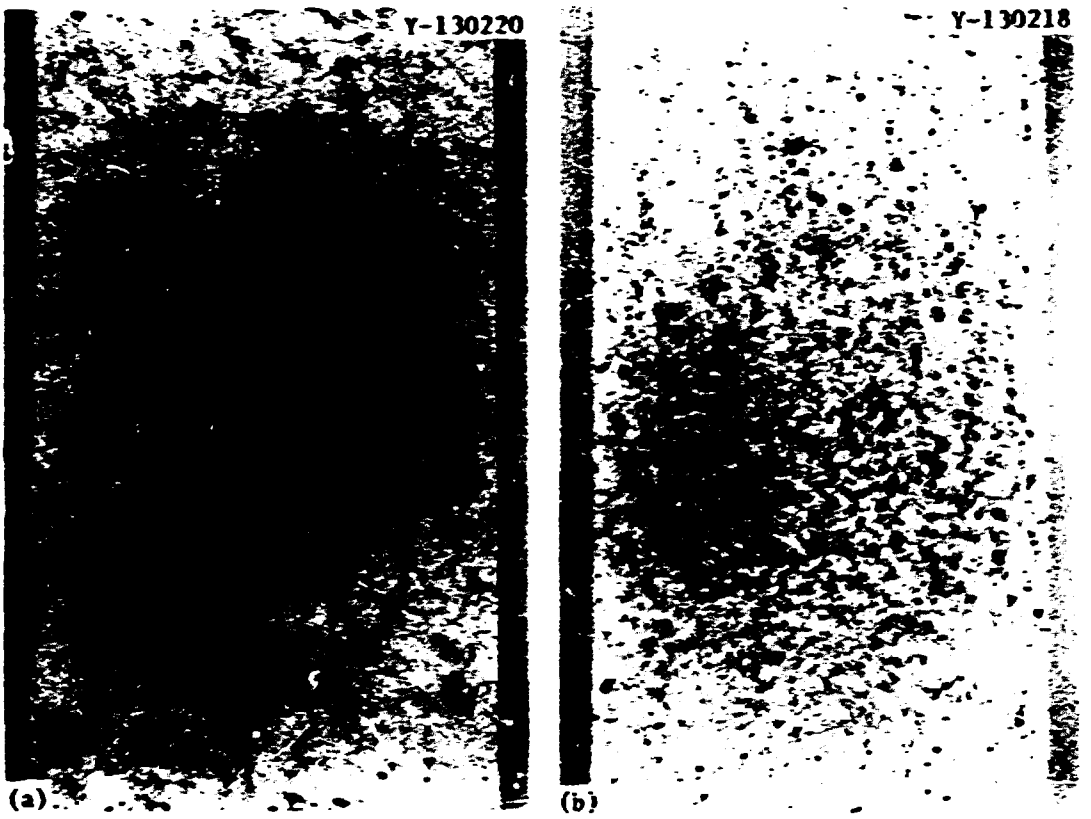

Fig. 3.33. Cross-Sectional Views of 13-mm-diam (0.5-in.) Matrix Pellets Showing the Effect of Initial Feed Particle Size on Microstructure. 5×. (a) Particle size up to 5 mm. (b) Below 300 μm.

properties plus the distribution by number of pore sizes. The areal analyses have been shown to be more desirable for inspection of fuel rods. For example, total microporosity measured by areal analysis is more consistent with coke yield measurement.

The causes and possible improvements for particle breakage during fuel rod fabrication have been investigated. Particle failure during the matrix injection step of fuel rod molding has been observed. The number of broken particles that result from rod molding depends strongly on injection pressure and, presumably, the strength of the coated fuel particles. Fuel particle characterization results for a batch of Biso-coated thoria particles indicate that the weakest particles may be concentrated in a narrow particle size range. Figure 3.34 illustrates coated particle thicknesses, determined by contact microradiography,

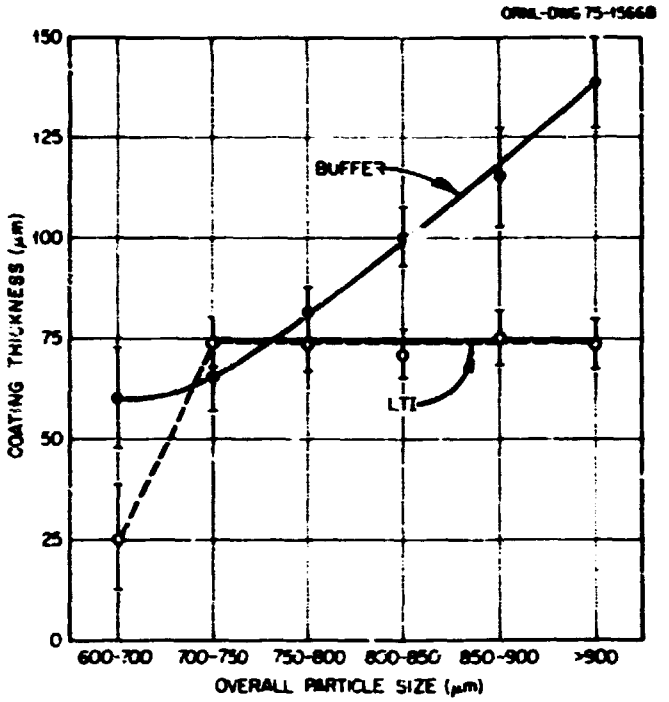

Fig. 3.34. Coating Thickness of Biso-Thoria Particles Versus Overall Particle Size (Fertile Batch A-572).

as a function of overall particle size. These results indicate that the buffer coating thickness varies with particle size, but the inner isotropic carbon coating is invariant with particle diameter at all but the very small particle diameters. The particles smaller than 700 μm have very thin inner isotropic carbon coatings. As a result of the thin coatings, the smallest particles are significantly weaker than the remainder of the batch. Table 3.6 lists coated particle crushing strength data that illustrate this size effect.

In addition, particle diameter measurements of large samples of 10,000 particles have indicated that the tails of the particle size distribution deviate significantly from a normal distribution. In particular, there are more of the very small particles than a normal distribution would predict. Failed particle analyses of the as-received coated particles indicated that 99% of the failed particles were smaller than 700 μm. Thus, these particle characterization results suggest that fertile particle breakage during fuel rod molding may occur selectively

Table 3.6. Crushing Strength of Sieved Fractions for Fertile Particle Batch A-572

Particle Sieved Fraction Size (μm)	Crushing Strength	
	(N)	(lb)
>900	17.4	3.9
850–900	17.4	3.9
800–850	16.5	3.7
750–800	14.7	3.3
700–750	16.5	3.7
600–700	6.2	1.4
Batch	18.2	4.1

among the smallest particles, and that the failed fuel fraction can be significantly improved by screening out the small particles before fuel rod fabrication. As these results are based upon the characterization of a single batch of coated fertile particles, they may not be typical. Additional work with more batches of particles is in progress in order to verify the preliminary conclusions. Similar characterizations of Triso-coated fissile kernels have indicated that the size distribution for fissile particles is primarily due to variations in kernel size. Thus, the fissile particles with defective coatings cannot be separated from the batch by screening.

3.7.3 Fuel Rod Inspection and Assay

A nondestructive uranium assay instrument is under development for the fabricated HTGR fuel rods. The technique selected for this application uses a ^{252}Cf neutron source to irradiate the uncarbonized fuel rods. The irradiating neutrons induce fission in the fissile material in a rod, and the resulting prompt fission neutrons are detected with ^{4}He-filled proportional counters. The detected count rate is directly related to the fissile uranium content and can be calibrated with rods of known uranium loadings.

The active ^{252}Cf assay method was selected after completion of a study of HTGR fuel characteristics and their effect on nondestructive assay techniques.[5,7] The primary characteristic of the HTGR recycled ^{233}U fuel is its high gamma radiation due to the inclusion of trace amounts of ^{232}U and its decay product nuclides.

In the analysis of nondestructive assay methods for ^{233}U, an evaluation of the use of the ^{233}U gamma rays as a measure of fissile material content was completed. A sample of ^{233}U with 250 ppm of ^{232}U that was near equilibrium with its decay products was scanned with three types of high-resolution Ge(Li) spectrometers. Two of the spectrometers are located at Lawrence Livermore Laboratory, and the measurements were conducted there by Raymond Gunnink. The results indicated that for all detector configurations the gamma-ray background due to the ^{232}U decay products masks the ^{233}U gamma-ray lines. A gamma-ray spectrum of ^{233}U measured at ORNL with a Ge(Li) detector is shown in Fig. 3.35. The detector is true coaxial with a total volume of 54 cm^3, a relative efficiency of 9%, and a resolution of 2.3 keV at 1332 keV. The labels of Fig. 3.35 near the peaks indicate the parent nuclide and the gamma-ray energy. There is no indication of any ^{233}U gamma-ray lines in this spectrum. Thus assay for ^{233}U by direct detection of ^{233}U gamma rays is not feasible if ^{232}U contents are above 100 ppm of uranium.

Active assay methods were also reviewed, and the ^{252}Cf interrogation system was selected for development. The advantages of this technique are (1) that the detected signal is uniquely determined by the fissile content of the rods and (2) that the fast neutron detectors can be made insensitive to gamma radiation.

The assay development program at ORNL is directed towards operation of an engineering-scale assay instrument for ^{233}U-loaded fuel rods. The assay instrument must be remotely operable and maintainable so as to function in-line in a commercial refabrication facility. The program to develop this capability began with the design and fabrication of a laboratory-scale system, which will be used to optimize the nuclear characteristics and operating parameters of a prototypic assay instrument. A schematic drawing of this development device is shown in Fig. 3.36. A 1.4-mg ^{252}Cf source is positioned at the center of a

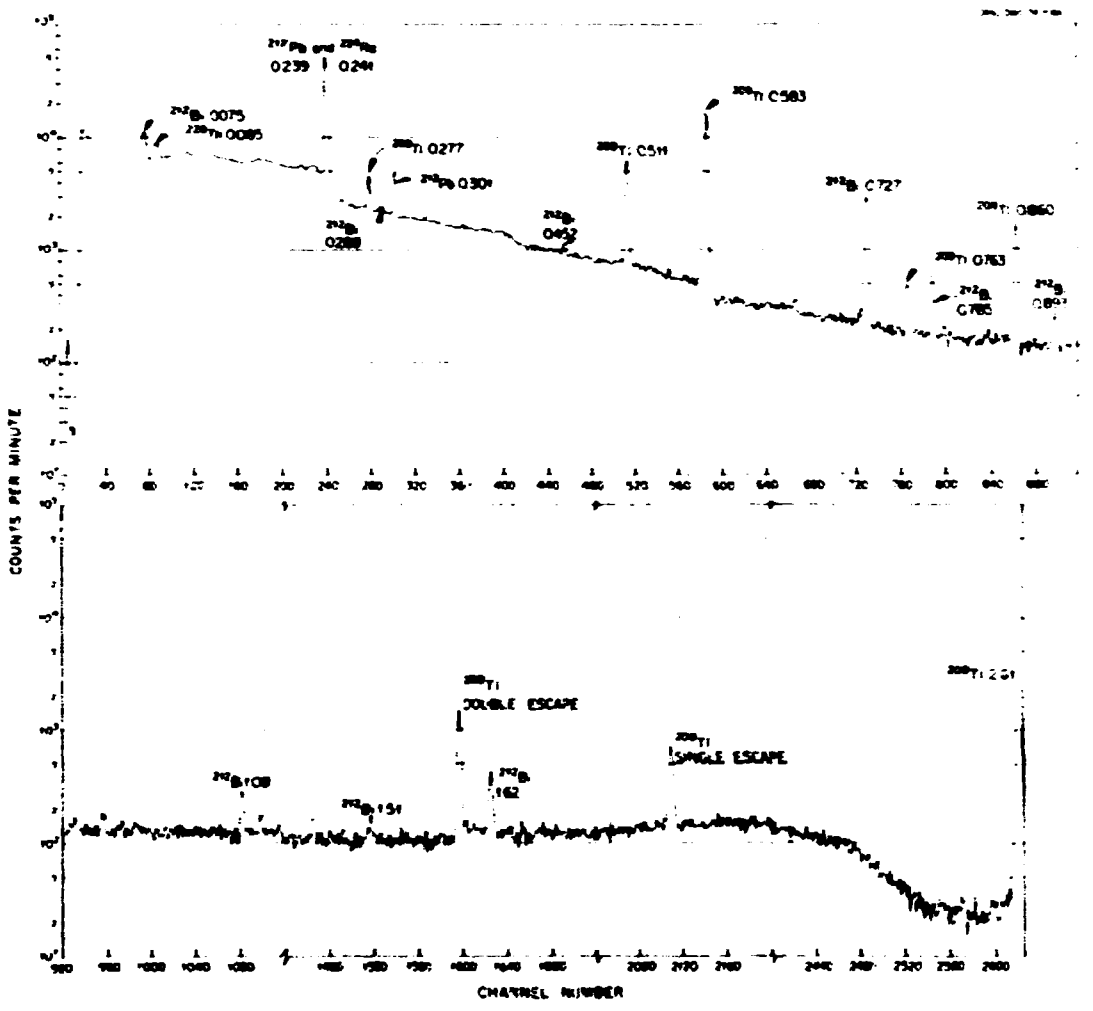

Fig. 3.35. Gamma Ray Spectrum ^{233}U with High ^{232}U Content.

cylindrical moderator assembly composed of graphite, polyethylene, and heavy water (D_2O). The fuel rods are positioned along the periphery of the moderator assembly. In this position they are exposed to well-thermalized neutrons, which selectively fission only the ^{233}U or ^{235}U atoms within the rods. The fission neutron detector, which is a ^{4}He proportional counter, records the number of prompt fission neutrons emitted from the sample. The calculated response function of this device has been previously reported.[5]

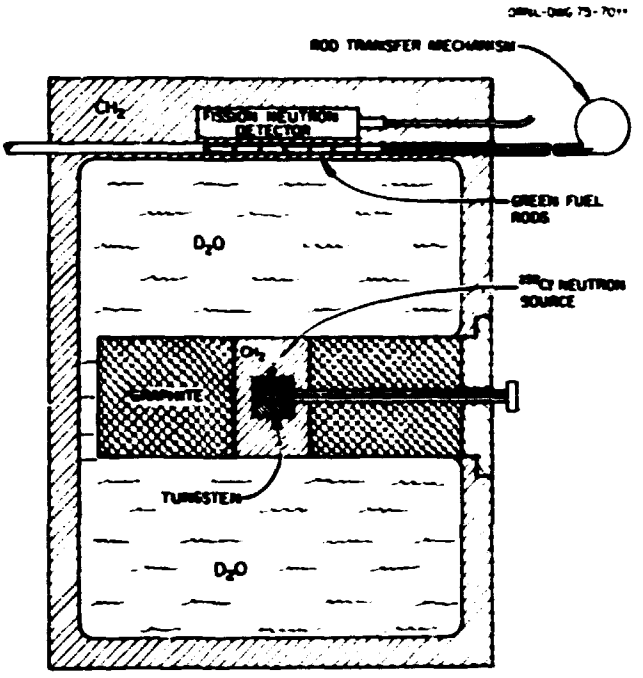

Fig. 3.36. HTGR Fuel Assay Development Device Prompt Fission Neutron Configuration.

The development assay device is to be located in an uncontaminated hot cell and operated semiremotely. The hot cell location offers several advantages:

1. The hot cell eliminates the need for expensive biological shields for the development device.

2. The hot cell operation will provide direct verification of remote handling procedures that will be incorporated in the prototypic assay instrument.

3. Handling of gamma-active ^{233}U samples is facilitated, while personnel exposure or contamination risks are minimized.

4. The hot cell remote manipulation equipment facilitates handling of the 1.4 mg ^{252}Cf source [radiation intensity of 100 R/hr at 0.3 m (1 ft)].

The current status of this program is that the cell is prepared for installation of the assay system and receipt of the ^{252}Cf source. The development equipment, which includes the ^{252}Cf irradiator, the fast neutron detectors, and the data processing electronics, is 80% complete.

A related development activity is the fabrication of uranium standards for the rod assay instrument. Delayed-neutron activation analysis is being used for this purpose to measure the relative and absolute ^{235}U content of individual Triso-coated fuel particles. The technique consists of irradiating a particle in a pneumatic tube facility in the Oak Ridge Research Reactor, then counting delayed neutrons, which are emitted by ^{235}U or ^{233}U in the kernel. A relative measure of a kernel's uranium density is found by dividing the delayed neutron counts by the volume of the kernel, which has been calculated from kernel diameter measurements taken from radiographs of the particle. An absolute measurement is done by irradiating a known ^{235}U or ^{233}U standard and comparing its delayed neutron count with that of a particle. In order to make particle-to-particle or particle-to-standard comparisons, each measurement must be corrected for thermal neutron self-shielding, for detector dead time, and for reactor power level changes, which occur during the course of a large number of measurements.

Three experiments have been completed. These evaluated the measurement technique itself and measured relative and absolute ^{235}U content of Triso-coated particles from two coating batches. The principal results are as follows: (1) The precision of the relative technique is about ±0.37% on a 95% confidence level when the reactor power level remains constant during the course of the measurements (i.e., when the series of measurements takes less than about 1 hr). (2) The kernel-to-kernel variation in the uranium density was ±3.6% on a 95% confidence level for 39 particles from one batch and ±3.2% for 38 particles from a second batch. (3) Limitations in the irradiation facility, which allow measurement of only one particle at a time, and reactor power variations, which reduce the precision of a long series of measurements, make the technique impractical for assay of large samples. In sum, the method is well suited for relative or absolute uranium assay of samples of individual particles.

An experimental effort is under way to develop a nondestructive fuel rod homogeneity inspection. A number of methods are being

evaluated to determine their applicability. These include x-ray attenuation, gamma-ray attenuation, passive counting of radioactive isotopes present in fuel rods, nuclear magnetic resonance, and x-ray fluorescence.

Radiation produced by typical commercial x-ray tubes is very intense; large, statistically significant numbers of counts are produced. The continuous x-ray spectrum produced by such tubes may be collimated and passed through a fuel rod. The x-rays are then detected with a thallium-doped NaI scintillation detector. The intensity of the beam is great enough that the signal from the detector is measured with an electrometer rather than a counting system. The measurements then give the total x-ray attenuation produced by all the mass components present in fuel rods. By relating the initial intensity of the x-ray beam to the intensity of the attenuated beam and using the results of calibration experiments, one may obtain the total mass distribution in fuel rods. This method has been shown to be feasible for determining the axial heavy metal homogeneity in fuel rods. The possibility of determining radial fuel homogeneity by interrogating the rod at different radial positions is being investigated.

The use of radioisotope gamma-ray sources is being evaluated as a means of determining total heavy metal, total mass, uranium, thorium, and light-element content and relative distribution in fuel rods. The radioisotope sources would replace the x-ray tube and power supplies in an attentuation system. A radioisotope source would be advantageous for use in a hot cell environment, as high-voltage power lines, x-ray vacuum tubes, and cooling systems are not required. In addition, the discrete gamma-ray energies simplify the analyses and can yield additional information as to the elemental mass distribution in fuel rods.

Three methods for measuring fuel rod homogeneity with radioisotope sources are being considered. The first configuration analyzes for the total mass distribution in fuel rods by using one gamma-ray energy in combination with an attenuation experiment. The second configuration uses a two-energy gamma-ray attenuation system such that the total heavy

metal and total light element content and relative distribution in fuel rods may be determined. A third category utilizes the differences of the thorium and uranium K absorption edges in determining the distribution of uranium and thorium and total light element content in fuel rods. In this latter method the radioisotope ^{169}Yb is to be used because it has gamma energies below, between, and above both the K absorptions edges of thorium and uranium. This isotope also has other advantageous characteristics: it has a fairly long half-life of over 32 days, it is fairly simple to fabricate into a source, it could possibly be reactivated while still encapsulated, its activity is such that an adequate number of counts can be detected, and its cost is less than $500 for typical sources of less than 2 Ci. Gamma-ray fluorescence as well as attentuation may be measured with the above configurations. Various detectors are being tested with the above mentioned systems: thallium-doped NaI crystals with photomultipliers, solid-state lithium-doped germanium crystal detectors, and intrinsic germanium crystal detectors. At this time, it seems as if the solid-state germanium detectors will be necessary with the system. The results of three gamma-ray attenuation experiments to determine total heavy metal content in fuel rods are shown in Table 3.7.

Table 3.7. Determination of Total Heavy Metal Content in Green Fuel Rods by Gamma-Ray Attenuation

Fuel Rod	Heavy Metal Loading, g/fuel rod	
	Actual	By γ-Ray Attenuation
HTR-3	5.0	4.9
HTR-4	3.9	4.1
HTR-6	2.5	2.7

A green fuel rod loaded with coated thorium particles and particles of ^{233}U with 10 ppm ^{232}U has been obtained. The fuel rod is four years old and in this respect has a radiation background typical of fuel rods to be produced in a recycle facility. The fuel rod will be studied as to the effect of its background radiation on the previously mentioned methods. The fuel rod will also be studied as to whether its gamma radiation can be used to determine the distribution of uranium within the rod. These experiments are continuing.

Nuclear magnetic resonance (NMR) is being evaluated as a means of determining ^{233}U and ^{235}U homogeneity in fuel rods. In this method the sample is placed in a magnetic field and an rf field supplied about the sample. At a specific frequency defined by the magnetic field and the characteristic nuclear magnetic moment of the nucleus the sample absorbs some of the rf energy. This method is specific as to isotopes of elements. This phenomenon exists in nuclei that have an odd number of nucleons. Thus the method should be sensitive to ^{233}U or ^{235}U. This method is attractive in that the detection is not affected by a gamma or particle radiation background. The phenomenon is being evaluated by testing nonradioactive model materials such as TaC, Eu_2O_3, and La_2O_3. These substances have been prepared in a size range similar to the weak-acid resin kernels used in Triso-coated particles. The isotopes of the above elements that have nuclear magnetic moments are ^{139}La, ^{151}Eu, ^{153}Eu, and ^{181}Ta. A sample of La_2O_3 has been sent to Varian Associates in Palo Alto, California. No data have yet been received. A wide-line state-of-the-art instrument is to be used there. The TaC and Eu_2O_3 have been sent to the NMR Laboratory at Y-12 in Oak Ridge, Tennessee. There a pulse-type instrument is to be used in studying the materials. If the results look encouraging, a ^{235}U sample will be sent to either laboratory for study. This method may be useful in other areas of HTGR fuel recycle and refabrication. Other radioisotopic or normal isotope analysis may be performed by this method.

3.8 FUEL ELEMENT ASSEMBLY (WORK UNIT 2106) — D. R. Johnson, A. J. Caputo, and W. G. Cobb

The fuel element fabrication development work is divided into four areas: (1) fuel element loading, in which green (unfired) fuel rods are loaded into the fuel element block; (2) carbonization and annealing, in which the loaded fuel element block is heated to about 1000°C to carbonize the pitch binder of the fuel rods and then annealed at 1800°C to remove residual volatiles and stabilize fuel rod dimensions; (3) end plug, dowel, and poison rod loading, in which poison rods are loaded into the element and graphite plugs and dowels are placed in the fuel holes and dowel holes and cemented into place; and (4) fuel element inspection, in which the assembled element is inspected and prepared for shipping to the reactor (or stored). Effort during the year has been confined to the carbonization and annealing area of this work.

3.8.1 Equipment Development

An engineering-scale remotely operable in-block carbonization and annealing furnace has been designed. The heating profile for fuel elements in the furnace is 10°C/min from ambient to 1800°C, followed by cooling at approximately 10°C/min to 200°C. A protective atmosphere is provided by flowing argon gas. The fuel blocks are unloaded at a surface temperature of 200°C or less. The throughput of the furnace is 16 blocks per day.

To maintain the desired throughput in a minimum of hot cell space, the furnace was designed to operate continuously. A fixed temperature profile will be maintained within the furnace; the desired heating and cooling rates will be maintained by conveying the fuel blocks through the furnace at a constant average speed. A vertical furnace was judged to be most efficient with respect to hot cell space and remote disassembly for maintenance. The fuel elements are introduced into the top of the furnace, a stack of elements is conveyed downward through the hot zone, and finally the cooled blocks are removed from the bottom of the furnace.

The furnace is designed as a three-module, vertically stacked unit, shown in Fig. 3.37. The top module is a preheat and low-temperature

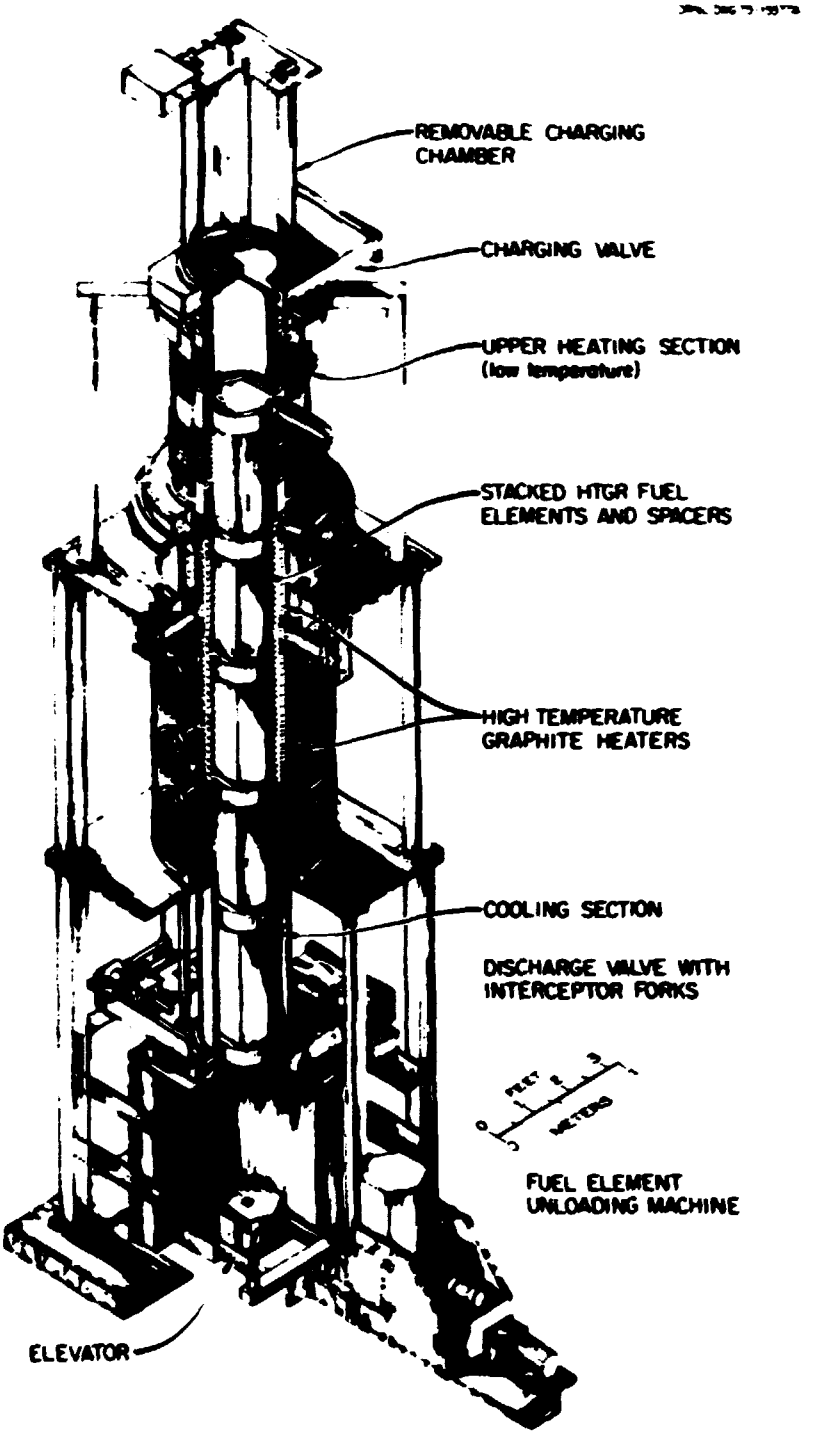

Fig. 3.37 In-Block Carbonization-Annealing Furnace.

zone, the middle module is the high-temperature zone (1800°C), and the bottom module includes the cooling zone and unloading chamber. The fuel element blocks are added to the top of the furnace by means of a loading chamber and move downward through the furnace in small, stepwise movements provided by an elevator mechanism in the unloading chamber. Separate support of the column is provided when it is necessary to remove the bottom block. Large slide valves maintain the argon atmosphere when blocks are added to or removed from the furnace. The preheat zone uses metallic heaters, whereas the rest of the furnace uses carbon resistance heating. The thermal design of the furnace has been confirmed with a detailed, computer-assisted heat transfer study. The furnace is designed for remote vertical disassembly using an overhead bridge crane and an electromechanical manipulator.

To complement the furnace design thermal analysis, heating rate studies using full-size graphite fuel elements were made with a large four-zone induction-heated furnace at the Y-12 plant. The furnace was loaded with two full-size elements plus additional graphite parts to simulate a load of approximately 2 1/4 elements. Under these conditions, 190 kW (≈85 kW/element) was required to obtain the desired heating rate of 10°C/min up to 800°C (the critical range for pitch coke yield) at the outer surface of the block. The heating rate of the center of the block was 9°C/min; thus, the fuel rods in the center of the block would be expected to have approximately the same microstructure as those near the edge. A power setting of 210 kW (≈95 kW/element) gave the desired 10°C/min heating rate up to 1200°C. Between 1200 and 1800°C, the maximum power available (230 kW or ≈105 kW/element) resulted in a heating rate of 7.5°C/min at the center of the element. From these data, we estimate that about 125 kW/element will be required to maintain the 10°C/min heating rate up to 1800°C. The furnace can accommodate this requirement. The radial and axial temperature variations for these runs are shown in Table 3.8. These temperatre variations would not appear to present significant problems in fuel fabrication.

Table 3.8. Temperature Variation in Full-Size Fuel Element

Nominal Temperature (°C)	Temperature Variations, °C	
	Radial[a]	Axial[b]
300	15	10
400	20	15
500	35	10
600	40	10
700	50	10
1200	65	10
1400	75	15
1600	50	25
1800	60	20

[a]Gradients at the top, middle, and bottom of the element were not significantly different.

[b]Gradients at the center and outer surface of the element were not significantly different.

3.8.2 Process and Materials Development

The final major process step in the fabrication of HTGR fuel rods is the carbonization and annealing of the rods. After the green rod is molded by the slug injection process, it is heated up to 1000°C to carbonize the pitch binder and then annealed at 1800°C to completely remove the residual pitch volatiles and produce a dimensionally stable rod. However, since the pitch is thermoplastic, the rod must be supported during carbonization to prevent dimensional distortion. In fresh fuel manufacturing, this can be accomplished by packing the rods in Al_2O_3 or graphite powder; however, this is not feasible for a remote process. Thus, for fuel refabrication, the green rods will be loaded directly into the graphite fuel element block and carbonized and annealed *in situ*.

In early accelerated irradiation tests rods carbonized in Al_2O_3 powder gave acceptable results, whereas rods carbonized in graphite tubes (to simulate in-block) contained fuel particles with broken outer coatings. The physical properties of the rods carbonized by the two

methods differed in several respects. Briefly, the in-tube processing resulted in high pitch coke yields (40–45%) and a high-density nonuniform matrix microstructure. The in-powder processing gave low pitch coke yields (15–20%), and a uniformly dispersed, lower density matrix microstructure. The high pitch coke yield of in-block carbonization was thought to be responsible for the initiation of breaks or tears in the particle coatings, resulting in subsequent particle failure during irradiation. As a result of these observations, optimum values of the composition of the fuel rod matrix and the heating rate during carbonization were determined such that the desired pitch coke yield and matrix microstructure were attained during in-block carbonization.

The fuel rod matrix contains graphite powder, a pitch binder, and a mold lubricant. The coke yield of the pitch can be lowered by increasing the heating rate during carbonization or by the use of low-coke-yield additives to the matrix. Pitch coke yield data as a function of heating rate and composition are summarized in Fig. 3.38. The desired 25% coke yield may be attained via an additive to the Ashland A-240 pitch

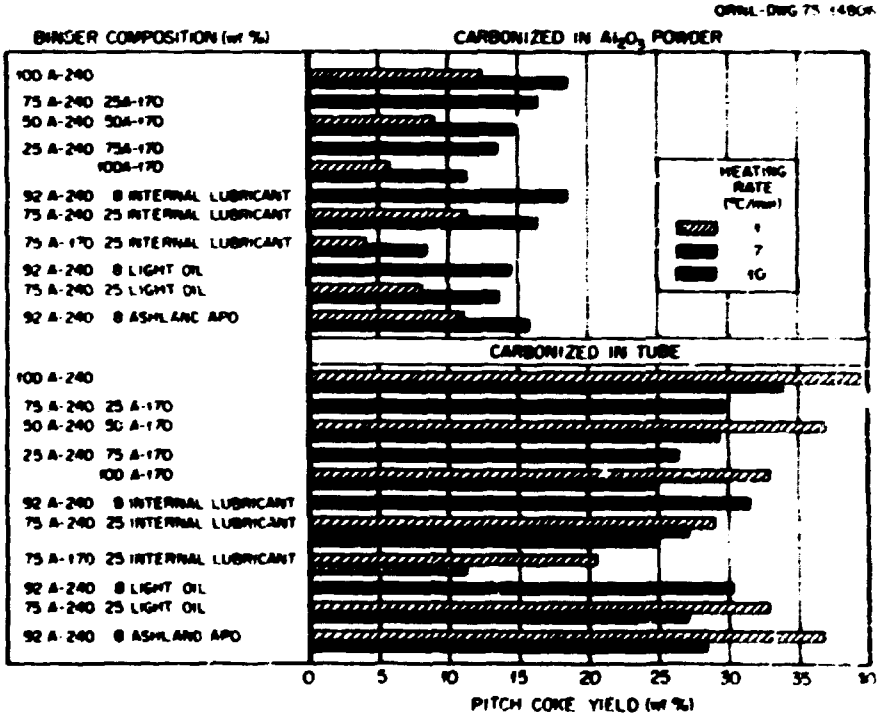

Fig. 3.38. Pitch Coke Yield of Fuel Rods Made With Various Binder Materials.

In-tube simulation of in-block carbonization using the A-240 pitch with additives produced a 25% coke yield and a matrix microstructure very similar to that previously obtained from carbonization in Al_2O_3 powder. The matrix structures obtained from carbonization, (1) in Al_2O_3 powder, (2) in-tube without additives at 37% coke yield, and (3) in-tube with additives at 26% coke yield are compared in Fig. 3.39.

One initial carbonization run was made in a 1/6 segment of an actual FSV element block at a 9°C/min heating rate. In this test using a matrix with additives, a matrix microstructure approaching that obtained by carbonization in Al_2O_3 powder was produced. The range of coke yields at the top, middle, and bottom of the block was not significant in this preliminary test.

The effect of particle strength on the failure of coated particles during in-block carbonization has been studied. The influence of coating parameters on particle strength and the details of the mechanical crushing strength test are discussed in Sect. 3.6 of this report. Also, the effect of molding pressure during fuel rod fabrication on particle failure is discussed in Sect. 3.7. The outstanding conclusion from our study was that Biso-coated thoria particles that had been annealed were less prone to failure than comparable unannealed particles. The data in Table 3.9 illustrate the beneficial effect of annealing. However, the behavior of Triso-coated fissile particles was not correlated with annealing or crushing strength.

3.8.3 Fabrication of Fuel Rods for Irradiation Tests

Detailed descriptions of the irradiation tests are published elsewhere.[36] The following is a brief description of the in-block carbonization and annealing experiments in those irradiation tests.

3.8.3.1 Experiments HT-26 and -27

The primary objective of these experiments was to study the matrix-particle interaction phenomenon associated with the in-block carbonization technique proposed for the fabrication of HTGR fuel rods. The two

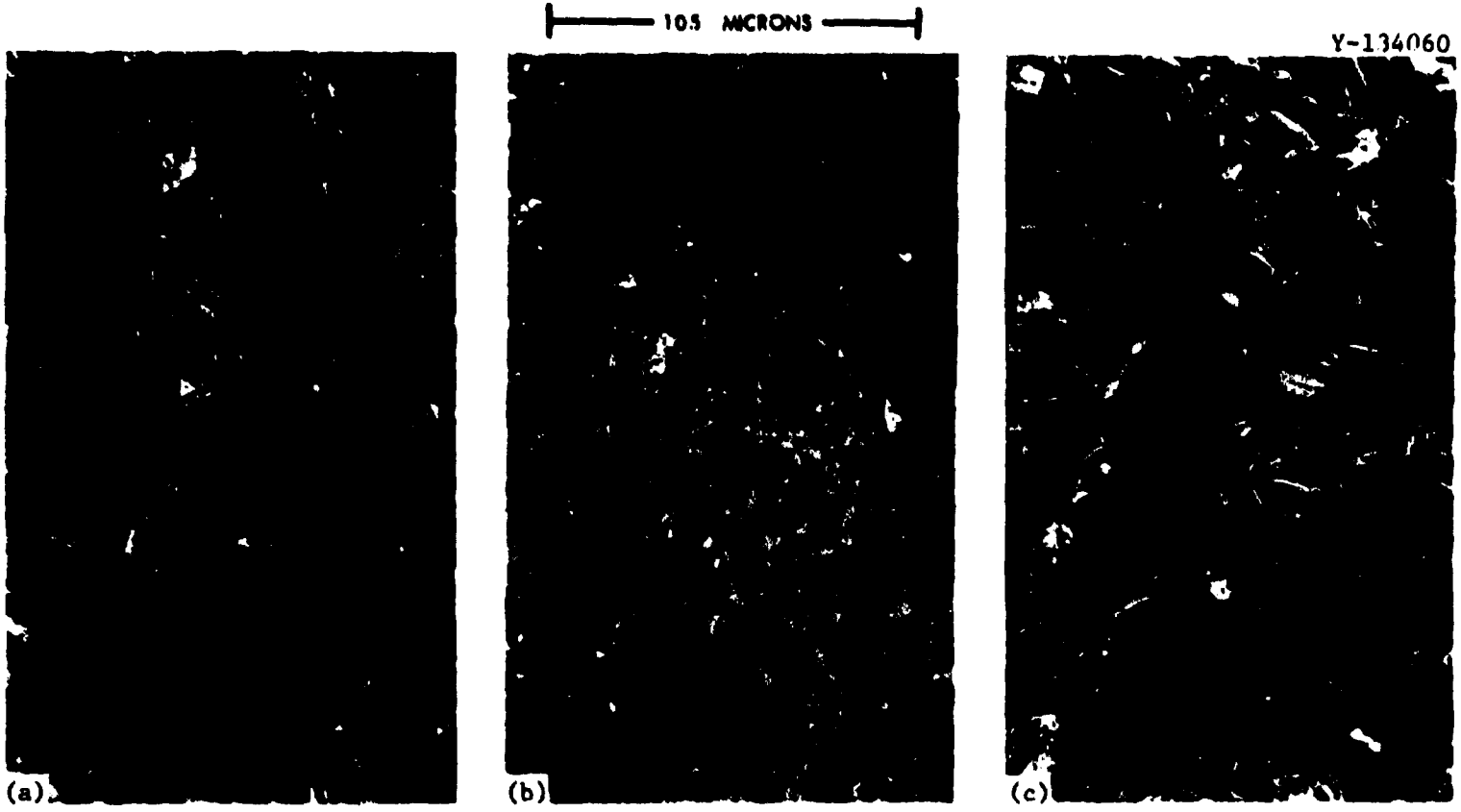

Fig. 3.39. Matrix Microstructure of Fired HTGR Fuel Rods Made with Ashland A-240 Pitch. 50×. (a) Carbonized in Al_2O_3 with no additive; pitch coke yield 17%. (b) Carbonized in graphite tube with no additive; yield 37%. (c) Carbonized in graphite tube with 15 wt % additive; yield 26%.

Table 3.9. Broken Particle Analysis of Fuel Rods[a] Containing Biso-Coated ThO_2 Particles

Starting Fuel Particles				Fired Fuel Rods			
				Carbonized in Al_2O_3 Powder		Carbonized in Graphite Tube	
Batch	Condition	Rupture Load (N)	Rupture Load (lb)	Pitch Coke Yield (wt %)	Failed[b] Fuel Fraction	Pitch Coke Yield (wt %)	Failed[b] Fuel Fraction
J-421	Unannealed	17.7	3.97	18.2	14×10^{-4}	32.7	$3? \times 10^{-4}$
J-422	Unannealed	21.7	4.88	17.2	5	32.3	24
J-421	Annealed	29.4	6.60	18.9	≈0	32.3	2
J-422	Annealed	30.7	6.91	18.9	≈0	28.3	≈0
J-409	Annealed	31.7	7.13	22.3	≈0	35.4	≈0

[a]Fuel rods leached with gaseous chlorine for . at 1500°C.

[b]Grams thorium recovered by chlorine leach per gram thorium in rod. Failed fuel fraction specification is 1×10^{-4}.

capsules had similar loading plans, with HT-26 and -27 exposed, respectively, to about half and about full HTGR design fluence at the capsule midplane. Each capsule was designed to be tested at two surface temperatures (about 900 and 1250°C). Three variables were investigated: (1) pitch coke yield, (2) strength of the fuel particle coatings, and (3) surface texture of the particles. High pitch coke yield (~40%), obtained by use of in-tube carbonization with A-240 pitch, was tested against three low pitch coke yields (20 to 25%) obtained by three techniques. These include in-tube carbonization and A-170 pitch, in-tube carbonization and A-240 pitch with low-coke-yield additives, and in-Al_2O_3-powder carbonization and A-240 pitch.

Both Biso-coated ThO_2 and Triso-coated weak-acid resin (WAR) fuel particles (6.5% enrichment) were used in all specimens along with strong-acid resin (SAR) carbon inert particles. Both type fuel particles were used at two strength levels, and the fissile particles were used with and without an outer LTI surface treatment.

Approximately 175 specimens were prepared for the actual experiments, characterization, and archive samples. Particle volume loadings were a nominal 58%, and the matrix densities varied from 0.52 to 0.71 g/cm^3 depending on pitch coke yield, which varied from 18 to 43%. The arrangement of the capsules along with the coke yield of the various matrices is shown in Table 3.10.

Table 3.10. Loading Plan for HT-26 and -27 Irradiation Test[a] to Study Matrix-Particle Interaction

Specimen Type	Approximate Surface Temperature (°C)	Matrix[b] and Particle[c] Types	Coke Yield (wt %)	Carbonization Mode
1	900	D, I	24–27	In tube
2	900	B, I	38–43	In tube
3	900	C, I	27–29	In tube
4	900	A, I	18–20	In Al_2O_3
5	1250	D, I	24–27	In tube
6	1250	B, I	38–43	In tube
7	1250	C, I	27–29	In tube
8	1250	A, I	18–20	In Al_2O_3
Reactor Midplane				
9	1250	A, II	18–20	In Al_2O_3
10	1250	C, II	27–29	In tube
11	1250	B, II	38–43	In tube
12	1250	D, II	24–27	In tube
13	900	A, II	18–20	In Al_2O_3
14	900	C, II	27–29	In tube
15	900	B, II	38–43	In tube
16	900	D, II	24–27	In tube

[a]HT-26 will operate two cycles and HT-27 four cycles.

[b]Matrix types are as follows: Type A contains high-coke-yield Ashland A-240 pitch carbonized in Al_2O_3; type B contains Ashland A-240 pitch carbonized in a graphite tube; type C contains low-coke-yield Ashland A-170 pitch carbonized in a graphite tube; and type D is current GAC matrix carbonized in a graphite tube.

[c]Particle types I consist of: Triso fissiles with outer LTI deposited at 1275°C from 100% MAPP gas, surface treated and annealed, and Biso-coated fertiles with unannealed reference coatings. Particle types II consist of: Triso fissiles with outer LTI deposited at 1325°C from 50% MAPP gas without surface treating or annealing, and Biso-coated fertiles with annealed reference coatings.

Because of the small amount of fuel contained in the test specimens, gaseous chlorine leach tests for broken particles were conducted on rods containing either all-fissile and all-fertile particles that had been processed at the same time as the test specimens. Both types of fissile particles, annealed surface treated and unannealed untreated, had comparable and rather high rupture strengths, 34 and 36 N (7.6 and 8.2 lb), respectively, which resulted in very low particle failure fractions regardless of the matrix or pitch coke yield. The ThO_2 particles used contained either unannealed or annealed coatings with rupture loads of 23 and 29 N (5.1 and 6.5 lb), respectively. The annealed particles had a very low particle failure fraction regardless of the matrix pitch coke yield. The unannealed ThO_2 particles with low rupture strengths had the highest particle failure fraction (34×10^{-4}) when carbonized in-tube using A-240 pitch at a coke yield of approximately 40%. The failure fractions of these particles when carbonized with matrix types A, C, and D of Table 3.10 were 16, 1, and 3×10^{-4}, respectively.

3.8.3.2 Experiment OF-2

The fuel refabrication objectives of the OF-2 test in ORR include the following: (1) Continue the study of the matrix-particle interaction phenomenon started in HFIR tests HT-26 and -27. The ORR tests are less accelerated than the HFIR tests, requiring one year rather than three months. (2) Test in-block carbonization of the GAC reference matrix by carbonizing and annealing rods in the actual graphite block used in the irradiation test capsule without disturbing the rods. Samples of fired rods were obtained by processing additional graphite blocks at the same time as the test block. (3) Test the ability to remove fuel rods that had been carbonized in-block from the graphite blocks after full-life irradiation. The variables for the test and the coke yield of the various matrices are shown in Table 3.11. The unannealed fertile (thorium) particles had a small failure fraction ($1\text{-}5 \times 10^{-4}$), and both the annealed fertile and unannealed fissile particles had failure fractions of approximately 1×10^{-4} or less.

Table 3.11. Variables for Matrix-Particle Interaction Study in Irradiation Test OF-2

Particle Batch[a]		Matrix[b] Type	Carbonization Mode	Coke Yield (%)
Fertile	Fissile			
25-mm-long (1-in.) Samples[c] Irradiated at 1150°C Center-Line Temperature				
U_1	U_1	A	In Al_2O_3	16–20
U_1	U_1	B	In tube	36–38
U_1	U_2	C	In tube	28–30
A_1	U_2	A	In Al_2O_3	16–20
A_1	U_2	B	In tube	36–38
A_1	U_1	C	In tube	28–30
25-mm-long (1-in.) Samples[c] Irradiated at 1350°C Center-Line Temperature				
U_1	U_2	A	In Al_2O_3	16–20
U_1	U_2	B	In tube	36–38
U_1	U_1	C	In tube	28–30
A_1	U_1	A	In Al_2O_3	16–20
A_1	U_1	B	In tube	36–38
A_1	U_2	C	In tube	28–30
51-mm-long (2-in.) Samples[c] Irradiated at 1350°C Center-Line Temperature				
U_1	U_1	C	In block	24–30
U_2	U_1	C	In block	24–30
U_3	U_1	C	In block	24–30
U_4	U_2	C	In block	24–30
A_1	U_2	C	In block	24–30
A_2	U_2	C	In block	24–30
A_3	U_3	C	In block	24–30
A_4	U_3	C	In block	24–30

[a]Fertile batches used were unannealed (U_1) and annealed (A_1). All fissile batches used were unannealed; U_1 and U_2 used frit coating distributor and U_3 used cone distributor.

[b]Matrix types are as follows: Type A contains high coke yield Ashland A-240 pitch carbonized in Al_2O_3; type B contains Ashland A-240 pitch carbonized in graphite tube; type C is current GAC matrix carbonized in a graphite tube.

[c]All samples 16 mm (5/8 in.) in diameter.

3.9 SAMPLE INSPECTION (WORK UNIT 2107) — W. H. Pechin

The purpose of this subtask is to develop techniques for obtaining, handling, and inspection of fuel samples at all stages of processing. During this period, development work on an electronic particle size analyzer was completed. Work was begun on techniques for sample handling and transfer for particles and fuel rods. A technique was developed to measure the fraction of particles with broken or permeable coatings by leaching with chlorine, either before or after the particles are consolidated into fuel rods.

3.9.1 Particle Inspection

3.9.1.1 Particle Size Analyzer — J. E. Mack

Development work on the particle size analyzer (PSA) has been completed. It is currently operating routinely in support of process development, providing data on particle size and sample count for the experiments on air blending and rod homogeneity, sample evaluation, and particle characterization studies, as well as sizing samples from furnace runs. The PSA measures each particle in the sample at rates up to 1500/min, completing sample analysis in one-fifth the time it had taken to read a particle sample radiograph, with five times the accuracy and no special sample preparation.

A Schottky barrier photodiode is used as the light detector, receiving a parallel homogenous light beam from a high intensity Fairchild FLV-104 visible-light-emitting diode (LED). It is located at the focal point of a 1-cm-focal-length converging lens which provides a uniform light field across the face of the photodiode. When a particle enters the light beam, the current output of the detector decreases by an amount proportional to the cross sectional area (shadow) of the particle. The signal is fed to an amplifier-converter, which converts the current drop to a voltage gain and amplifies it with a gain of 7000. The voltage pulse is then fed through an analog-to-digital converter to a pulse height analyzer, which records it in one of 1024 channels, with a resolution in pulse height of 4 mV.

The instrument is calibrated with a set of high-precision steel microspheres of four sizes ranging from 380 to 800 μm. Samples of this calibration set were sized with a light wave micrometer, and traceability to the National Bureau of Standards was established through ORNL secondary standards set PCC 71. Calibration of the analyzer against the steel microspheres can be completed within 5 min.

A secondary calibration standard permits upgrading the calibration curves between sample runs. Six wires of different diameters protrude radially from a Plexiglas hub and interrupt the light beam, creating pulses similar to those made by the coated particles. This wire disk is calibrated immediately following instrument calibration with the steel microspheres, and then used as a periodic calibration check. A suitable disk spectrum can be accumulated in 5 to 10 sec.

A number of improvements have been made on the PSA. A new singularizer drum was fabricated, allowing us to run particles as small as 250 μm. A new positive-action geared pulley and toothed belt drive system was added. A cyclone separator was designed and fabricated to receive the particles after measurement and collect them without damage. An isolation valve was designed and tested to provide a vacuum lock below the separator. A single-particle repeater was designed and fabricated for use in determining the absolute accuracy of the analyzer, as well as to determine the effects of particle shape ratio on size measurement. Coated particles characteristically produced size distributions with standard deviations of 3 to 7 μm for a single particle recirculated 200 times. In contrast, the nearly spherical steel microspheres showed standard deviations of less than 1 μm. Provisions are currently being made for glove box operation of the PSA to allow particle measuring of samples of pyrophoric material.

The reproducibility of the PSA over a period of six months has been shown to be excellent. The 95% confidence interval about the mean diameter is typically on the order of 2 μm for a sample of coated particles. The counting efficiency for a clean sample is essentially 100%. These characteristics along with the fast turnaround time have made the particle size analyzer a valuable piece of equipment in coated particle process development.

3.9.1.2 Particle Sample Transfer – J. E. Mack

A vacuum transfer system will be used to transport small quantities of fuel particles from the hot cell to a glove box outside the hot cell for particle analysis after each furnace operation. Since the particles will be pyrophoric after carbonization and conversion, the entire system must be closed from the atmosphere and transfer performed with oxygen-free gas. It must transport 100% of the particles received without any damage to the particles or their coatings, as no particle breakage or cross sample contamination will be acceptable. The particles themselves will be thermally and radioactively hot, and samples will be handled semi-automatically.

A test loop was designed and constructed to determine the feasibility of transferring unencapsulated particles over a large distance with a vacuum pump and a cyclone separator to receive the particles. An isolation valve was designed and fabricated to provide a vacuum lock between the transfer line and room atmosphere. A ball valve was modified to act as an isolation valve at the particle inlet.

The particles were transferred through 6.4-mm (1/4-in.) polyethylene tubing over a distance of 55 m (180 ft) with a pressure differential of 44 kPa (13 in. of mercury). The polyethylene tubing allowed particle velocity measurements to be taken with photoelectric sensors and a recorder. Particle velocities ranged from 3 to 8 m/sec (10–25 fps), with an average air speed of 15 m/sec (50 fps). Particle recovery was 100%, with individual particles being transferred and collected as efficiently as several thousand particles.

A new loop is being designed of stainless steel tubing to permit evaluation of particle wear and breakage as well as cross sample contamination in a more realistic system of rigid tubing and tube fittings. The application of particle sample transfer is illustrated schematically in Fig. 3.40.

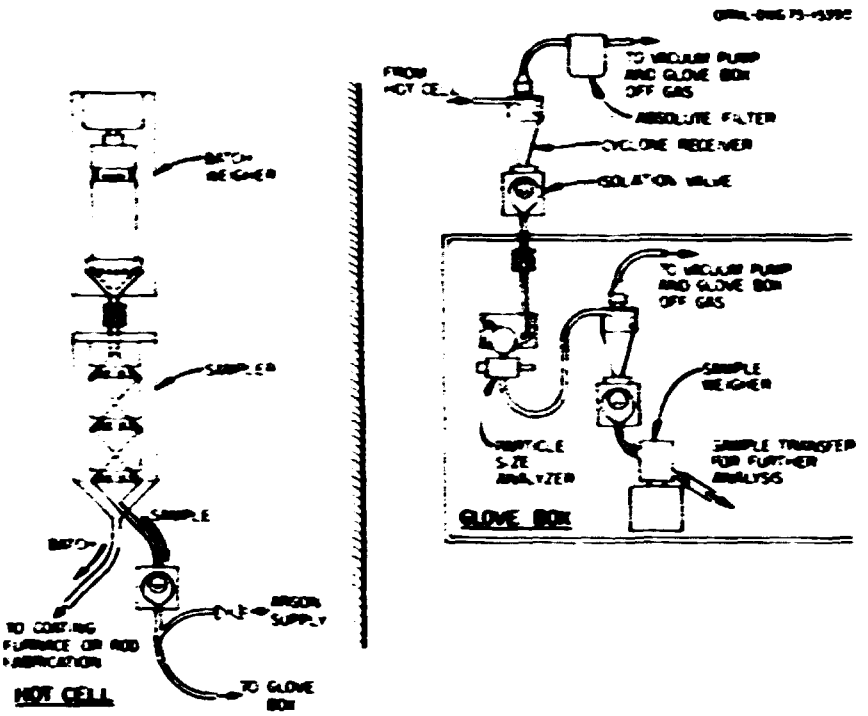

Fig. 3.40. Sample Transfer from in Cell to Sample Inspection Station Glove Box.

3.9.1.3 Particle Sample Subdivision — J. E. Mack and D. A. Dyslin

Design work has begun on a sampler capable of subdividing a small sample of coated fuel particles (1 to 10 g) into 10 representative subsamples utilizing the singularizer drum concept used successfully with the particle size analyzer. The rotation of the drum will be synchronized with that of a ten-pocket turntable beneath the drum. A stepping motor will be used to drive the system and index from pocket to pocket for sample removal. Any number of subsamples may be combined or recirculated back into the feed hopper for futher subdivision. A 10-g sample would be processed in less than 20 min.

3.9.2 Fuel Rod Inspection

3.9.2.1 Rod Sample Transfer — J. E. Mack and D. A. Dyslin

A number of fired and unfired fuel rods fabricated in the hot cell must be sent out of the cell to various sample inspection stations for

analysis. A system has been designed to load the rods into capsules, vacuum transfer the rods to a receiving station, unload the rods, and return the capsules. This operation must be performed without any structural damage to the rod, such as cracking or chipping, and without damaging individual particles. The method chosen for loading and unloading the rods involves a hollow capsule with "collars" inside each end for trapping spherical end plugs. These resilient ball plugs are pushed into and out of the capsule with a plunger driven by a small electric motor. The plunger never comes in contact with the rod and the clearance between the collars and the ball plugs is such that a 4.4-N (1-lb) force is sufficient to unload the rod. Chlorine leach analysis will be used to detect broken particles in the fuel rods.

A test loop was set up to evaluate the performance and determine the system requirements of a vacuum transfer system. The building off-gas system was used regulated to supply a vacuum with a maximum pull of 2 kPa (8 in. water) and a maximum air flow of approximately 9.4 std liters/sec (20 scfm), corresponding to a linear velocity of 10.7 m/sec (35 fps). The test loop was approximately 15 m (50 ft) long with five 0.3-m-radius (12-in.) bends and a number of 6.4-mm-diam (1/4-in.) holes for photoelectric sensors to measure capsule velocity. Figure 3.41 illustrates the velocity profile for a portion of the transfer line. Although the capsule lost considerable speed going into the bends, it accelerated quickly to nearly the same speed as the conveying air. The capsule velocity appears greater than that of the conveying air in several instances, although this is due to a buildup in the vacuum when the capsule was held in place before transfer, thus restricting the air flow, while the air flow reading had been taken before the capsule was placed in position.

A second loop was constructed to use smaller capsules and tubing: 25-mm (1-in.) diameter. The air flow requirement was correspondingly decreased to about 3.8 std liters/sec (8 scfm). A vacuum tee was installed at each end of the 21-m (70-ft) transfer line to send the capsule back and forth. The bends were made on a 0.46-m (18 in.) radius

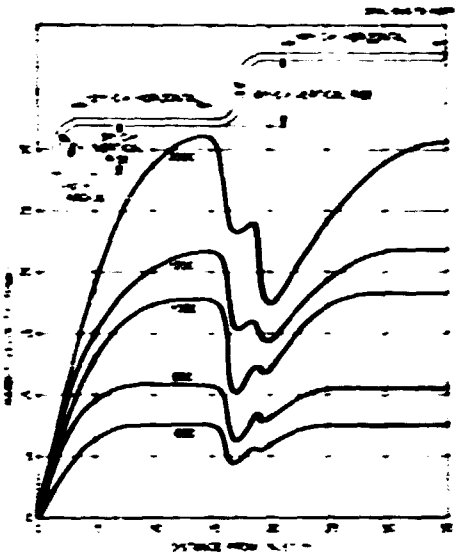

Fig. 3.41. Capsule Velocity as a Function of Position in a Transfer Line at Different Pressure Differences. Each curve is labeled with the air flow rate in linear ft/min measured in the absence of the capsule; corresponding values are 3.0, 4.1, 5.1, 6.1, and 10.2 m/sec. To convert capsule velocity to m/sec and line dimensions and distances from feet to meters, multiply by 0.305.

after the stainless steel tubing had been filled with a low-melting alloy to prevent collapse of the tube walls. The sections were then steam cleaned to remove this filling.

The capsule was transferred with an air flow of 3.8 liters/sec (8 cfm) at a pressure differential of 1.7 kPa (7 in. water), attaining a maximum velocity of 7.6 m/sec (25 fps) both in horizontal and vertical sections, decreasing to 5.5 m/sec (18 fps) around the bends. A 0.61-m (2-ft) dead air column below the vacuum tee provided sufficient cushioning to receive the capsule. A capsule loader and unloader will be placed at opposite ends of the transfer line. This method of operation will be evaluated upon completion of fabrication.

3.5.2.2 Particle Failure Fraction — D. E. LaValle

The determination of number of cracked or broken fuel particles is an important element in the characterization of fuels. The method now established is the treatment of the fuel at high temperatures with gaseous

chlorine, which removes the exposed heavy metal as volatile chlorides, which are then quantitatively recovered and analyzed. In previous experiments the advantages of chlorination at 1000°C became evident. Additional experiments at 1500°C showed significant reductions in chlorination times. We have now established as the standard procedure a chlorination time of 2 hr at 1500°C for rods and particles. The chlorine passes upward through a quartz tube supporting a hollow graphite tube, which holds the sample and is heated by induction. With fuel rods a partial flow through the 40%-porous rod is achieved by packing it snugly in the holder with porous carbon particles. Extensive chlorinations have been carried out on all types of rods and particles for both thorium and uranium determinations.

For irradiated fuel elements we developed an apparatus adaptable to operation in both a glove box and a hot cell. These systems, however, are still limited to resistance heating at 1000°C.

3.10 PLANT MANAGEMENT (WORK UNIT 2108) — W. R. Hamel

The objective of Work Unit 2108 is to develop and evaluate the instrumentation, control, and data handling technology required to support the demonstration of the remote refabrication of HTGR fuels.

The current and subsequent generations of instrumentation and control hardware appropriate for application to HTGR fuel refabrication processes involve the use of highly complex general-purpose devices such as minicomputer-based packages, microcomputers, and programmable logic controllers. These general-purpose devices will be the basic building blocks used in the design and construction of fuel recycle process control systems. Generally, recycle process control systems will comprise a network of these general-purpose devices and other types of hardware. The impact of factors such as synchronization and interfacing are obvious, and are being addressed in the refabrication development program by creating a real-time environment, with the operation of various engineering-scale process developmental equipment that is analgous to that expected in an actual recycle facility.

A development programmable logic controller and minicomputer have been procured and are being used in the control and operation of various engineering-scale mockup equipment.

3.10.1 Developmental LICS Mockup — W. R. Hamel

To evaluate two types of applicable general-purpose devices in a simulated process environment with engineering-scale refabrication machinery, the configuration shown in Fig. 3.42 was developed. The developmental Local Instrument and Control Subsystem mockup involves the use of a process control minicomputer and programmable logic controller to control the laboratory fuel rod fabrication machine, the fuel rod storage magazine loader-unloader, and the fuel block loading and verification mockup. Additionally, the development computer will be used to provide computational support to radioassay development equipment and electromechanical manipulator development equipment remotely located in TURF, Building 7930.

ORNL-DWG 75-6972

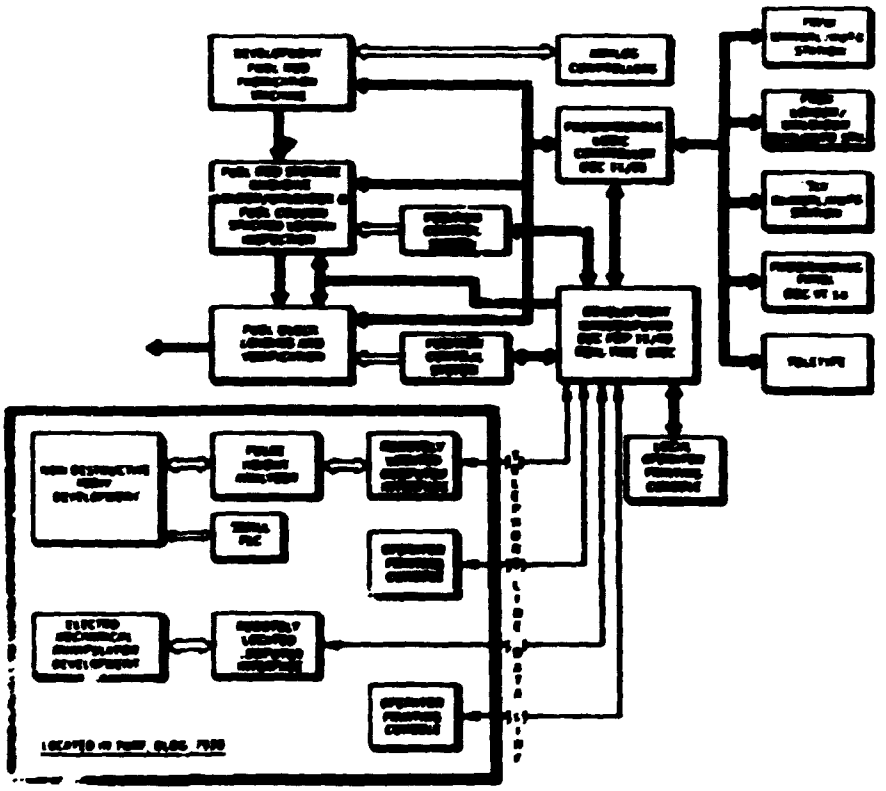

Fig. 3.42. Developmental LICS Mockup Configuration.

Currently, the development minicomputer and programmable logic controllers have been installed in Building 4508. The replacement of the original relay control system of the laboratory fuel rod fabrication machine is nearly complete. A Digital Equipment Corporation industrial 14/35 programmable logic controller was procured. See Sect. 3.10.2 for more details. The development computer, which is a Digital Equipment Corporation PDP-11/40, has been data-linked via telephone lines to the multichannel analyzer being used for nondestructive assay development in TURF Bldg. 7930. Details concerning the development computer are given in Sect. 3.10.3. The fuel rod storage magazine loader-unloader is scheduled for full automatic operation in January 1976. The LICS mockup is being designed such that all the equipment shown can be operated simultaneously. This type of operation will permit quantitative evaluation of real-time interfacing techniques between refabrication machines, programmable logic controllers, and minicomputers.

3.10.2 Programmable Logic Controller and Applications — B. J. Bolfing

Programmable logic controllers (PLC) are a relatively new general-purpose discrete control device intended to replace relay control systems. The refabrication process includes a multitude of discrete sequential operations that are ideally suited for PLCs. A PLC system has been procured and is now being used to control the laboratory fuel rod fabrication machine and is planned for use with the resin carbonization furnace particle handling loop.

The PLC system includes a Digital Equipment Corporation Industrial 14/35 controller, a VT/14 cathode ray tube display programming terminal, and a standard teletype. The Industrial 14/35 controller includes a central processor, 8K words of core memory, 128 input modules (expandable to 512), and 64 output modules (expandable to 256). Figure 3.43 shows the PLC installation in room 242 of Building 4508. The input-output module interfacing is wall mounted in the center background and the 14/35 processor and power supply are on the right. Figure 3.44 shows the VT/14 programming terminal in operation with a segment of control circuitry being displayed.

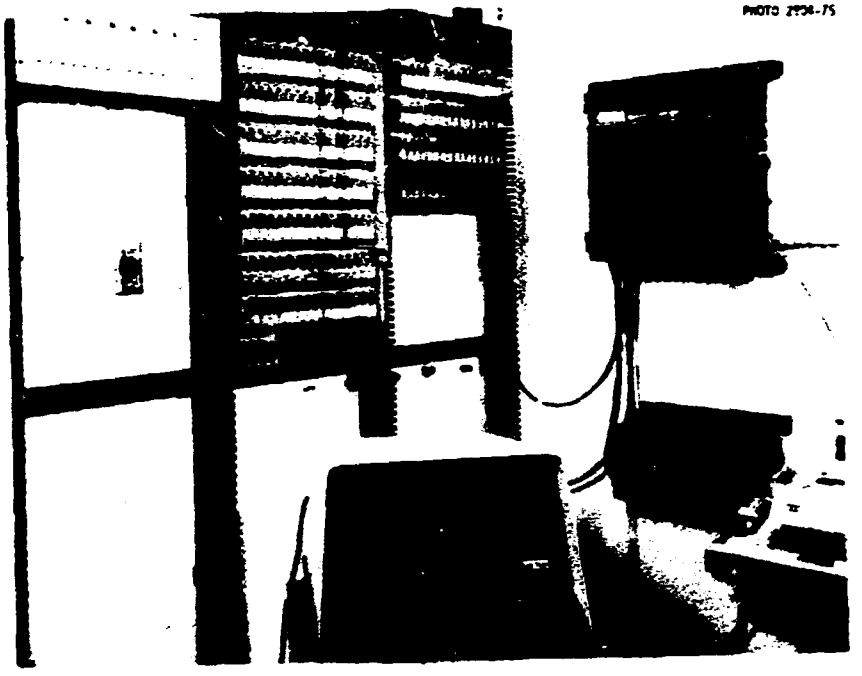

Fig. 3.43. Programmable Logic Controller System.

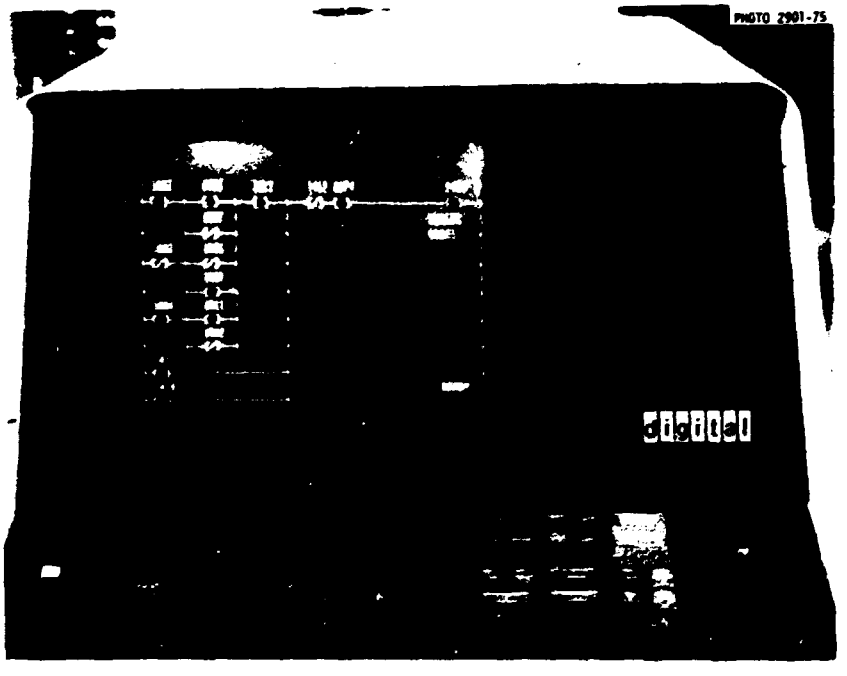

Fig. 3.44. PLC Programming Panel.

One of the primary objectives of controlling the laboratory fuel rod fabrication machine (LFRFM) with a programmable logic controller was to apply a mode of control that would allow complete automatic operation of the machine, including start-up and shutdown, while providing the operator with completely remote control of all machine actions.

Three modes of control (manual, semiautomatic, automatic) are provided. The automatic and semiautomatic control modes are implemented in the PLC software programming. The manual mode, however, is provided through the input-output forcing capability of the VT/14 programming panel (Fig. 3.44).

The PLC system was installed in room 242 of Building 4508. Signal lines were run about 46 m (150 ft) from the input and output modules in room 242 to the fuel rod fabrication machine located in room 254 of Building 4508. The PLC is remotely located because room 254 is a radioactive contamination control zone. Remotely locating the PLC also simulates signal transmission lengths expected in a hot cell installation.

The PLC solves Boolean expressions (logical AND/OR statements) that conditionally express output states as a function of input states, timer states, and output states. These expressions are stored in the core memory of the PLC and represent the control logic of the LFRFM. The control program is initially loaded into the core memory through the VT/14 programming terminal, which is designed for developing the control program in relay ladder diagram symbology. The real-time status of all inputs and outputs can be monitored with the VT/14. It can be used as a pushbutton manual controller by disabling the control program and then forcing specific outputs to desired states. The normal operating mode of LFRFM is the automatic mode, where the start-up, shutdown, and run sequence of the machine is automatically directed and monitored by the PLC. However, if a machine subsystem malfunction occurs, the machine is halted and further operation would be subject to an operator's "jog" command from the control panel. A "jog" command would return the malfunctioning subsystem to a reference position for repair or the initiation of the LFRFM shutdown sequence. The alarm conditions are

stored in PLC core memory and provide monitoring of limit switch failure, solenoid valve failure, and failure of commanded events to occur during a specified (or watchdog) time period.

The experience obtained to date demonstrates the versatility and reliability of PLC controls for remote refabrication equipment. The industrial 14/35 controller has been operating since June 1, 1975, with no hardware failures. The advantages of software-oriented PLCs over hardwired relay logic control implementation have been demonstrated by modifications made to the control program after initial PLC start-up. Similar modifications made to hardwired relay control systems would have resulted in additional rewiring costs.

The real-time monitoring capability of the VT/14 programming terminal provides a powerful tool for machine maintenance and troubleshooting for remote applications. Failures of in-cell sensors and actuators can be isolated through a simple pushbutton procedure out of cell with this device.

3.10.3 Development Computer System — B. O. Barringer

Initially, the development computer system is being used to support position control system requirements for the fuel rod storage magazine loader-unloader, and to provide computational support for nondestructive radioassay activities. Future applications will be associated with fuel block loading, fuel rod homogeneity inspection, development of recycle process data handling techniques, and computer support for the Industrial 14/35 programmable logic controller.

The development computer system has been delivered to Building 3500 for initial checkout and transferred to room 242 of Building 4508 in the configuration as shown in Fig. 3.45. The system is based around a standard Digital Equipment Corporation industrial package. This basic system includes the hardware shown and the real-time executive software (RSX-11M). There is sufficient memory to support either program development (FORTRAN and assembly language) and the simultaneous support of the fuel rod magazine loader-unloader mockup and the nondestructive radioassay activities. The 30-character/sec DECWRITER provided with

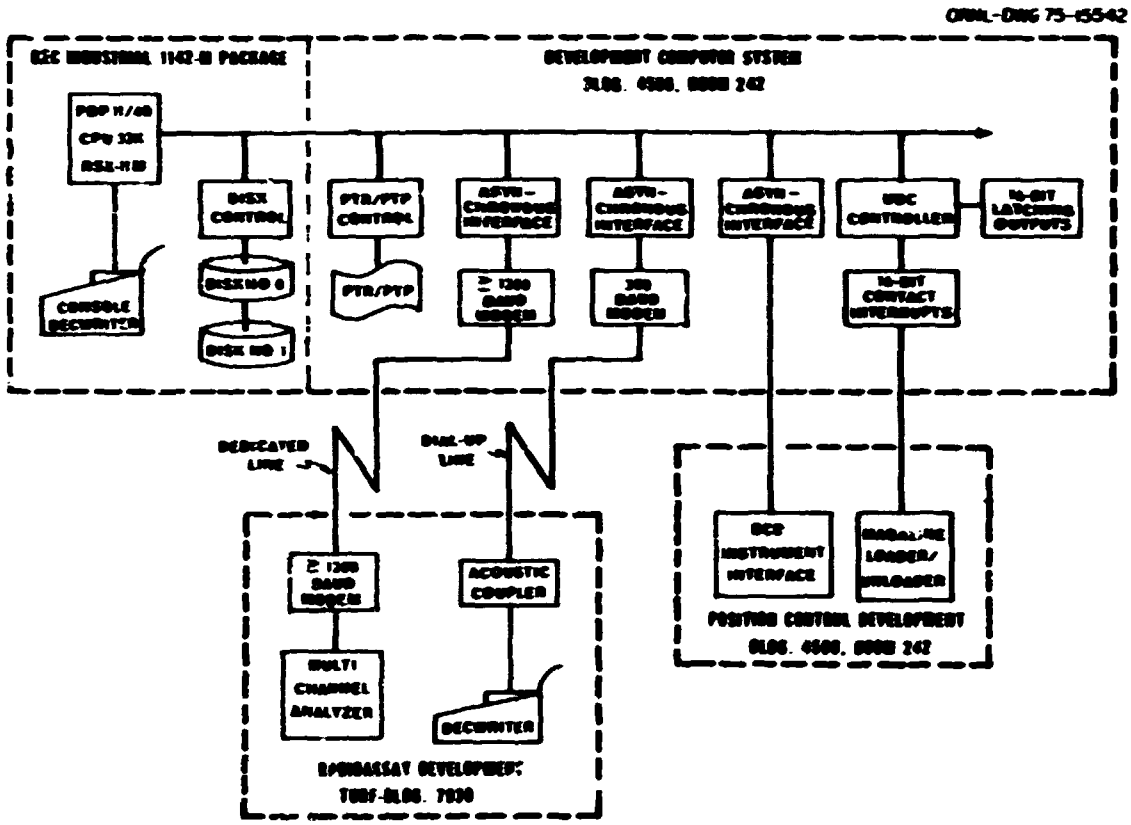

Fig. 3.45. Development Computer System.

the package is used as the console terminal. A high-speed paper tape reader-punch is included to provide an inexpensive compatible input-output medium. This will allow programs or data to be keypunched and placed on paper tape at the ORNL computer facility for loading into the minicomputer system.

The fuel rod storage magazine loader-unloader mockup includes a two-coordinate indexing system. The position control for the indexing table is provided by stepping motor drives with computer presetting and position encoder feedback. In addition, the system will require direct digital inputs and outputs. For this purpose 16 digital inputs and 16 digital outputs are provided via the Universal Digital Controller (UDC), which is a part of the development computer system.

As radioassay development will be located in TURF, dial-up communication lines will be used for the data link. Hardware is included

to provide one 300 BAUD line for a DECWRITER and one 1200 BAUD line (which may operate at up to 1800 BAUD) for the multichannel analyzer. A MODEM (data set) subsystem to handle the two communication lines is part of the development computer system. Two telephone lines (one dial-up line and one four-wire direct line) have been installed between TURF and Building 4508. Connection to the computer will require only dialing up the development computer. The calls will be automatically answered by the computer and connection established.

3.11 WASTE AND SCRAP HANDLING (WORK UNIT 2109) — J. D. Jenkins, M. S. Judd, and J. E. Van Cleve

During this reporting period the development efforts in the area of waste and scrap handling have undergone a substantial change of direction. During the earlier portion the overall program was directed toward the design and construction of an integrated refabrication pilot plant to be located in the TURF. Primary emphasis was placed on the production of reactor-grade fuel elements using bred ^{233}U. Waste and scrap materials handling during operation of the pilot plant would be centered around means for sorting, packaging, assaying, and removing the material from the cells for disposition in a temporary retrievable storage facility or for recycle to the head-end facility at Idaho. Little or no effort was expended on the problems associated with scrap reclamation within the refabrication plant or with incineration of low-uranium-content wastes peculiar to HTGR fuel refabrication.

Accomplishments during this period include (1) conceptual design of the equipment and facilities necessary to package waste and scrap materials remotely and remove the containers from the cell for disposal, (2) design of a storage facility and shipping containers for high-uranium-content waste cans, and (3) conceptual design of nondestructive assay equipment to determine the uranium content of both high- and low-level waste containers.[5]

The waste and scrap handling development program was reassessed in early 1975 when it appeared that the refabrication development program would be directed toward construction of a large-scale demonstration

facility (HRDF) rather than the pilot plant. Under this new concept, the problems associated with the waste and scrap materials became more immediate, and we were directed to concentrate the development effort in the areas of processing and reclaiming these waste and scrap materials peculiar to HTGR fuel fabrication. Accordingly, work was initiated in the area of reclamation of the perchloroethylene solution from the furnace off-gas scrubbers, burning of the residues obtained after perchloroethylene recovery, and reclamation of reject material from the product line.

At this point, bench scale experiments have been run to demonstrate the feasibility of distilling and reclaiming dirty perchloroethylene. Work is currently under way to design engineering-scale equipment to further test the techniques and obtain more quantitative operational information. In addition, some work has been initiated on the reclamation of reject fuel materials.

3.12 MATERIAL HANDLING (WORK UNIT 2110) — W. R. Hamel

The objective of Work Unit 2110 is to verify existing and to develop new remote material handling technologies necessary to support the remote refabrication of HTGR fuels. Toward this goal, work activities include: (1) the evaluation of the existing TURF material handling system, (2) survey of current research and development activities and commercial suppliers, and (3) the development of an automated material handling system concept consistent with HTGR fuel recycle requirements.

3.12.1 Evaluation of Existing TURF Material Handling System — J. G. Grundmann

Before proposing a work plan for the development of a manipulator with desired characteristics for HTGR fuel refabrication, an effort was initiated to become familiar with the mechanical and electrical equipment making up the TURF material handling system (i.e., PaR electromechanical manipulators, crane hoists, power cabinets, slide switch control boxes, and facility power and control wiring). This work included an examination

of engineering drawings and operators' manuals and operation of the actual equipment. This activity has been completed. The results of this study indicate that the TURF material handling system is of adequate mechanical configuration but extremely deficient in control functional capability and level of automation.

3.12.2 Material Handling Technology Survey — J. G. Grundmann

Existing material handling technology was extensively surveyed. Both research and development organizations and commercial equipment suppliers were contacted. A file of pertinent reports and product literature has been assembled. The following organizations that have active research and development programs in robots and manipulators were contacted:

1. Jet Propulsion Laboratory — NASA;
2. Marshall Space Flight Center — NASA;
3. Massachusetts Institute of Technology, the Charles Stark Draper Laboratory, Inc.;
4. The National Bureau of Standards, the Office of Developmental Automation and Control Technology;
5. Stanford Research Institute;
6. Rockwell International — Rocky Flats Arsenal;
7. Central Research Laboratory;
8. Fermi Laboratory;
9. Brookhaven National Laboratory.

The organizations listed below are involved in various types of research and development using the most recent remote TV viewing technology:

1. Allied Chemical Corporation, Idaho National Engineering Laboratory;
2. Marshall Space Flight Center — NASA;
3. Fermi Laboratory;
4. Rockwell International — Rocky Flats;
5. EG & G, Las Vegas, Nevada.

There are many commercial suppliers, both domestic and foreign, of manipulator and robot hardware. The product lines of those listed below have been studied in detail:

1. Programmed and Remote Systems Corporation (PaR);
2. Unimation;
3. MBA International, Inc.;
4. Central Research Laboratory;
5. Versatran, Inc.;
6. Prab Conveyors, Inc.;
7. Rancho Los Amigos Hospital;
8. Hill Rockford Company;
9. IBM Corporation;
10. Cincinnati Milacron;
11. Auto Place.

The following remote TV viewing system manufacturers have been contacted:

1. Dimension Television Corporation;
2. Martin Marietta Corporation;
3. MBA International, Inc.

3.12.3 Development of a Master-Slave Electromechanical Manipulator — J. G. Grundmann and R. C. Muller

Window-mounted mechanical master-slave manipulators with human-arm-like dexterity are used in most research-scale remote handling activities. Unfortunately, window master-slave manipulators cannot reach all in-cell locations in large hot cell facilities such as TURF. Since the TURF electromechanical manipulators are mobile and can be positioned at essentially any in-cell location, these devices must be extended to master-slave control capability to satisfactorily support the fuel refabrication equipment operation and maintenance. Research results have shown that an order of magnitude increase in operator electromechanical manipulator dexterity can be realized with a master-slave capability in comparison with conventional variable-rate controls. Considerable activity has been directed toward establishing a master-slave

capability with the TURF electromechanical manipulators. Highlights of these activities are given below.

1. A master arm designed by PaR for master-slave operation was obtained from UCNS, Y-12 Plant. The controls on this arm are inadequate for this application, but the mechanical structure will be usable after alterations.

2. Discussions with the PaR design engineers indicated that improvements had been made in the PaR manipulators. These improvements included a three-degree-of-freedom wrist joint and a stiffer telescoping tube hoist with adequate travel to reach the floor of all TURF hot cells. Purchase specifications were written and this equipment was ordered, delivered to TURF, inspected, and accepted.

3. A prototype analog servo loop was designed and installed on the Cell E PaR manipulator carriage to determine the accuracy capability of such servo loops. Repeatable and stable (nonoscillatory) positioning of the carriage with 0.25 mm (0.010 in.) dead band was demonstrated.

4. Simulation of the manipulator carriage was anticipated. To verify the accuracy of the simulation, experimental information regarding the carriage drive motor and servo loop was necessary. Experiments were conducted to verify: (a) carriage open loop response to input voltage, (b) carriage motor electrical and mechanical parameters, and (c) carriage closed servo loop position response to input voltage.

5. An IBM Continuous System Modeling Program (CSMP) computer simulation of the carriage was developed. This model's open and closed servo loop responses to step input voltage agreed with experimental results. The simulation is now ready for use in evaluation of various commercial hardware items to determine the optimum configuration.

6. An effort was directed at the problem of reliably and efficiently transmitting position and force information between in-cell and out-of-cell equipment. A digital serial communication link has been investigated as a possible solution since it has high noise immunity and requires only a few signal wires between in-cell and out-of-cell equipment. Detail design work on a prototype communication link has not yet been initiated.

3.12.4 Development of a Remote TV Viewing System – J. G. Grundmann

Since operator vision provides the primary feedback for manual operation of manipulators, the best visual coupling possible is imperative. In HTGR fuel recycle facilities, in-cell equipment density will be high. As a result, the view available from fixed shielded cell windows will be very restricted. Equipment may be visible, but only at long distances. To perform remote maintenance at crowded distant in-cell locations, mobile close-up vision augmentation is required. TV viewing systems are being investigated for this purpose.

A survey of manufacturers of remote TV viewing systems and also of TV viewing has been performed. Results of this survey indicate depth perception is the major deficiency of typical TV systems. Recently stereo TV (two cameras with different view angles) and 3D-TV have been perfected to largely offset this problem. One 3D-TV system is now commercially available and is sufficiently accurate to allow doctors to perform eye surgery. This 3D-TV system is being studied for possible use as an HTGR recycle remote TV viewing system.

3.12.5 Development of an Automatic Electromechanical Manipulator – J. G. Grundmann

To meet the requirements of production-scale HTGR fuel recycle facilities, automatic minicomputer control of electromechanical manipulators is necessary. The primary minicomputer functions are envisioned to be:

1. automatic "robot" execution of rapid transverses by mobile manipulators between in-cell working locations,
2. automatic "robot" execution of in-cell routine production tasks with a manipulator, and
3. automatic "robot" execution of some maintenance tasks, including tool changes, to speed completion of maintenance work.

Software development for some of these items was contracted to the N.B.S., Office of Developmental Automation and Control Technology, and this work will be completed by November 1, 1975. Hardware for the automatic production capabilities include the design and procurement of an interface to connect the development computer system (PDP-11/40) to the manipulator loops. This work has not yet been initiated.

3.13 REFERENCES

1. *Conceptual Design Report for HTGR Fuel Refabrication Pilot Plant (Phased Approach — Option A)*, ORNL internal document X-OE-4, (May 1, 1975); summarized in Chap. 4 of this report.
2. *HTGR Fuel Refabrication Pilot Plant, Oak Ridge National Laboratory, Oak Ridge, Tennessee. Final Environmental Statement*, WASH-1533 (August 1974).
3. J. E. Till, *A Comparison of the Potential Radiological Impact of Recycle ^{233}U HTGR Fuel and LMFBR Plutonium Fuel Released to the Environment*, ORNL-TM-4768 (January 1975).
4. J. E. Till, "A Comparison of Environmentally Released Recycle Uranium-233 HTGR Fuel and LMFBR Plutonium Fuel," *Proceedings of Fourth National Symposium of Radioecology, May 12–14, 1976, Corvallis, Oregon*, Dowden, Hutchinson, and Ross, Inc. (in press).
5. J. D. Jenkins, S. R. McNeany, and J. E. Rushton, *Conceptual Design of the Special Nuclear Material Nondestructive Assay and Accountability System for the HTGR Fuel Refabrication Pilot Plant*, ORNL-TM-4917 (July 1975).
6. *Code of Federal Regulations*, Part 70, "Special Nuclear Material."
7. J. E. Rushton, J. D. Jenkins, and S. R. McNeany, "Nondestructive Assay Techniques for Recycled ^{233}U Fuel for High-Temperature Gas-Cooled Reactors," *J. Inst. Nucl. Mater. Management* 4(1): 18–35 (Spring 1975).
8. G. E. Hansen and W. H. Roach, *Six and Sixteen Group Cross Sections for Fast and Intermediate Critical Assemblies*, LAMS-2543 (1961).
9. S. R. Bierman and E. D. Clayton, *Status of HTGR Criticality Safety Data Needs on U-Th Fuel Cycle*, unnumbered research report, Battelle Pacific Northwest Laboratories (June 1975).
10. S. R. McNeany and J. D. Jenkins, *Comparison of Hansen-Roach and ENDF/B-IV Cross Sections for ^{233}U Criticality Calculations*, ORNL-TM-5113 (January 1976).
11. P. A. Haas, *HTGR Fuel Development: Use of UO_3 to Load Cation Exchange Resin for Microsphere Preparation*, ORNL-TM-3817 (September 1972).

12. W. J. Lackey, W. H. Pechin, C. F. Sanders, F. C. Davis, and F. J. Furman, "Microsphere Coating," *Gas-Cooled Reactor and Thorium Utilization Programs Annu. Progr. Rep. Sept. 30, 1971*, ORNL-4760, pp. 45–52.

13. J. A. Carpenter, Oak Ridge National Laboratory, personal communication, July 15, 1975.

14. P. A. Haas, *Loading a Cation Exchange Resin with Uranyl Ions*, U.S. Patent 3,800,023 (March 26, 1974).

15. R. Whipple, General Atomic Company, personal communication, November 1974.

16. K. J. Notz and P. A. Haas, "Resin-Based Microsphere Development," *Gas-Cooled Reactor Programs Progr. Rep. Dec. 31, 1972*, ORNL-4911, pp. 27–32; note especially p. 31.

17. P. A. Haas, *HTGR Fuel Development: Loading of Uranium on Carboxylic-Acid Cation Exchange Resins Using Solvent Extraction of Nitrate*, ORNL-TM-4955 (September 1975).

18. C. C. Haws, B. C. Finney, and W. D. Bond, *Engineering-Scale Demonstration of the Sol-Gel Process: Preparation of 100 kg of ThO_2-UO_2 Microspheres at the Rate of 10 kg/Day*, ORNL-4544 (May 1971).

19. B. C. Finney and P. A. Haas, *Sol-Gel Process — Engineering-Scale Demonstration of the Preparation of High-Density UO_2 Microspheres*, ORNL-4802 (November 1972).

20. J. G. Moore, *Sol-Gel Process for Preparing ThO_2-UO_3 Sols from Nitrate Solutions by Solvent Extraction with Amines*, ORNL-4095 (October 1967).

21. D. R. Johnson, W. J. Lackey, and J. D. Sease, *The Effects of Processing Variables on HTGR Fuel Kernels Fabricated from Uranium-Loaded Cation-Exchange Resin*, ORNL-TM-4989 (August 1975).

22. R. B. Pratt, J. D. Sease, W. H. Pechin, and A. L. Lotts, "Pyrolytic Carbon Coating in an Engineering-Scale System," *Nucl. Appl.* 6(3): 241–55 (March 1969).

23. W. J. Lackey, W. H. Pechin, F. C. Davis, M. K. Preston, and R. S. Lowrie, "Microsphere Coating – 2104 (ORNL Lead)," *Gas-Cooled Reactor Programs Annu. Progr. Rep. Dec. 31, 1973*, ORNL-4975, pp. 26–37.

24. W. J. Lackey, W. H. Pechin, C. F. Sanders, F. C. Davis, and D. D. Cannon, "Microsphere Coating," *Gas-Cooled Reactor Programs Annu. Progr. Rep. Dec. 31, 1972*, ORNL-4911, pp. 33–45.

25. W. J. Lackey, J. D. Sease, D. A. Costanzo, and D. E. LaValle, "Improved Coating Process for High-Temperature Gas-Cooled Reactor Fuel," *Trans. Amer. Nucl. Soc.* 22(TANSAO 22): 194–95 (November 1975).

26. W. J. Lackey, D. P. Stinton, L. E. Davis, and R. L. Beatty, *Crushing Strength of HTGR Fuel Particles*, ORNL-TM-5132 (in press).

27. Personal communication with J. Holder, C.E.N., Grenoble, France, April 1975.

28. W. J. Lackey, W. H. Pechin, and J. D. Sease, "Measurement and Control of Shape of Fuel Particles for High Temperature Gas-Cooled Reactors," *Am. Ceram. Soc. Bull.* 54(8): 718–24 (1975). Also ORNL-TM-4673 (November 1974).

29. G. W. Weber, R. L. Beatty, V. J. Tennery, and W. J. Lackey, Jr., *Uranium Dispersion in the Coating of Weak-Acid-Resin-Derived HTGR Fuel Microspheres*, ORNL-TM-5133 (February 1976).

30. E. Gyarmati and H. Nickel, *Stationary and Dynamic Deposition of Silicon Carbide on Coated Fuel Particles*, JÜL-900-RW (November 1972); ORNL-tr-2733.

31. T. D. Gulden, *Deposition and Microstructure of Vapor-Deposited Silicon Carbide*, GA-8275 (Dec. 1, 1967).

32. E. H. Voice and D. N. Lamb, *The Deposition and Structure of Pyrolytic Silicon Carbide*, Dragon Project Report DP-677 (October 1969).

33. J. I. Federer, *Fluidized Bed Deposition and Evaluation of Silicon Carbide Coatings on Microspheres*, ORNL-TM-5152 (in preparation).

34. W. J. Lackey, J. D. Jenkins, and F. J. Homan, *Assessment of Coater Size for the Fuel Refabrication Prototype Plant*, ORNL-TM-4567 (July 1974).

35. R. A. Bradley, D. D. Cannon, F. C. Davis, C. R. Reese, J. D. Sease, and C. F. Sanders, "Fuel Rod Fabrication," *Gas-Cooled Reactor Programs Annu. Progr. Rep. Dec. 31, 1972,* ORNL-4911, pp. 44–56.

36. F. J. Homan, "HTGR Fuel Qualification," *HTGR Base Program Progr. Rep. Jan. 1, 1974–June 30, 1975,* ORNL-5108, in preparation, Chap. 6.

4. REFABRICATION PILOT PLANT (SUBTASK 220)

J. W. Hill J. P. Jarvis D. P. Reid F. C. Davis J. D. Sease

4.1 INTRODUCTION

The conceptual design for the HTGR Fuel Refabrication Pilot Plant has been completed and is assembled into an internal conceptual design report. No further design effort is planned for such a facility pending the outcome of design studies of an HTGR Recycle Demonstration Facility (HRDF).

4.2 OVERALL PLANT DESIGN (WORK UNIT 2200) — J. E. Van Cleve and A. R. Olsen

4.2.1 Purpose

The HTGR Fuel Refabrication Pilot Plant was conceptually designed to demonstrate the technology required for a commercial fuel refabrication plant that can produce recycle fuel elements for HTGRs using ^{233}U with radioactivity equivalent to material containing 500 ppm of ^{232}U and aged for up to 90 days. Such a plant must be safe, reliable, licensable, and economic. The technology must be available on a timely basis and ensure that any risks are comparable with those of a first-of-a-kind radiochemical plant.

The fuel element design is illustrated in Fig. 4.1. Characteristics of the particles to be used in the elements are given in Table 4.1.

In the HTGR, the initial core is fueled with thorium and ^{235}U (the uranium is 93% enriched in ^{235}U). Increasing amounts of ^{233}U are used as it is produced and recovered. Since the conversion ratio of the type of HTGR being marketed is about 0.7 with a fuel exposure time of four years, makeup ^{235}U must be used throughout the life of the reactor. However, if the ^{233}U is not recycled, the amount of ^{235}U required is approximately 1.6 times that required for operation in the recycle mode. To recycle fuel from the HTGR, it will be necessary to chemically reprocess the fuel, separate the various fuels, refabricate recycle fuel elements, and send these elements to the reactor. The ^{233}U, which is to be returned to the reactor, contains ^{232}U, which has decay products with

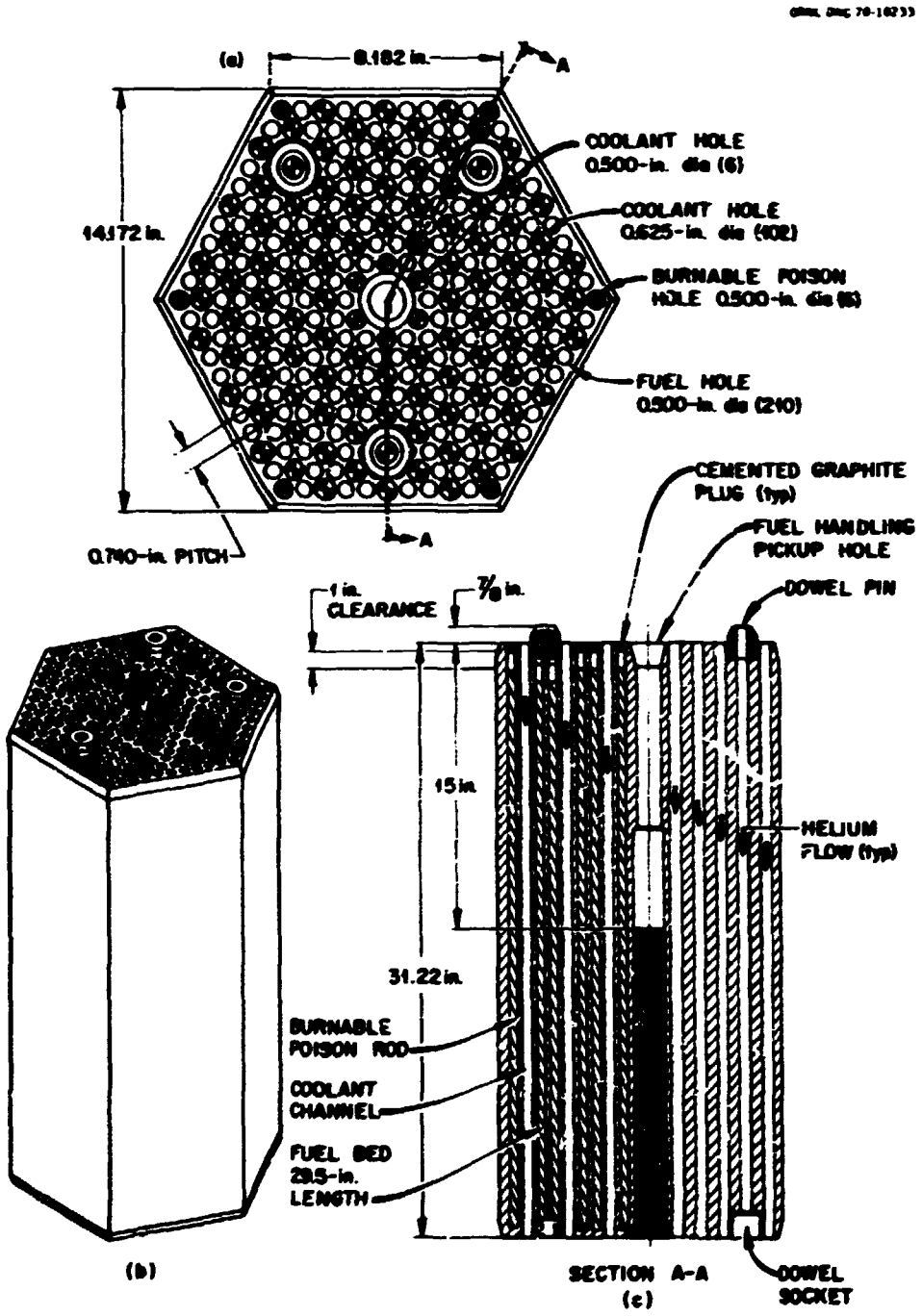

Fuel Element

Fig. 4.1. HTGR Fuel Element Design. To convert dimensions to millimeters, multiply by 25.4.

Table 4.1. Reference Recycle Fuel Particle Descriptions[a]

Property	Fissile Particle	Fertile Particle
Isotope	^{233}U	^{232}Th
Kernel composition	UC_2-UO_2-C	ThO_2
Kernel diameter, μm	400	500
Type coating[b,c]	Triso	Biso
Coating thickness, μm		
Buffer carbon	50	85
Inner dense carbon	30	
Silicon carbide	25	
Outer carbon	30	75
Total particle diameter, μm	670	820

[a]Particles will be bonded into fuel rods for insertion into hexagonal graphite block fuel elements.

[b]Triso designates three types of coating: buffer, silicon carbide, and dense pyrolytic carbon.

[c]Biso designates two types of coating: buffer and dense pyrolytic carbon.

high-energy gamma radioactivity. Thus, heavily shielded facilities and remote operations will be required to carry out refabrication operations. It is necessary also that the operations be suitably contained because of high alpha radioactivity. Thus, the operations and the equipment required for the refabrication of fuel with ^{233}U differ greatly from that required for fabrication of fuels containing naturally occurring isotopes. There is no experience on the remote refabrication of HTGR fuels on any scale, and there is very little experience with remote fabrication of fuels in general. The HTGR fuel refabrication pilot plant will provide this experience specifically for HTGR fuel, and the experience with remote operation will be valuable for the design of systems for refabrication of fast breeder reactor fuels.

4.2.2 General Description of Plant

The proposed pilot plant was planned for installation in the Thorium Uranium Recycle Facility (TURF), Bldg. 7930, at ORNL, except for the

uranium feed preparation system, which was to be located at Bldg. 3019, and the initial resin preparation, which was to be done in Bldg. 3503.

The TURF is a hot cell facility built particularly for pilot plant use. The pilot plant as conceptually designed is capable of performing all processing operations beginning with receipt of uranium nitrate solution and ending with the shipment of recycle fuel elements from the plant. The plant design throughput capacity is approximately 25 kg of heavy metal per day or about 2.5 product fuel elements per day. Working intermittently on a three-shift-per-day basis, the plant could produce about 200 fuel elements per year.

As designed, the pilot plant consists of ten major units or systems of equipment plus the necessary overall plant facility required to carry out necessary operations in fuel refabrication processing product verification, waste treatment and disposal, and materials handling.

4.2.3 Design Basis

This pilot plant, as conceptually designed, will produce about 150 recycle fuel elements for the Fort St. Vrain Reactor using ^{233}U and will demonstrate the following:

1. effective process and equipment designs for all fuel refabrication operations, including scalability to commercial plant capacities;
2. control of radiation hazards associated with the ^{232}U content of recycled ^{233}U fuel so that operating, maintenance, sampling, and analytical activities can be conducted safely;
3. feasibility of remote maintenance for all in-cell equipment through loading of the fuel elements;
4. practical methods for assay, quality control, and quality assurance for intermediates and the completed reactor grade fuel elements.

The refabrication pilot plant will be scaled to handle a heavy metal throughput of 25 kg of uranium and thorium per day, or 2.5 fuel elements per day on an intermittent basis. The demand for refabricated fuel for the 100-GWe reactor economy will be approximately 1000 kg/day in 1985. However, the first refabrication plants built will probably not exceed a capacity of 500 kg/day. On this basis, the HTGR fuel refabrication

pilot plant will be scaled at approximately 1/20 of commercial size. The rated capacity of the pilot plant is based on the total throughput of the flowsheet as restricted by the unit capacity of the slowest part of the process. The pilot plant will be designed to allow the test of at least one unit of each equipment item type that will be used in the commercial plant, and each unit will be either full size or a size that can be scaled to the commercial unit. To the extent possible, the commercial plant is expected to be designed by scale-up of certain units and by the use of multiple refabrication lines. Multiple refabrication lines will be required in commercial operations for reliability of the plant and because of criticality limitations. Because of this, the unit operations for the refabrication pilot plant will vary from 10 to 100% of the anticipated commercial plant size. The scale of the refabrication pilot plant is also set by the existing facility that is available for the work. The capacity of the pilot plant cannot be increased unless additional facilities are provided for incoming and outgoing shipments of materials. The scale on the lower side is set by the capacity of equipment representing an engineering-scale system. The scale of the pilot plant is very similar to that of a pilot plant that General Atomic is using for development of fabrication systems for nonrecycle fuel.

The design, construction, and operation of the HTGR fuel refabrication pilot plant will provide the following information for scale-up of refabrication processes to commercial size:

1. confirmation of design basis,
2. determination of equipment and process reliability,
3. determination of maintenance requirements,
4. confirmation of quality assurance procedures and standards,
5. confirmation of economic feasibility,
6. confirmation of licensability of systems,
7. confirmation of recycle fuel element design.

4.2.4 Process Equipment

The HTGR fuel refabrication pilot plant as conceptually designed consists of all equipment, facilities, and services necessary to prepare

recycle fuel elements using ^{233}U, with radioactivity equivalent to material containing 500 ppm of ^{232}U that has been aged for up to 90 days. The equipment shall be designed for remote installation, operation, and maintenance. The refabrication processing steps outlined in Fig. 4.2 will be performed by ten process systems described in the following sections.

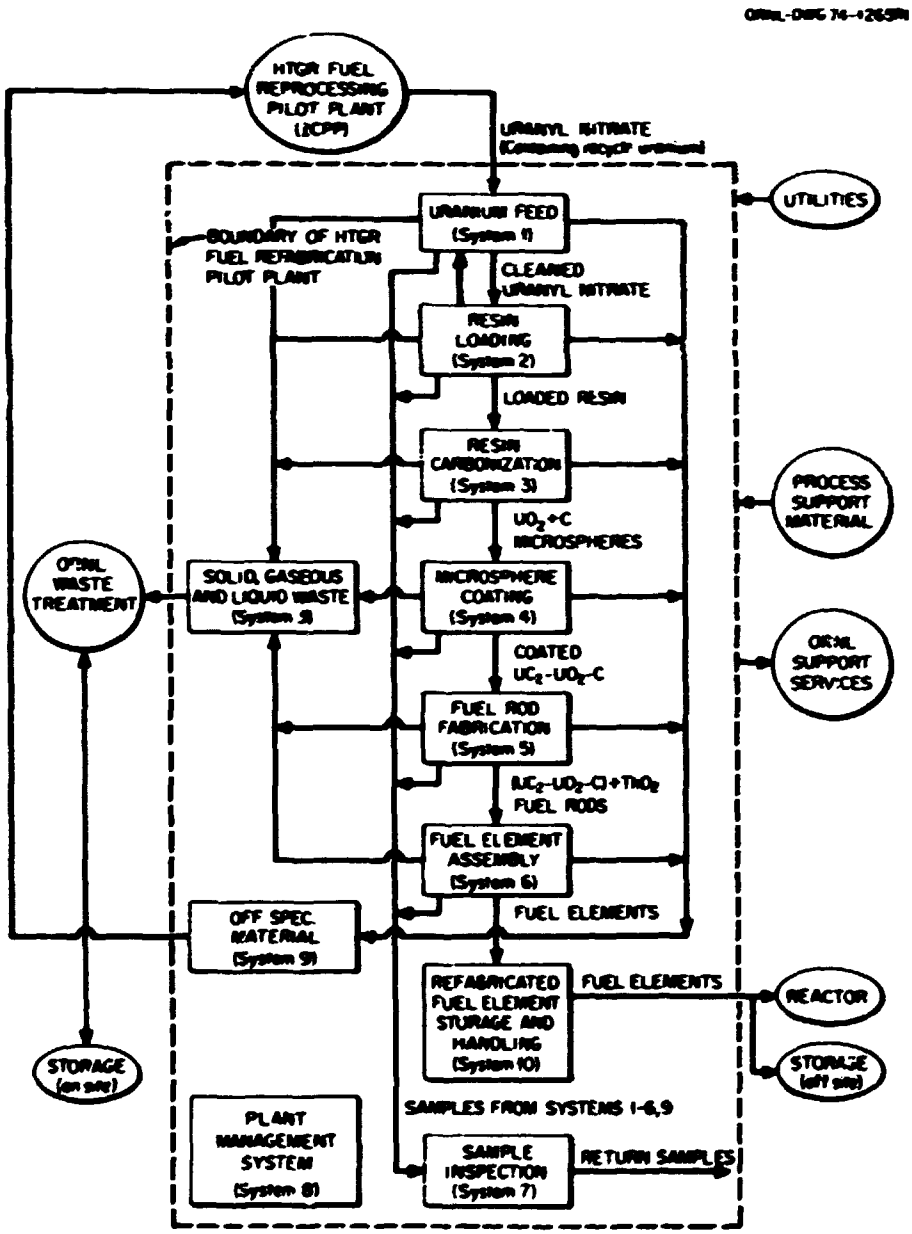

Fig. 4.2. Fuel Refabrication Pilot Plant Schematic Flowsheet.

Control instrumentation will be provided to operate the systems manually or semiautomatically. Most processing operations will normally be under the control of the local instrument and control subsystem, but the operators shall have the option of manual control. Decisions about production rates and handling rejects and backlogs shall be made by the operator. Maintenance and troubleshooting shall also be done in accordance with operator decisions.

Design of equipment and equipment location in the pilot plant shall be such as to preclude a criticality accident.

4.2.5 Facility

The Thorium Uranium Recycle Facility (TURF) is a three-story structure with a partial basement that was designed in accordance with the Southern Building Code for group-G industrial occupancy. It is constructed of structural steel, reinforced concrete, and masonry.

The first floor provides space for technical personnel offices, cell operation and maintenance, a receiving area, a fuel storage room, hot and cold change rooms, a compressor room, and an elevator room, as shown in Fig. 4.3.

The second floor provides space for chemical makeup, sampling of radioactive materials, a development laboratory, a shop, a maintenance area, mechanical and electrical equipment rooms, a cask decontamination station, a checking and holding area, and working space around Cell A.

The third floor, a high bay, includes the cell roof area and provides facilities for cell access and entry of cell services. It is equipped with a 0.44-MN (50-ton) overhead traveling bridge crane with a 44-kN (5-ton) auxiliary hoist. Some of the third-floor space is used for cell and building ventilation equipment, and other portions will be used as necessary for mockup of cell process equipment.

The facilities for receiving, handling, and storing radioactive materials consist of six heavily shielded cells served by an overhead crane and electromechanical manipulator system along with master-slave manipulators. In addition, there is an unshielded gloved maintenance cell, a fuel storage room, and a cask support and decontamination area.

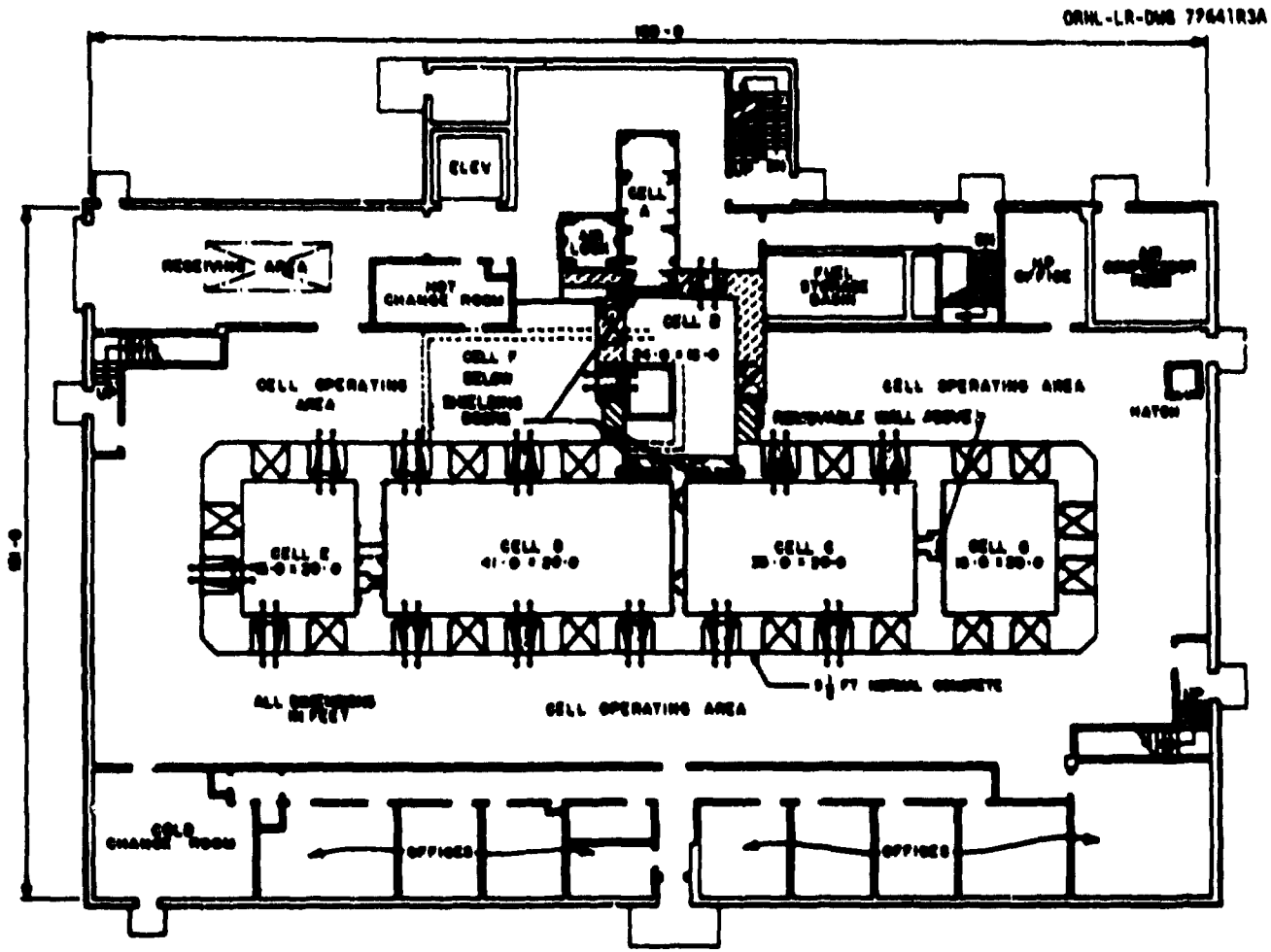

Fig. 4.3. First-Floor Plan of Building 7930 (TURF). To convert dimensions to meters, multiply by 0.305.

Figure 4.4 shows the four operating cells (Cells C, D, E, and G). These are described elsewhere.[1] A partial basement provides space for access to Cell F and for instaliation and maintenance of equipment in a pump room adjacent to Cell G.

The existing cells will accommodate the process systems involved, but modifications to the existing building will be required to provide the necessary services. The facility modifications include:
a two-story building addition and an addition to the third level on the east side of TURF,
increasing the plant air system,
providing for waste treatment,
adding a process gas storage and distribution system,
providing shielded transfer ports,
modifying the fuel storage basin,
adding a nonmoderating process cooling system,
adding an electrical substation,
adding the remaining viewing windows and master-slave manipulators,
adding a computer systems area.

4.3 SYSTEM 1 — URANIUM FEED PREPARATION (WORK UNIT 2201) — F. E. Harrington and T. F. Scanlan

4.3.1 Summary Description

The uranium feed preparation system is designed to receive uranyl nitrate product solution from the HTGR Reprocessing Pilot Plant at the Idaho Chemical Processing Plant (ICPP), purify it to reduce thorium content and radioactivity level by selective removal of particular ^{232}U decay products, and dispense the purified uranyl nitrate to a transport vessel for transfer to System 2 at TURF. The uranyl nitrate solution will be purified and dispensed on a campaign basis to support fabrication of 2.5 fuel elements per 24-hr day to a maximum of 45 kg of uranium.

This system will be located in Building 3019, which houses an established radiochemical production facility with suitable waste handling

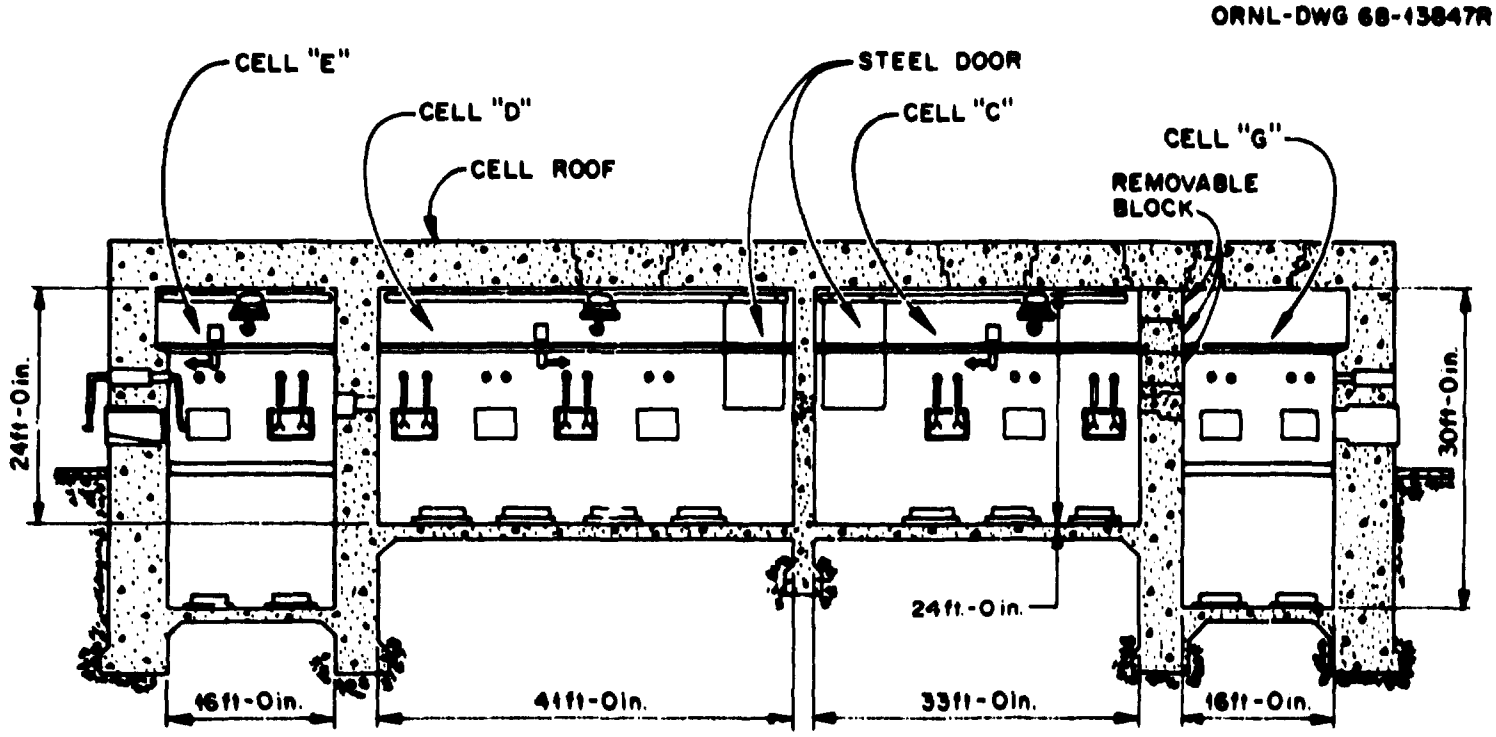

Fig. 4.4. Elevation View of TURF Operating Cells. To convert dimensions to meters, multiply by 0.305.

facilities and an experienced technical and operating staff employing well-developed operating and maintenance procedures. Therefore, approximately 90% of the equipment required for System 1 currently exists and has been operational from 5 to 25 years.

4.3.2 Conceptual Design Detailed Description

The functions to be performed are shown schematically in Fig. 4.5. The uranium feed preparation system will receive uranyl nitrate shipments from both ICPP and TURF in 10-liter shipping casks. The casks are then conveyed to a receiving station, where the uranyl nitrate solution is vacuum transferred to either the recycle receiving vessel (if returned from TURF) or the ICPP product receiving vessel (if received from ICPP). The quantity of uranium received is established by measurement at these two tanks. Solution in the recycle receiving vessel is then transferred to solvent extraction (SX) feed makeup tank for recycle purification, while solution in the ICPP product receiving vessel is transferred to the liquid storage facilities to await purification processing. Greater than 90% of the ICPP solution received is expected to meet purified product requirements after a single pass through the ion exchange (IX) column.

A typical purification campaign will consist of three successive IX runs of 15 kg of uranium each. For each IX run, approximately 20 kg of uranium is transferred from the storage facility to the IX feed makeup tank, adjusted, and fed through the IX column, where essentially 100% of the ^{228}Th and ^{224}Ra are selectively removed from the solution, thus breaking the ^{232}U decay product chain. Each batch of purified product is then transferred to the campaign tank, where the three batches are blended to form the feed solution for each TURF fuel refabrication campaign.

ICPP product containing excessive ionic impurities, IX elutrient, and all other recycleable liquid scrap will be transferred to the SX feed makeup tank for uranium recovery by a solvent extraction technique. Uranium is extracted from solution by countercurrent contact of an aqueous uranium-bearing feed stream and an immiscible organic extractant

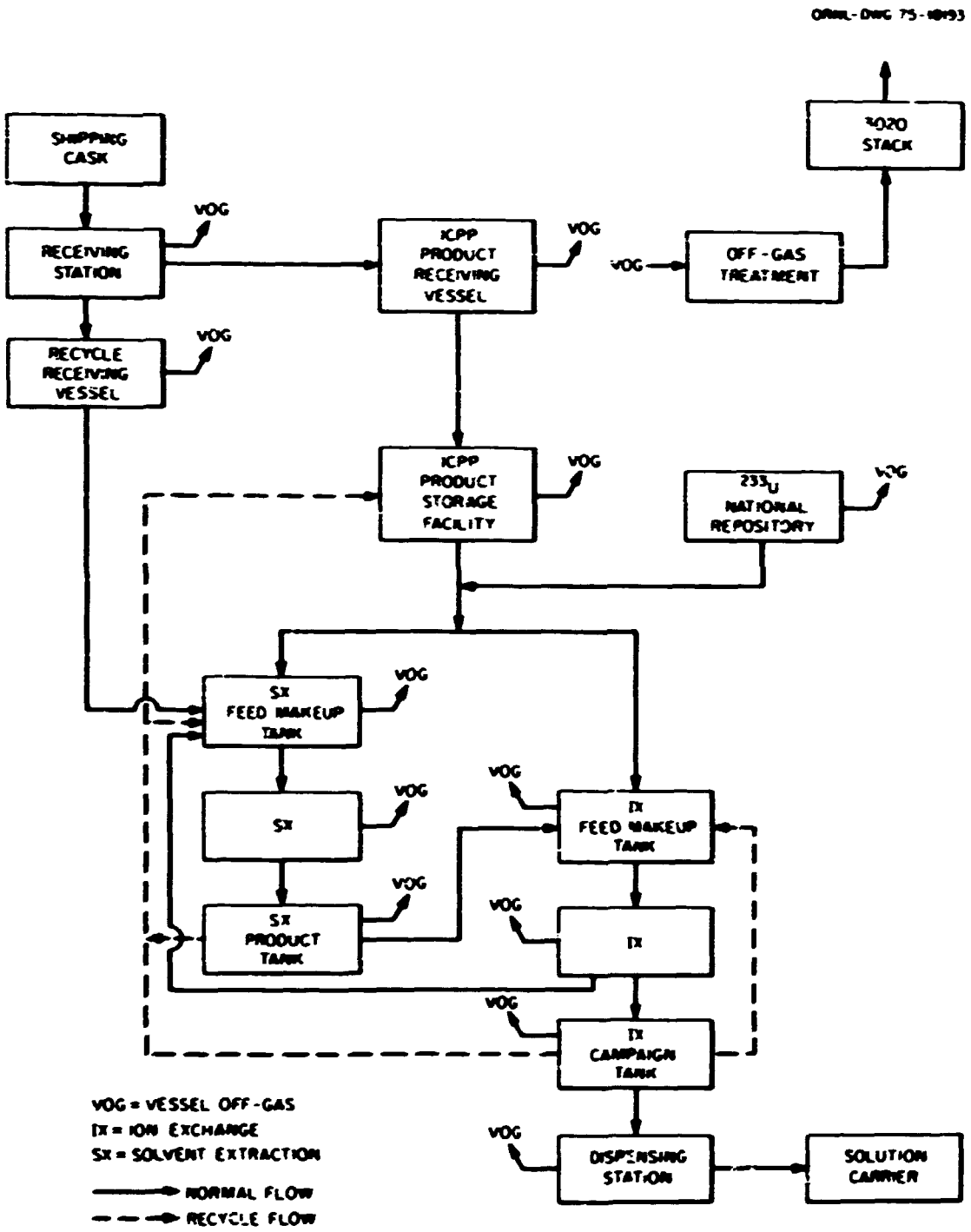

Fig. 4.5. Uranium Feed Preparation Process Schematic.

in an air-pulsed column. Further purification is achieved in a scrub column, and finally the uranium is stripped and returned to the aqueous phase in a third column. The purified SX product is then concentrated and normally transferred to the IX feed tank. Alternatively it may be transferred to the storage facility when the SX run does not coincide with the need for an IX batch.

Purified uranyl nitrate solution to be transferred to TURF is pumped from the campaign batch tank into the solution carrier. The purified uranyl nitrate will usually be transported to TURF in three batches of approximately 125 liters each.

The Off-Gas Cleanup Subsystem provides for two new radon retention trains in parallel before the vessel off-gas (VOG) enters the existing building VOG system. Each radon retention train consists of a chiller, dryer, charcoal absorber, and filter. The charcoal bed retains the radon for longer than 10 half-lives. The subsystem design capacity is 500 cfm (0.236 m^3/sec) flow while a minimum vacuum of 0.5 in. (13 mm) H_2O is maintained at the vessel vent ports. The dryer employs molecular sieves to remove water, which would interfere with radon absorption from the VOG.

The Liquid Waste Disposal Subsystem utilizes existing equipment to monitor and recycle or dispose of the liquid waste.

4.4 SYSTEM 2 — RESIN FUEL KERNEL PREPARATION (WORK UNIT 2202) — C. C. Haws and F. E. Harrington

4.4.1 Summary Description

The resin fuel kernel preparation system will be designed to receive ion exchange resin kernels purchased from a commercial supplier, upgrade them by rejecting those that do not meet the criteria for size and shape, and convert the resin from the sodium to the hydrogen form. Aqueous uranyl nitrate, received from System 1, will be converted to an acid-deficient solution and contacted with the upgraded resin kernels to load them with uranium. The loaded kernels will be dried and transferred to the Resin Carbonization System. The resin upgrading operation is

nonradioactive, so the equipment is to be located in a clean area of Building 3503, which allows for direct maintenance and operation. The remainder of the system will occupy the northern half of the east wall in Cell C of TURF.

4.4.2 Conceptual Design Detailed Description

Schematic diagrams showing the major operations for resin preparation and resin loading are included as Figs. 4.6 and 4.7.

In resin preparation portion of System 2, a weak-acid ion exchange resin (sodium form) is received from a commercial supplier and passed through size and shape classification equipment to accumulate a supply of spherical kernels within the correct size range. Currently, less than 10% of the resin in the as-received condition meets the size and shape requirements, making the expected accumulation rate of acceptable resin kernels approximately 6 liters/day using the proposed equipment. Next the acceptable resin kernels are conditioned by sequential treatment with HNO_3 and NaOH, then finally converted from the sodium form to the hydrogen form by treatment with HNO_3 followed by a water rinse. The converted, rinsed resin (now 11 liters because of swelling) is then placed in resin transfer flasks for transport to the TURF.

The resin loading portion of System 2 receives both the conditioned resin from Building 3503 and purified uranyl nitrate solution from Building 3019 (System 1). A typical equipment arrangement is shown in Fig. 4.8. Approximately 40 liters of uranyl nitrate solution is required for loading each resin batch. The purified uranyl nitrate is made into an acid-deficient solution by a solvent extraction technique in which nitrate (NO_3^-) is removed from the uranyl nitrate solution by contacting it with an organic extractant (Amberlite LA-2) dissolved in a hydrocarbon dilutant (diethyl benzene). During the resin loading operation, both makeup uranyl nitrate and the spent nitrate solution leaving the resin loading column are mixed and continuously processed through the nitrate extraction contactor to maintain the correct ratio of nitrate to uranium for efficient loading. The organic extractant is recycled to the nitrate extraction contactor after any remaining uranium is scrubbed out, and the solution is regenerated with NaOH and Na_2CO_3.

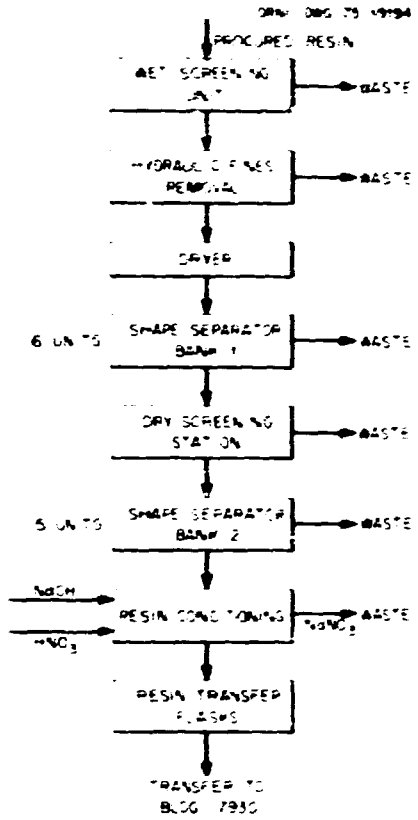

Fig. 4.6. Resin Preparation Process Schematic Flowsheet.

For the resin loading operation, approximately 11 liters of conditioned resin is transferred from the receiving site into the loading contactor. Then, heated (≈50°C) acid-deficient uranyl nitrate is introduced at the bottom of the resin loading contactor at a rate of about 4 liters/min, causing fluidization of the resin kernels. The uranium in the solution is transferred to the resin via ion exchange action, and the spent nitrate solution is returned to the nitrate extraction contactor for adjustment. Excess water in the uranyl nitrate solution is eliminated by continuous passing a stream of feed solution through an evaporator.

The resin loading operation is considered complete when the pH difference between the influent and effluent streams of the resin loading column is less than or equal to 0.02 units.

The loaded resin is next transferred to a drying vessel and dried by a forced hot-air system. The dried batch of resin kernels is discharged

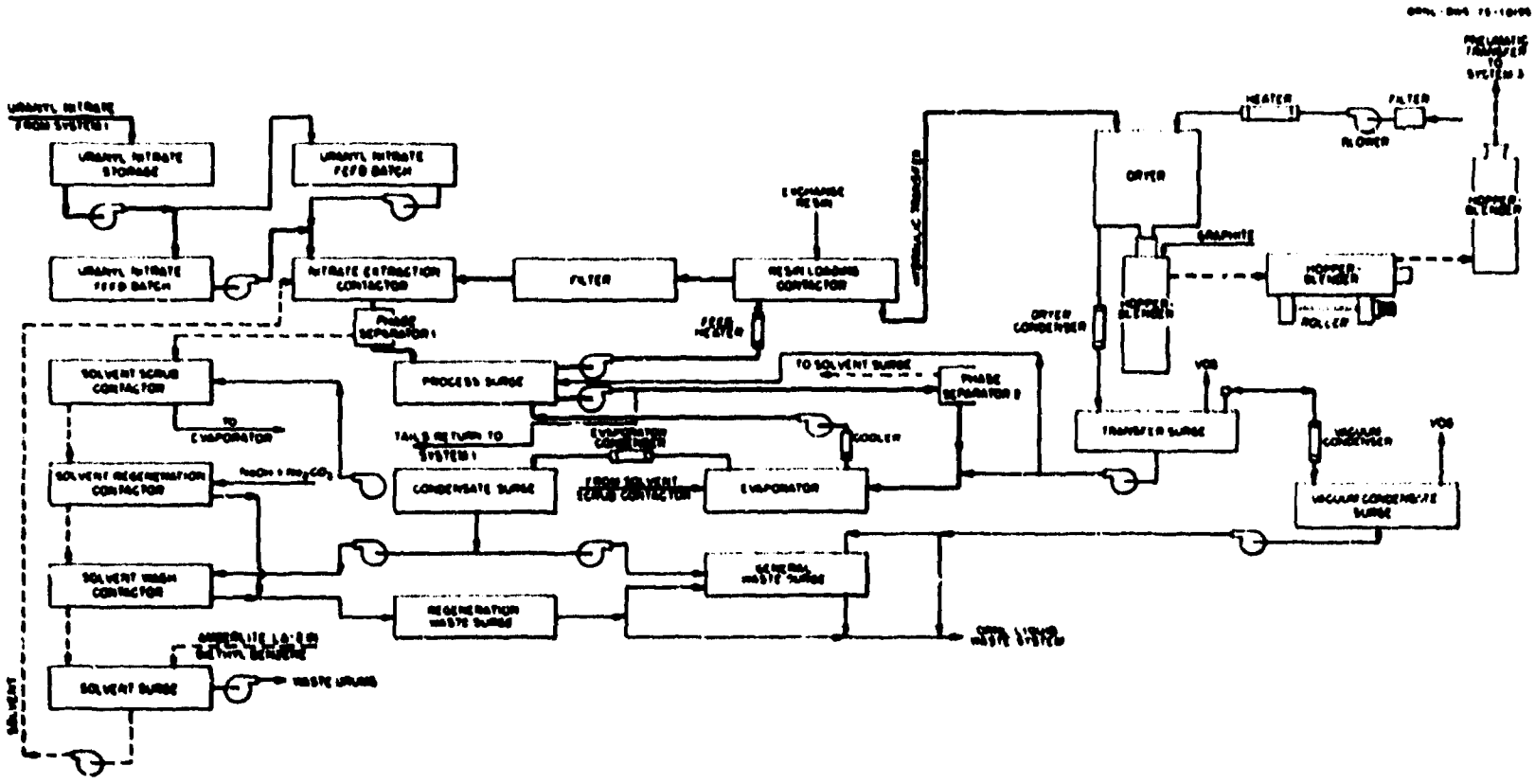

Fig. 4.7. Resin Loading Process Schematic Flowsheet.

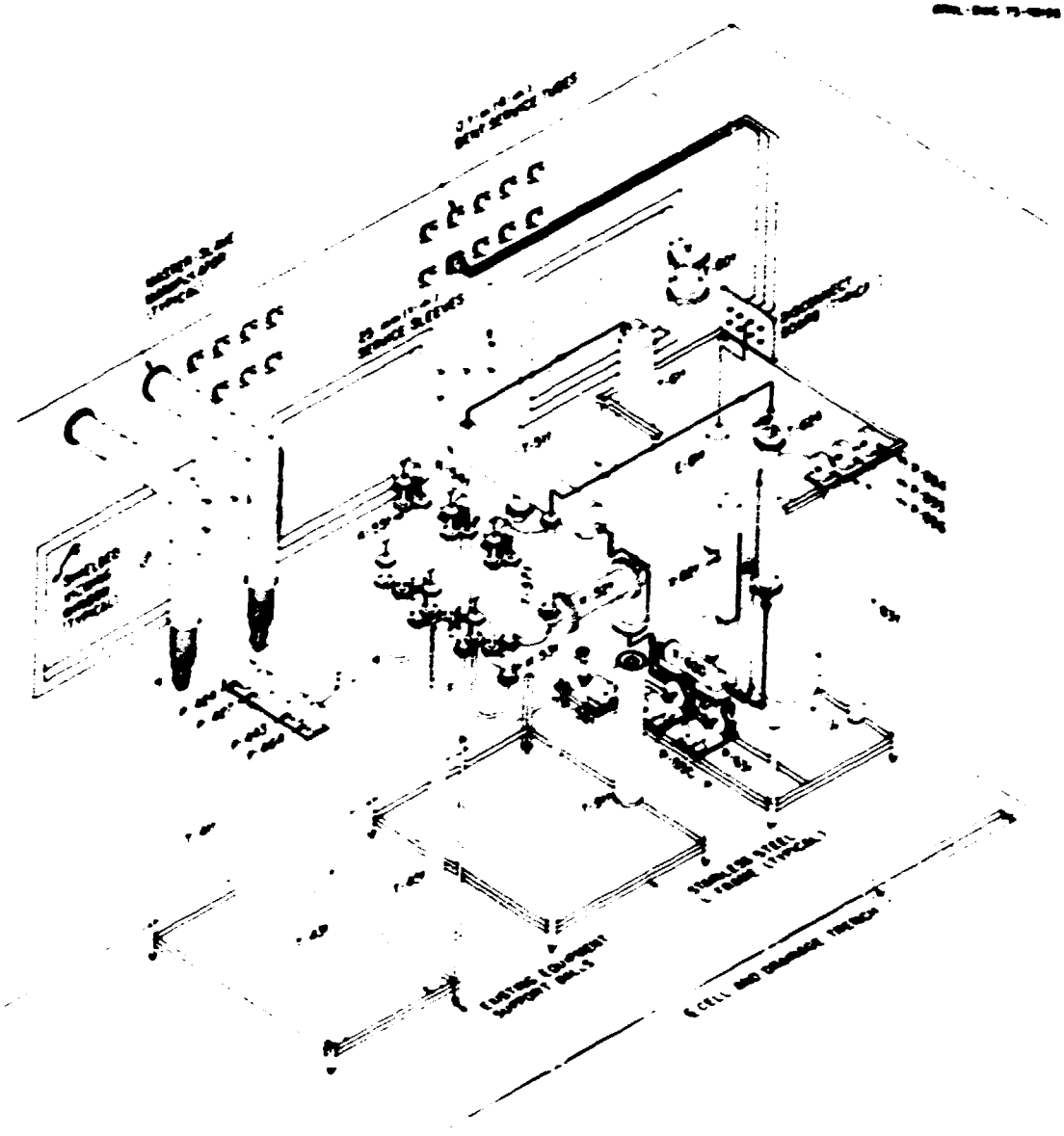

Fig. 4.8. Typical Equipment Arrangement for Resin Loading.

to a hopper-blender, coated with graphite, and pneumatically transferred to the receiving hopper of System 3. En route to System 3, the batch passes over a sample riffle, where two samples are removed for quality assurance.

Waste from organic extractant regeneration and waste from the evaporator are collected in separate tanks for uranium assay before discharge to the Cell C drain of System 9.

Off-gases from the various processing operations are passed through a condenser to cool them to about 4°C (40°F). Condensed liquids are routed to the condensate waste tank and the dry gas is passed over charcoal for adsorption of radon. Any decay products escaping the charcoal are collected by an HEPA filter before the gas is vented into the hot off-gas of System 9.

4.5 SYSTEM 3 – RESIN CARBONIZATION (WORK UNIT 2203) – C. B. Haynie and D. R. Johnson

4.5.1 Summary Description

The resin carbonization system is designed to receive dried uranium-loaded resin fuel kernels from System 2. The system will upgrade the kernels by rejecting those that do not meet the criteria of size or shape. The remainder will be carbonized, weighed, and sampled. The sample will be analyzed in System 7. On the basis of the analysis, acceptable lots are transferred to the microsphere coating system and unacceptable lots are transferred to the reject weigher in System 4 and ultimately to the Reprocessing Pilot Plant for reclamation. All the carbonization equipment will be located in Cell C of TURF, occupying the two southern window modules on the east wall. The arrangement of the system is shown in Fig. 4.9.

4.5.2 Conceptual Design Detailed Description

The functions to be performed are shown schematically in Fig. 4.10. The resin carbonization system will receive approximately 6 kg/day of uranium-loaded and dried resin kernels from System 2 in three batches of 2 kg each at approximately 4-hr intervals. Each 2-kg batch is received

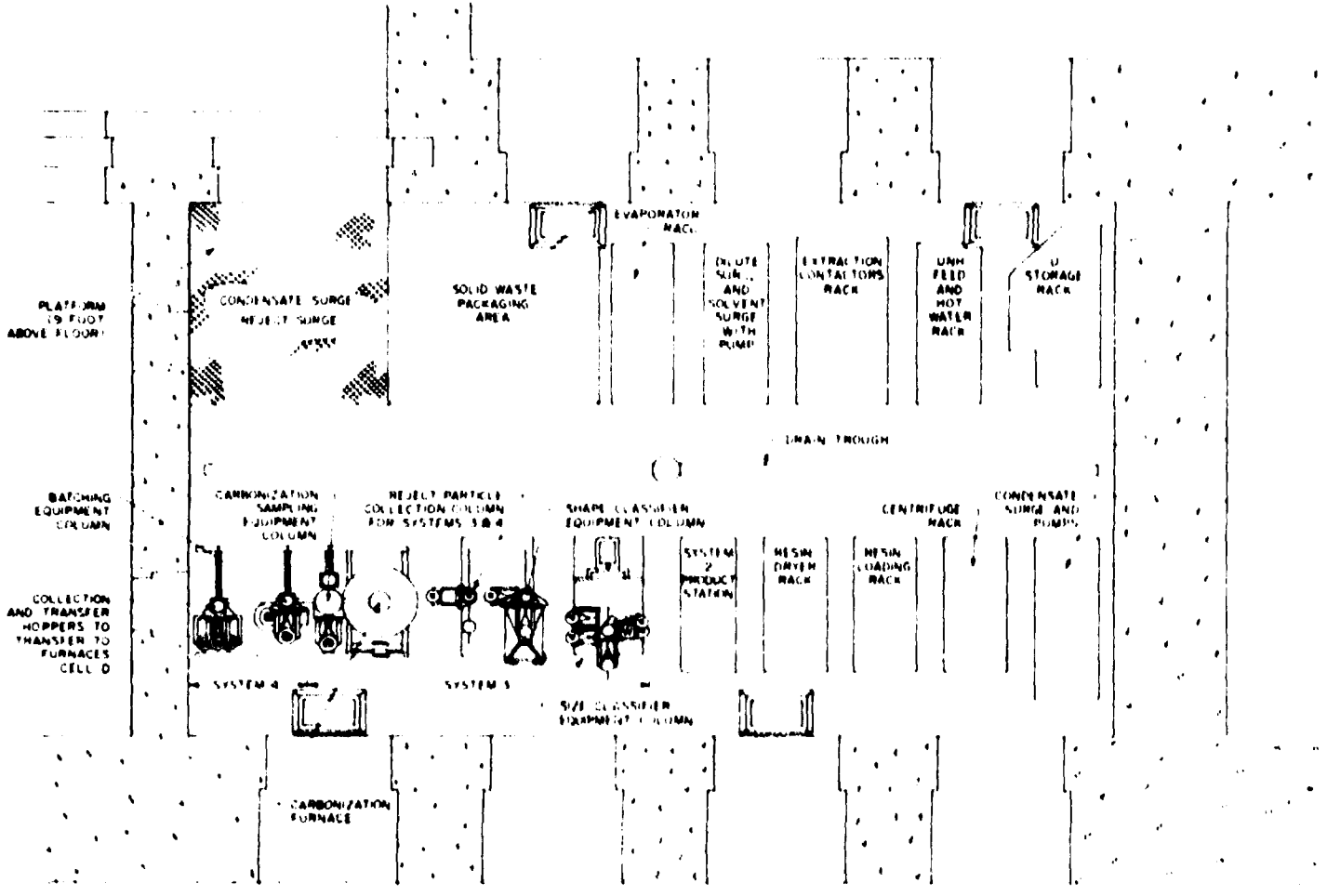

Fig. 4.9. Cell C Equipment Arrangement.

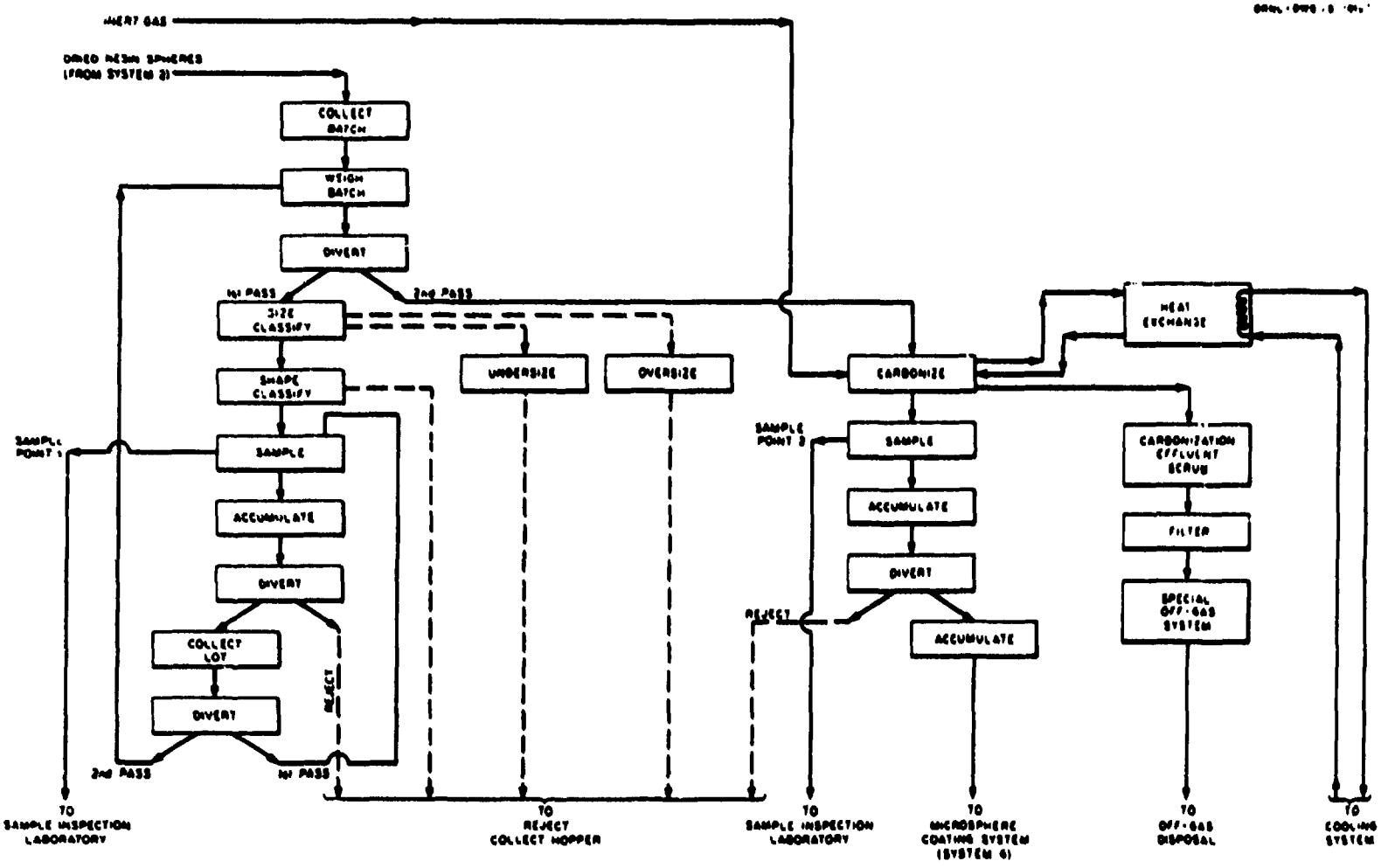

Fig. 4.10. Resin Carbonization Process Schematic Flowsheet.

in the first collection hopper and fed to a bulk precision weigher and weighed, and the weight is recorded. The weighing operation requires minimal time (2–5 min). The batch is then fed into a size classifier, where a set of vibrating screens separates the undersize and/or oversize kernels from the acceptable kernels. This operation requires approximately 0.5 hr. The acceptable kernels are collected and fed to a shape classifier, where the misshapen and broken kernels are separated from the true spheres by the use of a vibrating slanted plate. Shape classification of a batch requires approximately 3 hr. The upgraded kernels are then fed through a sampler, and the sample is transferred to the sample inspection laboratory for analysis. The sampling operation requires 2 to 5 min, and the analysis should require no more than 0.5 hr.

Depending upon the sample analysis, the batch is either rejected or pneumatically transferred to a collection hopper, which collects and combines the three batches of kernels into the 6-kg lot. After the lot is combined it is again fed through a sampler to verify its acceptability. Depending upon the sample analysis, the lot is either rejected or fed to a precision weigher and weighed. The weight is recorded so that material accounting can be done after the lot has been combined.

The accepted kernels are pneumatically transferred into the carbonization furnace through a specially designed three-way valve, which allows a common entry-exit line in the bottom of the furnace vessel. Figure 4.11 shows the furnace. The kernels are fluidized in the furnace with argon as the furnace temperature is elevated to carbonize the organic material in the resin of the kernels. Approximately 33% of the weight of the kernels is lost by the volatile of the resin. The effluents from the furnace are directed through a scrubber and radon decay trap filters, and are finally exhausted up the system combustible-gas stack. Upon completion of carbonization, the fluidizing gas is stopped, and the lot drains from the furnace under a protective inert atmosphere. The carbonized kernels are pyrophoric and must be maintained in this inert environment until they are coated. The carbonizing operation will require approximately 4 hr. The carbonized kernels are fed through a second sampler, and the sample is transferred to the sample inspection laboratory. The sampling

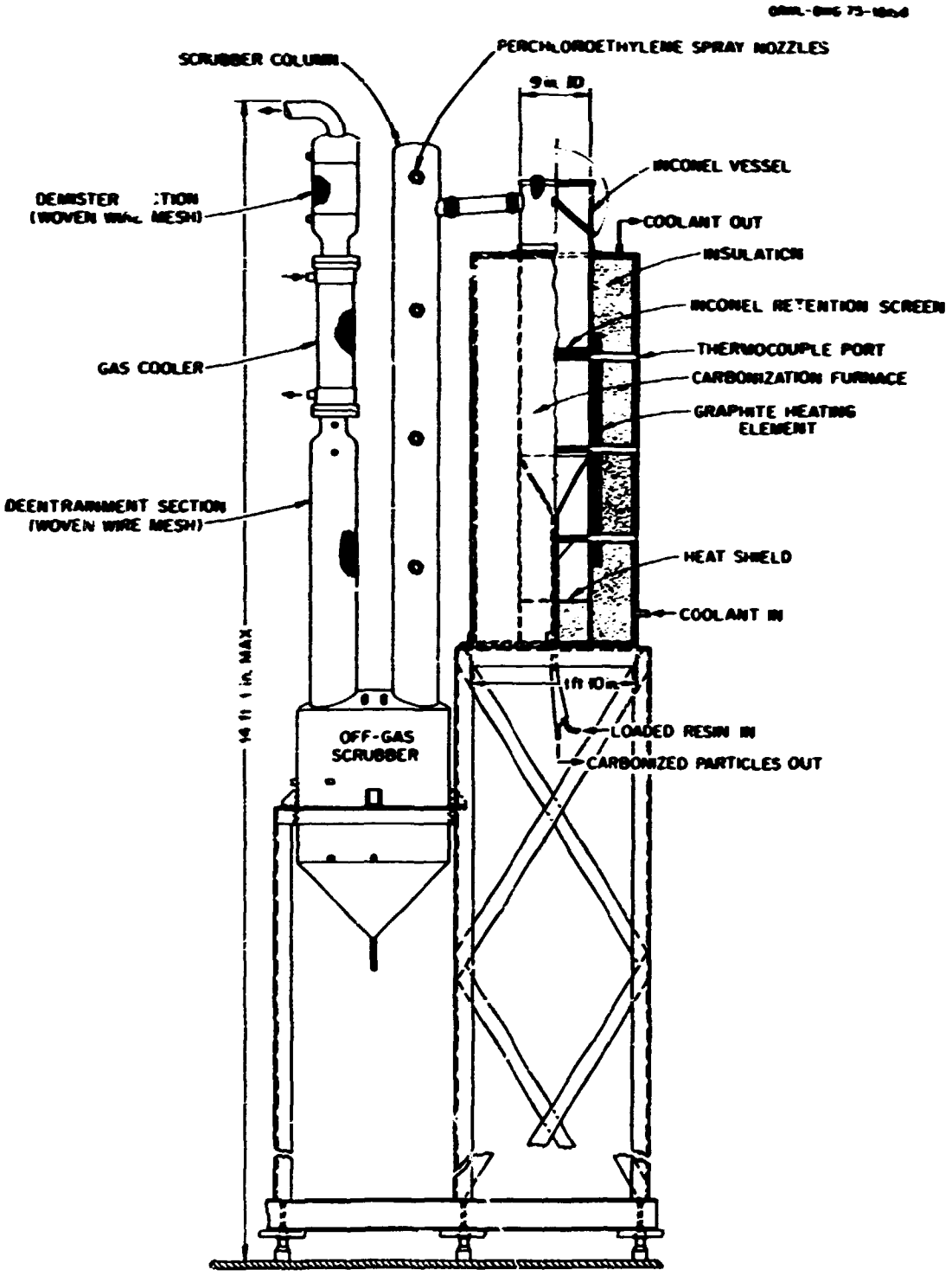

Fig. 4.11. Carbonization Furnace Installation.

and required analysis will require approximately 2 hr to complete. Depending upon the sample analysis, the carbonized lot is either rejected or pneumatically transferred to System 4 for coating. The total time required to carbonize the 6-kg lot is 18 hr.

In general, the equipment constituting the various subsystems of the carbonization system is small, and several of these components will be mounted on each of several vertical equipment racks. Fuel kernels are transferred from component to component on a vertical support by gravity flow, but the kernels in the bottom components on a support are pneumatically transferred to the top component on the next support.

In the event that System 4 becomes temporarily inoperative, loaded and dried resin can be received from System 2 for three days and stored in the precarbonization equipment. However, because of the reactive nature of the carbonized product, the carbonization furnace will not be operated unless System 4 is prepared to receive the carbonized kernels.

4.6 SYSTEM 4 – MICROSPHERE COATING (WORK UNIT 2204) – M. K. Preston and W. J. Lackey

4.6.1 Summary Description

The microsphere coating system will be designed to receive one approximately 3.5 kg lot of carbonized kernels loaded with uranium oxide (UO_2) and subdivide this lot into appropriately sized batches for further processing. The kernels will be pyrophoric as received and consist of elementary carbon and uranium oxide. Approximately 75% of the uranium oxide will be converted to uranium carbide. After conversion the kernels will be given four coatings, a buffer coat of low-density carbon, an inner coating of high-density carbon, a coating of silicon carbide (SiC), and an outer coating of high-density carbon. The coated particle is no longer pyrophoric. These coatings will serve as cladding material to maintain microsphere integrity and contain fission products.

To ensure proper particle composition and coating properties, the batches shall be sampled for analysis at key points in the system. If a sample does not meet specifications, the batch will be rejected to waste

particle reclamation. After all the precoating and coating processing, the fuel particles will be sized, and those particles that are of proper size and composition will be transferred to the fuel rod fabrication system (System 5).

4.6.2 Conceptual Design Detailed Description

A schematic diagram of the operations to be performed is shown in Fig. 4.12. The system can be divided into four functional sections: the precoating section, coating section, postcoating section, and reject particle handling section. The precoating section and the reject particle section are located in the southeast corner of Cell C (Fig. 4.9), while the coating and postcoating sections will be located in the north half of Cell D (Fig. 4.13).

The precoating section is maintained in an inert atmosphere to protect the pyrophoric kernels. The section starts with a collection hopper that receives one 3.5-kg lot of carbonized kernels. The lot is divided into process batches, usually six, which are dispensed one at a time for processing. Each batch is weighed in a precision scale and then pneumatically transferred into one of two parallel coating furnace loops. The furnace coating loop is the main part of the system and constitutes the coating section. It includes the furnace itself, the coating chamber handling subsystem, the carbon and silicon carbide coating effluent scrubbers, and the furnace maintenance equipment. A typical installation is shown in Fig. 4.14.

The fuel particles are pneumatically transferred through the top of the furnace and fall to the bottom of the coating chamber onto a porous graphite disk. The batch is first fluidized with argon and then heated to about 1800°C to obtain the desired conversion ratio. After the particles are converted, the coating chamber elevator assembly lowers the coating chamber from the furnace. When the coating chamber is clear of the bottom of the furnace, a manipulator assembly grasps it and dumps the batch into the receiving hopper of a scalping screen, which is in the loop to remove large carbon pieces generated during the coating operations. The particles are pyrophoric until the first coating is applied; thus the coating loop is maintained in an inert argon enclosure.

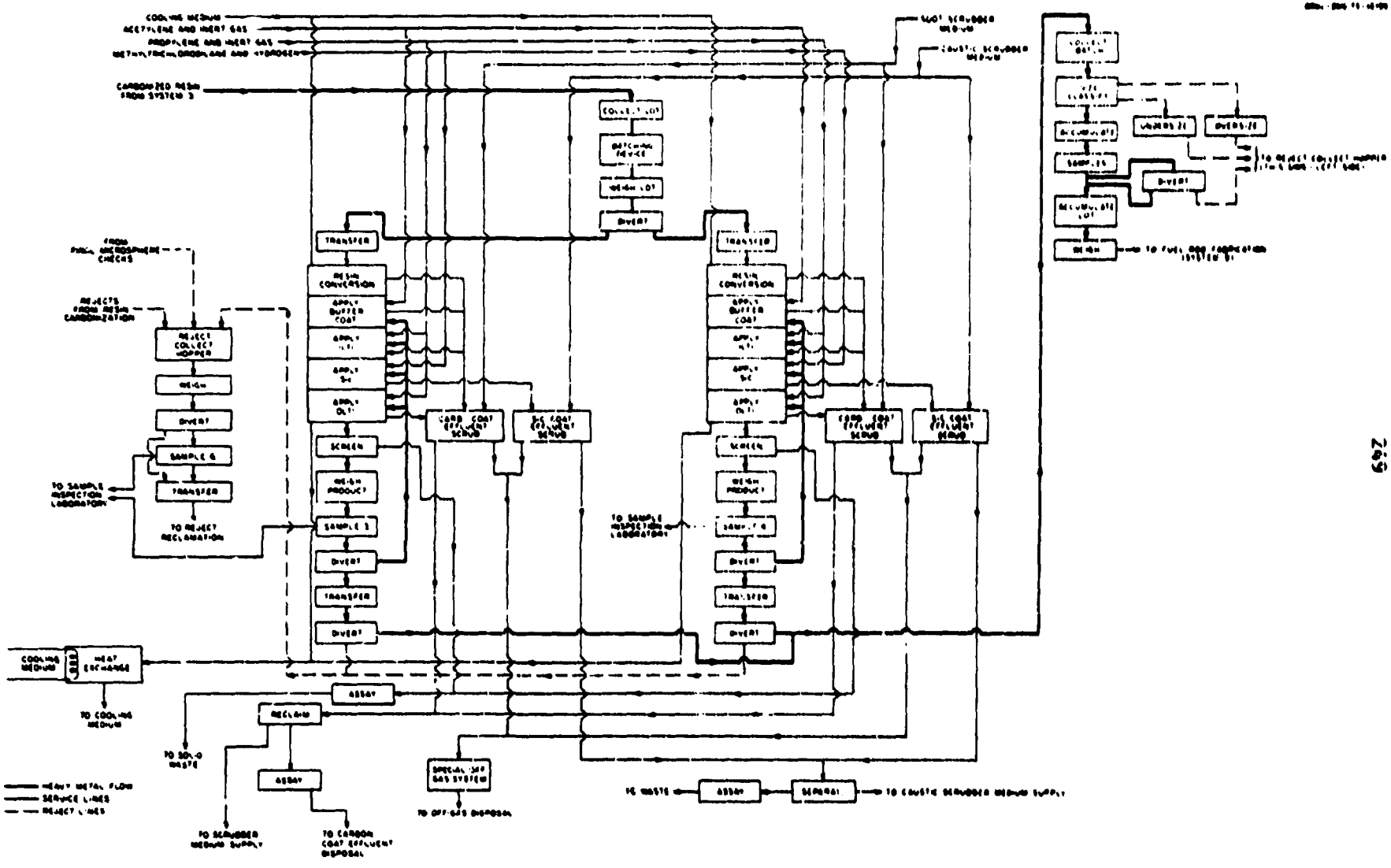

Fig. 4.12. Microsphere Coating Process Schedule Flowsheet.

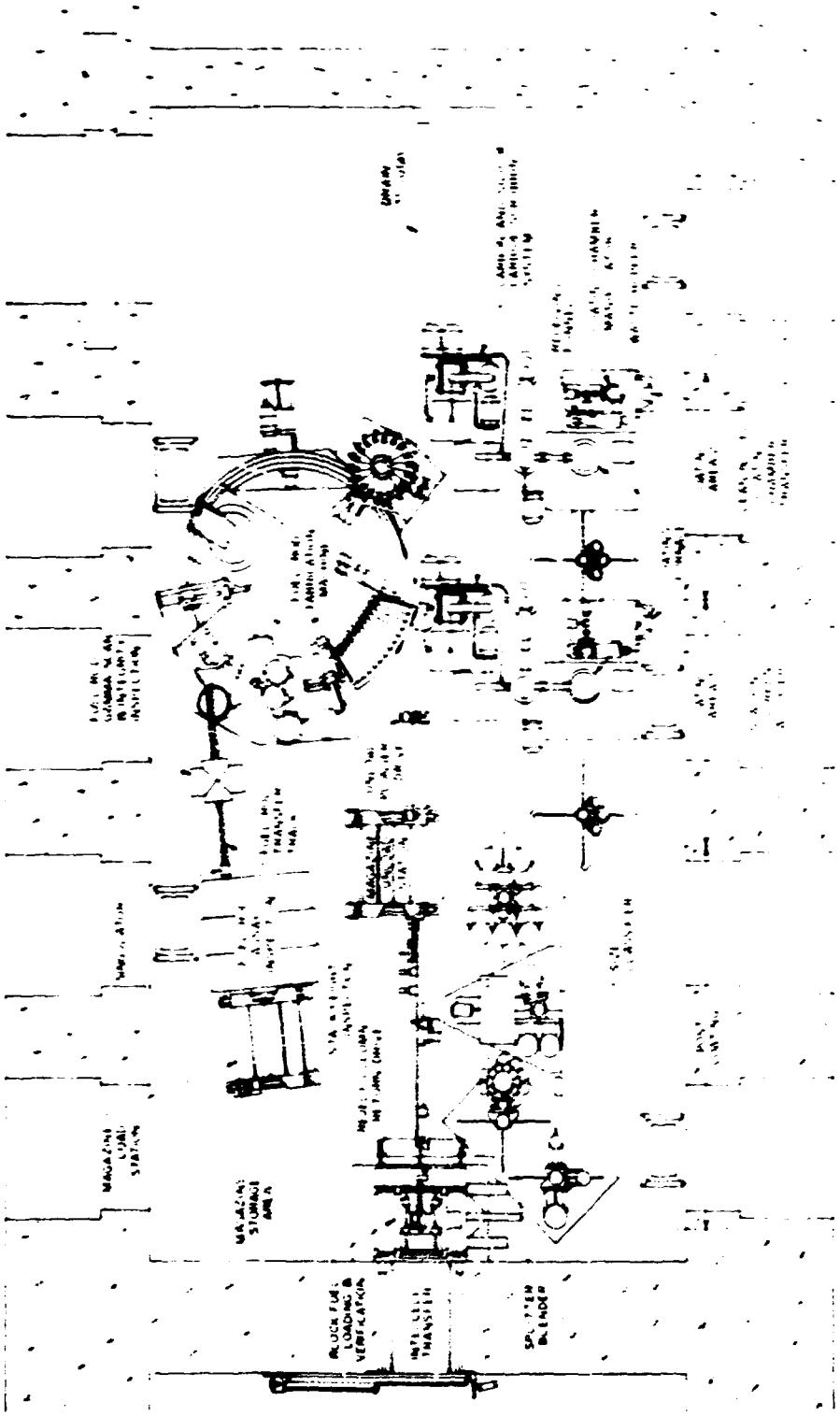

Fig. 4.13. Cell D Equipment Arrangement.

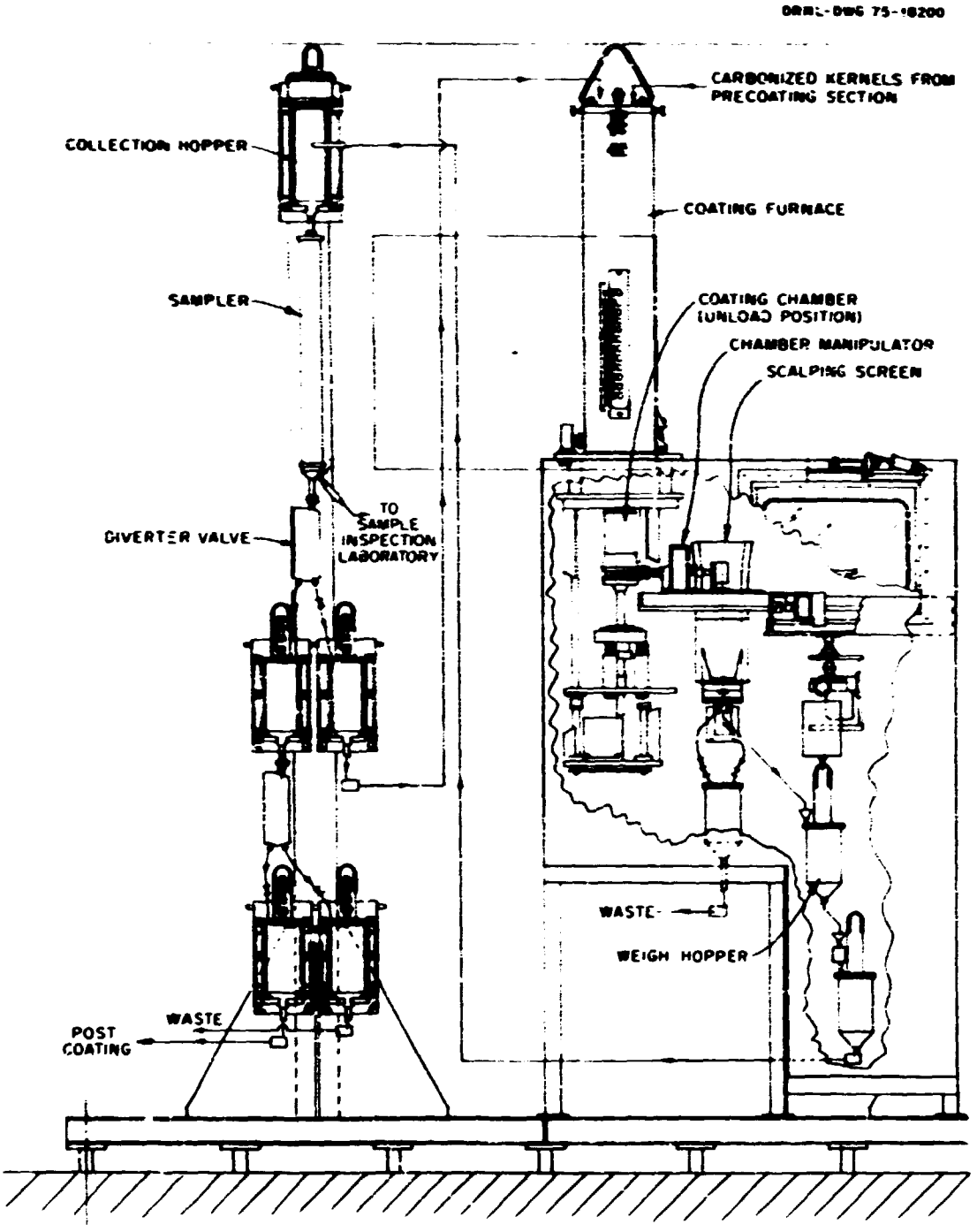

Fig. 4.14. Typical Microsphere Coating Loop.

The receiving hopper feeds the converted batch to the scalping screen, which is a vibrating feeder screen. The particles pass through the screen and are collected in a precision weigher. After weighing, the batch is passed through a sampler, and the sample is sent to the sample inspection laboratory for a comprehensive analysis.

Depending upon the sample analysis, the batch is either rejected to the reject particle handling section or pneumatically transferred back to the furnace for the first coating. After each coating, the batch is passed through the scalping screen, weigher, and sampler and returned to the furnace until it is either rejected or receives all four coatings. After all four coatings have been applied, the batch is diverted to a collection hopper that starts the postcoating section.

The collected microspheres are fed to a size classifier, in which a set of vibrating screens separates the undersize and/or oversize particles from the acceptable particles. The sized batch is collected and fed through a sampler. If the batch is acceptable, it is transferred to a collection hopper, where the entire lot is re-collected, weighed, and transferred to the fuel rod fabrication system (System 5).

Effluents from the furnaces are directed through two scrubbers to remove particulate and gaseous wastes generated in the furnace during the coating and converting processes. Perchloroethylene is used in one to remove hydrocarbon wastes, and an aqueous solution of NaOH is used in the other to neutralize the HCl gas generated during the SiC coating.

Components of various subsystems are mounted on vertical equipment racks to allow the use of gravity flow as much as possible to transfer the microspheres. Pneumatic transfers will be used when particles reach the bottom component of an equipment rack.

It is estimated that 5 hr is required for fully coating a batch, including time for sample analysis, weighing, and other particle handling.

4.7 SYSTEM 5 — FUEL ROD FABRICATION (WORK UNIT 2205) — R. I. Deaderick and R. A. Bradley

4.7.1 Summary Description

The Fuel Rod Fabrication System will be designed to perform the various processes and inspections required to produce fuel rods suitable for

use in the HTGR fuel element (see Fig. 4.1, p 226). The system will receive coated fissile fuel particles from the microsphere coating system (System 4), receive coated fertile and shim particles procured from external sources, blend these in appropriate proportions, and form fuel rods by the slug injection technique. The system will also include the required inspections to qualify the fuel rods as to dimensions and to fuel loading. The fuel rod machine will consist of a number of independently operating stations connected by a common nonsynchronous closed-loop transfer table. The formed fuel rods will be transferred to sequential inspection stations consisting of a fuel rod gamma scan inspection, a fuel rod integrity inspection, and a radioassay inspection. The fuel rods will then be placed in storage magazines for transfer to the fuel element assembly system (System 6), where the fuel rods will ultimately be loaded into a fuel block. The nominal throughput of this system will be 10,900 fuel rods per 24-hr day. The equipment will be located along the west side of Cell D, as shown in Fig. 4.13.

4.7.2 Conceptual Design Detailed Description

A schematic diagram showing the operations to be performed is shown in Fig. 4.15. The system begins with the fuel rod fabrication machine shown in Fig. 4.16. This machine forms fuel rods approximately 13 mm in diameter and 50 mm long (0.5 by 2 in.) in reusable molds. The molds are moved on the 2.4-m-diam (8-ft) circular conveyor, which is a smooth flat steel ring continuously moving in a horizontal plane. When a mold is moved to an operating station, escapement fingers and clamps precisely handle and locate the mold while the necessary production operation is performed.

For the purpose of this detailed description, the mold lubrication station may be regarded as the beginning of th fuel rod fabrication process. There lubricant is injected into the mold, and a rotating brush cleans and lubricates the inside surface. The lubricated mold is then carried to the bottom punch feeder, where a stainless steel spool is inserted into the mold and serves as a base for the formation of the fuel rod. A vibratory feeder and singularizer drops this punch into the top of the mold. A plunger then strokes into the mold to check proper positioning of the punch. If the punch is not properly positioned, the mold can

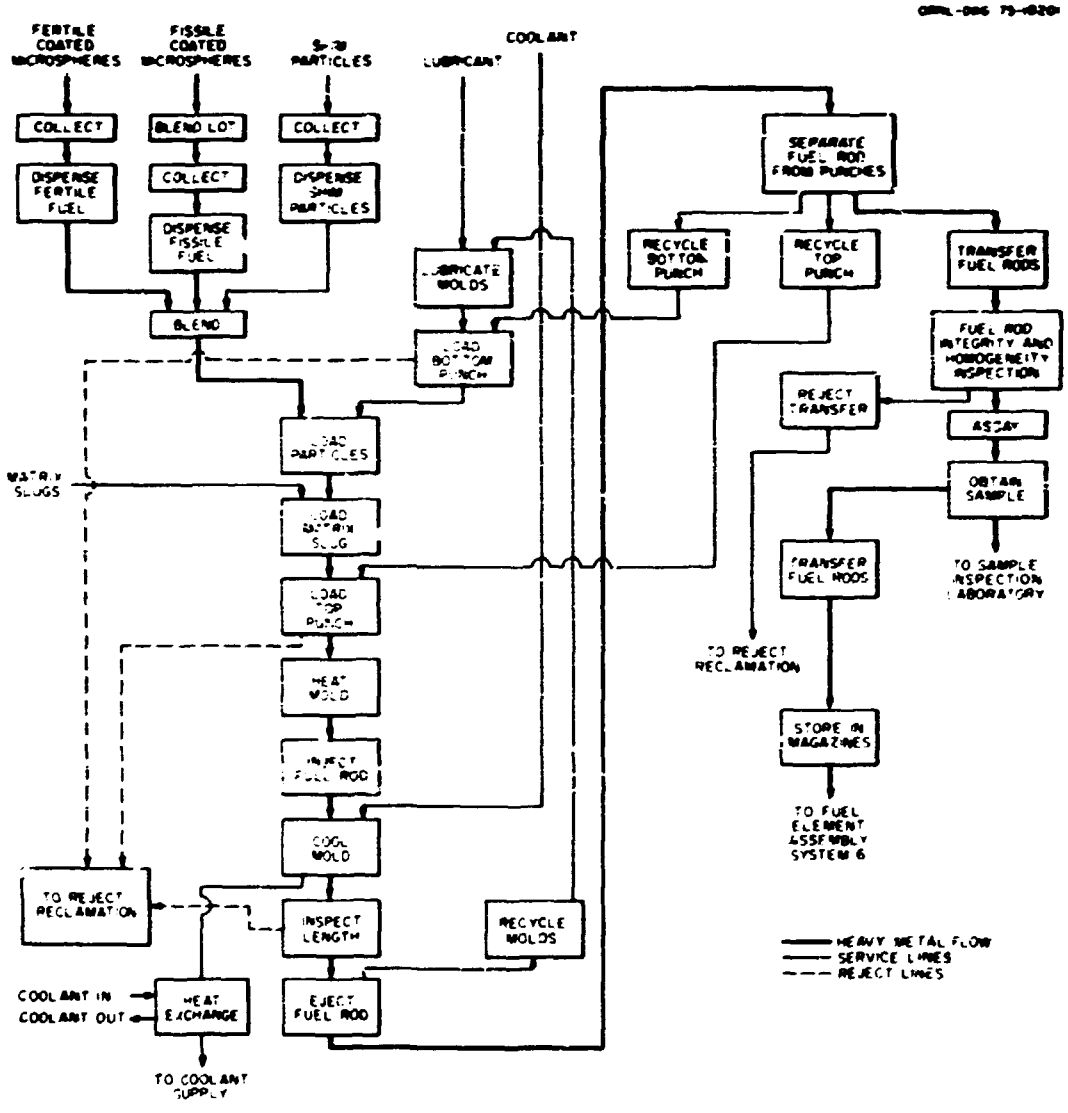

Fig. 4.15. Fuel Rod Fabrication Process Schematic Flowsheet.

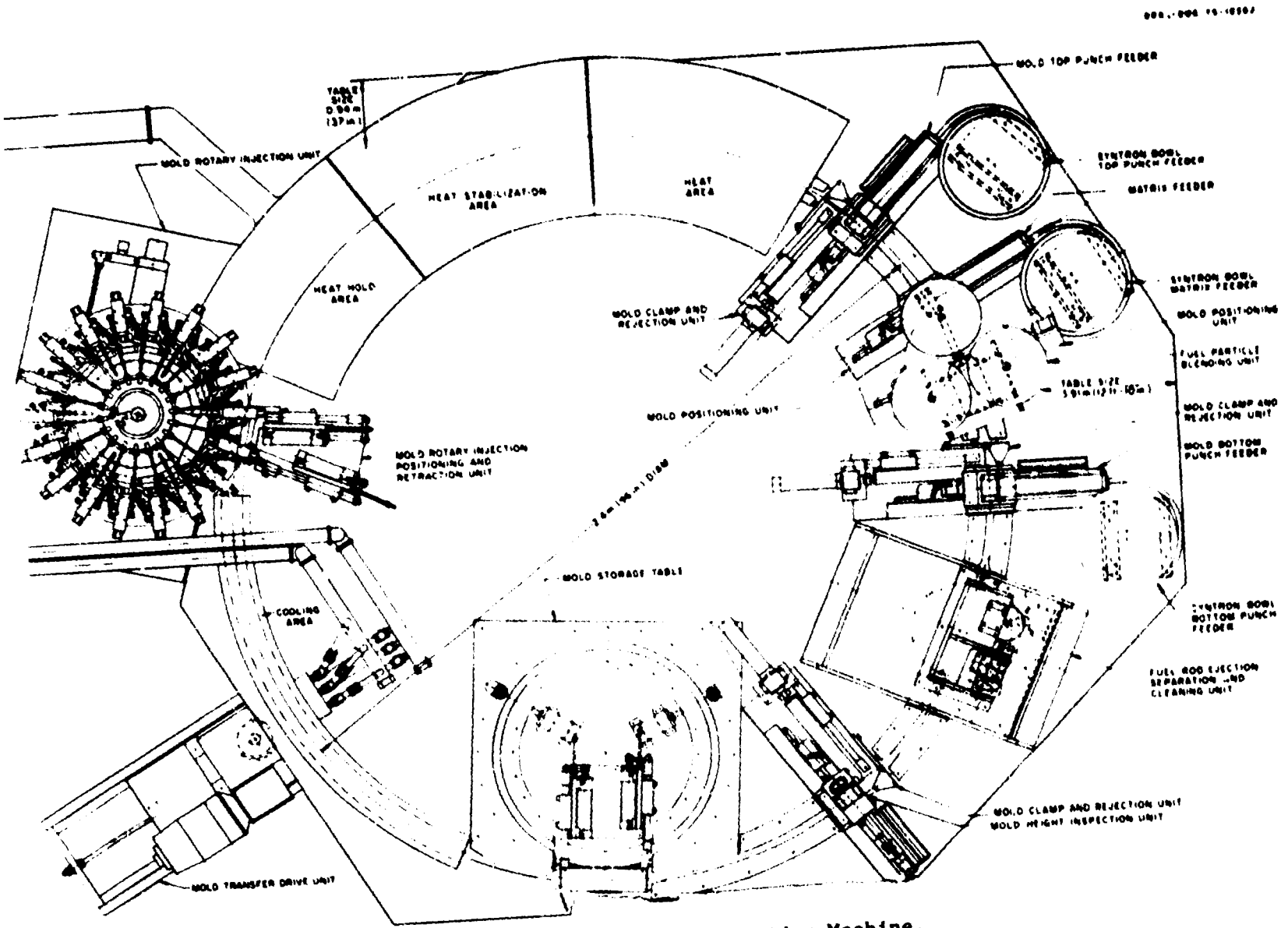

Fig. 4.16. Fuel Rod Fabrication Machine.

be rejected from the transfer table, and subsequent operations at the next mold position would not be performed.

After properly receiving the bottom punch, the mold is carried to the particle dispenser unit, which comprises three hoppers containing fissile, fertile, and shim particles. The desired quantity of each particle is dispensed volumetrically, blended, and dropped through a funnel and a telescoping tube into the mold.

After the particles are loaded into the mold, the mold is carried to the matrix slug feeder, where a matrix slug is positioned on top of the particles in the same manner as the bottom punch was introduced. Matrix slugs are preformed outside the hot cell facility and are transferred by the cell handling equipment into the vibratory feeder bowl as needed. The mold is next carried to the top punch feeder, which is identical to the bottom punch feeder including the rejection unit. The loaded molds next move through a mold heating section, where infrared strip heaters bring the molds up to a temperature of approximately 180°C.

After each mold with its contents has been brought to temperature, it is transferred to the matrix injection press, which is an 18-station unit mounted on a rotary indexer. As the heated molds are being indexed around the injection press platen, a force of up to 1.78 kN (400 lb) is being applied to the top punch by an air cylinder. The rod formation procedure is depicted in Fig. 4.17. Molds having completed the pressing cycle are then moved back to the transfer track and through an insulated tunnel, where refrigerated air is circulated to cool the mold to 30°C or below. After the molds are cooled they move onto a mold storage ring installed on the inside of the mold transfer ring circle.

Before the fuel rods are ejected from the molds, there is a final height inspection unit, which measures the height of the mold contents, and out-of-tolerance units are shifted to a reject basket instead of passing onto the mold ejection rod separator station.

The fuel rod ejection station is mounted on the same rotary indexing device as the mold lubrication station. An air-activated ram ejects the molded rod and the punches through the bottom of the mold into a device that uses cams and plungers to separate the fuel rod from the top and

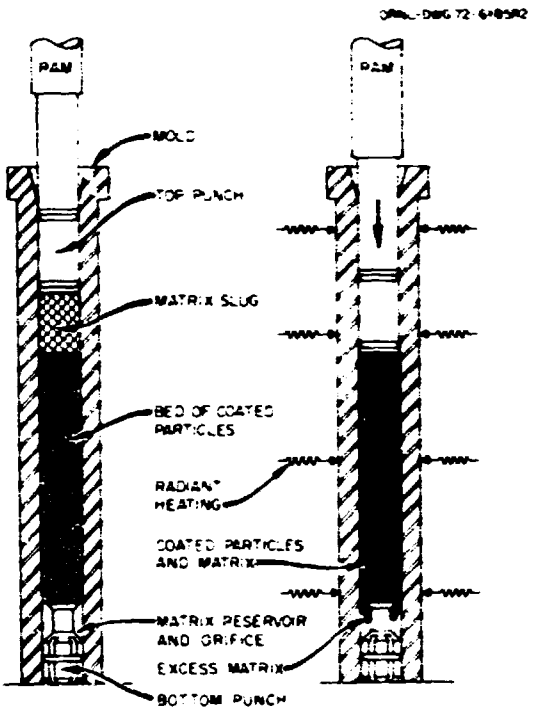

Fig. 4.17. Slug Injection Technique for Making Fuel Rods.

bottom punches. The fuel rod is ejected onto an air-levitated fuel rod transfer track, and the top and bottom punches are dropped into separate baskets for return to the respective parts feeders. On the subsequent index the empty mold is moved to the mold lubrication subsystem for a repetition of fuel rod fabrication process.

Fuel rods are discharged singularly from the fuel rod fabrication machine at a maximum rate of one fuel rod every 8 sec and conveyed through inspection and storage to the fuel element loading machine.

After a fuel rod is released it is inspected with a gamma scanner and with an air ring, which checks for voids and pits on the surface of the fuel rod. There is a reject slide provided after this operation. Acceptable fuel rods will be subject to an assay using a californium source embedded in cylindrical shielding. The rod is then fed into a fuel rod storage and transfer magazine. The loaded magazines are moved with a manipulator to storage racks for accumulation of production before being loaded into the fuel element in System 6.

4.8 SYSTEM 6 — FUEL ELEMENT ASSEMBLY (WORK UNIT 2206) — W. G. Cobb and A. J. Caputo

4.8.1 Summary Description

The fuel element assembly system is designed to perform the various assembly operations and inspections required to complete the production of a fuel element for use in High-Temperature Gas-Cooled Reactors. The system will receive procured fuel block components from the materials handling system (System 10) and formed fuel rods from the fuel rod fabrication system (System 5). The system will load the fuel rods into the graphite fuel blocks, restrain them during an in-block carbonization and annealing process, remove the restraints, clean the block surfaces, install fuel column end plugs and dowels, cure the cement binding them to the block, and load the assemblies into containers for shipment. The system will verify each operation; inspect for dimensional accuracy, integrity, and the presence of contaminants; provide samples for verification of performance; and provide a complete record for each fuel element establishing its usability. The nominal throughput of this system will be 2.5 fuel elements per 24-hr day. The equipment will occupy the south central portion of Cell D and all of Cell E, as shown in Figs. 4.13 and 4.18.

4.8.2 Conceptual Design Detailed Description

A schematic diagram of the functions to be performed is shown in Fig. 4.19. A fuel block container is lowered by a grapple through a roof port and into a rotatable, six-station storage platform in Cell E. The grapple is located in a removable housing, which contains an isolation valve and sealing provision to maintain cell containment. A specialized lift is provided for removing and installing the container covers. A second storage carousel provides storage for 12 dummy blocks and the spacer pallets required for the furnace operation.

An in-cell dedicated hoist uses a specialized grapple to remove a fuel block from its container and transfer it onto a shuttle table of an intercell transfer device. The shuttle table is transferred into Cell D by the action of a motor-driven screw, and is so designed that

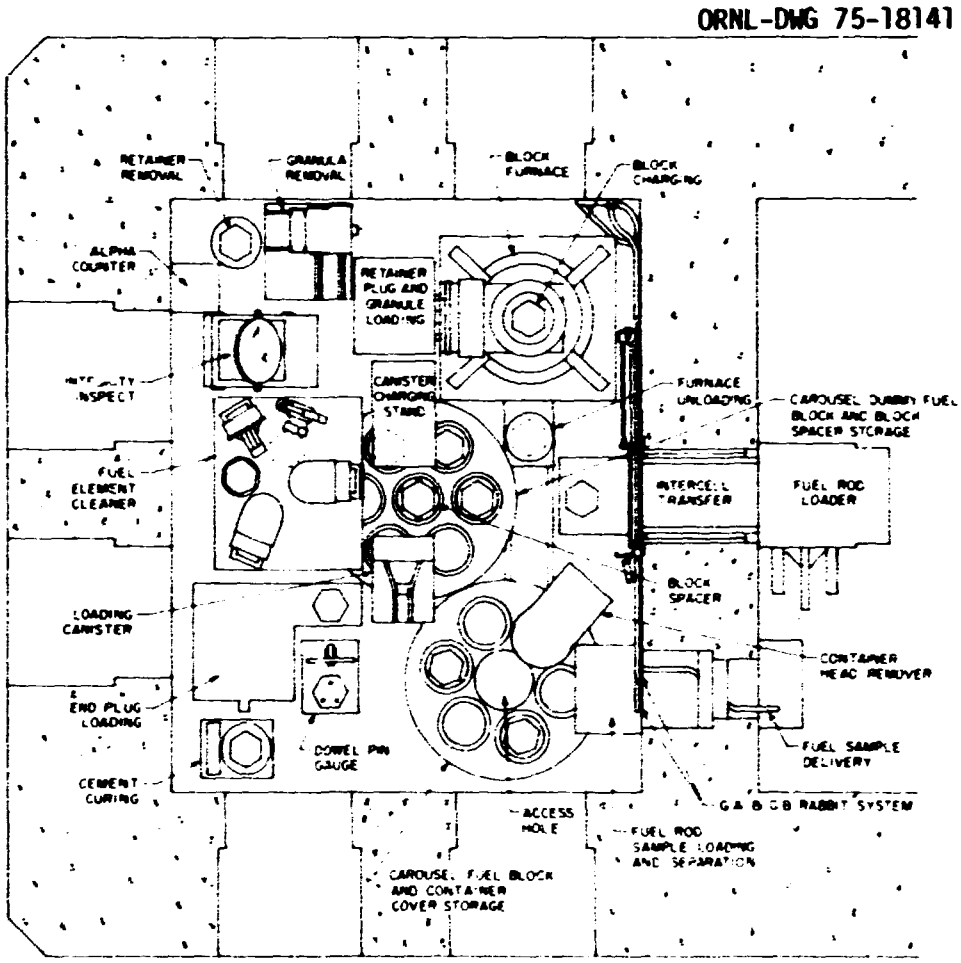

Fig. 4.18. Cell E Equipment Arrangement.

the entire mechanism moves within the Cell wall, permitting a sliding gate valve to isolate the passage from Cell E atmosphere. Another sliding gate valve seals the passageway opening into Cell D, providing for isolation of the two cells. After this gate is opened, a pneumatic cylinder lifts the block from the shuttle table to the loading position under the fuel block loading machine.

Within Cell D a column of fuel rods is discharged from a storage magazine and measured for length acceptability. The rods are then fed singly to the fuel block loading machine. By using programmed coordinates and a final true positioning device, the fuel block loader is sequentially positioned over each fuel cavity. Each fuel rod is

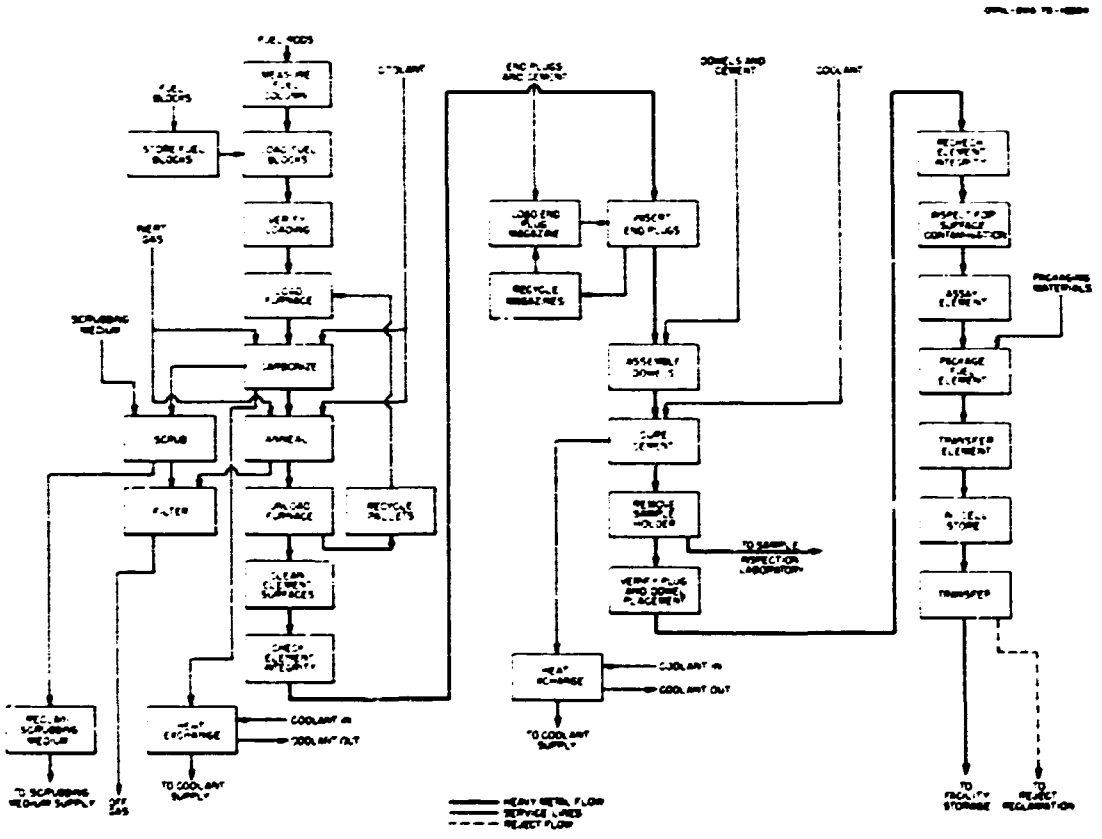

Fig. 4.19. Fuel Element Assembly Process Schematic Flowsheet.

individually loaded, and its position is verified by a depth measuring device. The loaded blocks are returned to Cell E and transported by the hoist to a fuel column restraint loading stand. This equipment finishes filling the fuel cavity with a granular material, which maintains a space for fuel column expansion during fuel burnup. A furnace spacer pallet, positioned on top of the fuel block, fits down around the block sides to restrain the granular material.

The block is then loaded into a portable charging chamber and then lifted to the top of the carbonization and annealing furnace. This furnace is a continuous-throughput vertical-tube controlled-atmosphere type using electrical resistance heaters; it is illustrated in Fig. 4.20. The blocks are charged from the chamber into the furnace through an isolating gate valve and travel vertically downward through a series of heating and cooling zones until discharged through a lower isolation valve. An interceptor fork provides temporary support for the column while the lower chamber is isolated and opened for removal of the processed element by the furnace unloading device. The discharge chamber is then closed, purged, and reopened to the furnace, and the elevator reengages the column of elements. An argon purge sweeps the furnace during processing and is cleaned by a perchloroethylene scrubber system before release to the plant off-gas system. The fuel element is then transported to a vacuum machine, which removes the granular material from the fuel cavities, and then to a cleaning machine, which vacuums and brushes all surfaces of the element.

The block is next positioned for loading an end plug in each fuel cavity. The device is positioned sequentially over each hole, and a feed shuttle loaded with a plug from a supply magazine positions the plug directly over the fuel hole so that a downward stroke of a punch drives the plug into the hole.

The three dowels are screwed into their recesses by means of a manipulator-held low-torque motor. These dowels and the hole plugs when inserted have dry cement molded into a peripheral groove, and this cement is fused and cured by heating the top end of a completed assembly with resistance heaters.

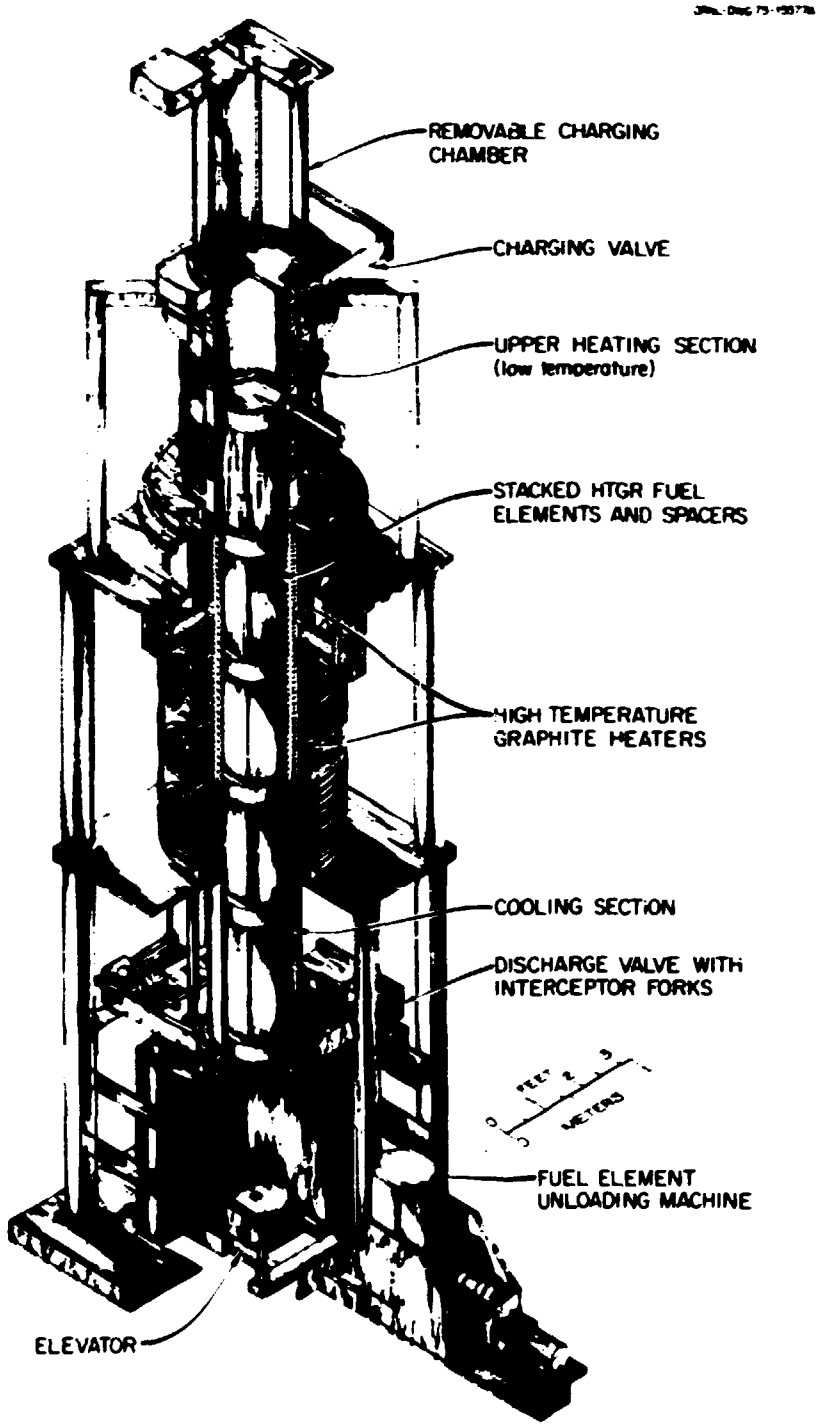

Fig. 4.20. Carbonization and Annealing Furnace.

A transparent rotatable platform mounted in front of a cell window with adjustable mirrors above and below allow visual inspection of all through holes and exposed surfaces. Accuracy of dowel positioning is checked with an overlay inspection plate referencing to the block datums. Dowel heights are checked with a manipulator-hand-held height gage. To monitor contamination of block surfaces with radioactive particulates, prepared swabs maneuvered with a manipulator wipe the surface and are placed into a shielded cavity containing the assay equipment.

4.9 SYSTEM 7 — SAMPLE INSPECTION (WORK UNIT 2207) — D. A. Dyslin and W. H. Pechin

4.9.1 Summary Description

The sample inspection system is designed to receive samples from all stages of processing in the Fuel Refabrication Pilot Plant, determine the various required physical and chemical characteristics, transfer this information to System 8, plant management, return expended or unused sample material to System 9, waste handling, and transfer suitably packaged archive material to storage. The system will perform about 240 inspections per day on 95 samples. The design must provide for the alpha containment and gamma shielding of the material being inspected. The inspection laboratory will be located in a new addition to the south end of TURF.

4.9.2 Conceptual Design Detailed Description

The inspections to be performed are shown schematically in Fig. 4.21. This system is not a straight-line step process but a complex multibranched system. The basic inspection functions are performed by 16 subsystems, which are described below:

Radioassay Subsystem determines the fissile content of fuel rods and particles by exposing them to a ^{252}Cf neutron flux and counting either the prompt neutrons from fission or the delayed neutrons from fission products.

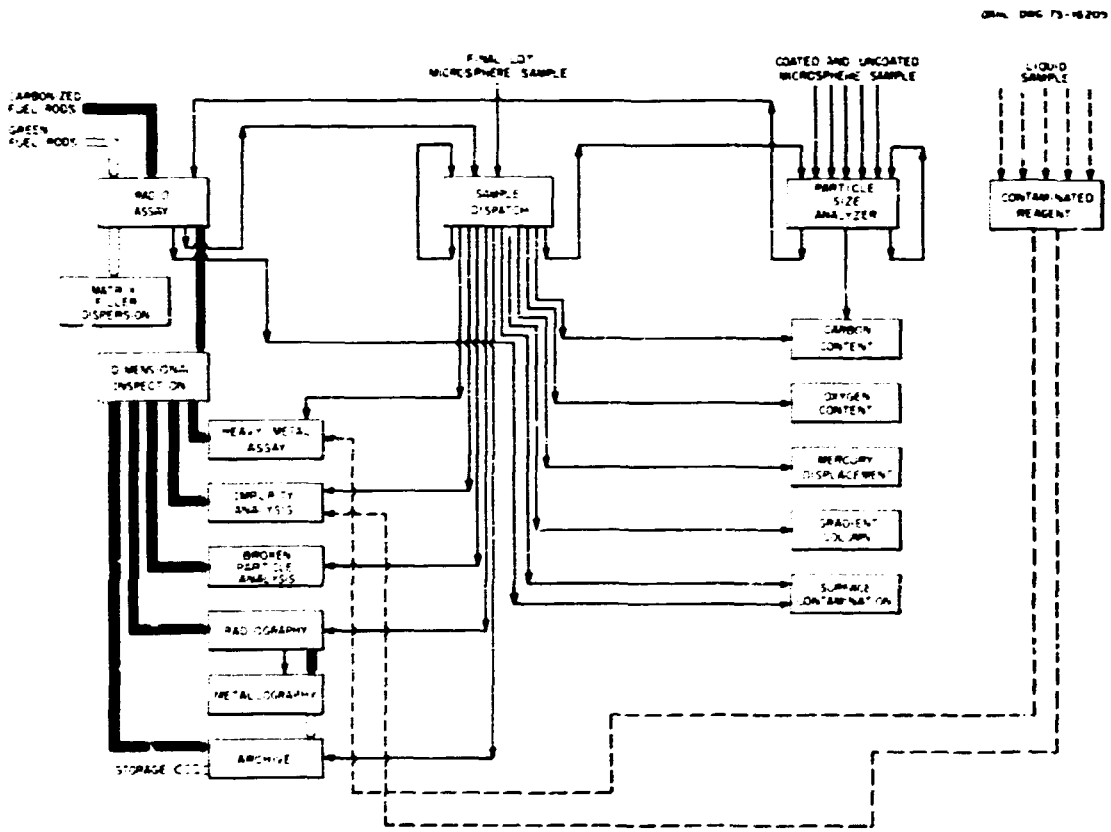

Fig. 4.21. Sample Inspection Process Schematic Flowsheet.

Particle Size Subsystem determines the mean and standard deviation of diameter and the mean particle weight of a particle sample by using a calibrated photocell, counter, and scale.

Contaminated Reagent Subsystem receives all liquid samples from in-cell, performs those analyses required on contaminated liquid samples except for heavy metal assay, and transfers the liquid samples to the heavy metal assay subsystem as required.

Noncontaminated Reagent Subsystem determines the physical and chemical properties of noncontaminated reagents for operation of the Resin Loading System.

Surface Contamination Subsystem determines the level of alpha activity on the surface of the outer low-temperature isotropic coating by counting a known weight of fuel particles in a gas-flow proportional alpha counter.

Matrix Filler Dispersion Subsystem determines the amount and distribution of filler in the rod matrix by dividing a rod into three segments and removing and weighing the pitch to determine the amount in each segment.

Gradient Column Density Subsystem determines the densities of the LTI pyrocarbon and silicon carbide coatings by determining the rest position of coating fragments placed in a fluid column having a linear gradient of known fluid density.

Carbon Content Subsystem determines the carbon content and carbon-to-uranium ratio of particles by burning the carbon from a sample in a controlled argon-oxygen atmosphere, collecting the CO_2 in absorption columns, and measuring the column weight change.

Mercury Displacement, Density, and Porosity Subsystem determines particle density and coating porosity by utilizing a commercially available porosimeter adapted to glove box operation.

Radiography Subsystem produces radiographs of coated particles to determine size distribution, coating thickness, and shape of fuel rods to determine relative distribution of fissile, fertile, and shim particles.

Broken Particle Subsystem determines the fraction of microspheres having broken coatings in particles and fuel rods by chlorinating a sample at 1500°C to convert exposed heavy metal to the chloride, which is collected in a condenser. The condenser is washed with hydrochloric acid, and the resulting solution is analyzed for uranium and thorium.

Dimensional Subsystem determines the dimensions and weight of fired fuel rods to ascertain the coking yield of the matrix material utilizing a modified commercial air gage and a balance.

Metallography Subsystem allows visual micro and macro examination of polished sections of microspheres and fired fuel rods. Quantitative measurements will also be made of the anisotropy of coatings and the amount and size of porosity in the fuel rod matrix. The subsystem uses modified commercially available metallographic equipment. Anisotropy will be determined by measuring the angular dependence of reflectivity of plane-polarized light. The size and spatial distribution of the matrix porosity will be measured by a commercially available image analyzer.

Heavy Metal Assay Subsystem determines the heavy metal content of liquid, particle, and fired fuel rod samples. Particle and rod samples must first be crushed and ignited in oxygen, and the residue leached with acid to dissolve the heavy metal. The resulting solution is analyzed for uranium and thorium.

Impurity Subsystem prepares a sample that will be transferred out of the sample inspection system laboratory for impurity analysis by spark source mass spectrometry.

Oxygen Content Subsystem determines the oxygen content of converted fuel kernels by reacting the sample with carbon at 2000°C in argon to convert the oxygen in the sample to CO. The CO is converted to CO_2 with hot copper oxide and absorbed on Ascarite. The oxygen is determined by measuring the weight change of absorption towers located in the furnace off-gas train.

4.10 SYSTEM 8 — PLANT MANAGEMENT (WORK UNIT 2208) — B. C. Duggins and R. A. Bradley

4.10.1 Summary Description

The plant management system, System 8, is an information handling system, which is designed to assist in the operation and evaluation of the fuel refabrication processes by:

1. collecting and storing information that will be required for quality assurance documentation of refabricated fuel,
2. performing calculations that will be required in the operation of the process systems,
3. collecting and storing information that will be required for the evaluation of the plant performance, and
4. maintaining a running inventory of fissile material for criticality safety and special nuclear material accountability.

In addition, the plant management system will serve as the interface for information flow between the various process systems and support systems such as sample inspection. This system also provides basic support functions to the operation of the local instrument and control subsystems of the process systems.

4.10.2 Conceptual Design Detailed Description

The plant management system is basically an automated information management system to be configured from minicomputer class equipment. A 16-bit minicomputer with line printer, magnetic tape and disk bulk storage devices, and other peripherals will be used.

Figure 4.22 shows the information flow between this system and process systems. Details concerning data type, acquisition rates, and quantities are available in the System Design Description. The software structure is shown in Fig. 4.23. Data bases will be maintained for process variables, process support data, and fissile inventory. Quality assurance documentation will be generated from the process support data base.

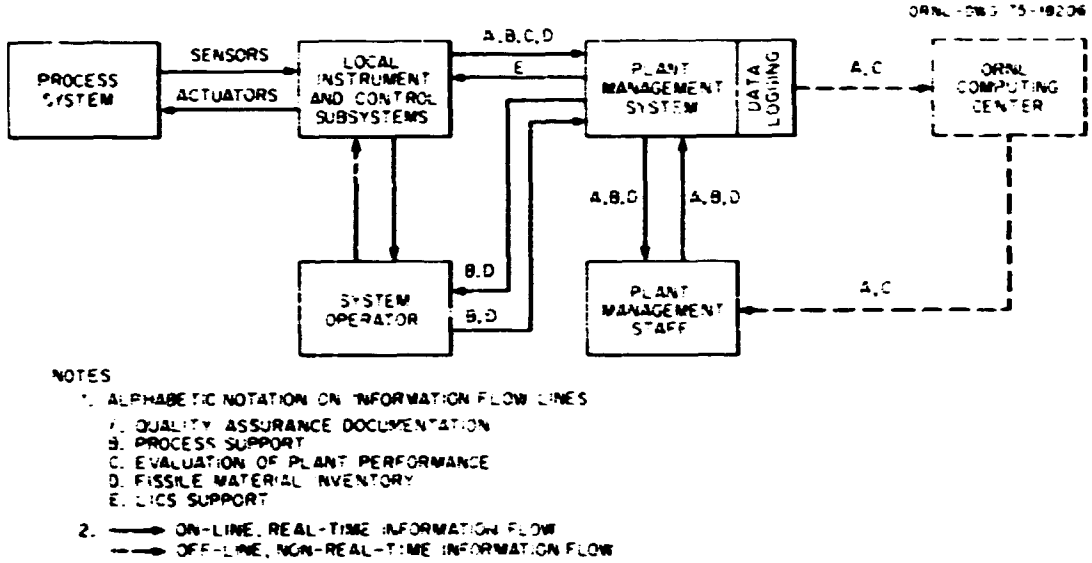

Fig. 4.22. Diagram of Information Flow Between Plant Management System and the Process Systems.

4.11 SYSTEM 9 — WASTE HANDLING (WORK UNIT 2209) — J. P. Jarvis and A. R. Olsen

4.11.1 Summary Description

This system will be designed to provide for the handling of waste materials from the processes located in Building 7930 (TURF). The materials to be handled include the following: (1) solid reject or scrap material with significant fissile or fertile element content suitable for reclamation, (2) solid material with low fissile material content [less than 0.35 kg/m^3 (10 g/ft^3) ^{233}U] to be sent to a retrievable storage facility, (3) liquids containing uranium suitable for immediate recycle within the refabrication process systems, (4) liquid wastes with low levels of fissile and fertile material appropriate for transfer to the appropriate ORNL contaminated liquid process system, (5) organic liquid wastes that must be treated and stored, and (6) gaseous wastes from processing operations and containment areas. The equipment will be located throughout the building.

ORNL-DWG 75-4072

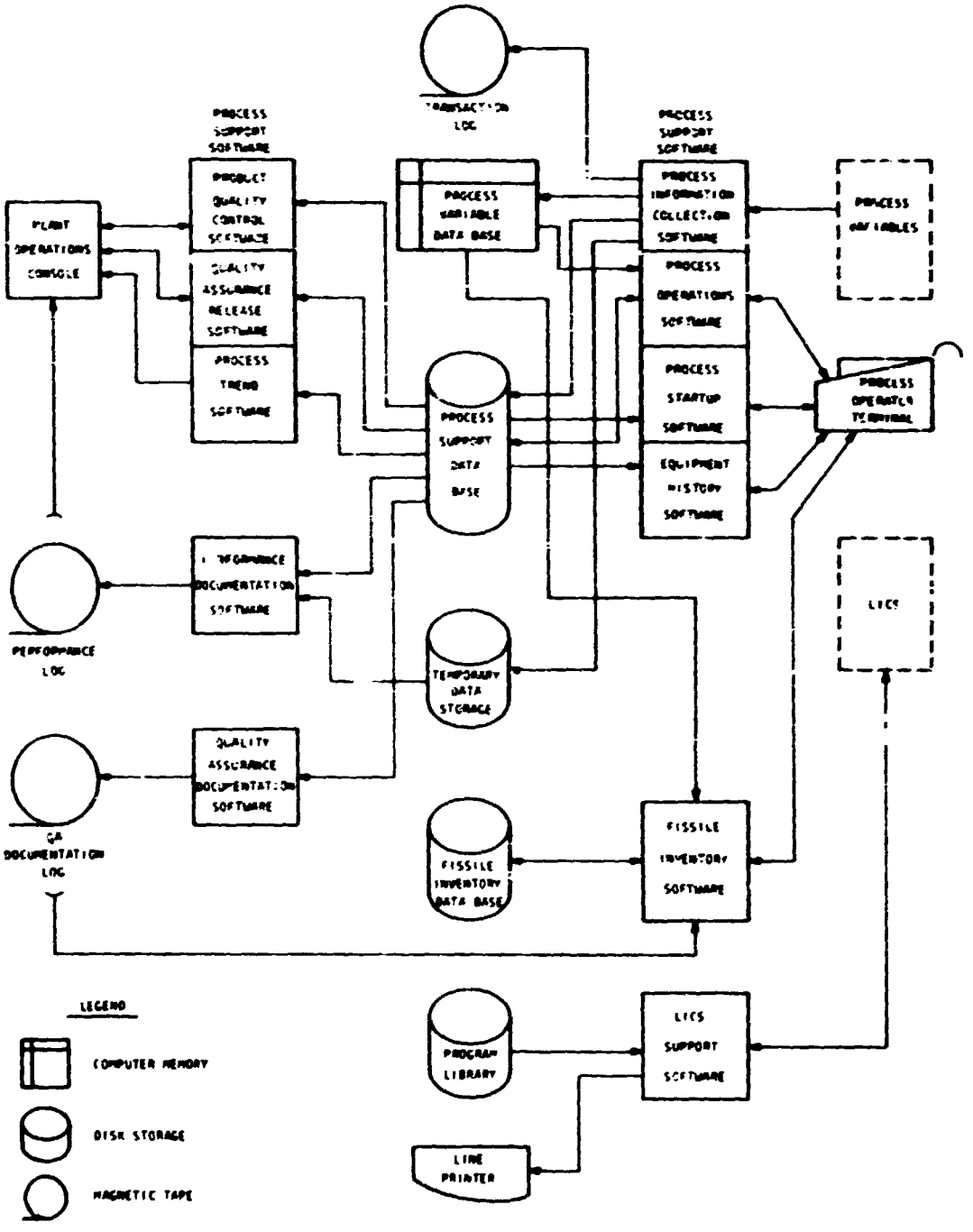

Fig. 4.23. Process and Plant Support Software Block Diagram.

4.11.2 Conceptual Design Detailed Description

Provisions are made for collecting, monitoring, assaying, packaging, moving, and storing or disposing of the materials described in the paragraphs that follow.

Liquid Aqueous Radioactive Waste — The existing radioactive hot drain and hot off-gas (RHD-HOG) will be used to collect liquid and/or gaseous waste from equipment that does not contain fissile material. This system has been described.[1] Connections are provided in the process cells for collection and transfer of wastes to stainless steel tanks that are filled with borated glass Raschig rings. Equipment is provided for sampling the contents of the tanks and for addition of depleted uranium or other chemicals if required. Disposal is to the ORNL waste collection and treatment system.

Aqueous solutions containing recoverable quantities of fissile material should be generated only by System 2 operations. Provisions for collection, analysis, and transfer of this material back to System 1 in Building 3019 will be part of System 2.

Waste from other equipment containing fissile material is collected in the radioactive hot drain recoverable (RHDR) system. Piping for this system is sized to protect against accumulation of a critical mass of fissionable material, and the storage tank is filled with borated Raschig rings. Estimated average quantities of aqueous liquid waste generated are listed in Table 4.2.

Liquid Organic Radioactive Waste — As indicated in Table 4.3, only small quantities of contaminated organic wastes will be generated. These will be absorbed on suitable materials to convert them to low-level solid wastes for disposal.

Solvent used in off-gas scrubbers for Systems 3, 4, and 6 will be recovered in System 9 for reuse. Tetrachloroethylene containing suspended solids (mostly carbon soot) and dissolved light oils and tars will be distilled, with the clean solvent being returned to the process systems and the solids being collected in the still pot for removal and transfer to the solid waste handling system.

Table 4.2. Estimated Average Quantities of Aqueous Liquid Waste Generated by the HTGR-FRPP

Source	Material Composition	Quantity (liters/day)
Uranium feed preparation and resin loading, Systems 1 and 2	Evaporatory condensate	50
	Caustic carbonate from solvent regeneration	35
Microsphere coating, System 4	Spent caustic from HCl scrubbers (NaOH + NaCl)	500
Miscellaneous	Decontamination solution: water, Turco, acids, etc.	190
Floor drains, service sinks, etc.; process waste system	Water (negligible radioactivity)	380

Table 4.3. Estimated Average Quantities of Organic Liquid Waste Generated by HTGR-FRPP

Source	Material Composition	Average Quantity Generated[a] (liters/day)
Resin fuel kernel preparation, System 2	0.2 *M* Amberlite LA-2 in diethylbenzene	3
Resin carbonization, System 3	Organic scrubbing media plus condensable hydrocarbons	<4
Microsphere coating, System 4	Organic scrubbing media plus condensable hydrocarbons	<4
Fuel element assembly, System 6	Organic scrubbing media plus condensable hydrocarbons	<2
Cleaning and decontamination of equipment in cell A	Solvents to clean bearings, etc.	<1

[a]Radioactivity negligible.

Low-Level Solid Radioactive Wastes — Both combustible and noncombustible wastes will be packaged in 115-liter (30-gal or 4 ft^3) drums in Cells C, D, and E or at the point of origin, such as the sample inspection system. A ^{233}U assay system is to scan waste drums positioned on a rotating table with sodium iodide detectors. A standard containing ^{233}U from the fuel batch being processed is compared with the waste sample being assayed. A gamma ray absorption comparison is made for each waste drum with a source of the 2.6-MeV gamma rays being counted by the assay apparatus. These drums will be assayed and packaged in 55-gal (208-liter) drums, for shipment to the ORNL retrievable storage facility, in an out-of-cell packaging station. The estimated quantity of such waste generated per day is shown in Table 4.4. The maximum radiation level of this material per cubic foot (0.028 m^3) is estimated from a maximum of 0.35 kg/m^3 (10 g/ft^3) of ^{233}U containing 500 ppm ^{232}U. This estimate for material aged various times is: 90 days, 3.75 mrem/hr; 2 years, 24.0 mrem/hr; and 10 years, 42.5 mrem/hr.

Table 4.4. Estimated Average Quantites of Low-Level Contaminated Solid Waste Generated by the HTGR-FRPP

Material Description	Quantity	
	(m^3/day)	(ft^3/day)
Irreparable in-cell process equipment and components	0.028	1.0
Manipulator boots	0.028	1.0
Miscellaneous tools, plastic bottles, seals, gloves, in-cell filters, plastic sheet, etc.	0.17	6.0
Coating chambers, fritted plates	0.085	3.0
Soot from solvent reclamation system	0.017	0.6
Excess matrix	0.007	0.25
Total	0.34	11.85

High-Level Solid Wastes — The estimated production of solid wastes having high uranium content is given in Table 4.5. These materials will be packaged in critically safe containers for transfer to a retrievable storage site or to a reclamation process. Reject fissile material cans are about 90 mm diam by 230 mm long (3 1/2 by 9 in.). They are designed to receive up to 1 kg ^{233}U containing 500 ppm ^{232}U aged 90 days after removal of decay products. The estimated radiation level for material aged various times is: 90 days, 750 mrem/hr; 2 years, 4.8 rem/hr, and 10 years, 10.1 rem/hr. A combination calorimeter-gamma scan device will be used for assay of these cans.

Gaseous Wastes — The source, composition, and estimated volumes of off-gases that will be generated are given in Table 4.6. The combustible gases generated in Systems 3, 4, and 6 will be pretreated in the respective systems for removal of radioactive and particulate components before they are delivered to System 9. These gases are monitored for radioactivity and oxygen content and exhausted through local stacks on the TURF roof. The Hot Off-Gas system, which receives vessel off-gases and the cell containment system, has been described.[1] Gaseous alpha-contaminated waste from the sample inspection glove box line (System 7) is filtered; monitored for radioactivity, pressure, and flow; and discharged either from a separate stack or from the existing cell off-gas system.

4.12 SYSTEM 10 — MATERIALS HANDLING (WORK UNIT 2210) — J. P. Jarvis and A. R. Olsen

4.12.1 Summary Description

The Materials Handling System will be designed to provide the equipment and facilities required to receive, handle, store, and ship materials required for or resulting from operation of the fuel refabrication processes. This function will be limited to activities outside the process cells. Materials will be delivered to or removed from shield penetrations, which are provided as part of other plant systems.

Table 4.5. Estimated Average Daily Production of High-Uranium-Content Solid Waste Material

Material Form	Quantity ($g^{233}U$/day)	Source
Loaded and dried resin	247	Resin loading reject and samples
Carbonized resin[a]	161	Resin carbonization reject and samples
Converted resin[a]	[illegible]	Resin conversion rejects and samples
Coated particles	530	Particle coating reject and samples
Green rods	13	Reject rods, samples, and assay calibration standards
Carbonized rods	11	QA samples
Reject blocks[a]	12	Reject blocks
Coated particles and carbon	18	Coating chamber scrapings and frits
Epoxy-impregnated rods	0.15	Metallographic mounts
U_3O_8 ash	3	Sample inspection station

[a]Routine production of this type of waste is not anticipated. Figures represent daily average, but in fact an infrequent large batch will have to be dealt with.

Table 4.6. Estimated Maximum Gaseous Radioactive Waste from the HTGR Refabrication Pilot Plant

Source	Composition	Flow (scfm)	Flow (std m^3/sec)	Destination
Cell exhaust	Air	9500	4.5	HFIR stack
Miscellaneous off-gas from vessel purge and pneumatic transfer operations	Air, Ar, etc. with particulate alpha activity	600	0.28	HFIR stack
Coating carbonization and annealing furnace	Ar, He, combustible gases	80 total 20 each	0.038 0.0095	Local stack Local stack
Sample inspection system gloveboxes and hoods	Air Ar, etc. with particulate alpha activity	90 normal 560 max	0.043 0.26	Either stack Either stack

4.12.2 Conceptual Design Detailed Description

Facilities are provided for handling and storage of product fuel elements, archive samples, and high-level solid waste cans in the existing TURF fuel storage basin.

Materials Required for Refabrication of Recycle Fuel Elements — The necessary materials for recycle element refabrication are listed in Table 4.7. These items plus the required process support chemicals and materials are received and stored in TURF. Uranyl nitrate feed is transported from Building 3019 to TURF via a special shipping carrier and trailer.

Product Fuel Elements — Completed fuel elements are removed from Cell E through the roof port into a container and transfer shield for transfer to the TURF fuel storage basin for interim storage.

Solid Waste Materials — Canned waste materials are withdrawn from the process cells into shielded carriers for transfer to interim storage.

Samples — This system provides shielded carriers for delivery of radioactive samples to hot cell facilities outside the TURF and archive samples from System 7 to the fuel storage basin.

Table 4.7. Materials for Refabrication of Fuel Elements

Material or Equipment	Quantity for 24-hr Run	Type Storage Area in TURF
Uranyl nitrate solution, kg U	4	Alpha contained and shielded
Coated thorium particles, kg	15	Alpha contained
Empty graphite blocks	3	General
Graphite plugs	675	General
Graphite dowels	9	General
Poison rods	6.18	General
Graphite cement, liter (pt)	0.47 (1)	General
Fuel packaging material, m^3 (ft^3)	0.28 (10)	General
Shim particles (graphite), kg	15	General
Matrix slugs 13 mm diam by 25 mm (1/2 by 1 in.)	10,000	General

4.13 REFFRENCES

1. J. W. Anderson, S. E. Bolt, and J. M. Chandler, *Safety Analysis for the Thorium-Uranium Recycle Facility*, ORNL-4278 (May 1969).
2. R. W. Horton (comp.), *Safety Analysis: HTGR Support Program in Building 3019 Pilot Plant*, ORNL-TM-3567 (March 1972).
3. R. W. Horton (comp.), *Criticality Analysis: HTGR Assistance Program in Building 3019*, ORNL-TM-3469 (March 1972).

5. RECYCLE FUEL IRRADIATIONS (SUBTASK 230)

F. J. Homan

5.1 INTRODUCTION — F. J. Homan

During the present reporting period the entire Thorium Utilization (ThU) Program was reorganized, and the recycle fuel irradiations work was designated Subtask 230. Subtask 230 was organized into five work units:

Work Unit 2300: fuel performance assessment,

Work Unit 2301: capsule irradiations,

Work Unit 2302: Peach Bottom irradiations,

Work Unit 2303: large-scale recycle element (LSRE) irradiations,

Work Unit 2304: refabricated fuel recycle element (RFRE) irradiations.

The work on recycle fuel irradiations has always been part of the National Fuel Development Program Plan for the Steam Cycle HTGR. At the end of the reporting period this program plan was reorganized around four goals:

Goal 1: qualify initial and makeup (I.M.) fuel and processes for the large HTGR,

Goal 2: qualify reference recycle fuel and manufacturing processes for the large HTGR,

Goal 3: qualify backup to developmental reference I.M. and recycle fuel,

Goal 4: development of essential technical support.

Coincident with the reorganization of the National HTGR Fuel Development Program was a reorganization within ERDA. The Thorium Utilization Program was moved from the Division of Reactor Research and Development to a newly created Division of Nuclear Fuel Cycle and Production. For the National HTGR Fuel Development Program this meant that the funding for program activities was coming from two separate divisions of ERDA — RRD and NFCP. It has always been recognized that there are many parallel activities involved in the development of fresh and recycle fuel, and in fact the same personnel and irradiation facilities at ORNL are used in both programs. It was therefore logical to move money from the ThU Program to the HTGR Base Program so that all the money for HTGR fuel development would be in one program, and in one ERDA division. This was accomplished, in part, in June 1975.

While these changes were made at the end of the reporting period, it has been decided to structure this report around the new funding arrangement — both to establish a sound framework for future reporting, and to provide continuity for the fuels work reported in this annual report. Accordingly, all work done in support of the four goals previously listed for the HTGR fuel development program is reported elsewhere,[1] including work supported by both the Base Program and the ThU Program.

The work formerly associated with the five work units listed for Subtask 230 of the ThU Program has been incorporated under goals 2, 3, and 4 of the National HTGR Fuel Development Program. Some work is still funded from the ThU Program, under work units 2302 and 2303 of Subtask 230. In addition, there is some jointly funded work (HTGR Base Program and Subtask 210 of the ThU) on kernel carbonization and conversion, SiC and pyrocarbon characterization, and process latitude investigations. This work is reported in Chap. 3 of this report.

5.2 PEACH BOTTOM IRRADIATIONS (WORK UNIT 2302)

Seven Recycle Test Elements (RTE) have been irradiated in the Peach Bottom Reactor. Three were removed and partially examined previously.[2,3] The Peach Bottom Reactor was shut down in October 1974, terminating irradiation on the four remaining RTEs at about half of peak large HTGR exposure. Progress on the postirradiation examination of the RTEs is reported below. This work is scheduled for completion during FY 1976, with a final report on the RTEs to be issued in September 1977.

5.2.1 Postirradiation Examination of RTE-7 — E. L. Long, Jr.

The operating history and results from the earlier examinations of RTE-7 have been reported.[3] Two fuel rods had not been examined metallographically until this reporting period because we did not have the capability required to polish irradiated ThC_2. The fuel rods examined in this reporting period were RTE-7-3-3-3 and RTE-7-5-5-5, which contained $(2Th,U)O_2$ Biso with ThC_2 Biso and UC_2 Triso with ThC_2 Biso fuel mixtures, respectively. The fuel rod that contained mixed oxide operated at a

design center-line temperature of 1215°C, and the rod that contained UC_2 operated at 1120°C. This element had accumulated 252 equivalent full-power days of exposure, and the average element burnup was predicted by GAC to be 2.4% FIMA. A peak neutron fluence of about 1×10^{22} n/cm^2 (>0.18 MeV) was achieved.

Metallographic examination of a transverse section through the fuel rod that contained the Biso-coated $(2Th,U)O_2$ and ThC_2 kernels revealed no unusual microstructural features. There was no evidence of failure or potential failure of either the fissile or fertile particles, nor was there any measurable amount of amoeba effect. A typical fissile particle from this rod is shown in Fig. 5.1.

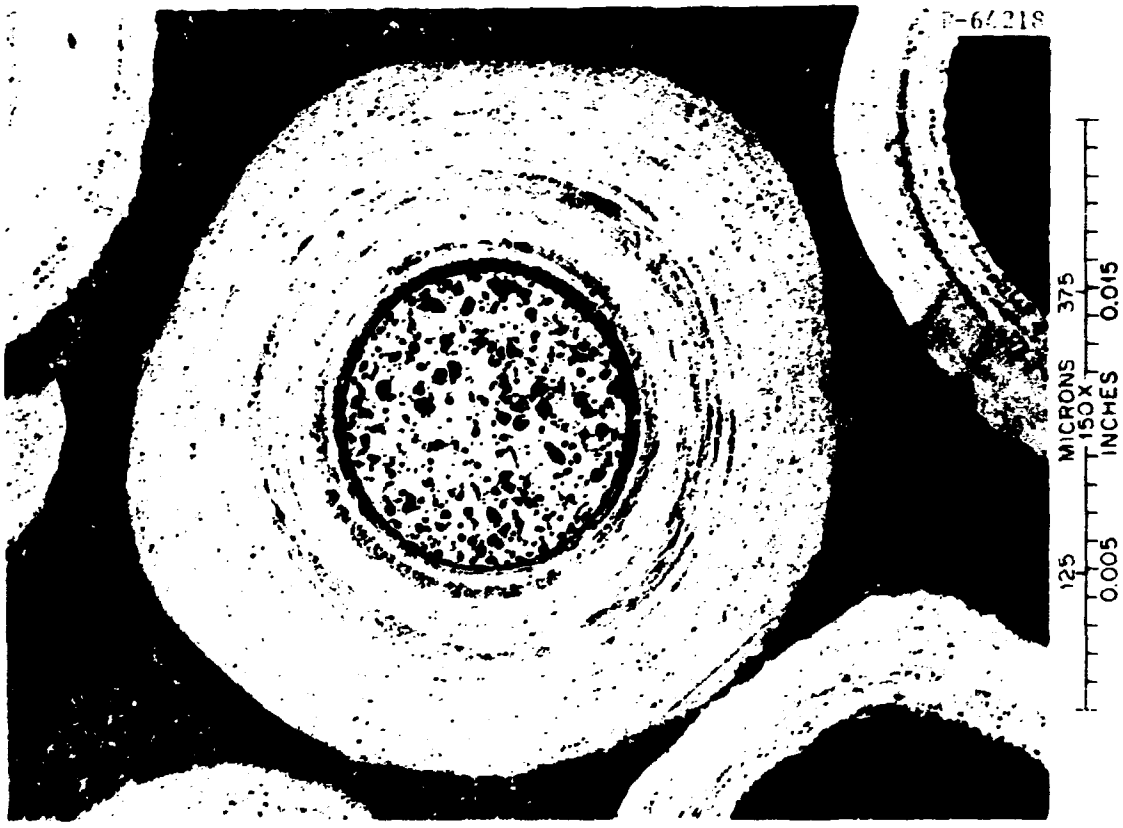

Fig. 5.1. Typical Biso-Coated $(2Th,U)O_2$ Fissile Particle from RTE-7-3-3-3.

Examination of a transverse section through the fuel rod that contained the Triso-coated UC_2 and Biso-coated ThC_2 kernels (PTE-7-5-5-5) revealed no evidence of amoeba effect in either the fissile or fertile particles. We noted one fissile particle that had failed and had the appearance of a pressure-vessel-type failure [Fig. 5.2(a)]; 325 fissile particles were exposed in this plane of polish. Although this one failed particle represents a failure fraction of only 0.3%, an upper limit of 1.7% failed particles is indicated at a 95% confidence interval. Examination of the Triso coatings at high magnification revealed that a slight reaction had occurred at the interface between the inner LTI and SiC on the cold side of the fissile particles. This reaction formed graphite flakes that extended from the inner surface of the SiC into the inner LTI for about 3 μm. This reaction also resulted in slight attack on the inner surface of the SiC layer to a depth of 1 to 2 μm. The appearance of this reaction on the cold side of the particles suggests that the rare-earth fission products are responsible. A typical fissile particle is shown in Fig. 5.2(b), and the appearance of the graphitized region adjacent to the SiC is shown in Fig. 5.3.

5.2.2 Postirradiation Examination of Fuel Rods from RTE-4 — E. L. Long, Jr.

The results from the physical examination of the fuel rods from RTE-4 that had been in the Peach Bottom Reactor for 384 equivalent full-power days have been reported previously.[2] The metallographic examination was delayed until we had the capability to polish carbide fuels. The mechanical polishers have been installed in the hot cells, and the polishing techniques have been refined to enable us to adequately prepare Triso and Biso systems for metallographic evaluation.

The fuel loading combinations and forms for RTE-4 are shown in Table 5.1. The fuel examined from body 1 operated at an estimated maximum end-of-life temperature of 760°C and contained Biso-coated dense UC_2 fissile particles and Biso-coated ThC_2 fertile particles. Examination of a transverse section revealed no particles that failed as a result of the irradiation test; however, two of the Biso coatings had been

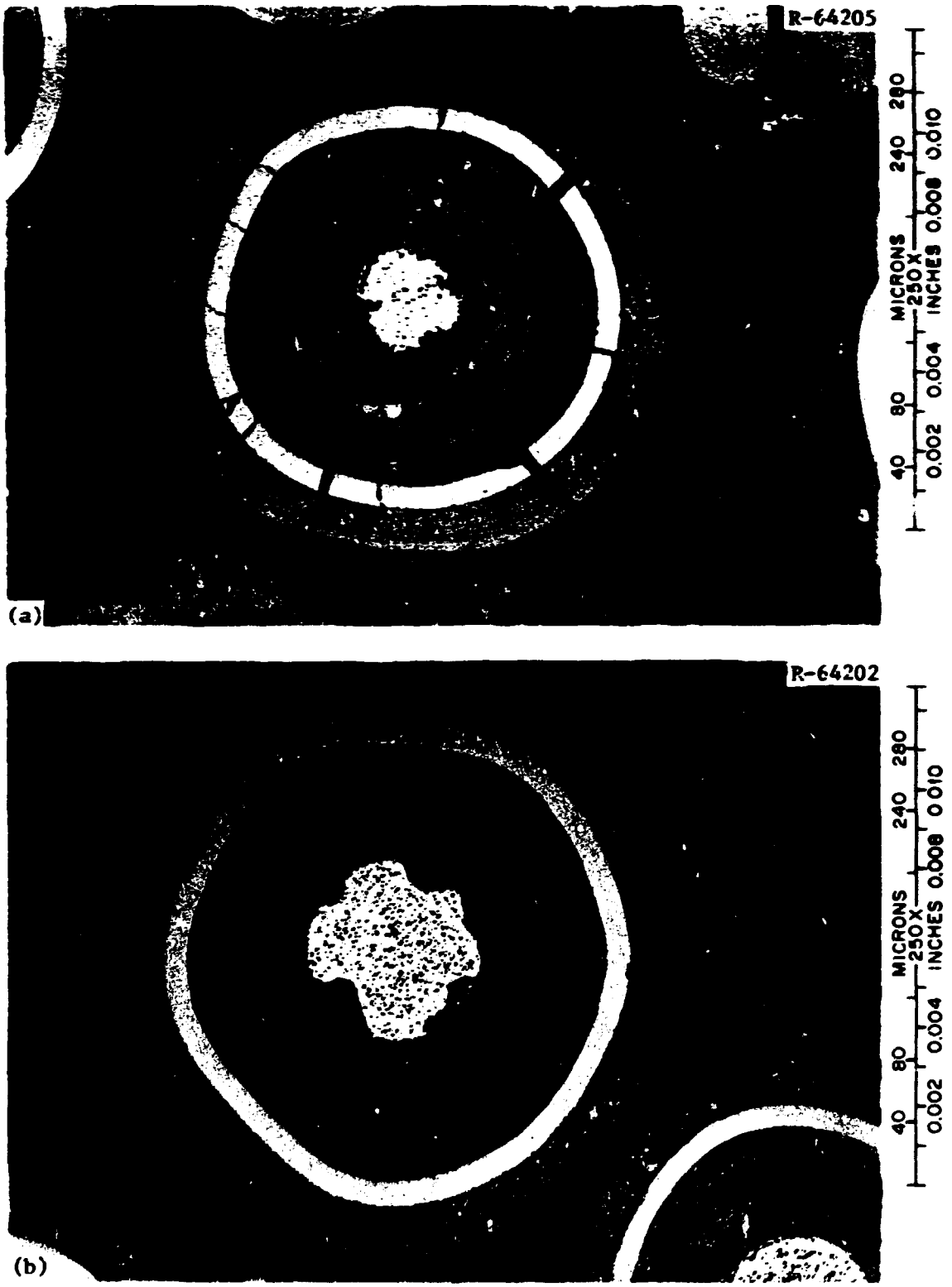

Fig. 5.2. Triso-Coated UC_2 Fissile Particles from RTE-7-5-5-5. (a) Pressure vessel failure. (b) Typical particle.

Fig. 5.3. Localized Graphitization of Regions (Arrows) of the Pyrocarbon Coating Adjacent to Inner Surface of SiC Layer on the Cold Side of the Particle. Polarized light.

Table 5.1. Fuel Loading Scheme for RTE-4

Body	Fuel Type	Fuel Form	Fuel Particle Type	
			Fissile	Fertile
6	e	Blended[a] bed	UC_2 Biso	ThC_2 Biso
5	d	Rods[b]	$(2Th,U)O_2$ Biso	ThC_2 Biso
4	f	Rods[c]	UC_2 Triso	ThC_2 Biso
3	a	Blended[a] bed	$(4.2Th,U)O_2$ Biso	ThC_2 Biso
2	f	Blended[a] bed	UC_2 Triso	ThC_2 Biso
1	e	Rods[c]	UC_2 Biso	ThC_2 Biso

[a] Blended beds contain graphite powder as a bed stabilizer to prevent segregation.

[b] Carbonized in covered graphite tray.

[c] Carbonized in fuel body.

broken during fabrication. There was no evidence of amoeba effect with either the UC_2 or ThC_2 kernels. Although none of the coatings showed indications of potential failure, the coatings on the UC_2 kernels contained sooty regions that delineated layers in the PyC. Also, in numerous particles the outermost layers contained cracks that propagated into the coatings for 20 to 30 μm. Typical fissile particles from this fuel rod are shown in Fig. 5.4.

Fig. 5.4. Typical Biso-Coated UC_2 Fissile Particles from Fuel Rod RTE-4-1-1-3.

A fuel system of Triso-coated dense UC_2 and Biso-coated ThC_2 was included in this element for comparison. We selected from body 4 a fuel rod that had a maximum end-of-life fuel temperature estimated to be 1100°C. Examination of a transverse section through this fuel rod revealed no evidence of amoeba in either the UC_2 or ThC_2. A typical fissile particle is shown in Fig. 5.5. Examination of 526 Triso-coated

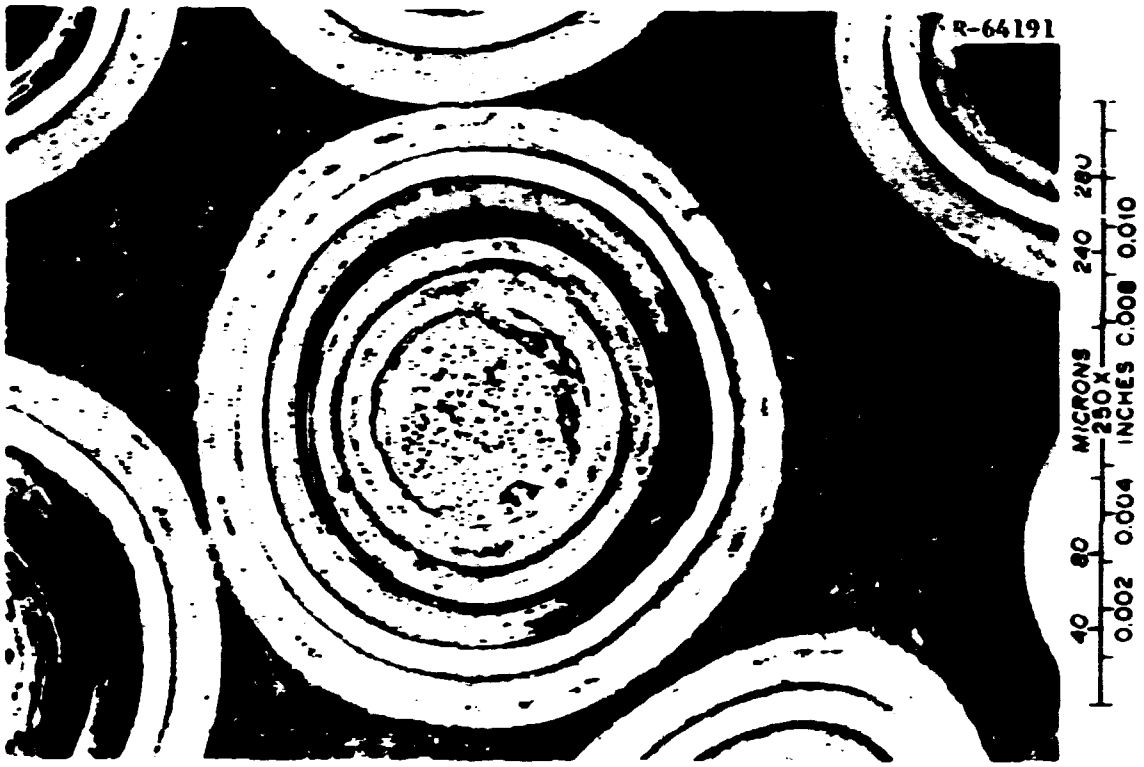

Fig. 5.5. Typical Triso-Coated UC_2 Fissile Particle from Fuel Rod RTE-4-4-1-3. This particle was located 2 mm from the outer surface of the rod; the cold side of the particle is on the right.

UC_2 particles revealed that 3% of the SiC coatings contained straight-line fractures, and in 1% the outer LTI had failed also. Examination of the fissile particles under polarized light revealed that the inner LTI had graphitized on the cold side of the particle, and the inner surface of the SiC was slightly attacked to a depth of 5 μm. A failed particle is shown in Fig. 5.6, in bright field and polarized light. Electron microprobe analysis showed that the graphitized regions of the inner LTI contained the rare-earth fission products — La, Ce, Pr, and Nd — as shown in Fig. 5.7. About 10% of the fissile particles contained tears that extended about halfway through the outer coatings, as shown in Fig. 5.8. This is the first example of matrix-particle interaction that we have observed in fuel rods that had been carbonized in an RTE graphite fuel body. Although none of the Biso-coated ThC_2 particles had failed as a result of the irradiation test, two were found that had been crushed during fabrication.

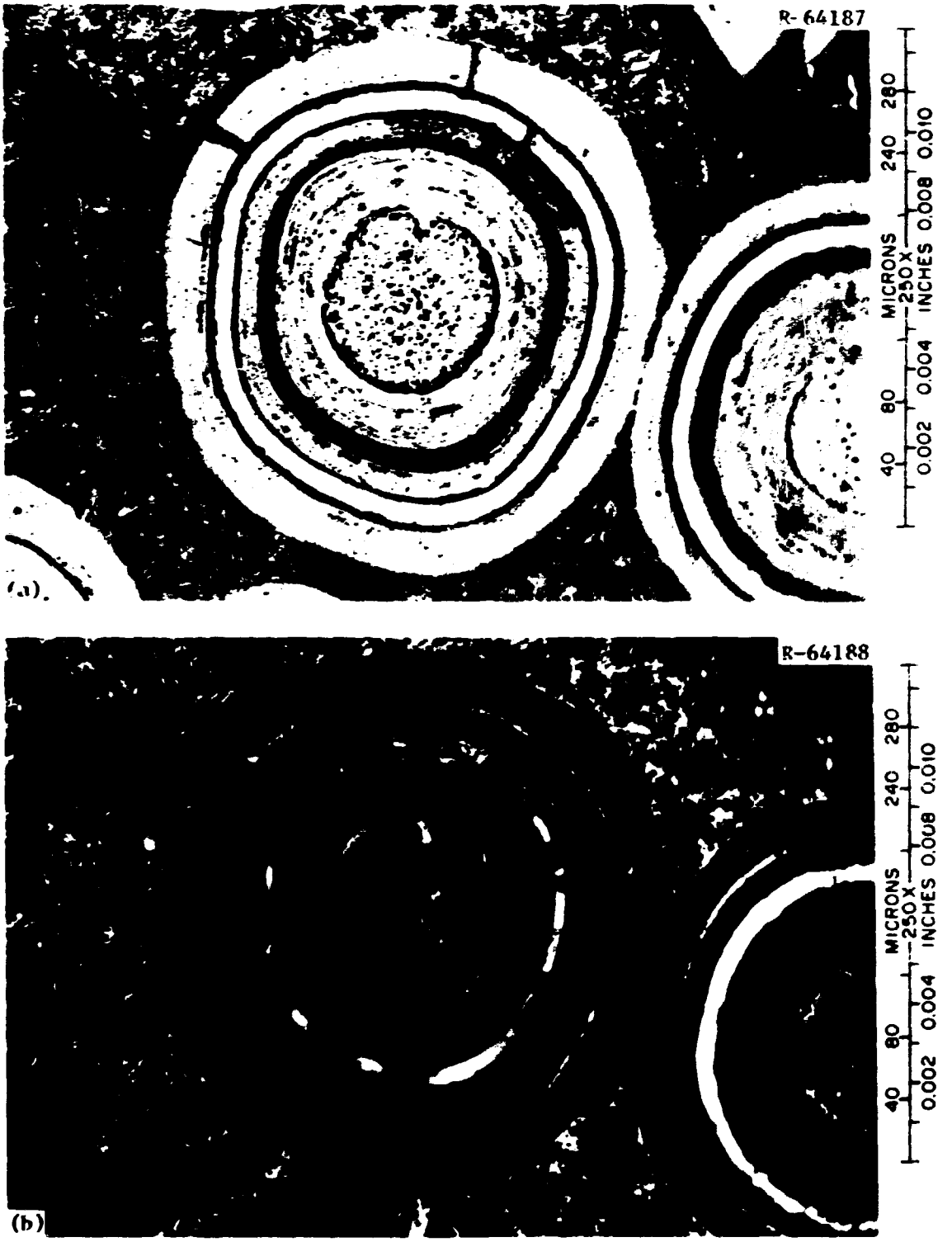

Fig. 5.6. A Failed Triso-Coated UC_2 Fissile Particle from Fuel Rod RTE-4-4-1-3. This particle was located 1 mm from the outer surface of the rod; the cold side of the particle is at the top. (a) Bright field. (b) Polarized light.

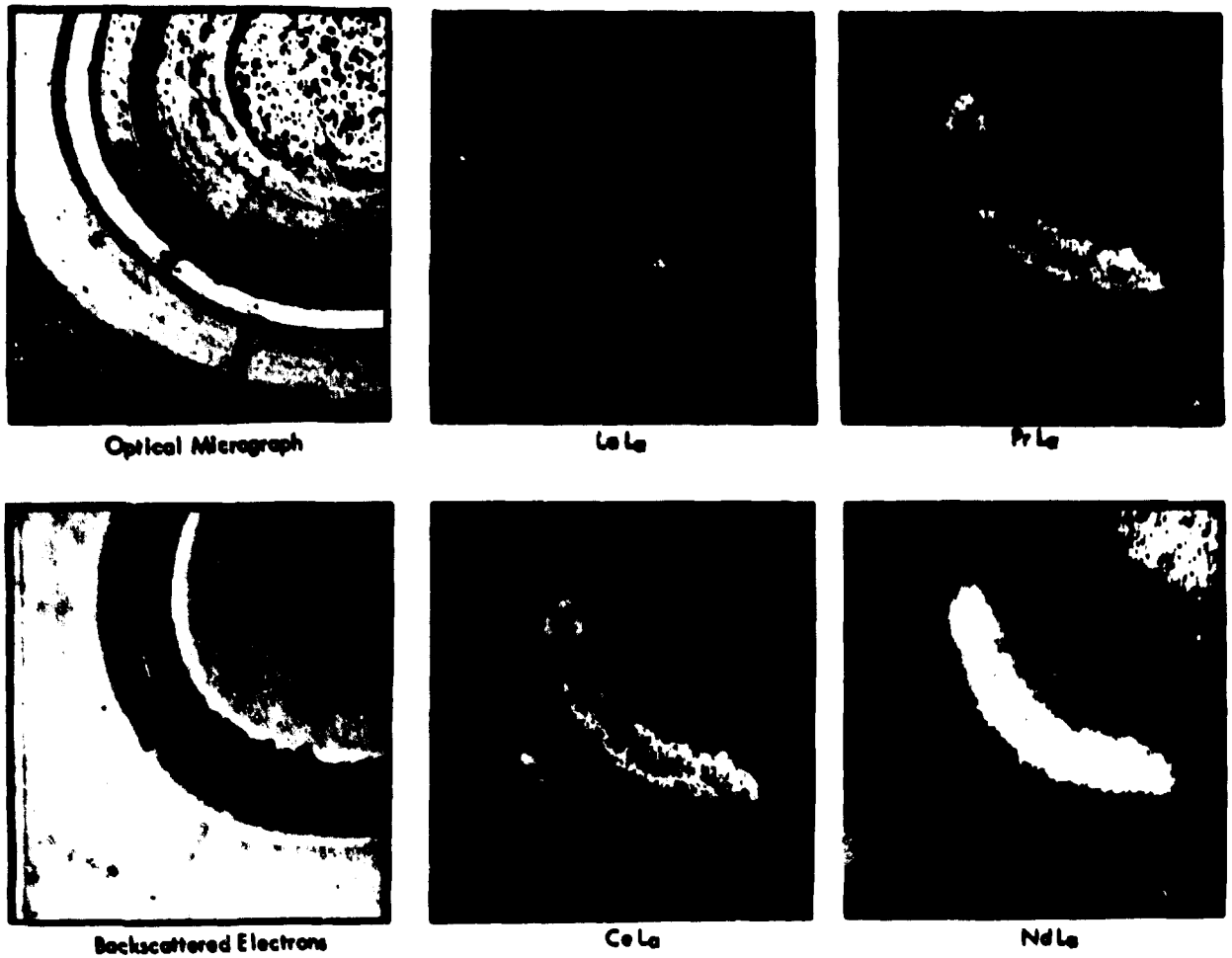

Fig. 5.7. Location ot Rare-Earth Fission Products on the Cold Side of the Fissile Particle Shown in Fig. 5.6, as Determined by Electron Microprobe Analysis.

Fig. 5.8. Tear in the Outer Coating of a Fissile Particle as a Result of Matrix-Particle Interaction in Fuel Rod RTE-4-4-1-3.

The fuel system contained in rods in body 5 consisted of Biso-coated $(2Th,U)O_2$ and Biso-coated ThC_2. The fuel rod selected for metallographic examination operated at an end-of-life maximum temperature estimated to be 1090°C. Examination of a transverse section through this fuel rod revealed no measurable amoeba, nor was there any evidence to indicate potential failure of either the fissile or fertile coated particles. Two Biso coatings that had been crushed during fabrication were found in this section.

Body 2 contained a blended bed of Triso-coated dense UC_2 fissile particles and Biso-coated ThC_2 fertile particles and can be compared with the fuel rods in body 4 that contained the same fuel system. The microstructural appearance of the blended bed was similar to coated particles contained in the fuel rods, with one exception. Graphitization of the cold side of the inner LTI was found in the fissile particles across the entire cross section of the fuel rods, whereas this effect

was not observed in any of the particles in the loose bed sample. The maximum fuel temperature of the loose bed sample was estimated to be about 100°C cooler than the fuel rod, and the thermal fluence (≤ 2.38 eV) was about the same (2.1×10^{21} n/cm^2). The above apparent discrepancy points out the need for detailed thermal analyses of the RTE experiments to take into account the changes in dimensions and relative thermal conductivities with fast neutron damage. A detailed thermal analysis of the RTE experiments is under way.

Body 3 contained a blended bed of Bisc-coated $(4Th,U)O_2$ fissile particles and Biso-coated ThC_2 fertile particles. The sample examined metallographically from this body operated at an estimated maximum end-of-life fuel temperature of 1120°C. There was no evidence of amoeba in either the fissile or the fertile particles; nor was there any indication of potential failure in any of the particles.

The blended bed contained in body 6 was a mixture of Biso-coated UC_2 and Biso-coated ThC_2 particles. The sample examined from this body operated at an estimated maximum end-of-life fuel temperature of 1025°C. This sample was compared with the fuel rods from body 1 that contained the same fuel system but ran at a lower temperature (760°C). The microstructural features in the particles from both bodies were similar in appearance; that is, no measurable amoeba and no indications of potential failure in either the fissile or fertile particles. The short radial cracks noted in the peripheral regions of the Biso coatings on the UC_2 kernels in the fuel rods were also present in the loose-bed sample, indicating that it was a coating property problem and not a fabrication problem.

5.2.3 Postirradiation Examination of RTE-2 — E. L. Long, Jr.

The third in a series of recycle test elements, RTE-2, was discharged from the Peach Bottom Reactor in mid-September 1973, after 701 effective full-power days. The element was received at ORNL in March 1974, and disassembly started in mid-April. The overall appearance of the element was excellent, with no evidence of any localized regions of attack. A sooty deposit was present in the region of the lower spacer-ring of the

graphite sleeve. This sooty deposit rubbed off easily, exposing the as-machined surface. After the upper and lower graphite reflector sections were cut off, the six graphite fuel bodies were pushed out of the graphite sleeve. The appearance of the fuel bodies was excellent. The fuel loading combinations for each of the bodies are given in Table 5.2.

Table 5.2. RTE-2 — Fuel Loading and Operating Temperatures

Body	Estimated max EOL Temperature[a] (°C)	Fuel Type	Fuel Bed Type	Coated Particles	
				Fissile	Fertile
6[b]	1050–1140	f	Rod[b]	UC_2 Triso	ThC_2 Biso
5	1220–1300	a	Blended[c] bed	$(4Th,U)O_2$ Biso	ThC_2 Biso
4[b]	1240–1260	e	Rod[b]	UC_2 Biso	ThC_2 Biso
3	1320–1360	f	Blended[c] bed	UC_2 Triso	ThC_2 Biso
2[d]	1020–1190	d	Rod[b]	$(2Th,U)O_2$ Biso	ThC_2 Biso
1	620–1080	e	Blended bed	UC_2 Biso	ThC_2 Biso

[a]Maximum End-of-Life Temperature Range Along Length of Individual Bodies, Estimated from As-Fabricated Dimensions. Detailed thermal analyses under way incorporate irradiation-induced dimensional changes. The detailed thermal analyses will be included in the final report on the recycle test elements.

[b]Carbonized in fuel body.

[c]Blended beds contain graphite powder that was added as a bed stablizer to prevent segregation.

[d]Carbonized in covered graphite tray.

A representative number of fuel rods (about 40%) were removed by tapping the graphite bodies on the cell floor. As has been the experience with the previous recycle test elements, the fuel rods that had been carbonized in the graphite bodies (bodies 4 and 6) were more difficult to remove than

those carbonized before being loaded in the graphite body (body 2). The general appearance of the fuel rods carbonized in the bodies was good, with only slight evidence of debonding of particles. Most fuel rods had separated at the original interfaces; in a few instances, two fuel rods stuck together. The two fuel rod segments bowed noticeably; this contributed to the degree of difficulty in removal from the graphite body. "Sooty" regions were noted along the fuel rods from body 4; the rods from body 6 were free of surface deposits. Examination of the fuel rods from body 4 revealed that the sooty regions were rust-colored. As shown in Table 5.2, the fuel rods from body 4 contained a Biso-Biso fuel system, while those from body 6 contained a Triso-Biso system and operated at a lower temperature. We also noted that the graphite spine sample from body 4 was more radioactive than that from body 6: about 5 R at 0.61 m (2 ft) vs 200 mR. The spine sample from body 3, which contained a Triso-Biso fuel system (>1300°C), was also at a radiation level of about 200 mR.

The ORNL fuel rods (carbonized before loading) in graphite body 2 were easily removed. The general appearance of the fuel rods was excellent, with only slight evidence of debonding. Of 24 fuel rods removed from this body, three were found broken near mid-length. The breaks were "clean," and examination of the fracture surfaces revealed no broken coatings. Examination of the surfaces of the fuel rods from one hole revealed nine particles that had failed in service.

The results of the dimensional inspection of the ORNL fuel rods from body 2 are shown in Table 5.3. Each fuel rod diameter change reported is an average of six diametral measurements on each of four fuel rods on the same horizontal plane, or 24 measurements per fuel rod position. Only one length measurement was made per rod; but this represents an average value of four measurements per fuel rod position. The fuel rods shrank nearly isotropically; measured $(\Delta D/D)/(\Delta L/L)$ values ranged from 0.82 to 1.08.

Dimensional inspection of the fuel rods carbonized in graphite bodies 4 and 6 showed average diameter changes of −7.73 and −3.24%, respectively. The fuel in body 4 was a Biso-Biso system and was expected

Table 5.3. Dimension Changes vs Fast Fluence for ORNL Fuel Rods from RTE-2, Body 2

Fuel Rod Position	Change, %		$\frac{\Delta D/D}{\Delta L/L}$	Fast Fluence, >0.18 MeV (n/cm^2)
	Diameter	Length		
1[a]	−2.20	−2.29	0.96	2.52×10^{21}
2	−2.57	−3.15	0.82	2.65
3	−2.80	−3.13	0.89	2.75
4	−2.61	−2.89	0.90	2.82
5	−2.91	−3.08	0.94	2.88
6	−3.16	−2.93	1.08	2.92
Av	−2.71	−2.92	0.93	2.75

[a]Bottom fuel rod.

to shrink more than the Triso-Biso system in body 6. The average fast fluence (>0.18 MeV) along body 4 was 2.8×10^{21} n/cm^2 and 1.4×10^{21} n/cm^2 along body 6.

Transverse sections through fuel rods from the maximum temperature regions from bodies 2, 4, and 6 were examined metallographically. A fuel rod from body 2 showed no coating failures or indications of coating failures out of 53 $(2Th,U)O_2$ Biso-coated fissile particles. There was no evidence of kernel migration in either the fissile or fertile particles. No coating failures were found in the ThC_2 Biso fertile particles. The appearance of particles from body 2 is shown in Fig. 5.9.

Examination of 611 UC_2 Biso fissile particles through a fuel rod from the high-temperature region of body 4 revealed no failures. The only significant change noted in the coatings on the fissile particle was the densification and an accompanying increase in the anisotropy of the buffer layer. Examination of the ThC_2 Biso fertile particles revealed no failures. There was no evidence of migration of either the fissile or fertile kernels. Typical fissile particles are shown in Fig. 5.10.

Examination of 433 UC_2 Triso fissile particles through a fuel rod from the high-temperature region of body 6 revealed four particles with

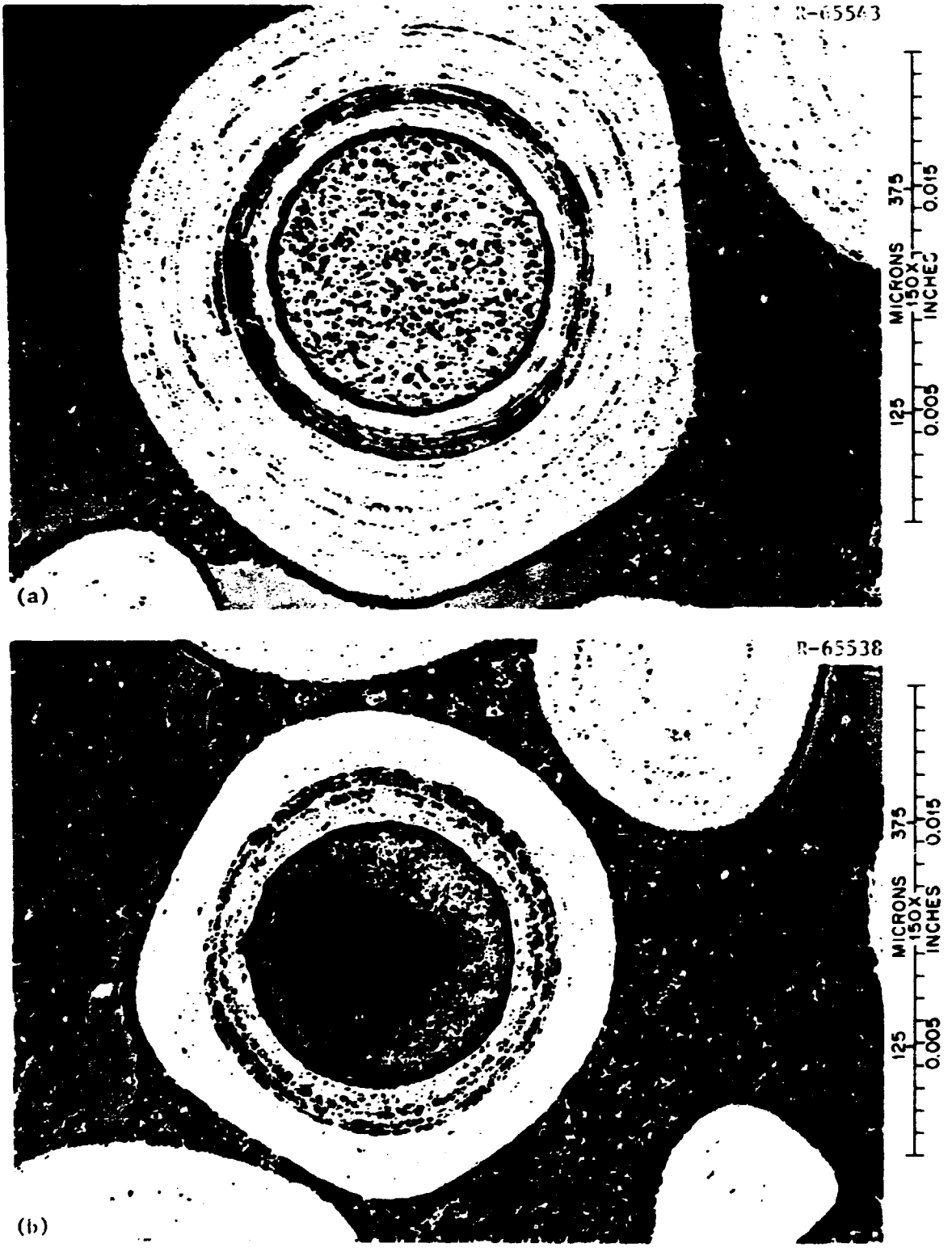

Fig. 5.9. Typical Coated Particles from the Mid-Radius of Fuel Rod RTE-2-2-1-6. (a) $(2Th,U)O_2$ Biso fissile. (b) ThC_2 Biso fertile.

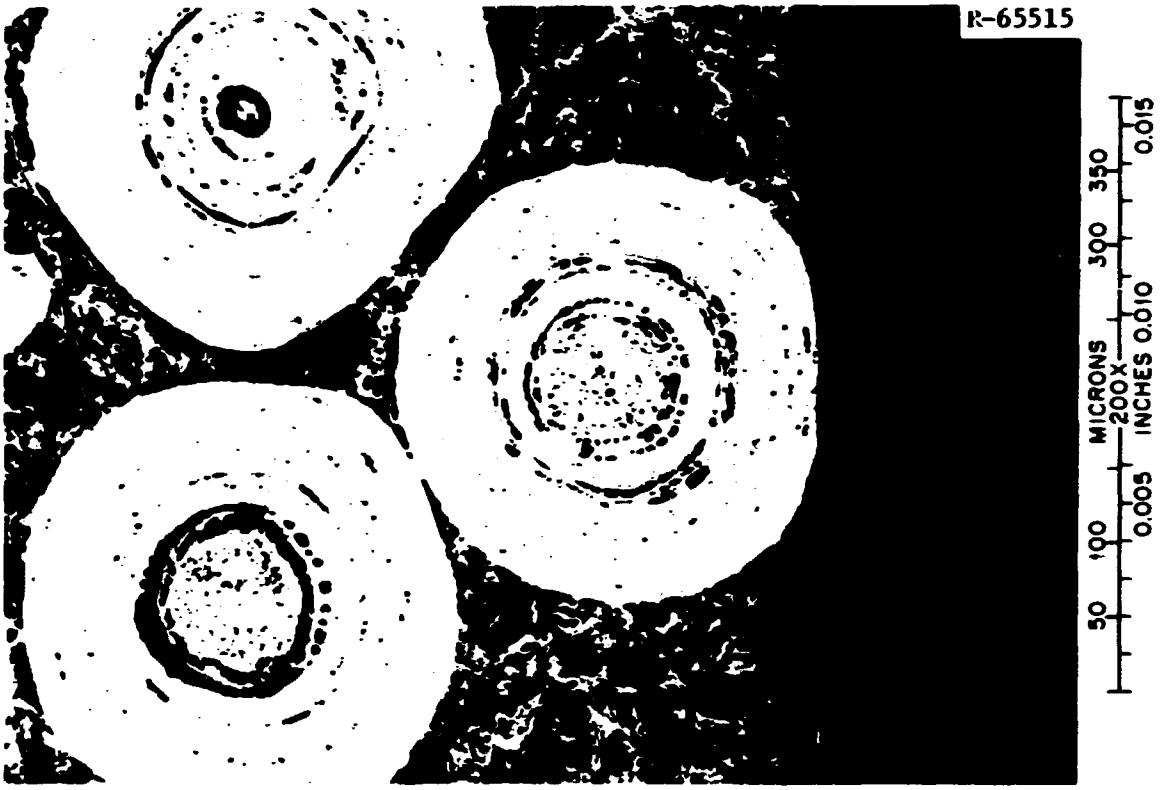

Fig. 5.10. Typical UC_2-Biso Fissile Particles from Fuel Rod RTE-2-4-1-1.

failed PyC and SiC coatings; the outer LTI coatings had failed on 14 particles. The failures were in the form of radial cracks and were of a mechanical nature. Tears that indicated matrix-particle interaction were present in the outer LTI layers of about 25% of the particles (Fig. 5.11).

Graphitization of the cold side of the inner LTI was noted in the fissile particles across the diameter of the fuel rod. Graphitization of the inner LTI is normally associated with the collection of rare-earth fission products on the cold side of fissile particles (Fig. 5.12). There was no measurable amount of attack of the SiC from fission products. One fissile particle was found that contained a defective SiC layer. A portion of the SiC had chipped off in the final stages of SiC deposition, as shown in Fig. 5.13. Examination of the Biso ThC_2 fertile particles revealed no failures, although a large fragment of a Biso

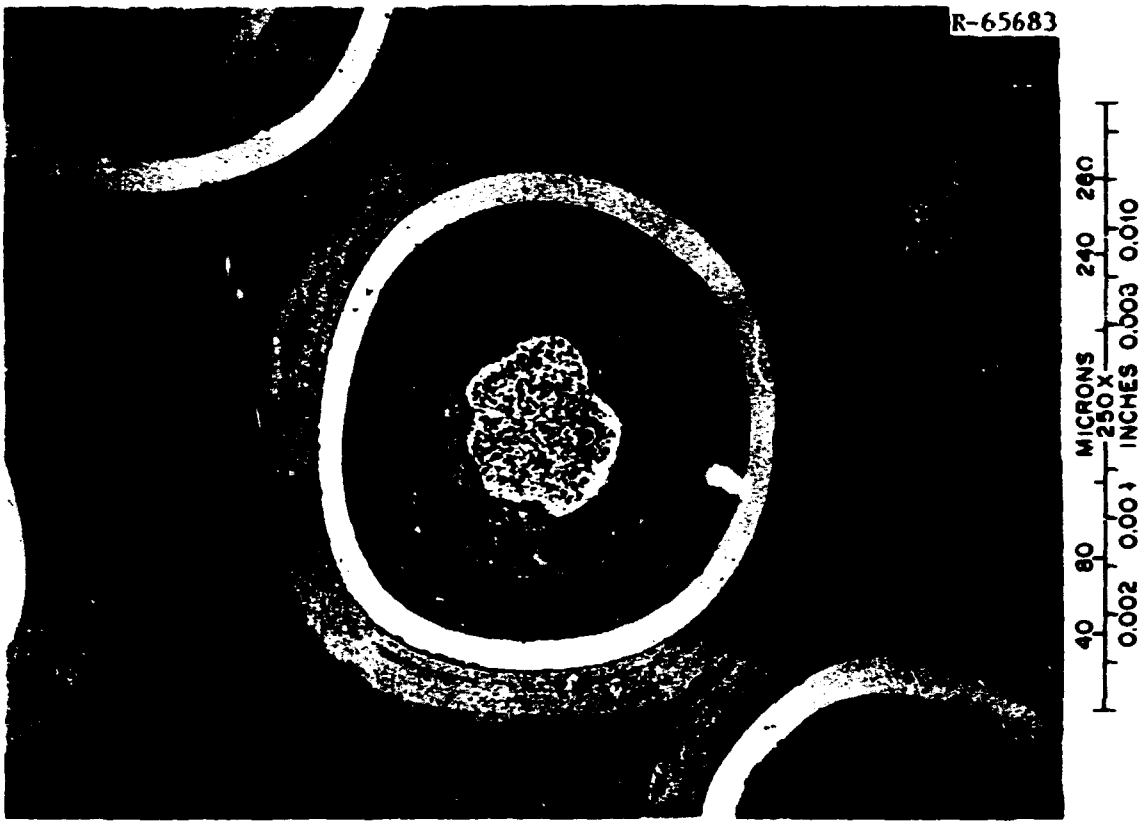

Fig. 5.11. Appearance of a Triso-Coated UC_2 Fissile Particle from Fuel Rod RTE-2-6-1-1. The outer coating failed as a result of matrix-particle interaction.

coating partially surrounded a Triso-coated particle. There was no evidence of kernel migration in either the fissile or fertile particles.

Samples were taken from the maximum temperature region of each of the bodies containing the blended beds and examined metallographically. No unusual microstructural features were observed in the sample from body 5 that operated at an estimated maximum end-of-life temperature of 1300°C. There was no evidence of migration of either the $(4Th,U)O_2$ fissile or the ThC_2 fertile kernels, nor was there any indication of failure or potential failure of either the fissile or fertile particles.

Examination of the Triso-coated UC_2 fissile particles from body 1 revealed no unexpected changes. The estimated maximum end-of-life fuel temperature in this body was 1080°C. The kernels contained numerous relatively small fission-gas bubbles and showed no evidence of migration.

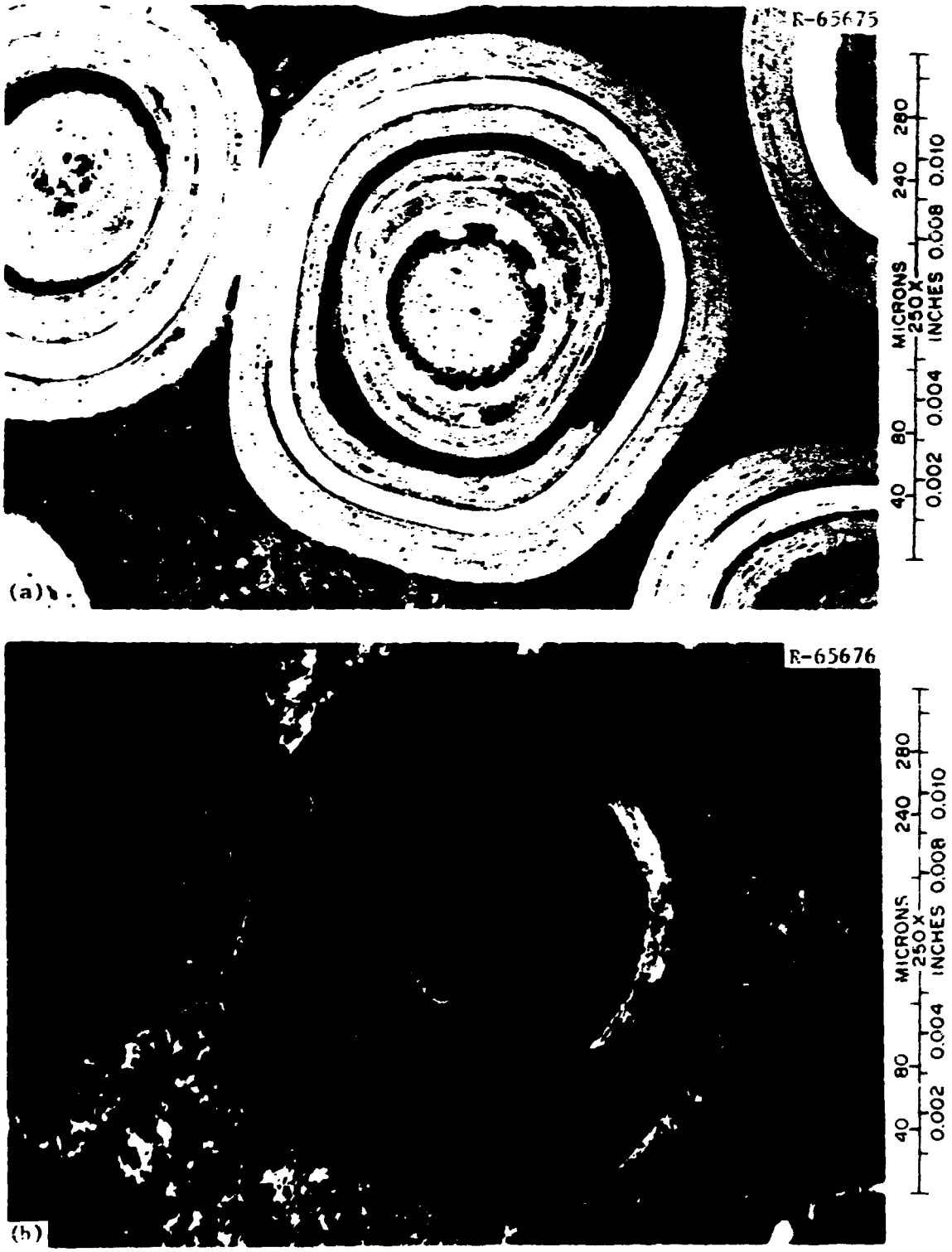

Fig. 5.12. Typical Triso-Coated UC_2 Fissile Particle from Fuel Rod RTE-2-6-1-1. Graphitization of the inner LTI occurred on the cold side (right) of the particle. (a) Bright field. (b) Polarized light.

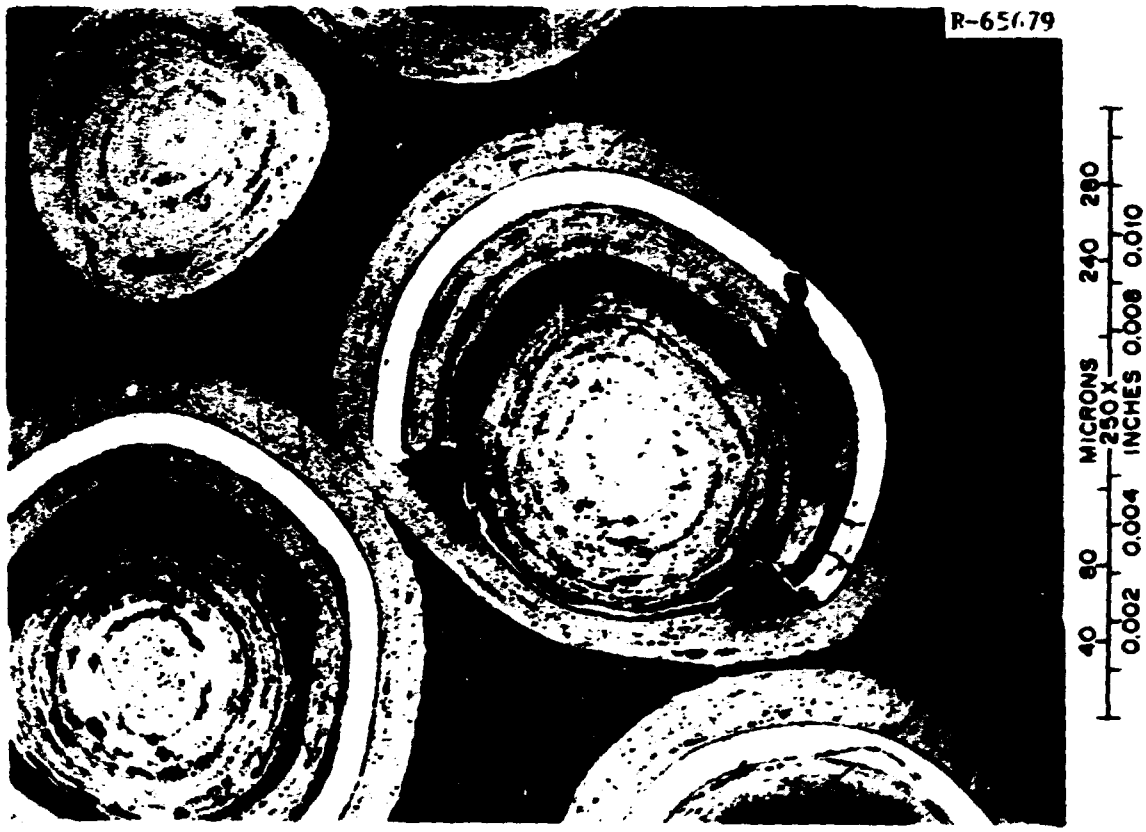

Fig. 5.13. A Triso-Coated UC_2 Fissile Particle with a Defective SiC Coating from Fuel Rod RTE-2-6-1-1.

Examination of the coatings under polarized light clearly revealed a thin (3 to 4 μm) sealer coat that had been put on the buffer coating before deposition of the outer LTI coating. There were no deleterious effects of the coatings due to the presence of the sealer coat. No failed particles were observed out of 378 examined. Examination of the Biso-coated ThC_2 fertile particles revealed no evidence of kernel migration or coati · failures.

Examination of the Triso-coated UC_2 particles from body 3 showed significant differences compared with the Biso-coated UC_2 particles described above. The estimated maximum end-of-life fuel temperature for the fuel in this body was 1360°C. A count of 472 Triso coatings revealed that 17 SiC coatings (3.6%) had failed. Statistically this represents a failure fraction range between 2.8 and 5.4%, at a 95% confidence level. The failures were in the form of straight-line radial

cracks. Examination of the coatings under polarized light revealed that the failures in the coatings were associated with graphitized regions in the inner LTI layers. The apparent graphitization of the inner LTI layers had been associated with the collection of the rare-earth fission products La, Ce, Pr, and Nd on the cold side of the particles in Triso-coated UC_2 in a prior recycle test element (RTE-4). This same effect was observed in the same fissile particles used in the fuel rods in body 6 of this element. No tears in the outer surface regions were seen in any of the fissile particles: this supports the matrix-particle interaction observation made for the fuel rods contained in body 6 of this element.

Thus, it appears the performance limits of the SiC layers in this batch of Triso-coated UC_2 particles have been exceeded in this recycle element. Detailed thermal analyses will be performed on this and other recycle elements in the future by General Atomic Company in an effort to better define the operating conditions of this element. Representative fissile particles from bodies 1, 3, and 5 are shown in Fig. 5.14.

5.2.4 Postirradiation Examination of RTE-8 — E. L. Long, Jr. and T. N. Tiegs

The fourth in a series of seven recycle test elements, RTE-8, was shipped from the Peach Bottom Reactor site to ORNL in March 1975. This element resided in the reactor for 897 equivalent full-power days. The fuel loading combinations and carbonization mode for the fuel rods used in this element are shown in Table 5.4. The overall appearance of the element was normal, with no unusual or unexpected features. The fission-product trap and end fittings were cut off and the six fuel bodies removed from the graphite sleeve. Dimensional measurements taken on graphite components of the fuel element include the sleeve, fuel bodies, spines, and fuel rods. The results were compiled and forwarded to General Atomic Company for incorporation in the detailed thermal analysis for the RTE series.

Fuel rods were removed from holes 1, 5, and 7 in bodies 2, 3, 5, and 6 and holes 1, 3, 5, and 7 in body 4. Loose particle samples were taken

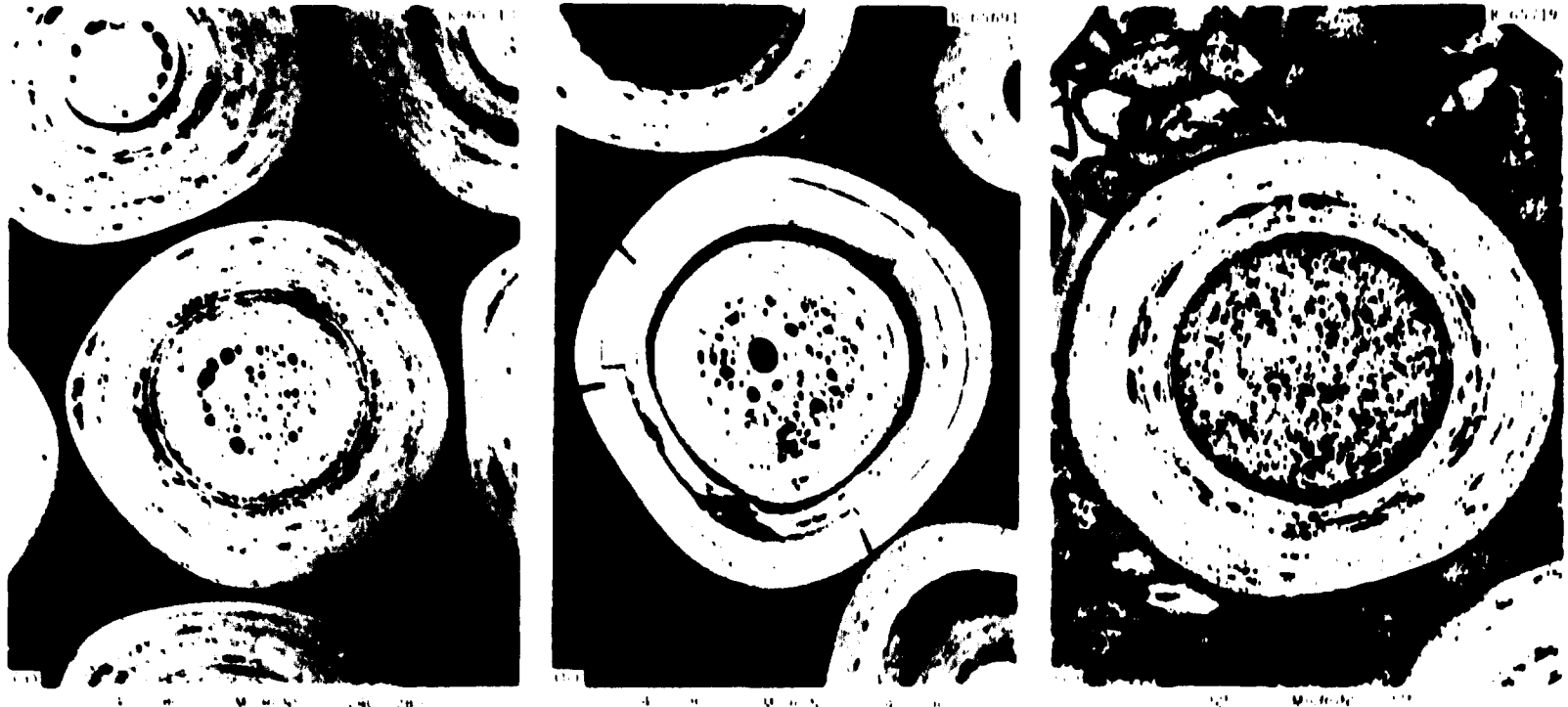

Fig. 5.14. Fissile Particles from Blended Beds Contained in Fuel Bodies 1, 3, and 5 of RTE-2. (a) Biso-coated UC_2. (b) Triso-coated UC_2. (c) Biso-coated $(4Th,U)O_2$. Reduced 34.5%.

Table 5.4. Fuel Loading Scheme for RTE-8

Body	Fuel Type	Fuel Particle Type	
		Fissile	Fertile
6	f[a]	UC_2 Triso	ThC_2 Biso
5	i[a]	UC_2 Triso	ThC_2 Triso
4	d[b]	$(2Th,U)O_2$ Biso	ThC_2 Biso
3	e[a]	UC_2 Biso	ThC_2 Biso
2	i[a]	UC_2 Triso	ThC_2 Triso
1	f[c]	UC_2 Triso	ThC_2 Biso

[a]Carbonized in fuel body.

[b]Carbonized in covered graphite tray.

[c]Blended bed containing graphite powder that was added as a bed stabilizer to prevent segregation.

from hole 1 in body 1. All fuel was visually inspected with the stereomicroscope and photographed. The rods appeared in good condition with virtually no debonding.

Fuel was selected from the highest temperature region of each of the fuel bodies and submitted for metallographic examination. The results of these examinations are summarized below.

Body 2. The Triso-coated UC_2 particles appeared in good condition, with no graphitization of the inner LTI. Many particles had broken outer LTIs. Particles from the same batch were also irradiated in RTE-7, where cracks were observed. This element was irradiated for a longer period, and evidently the outer LTIs have shrunk considerably with increased exposure. The Biso-coated ThC_2 particles were in good condition, with no amoeba observed. The buffer separated from the inner LTI and densified around the kernel in some particles. Typical fissile and fertile particles from body 2 are shown in Fig. 5.15.

Body 3. No failed Biso-coated UC_2 or ThC_2 particles were observed. No graphitization, matrix-particle interaction, or amoeba was seen. Particles were in good condition, though some had faceted coatings or misshapen kernels (Fig. 5.16).

Fig. 5.15. Typical Particles from Fuel Rod RTE-8-2-7-7. (a) Triso-coated UC_2. (b) Triso-coated ThC_2.

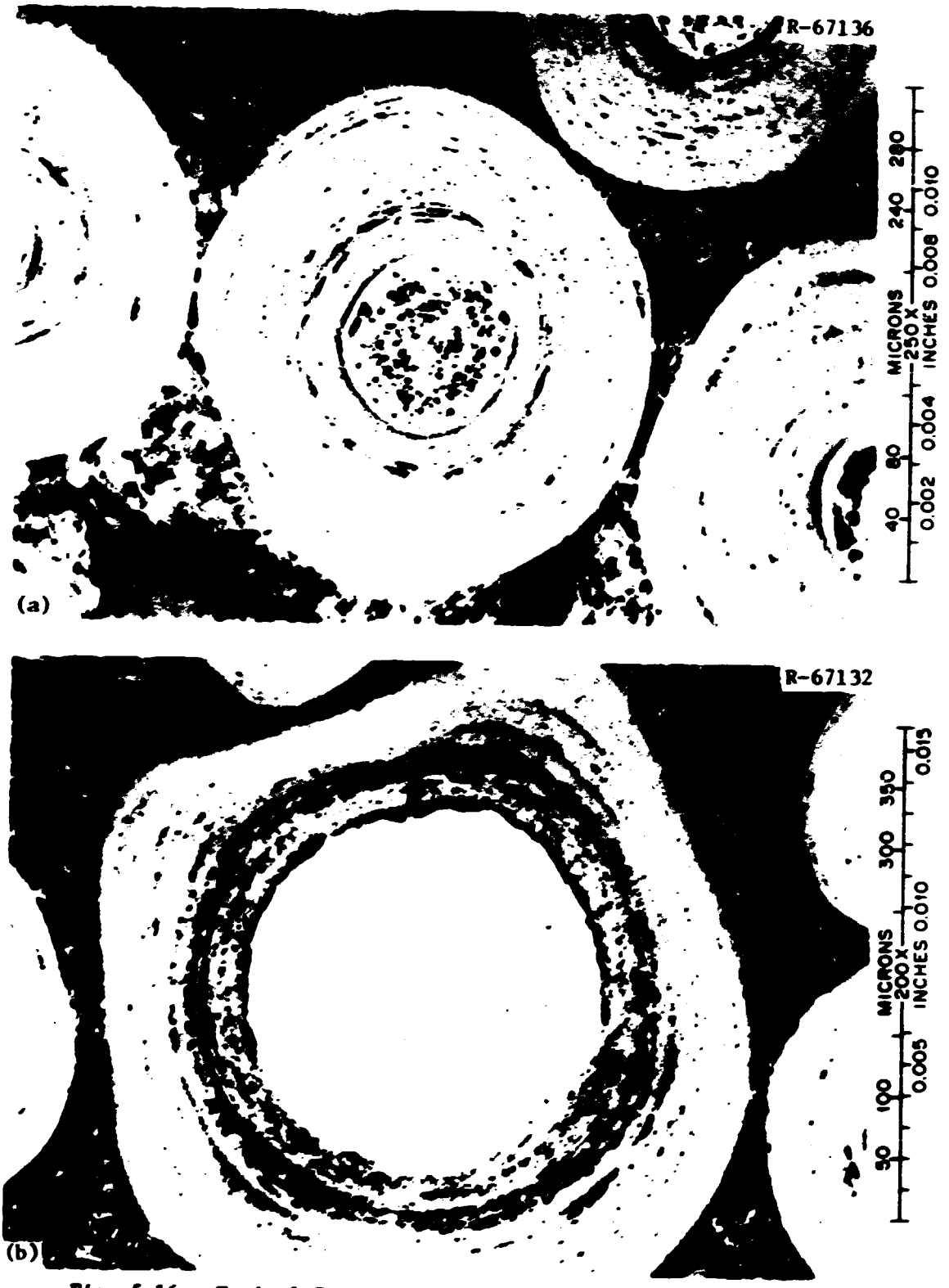

Fig. 5.16. Typical Particles from Fuel Rod RTE-8-3-1-7. (a) Biso-coated UC_2. (b) Biso-coated ThC_2.

Body 4. No failed particles or matrix-particle interaction was observed. Particles were in good condition, though some had faceted coatings. Slight amoeba was observed in $(2Th,U)O_2$ particles (<5 μm). A typical fissile particle is shown in Fig. 5.17.

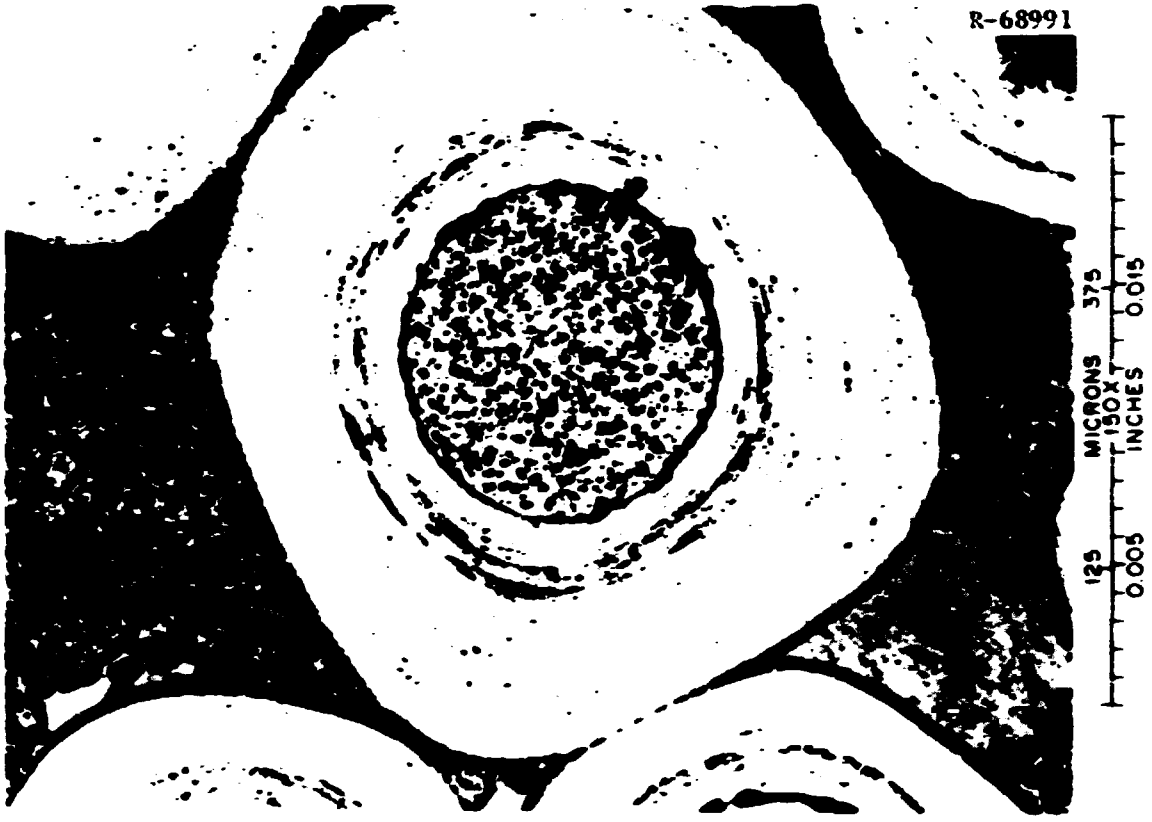

Fig. 5.17. Typical Biso-Coated $(2Th,U)O_2$ Fissile Particle from Fuel Rod RTE-8-4-5-1.

Body 5. Most Triso-coated UC_2 particles (≈90%) showed graphitization of the inner LTI on the cold side of the particle, with evidence of slight attack of the SiC (<5 μm) (see Fig. 5.18). There were many broken outer LTIs, and the reason is the same as for body 2. The buffers separated from the inner LTI and densified around the kernel of the Triso-coated ThC_2 particles. The outer LTIs on about half of the fertile particles had failed from fast-neutron damage (Fig. 5.19).

Fig. 5.18. Triso-Coated UC_2 Particle from Fuel Rod RTE-8-5-7-1. (a) Bright field. (b) Polarized light. The cold side of the particle is at the top of the figure. Note that graphitization of the inner LTI is apparent in polarized light.

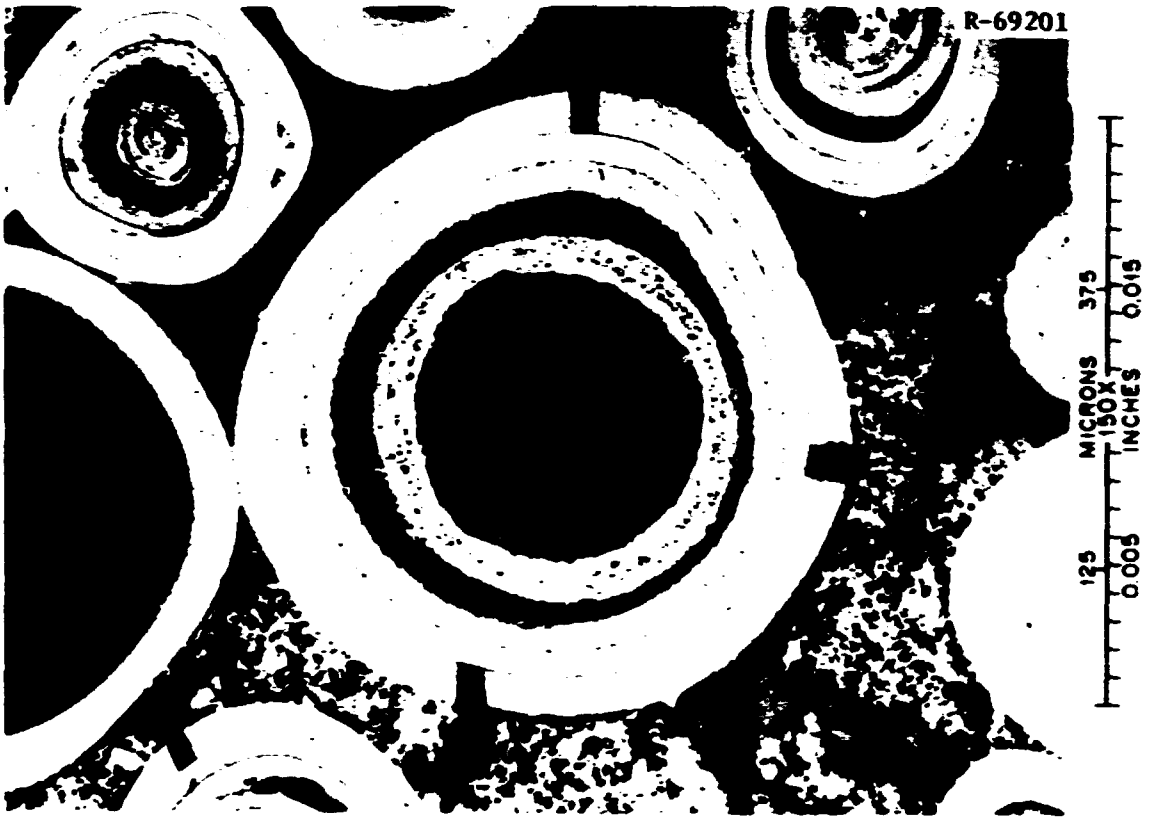

Fig. 5.19. Triso-Coated ThC_2 Fertile Particle from Fuel Rod RTE-8-5-7-1. The failed outer LTI is a result of fast-neutron damage.

Body 6. The UC_2 particles appeared in good condition, with no graphitization of the inner LTI. Many particles had broken outer LTIs, and the reason is the same as for body 2. The ThC_2 particles were in good condition though some had faceted coatings. No amoeba was observed.

The metallographic results for the sample of loose particles from body 1 are not available and will be reported later.

5.3 LARGE-SCALE RECYCLE ELEMENT IRRADIATIONS (WORK UNIT 2303)

The FSVR test element program will not begin until Spring 1977, when the first elements are scheduled to begin irradiation. Preliminary planning was accomplished during the reporting period, and more substantive accomplishments will be reported in the next progress report.

Briefly, the ORNL portion of the test element program will include about 90 test fuel rods to be irradiated in each of three standard FSVR fuel elements. The remaining fuel in the elements will be either production FSVR fuel or test fuel from other sites. General Atomic Company will coordinate the test with the reactor owner (Public Service Company of Colorado), and will be testing fuel and graphite in the same test element series. The fissile fuel particles for the FSVR test elements were manufactured during the reporting period and are undergoing preliminary capsule testing in the OF-2 capsule. Similar fuel, manufactured in laboratory-scale equipment, was irradiated in the HRB-9 and -10 capsules, and it performed very well. All the fuel rods for the FSVR test elements will be manufactured in engineering-scale equipment being developed for the HTGR Recycle Demonstration Facility. General Atomic Company will be providing the fertile fuel, shim material, and matrix material for the test.

5.4 REFERENCES

1. F. J. Homan, "HTGR Fuel Qualification," Chap. 6 in *HTGR Base Program Progr. Rep. Jan. 1, 1974–Dec. 31, 1975*, ORNL-5108 (in preparation).
2. E. L. Long, "Recycle Test Elements," *Gas-Cooled Reactor Programs Annu. Progr. Rep. Dec. 31, 1973*, ORNL-4975, p. 153.
3. E. L. Long, R. B. Fitts, and F. J. Homan, *Fabrication of ORNL Fuel Irradiated in the Peach Bottom Reactor and Postirradiation Examination of Recycle Test Elements 7 and 4*, ORNL-TM-4477 (September 1974).

6. ENGINEERING AND ECONOMIC STUDIES (SUBTASK 310)

F. J. Homan

6.1 INTRODUCTION — M. S. Judd

The purpose of Subtask 310 is to guide the HTGR Fuel Recycle Program toward commercial application in the late 1980s. It utilizes the work done in other subtasks to provide the liaison between the development efforts and the design of a commercial recycle facility. The long-range objectives are:

1. to provide the economic analysis and program coordination in the areas of fuel cycle alternatives, environmental impact, safety analysis, and safeguards procedures that will permit the development of a commercial HTGR fuel recycle industry that will provide the dual benefits of low fuel cycle costs and maximum utilization of natural resources;
2. to ensure that the process evaluation and equipment development activities under way in Task areas 100 and 200 remain relevant to the design of a commercial recycle facility.

Subtask 310 is composed of the following work units:

Work Unit 3100 — Fuel Cycle Systems Analysis
Work Unit 3101 — Analysis of Reprocessing Techniques
Work Unit 3102 — Analysis of Refabrication Techniques
Work Unit 3103 — Environmental, Safeguards, and Safety Analysis

6.2 ECONOMIC ANALYSIS OF HTGR FUEL RECYCLE (WORK UNIT 3100) — W. E. Thomas

The objectives of this work are to economically analyze fuel cycle alternatives. Part of this activity involves cost estimation of the reprocessing and refabrication steps, including capital, operating, and hardware costs. A computer code is now under development to implement this analysis.[1]

The code is designed to describe not only costs in individual fuel recycle facilities, but the fuel recycle needs of the HTGR segment of a growing reactor economy. In its present state of development, the

BLANK PAGE

capability is confined principally to calculating annual mainstream and scrap recovery process throughputs in fresh fuel fabrication. The code works from reactor build schedules and fuel specifications to determine approximate HTGR growth and changing fuel fabrication requirements over a 20-year projection.

Figure 6.1 shows the intended overall procedure to be followed by the code in arriving at costs. At present the code is functional in approximately the upper half of the figure. A user may classify all HTGRs to be served by fuel cycle plants into as many as four different types, and may specify the number of each type to be built each year. For example, types may be differentiated according to such characteristics as size, fuel residence time, fuel specification and loadings.

The code computes the quantities of fuel — uranium and thorium — charged and discharged from all HTGRs (by type) over a 20-year history. The number of fuel elements, both control and regular, is obtained, enabling the determination of fabrication and reprocessing requirements. The possibility of delay in the availability of reprocessing facilities can also be included by a date specification.

Fresh fuel fabrication, chemical reprocessing, and refabrication are each subdivided into major processes, examples of which are fuel rod manufacture and fuel element assembly. Annual process throughputs are computed with user-supplied information on reject fractions, waste fractions, and scrap recovery parameters. Fissile and fertile particles may be specified as any combination of Biso and Triso to determine coating throughputs and gross heavy metal content, as well as secondary burner throughput in chemical processing.

The annual throughputs determined for each major step in chemical reprocessing, fabrication, and refabrication form the basis for estimating units of equipment required, space requirements, and costs. The expansion of recycle plant capacity need not be assumed as proceeding continuously. Rather, the user can specify discrete plant expansion schedules with equipment sized for maximum throughput between expansion dates.

ORNL-DWG 76-4046

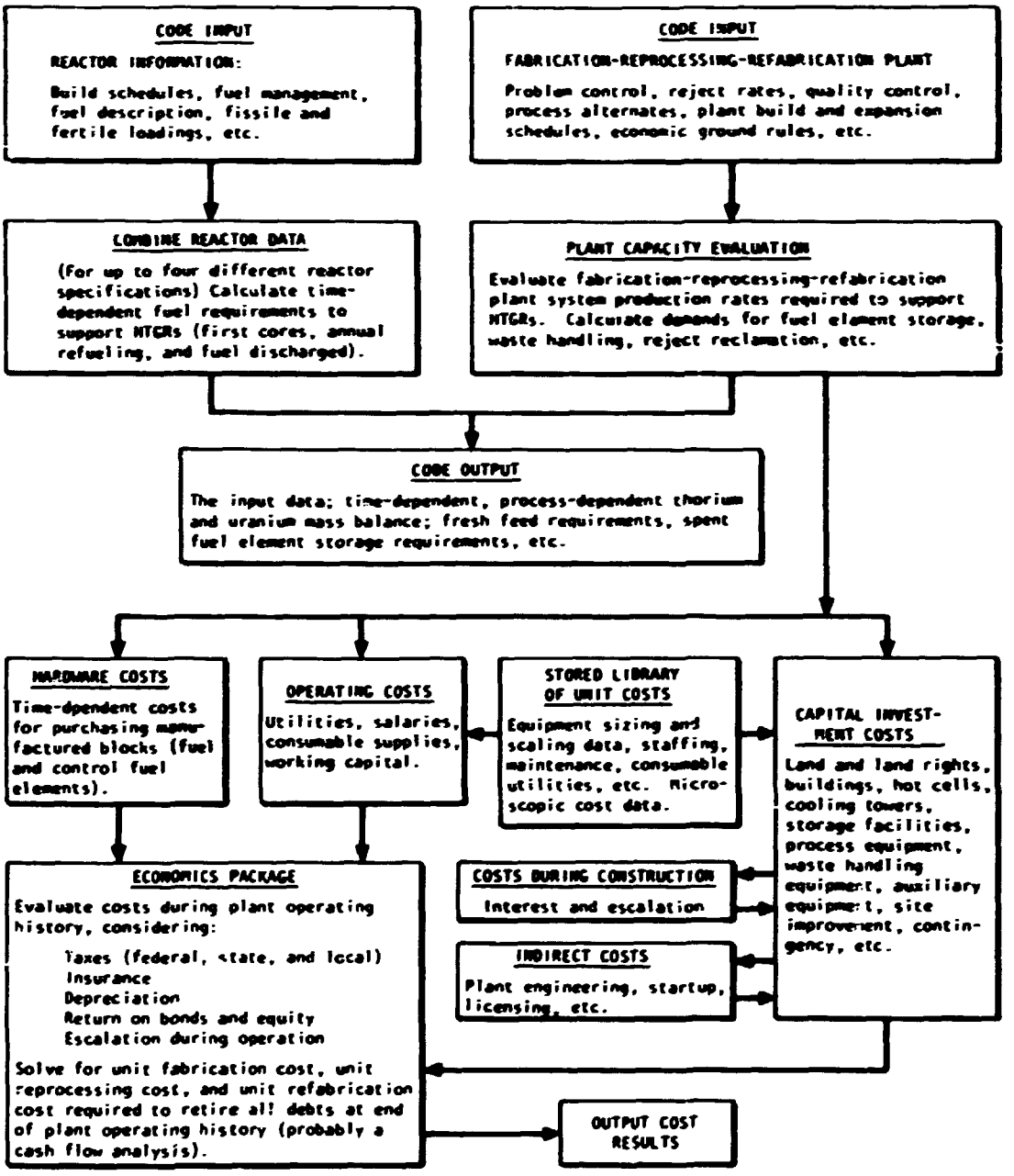

Fig. 6.1. Outline of Code Logic.

6.3 ANALYSIS OF SHIPPING, RECEIVING, AND STORAGE OF HTGR FUEL (WORK UNIT 3101) — J. W. Snider

Shipping, receiving, and storage of spent HTGR fuel elements at a commercial reprocessing plant [50,000-MW(e) economy] were evaluated. Since the design and construction of the reactor will probably be carried out over a significant time period, a full-capacity (1.5 tons of heavy metal per day) reprocessing plant will not be required at first. Three alternatives of receiving and storage were considered:

1. a full 50,000 MW(e) reactor economy HTGR reprocessing plant,
2. smaller multiple reprocessing plants, and
3. a single modular plant.

Both a staggered reactor discharge and a seasonal reactor discharge were considered. The seasonal reactor discharge was considered for two 50% discharges six months apart and for a 67% discharge and a 33% discharge six months apart. The seasonal reactor discharge was assumed to occur over a six-week period. Considerations and conclusions for the three alternatives are presented.

6.3.1 Full-Scale Commercial Plant — J. W. Snider and D. C. Watkin

A study of primary burning[2] had indicated that at least one-fourth to one-half of an annual reactor discharge should be burned during a burner campaign with the total discharge preferred. Thus, the accumulation of large numbers of spent fuel elements from a single reactor for feed to the crusher during a burnup campaign is required. It was assumed that the fuel was moved from the reactors as quickly as possible and that the fuel elements were not sorted before shipping as to fuel type (IM, 23R, and 25R).

With the availability of two shipping casks (rail) per reactor, shipping 48 spent fuel elements per trip and also returning the 23R and 25R recycle fuel elements, the cask fleet can transport only five annual reactor discharges [1000 fuel elements for discharge for a 1160-MW(e) reactor] per month. Thus, the cask fleet is operating ten months per year (see Table 6.1).

Table 6.1. Estimated Turnaround Times for the Shipping Casks

Procedure	Time (days)
Spent Fuel Shipping	
Travel to reactor 1[a]	5
Loading at reactor 1 (1/day + 2-day queue)	7
Travel to reprocessing plant	5
Unloading at reprocessing plant (4/day + 4-day queue)	5
TOTAL	22
Recyle Fuel Shipping	
Travel to reactor 2[a]	5
Unloading at reactor 2 (2/day + 2-day queue)	5
Travel to reactor 1	5
TOTAL	15
Average Time of Shipping	
Spent fuel (100% × 22 days)	22
Recycle fuel (40% × 15 days)	6
AVERAGE	28

[a]Reactors 1 and 2 are in different seasonal discharge schemes.

The receiving area was assumed to have a daily capacity of 4 times the average daily plant capacity. This results in the handling of about 12 casks per day or the unloading, can emptying, sorting, recanning after sorting, and placing into storage about 600 spent fuel elements per day. Single-can handling of four elements in the cask cans and four or six elements in the storage cans presents a significant movement problem with can emptying, loading, and can moving.

We conceived a system that moves the cans in groups of 12, and the sorting is done whenever the cans are removed from storage, when the daily flow of fuel elements is near the plant average. A schematic flowsheet showing the sequence of operations is shown in Fig. 6.2. In this concept the 12 containers from a cask are transferred into a carousel-type container holder and transferred with a crane to a

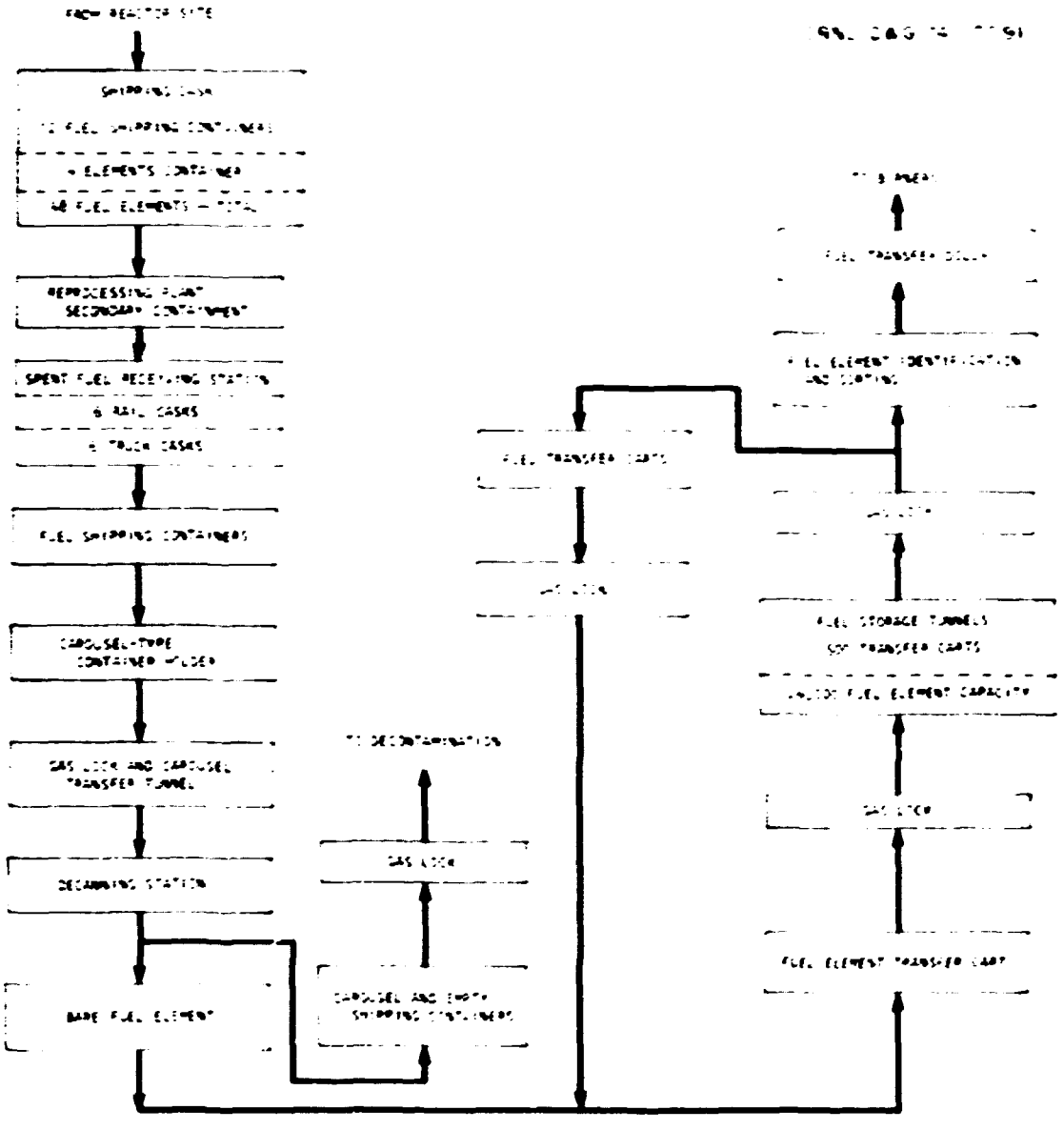

Fig. 6.2. Fuel Element Handling Sequence Assumed for this Study.

carousel conveyor tunnel. There the carousel is transferred to a floor hatch beneath where the spent fuel elements are transferred into a fuel element transfer cart (Fig. 6.3). The contents of a cask are held by a transfer cart (Fig. 6.4). The cart is inserted into a below-floor storage tunnel, where it is advanced in a manner similar to that of a push-through furnace (Fig. 6.5). Cooling gas passes through the tunnel for heat removal. The tunnel contains one annual reactor discharge when it is full. At the end opposite to where the cart was inserted into the tunnel it is removed, and there elements are sorted. The empty cart is returned through a cart return enclosure. It is refilled with elements and inserted into a tunnel or inserted empty. The elements may be stored bare within the cart (Fig. 6.4).

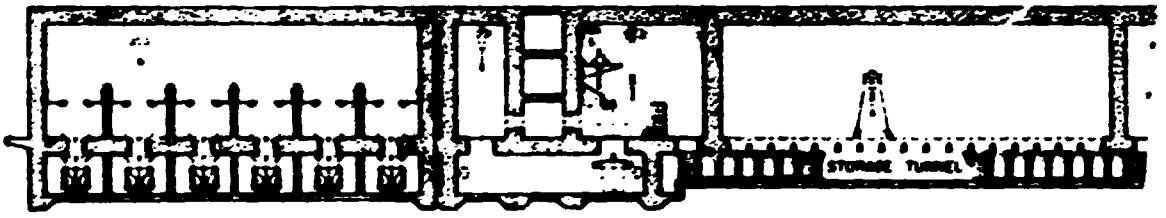

Fig. 6.3. A Sectional View of the Six Rail Receiving Stations, the Carousel Conveyor Tunnel, the Fuel Element Transfer Bay, and the Storage Tunnel.

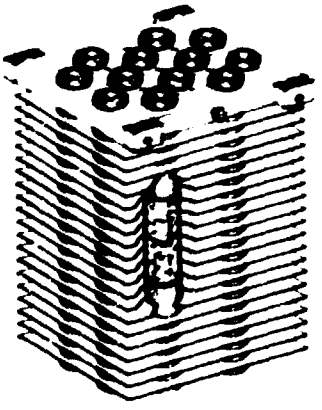

Fig. 6.4. Transfer Cart Used for Spent Fuel Storage and Transfer.

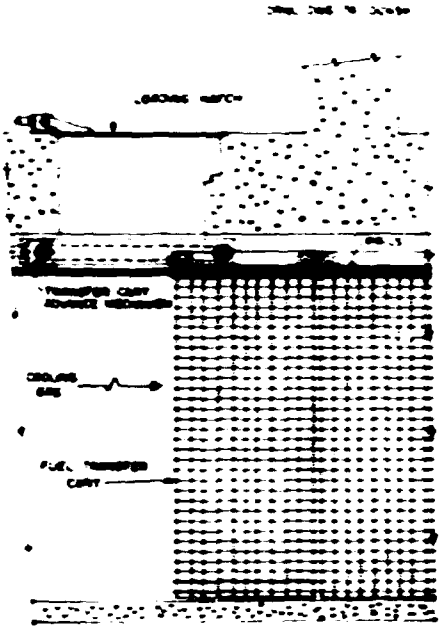

Fig. 6.5. A Sectional View of the Storage Tunnel, Showing Transfer Carts and Advance Mechanism.

The 12 empty shipping containers from the carousel are transferred to the decontamination cells and then returned to the receiving area via a container conveyor. Figure 6.6 shows a plan view of such a storage area with six rail and and six truck receiving stations, 28 tunnels for 28 reactor discharges and the related areas and corridors for a functional facility.

The most significant conclusion drawn from this study was that single-can movements within a storage-sorting area are impractical and that the total cask load should be moved within the storage-sorting area to minimize the number of transfers.

6.3.2 Multiple Small-Scale Plants — D. C. Watkin

A hypothetical small-scale fuel reprocessing plant was considered for a two-burner head-end system. This plant can handle up to about 15 reactors, depending upon the primary burner size. We actually considered a 10-reactor reprocessing plant using smaller burners. This size plant represents the smallest increment of system components

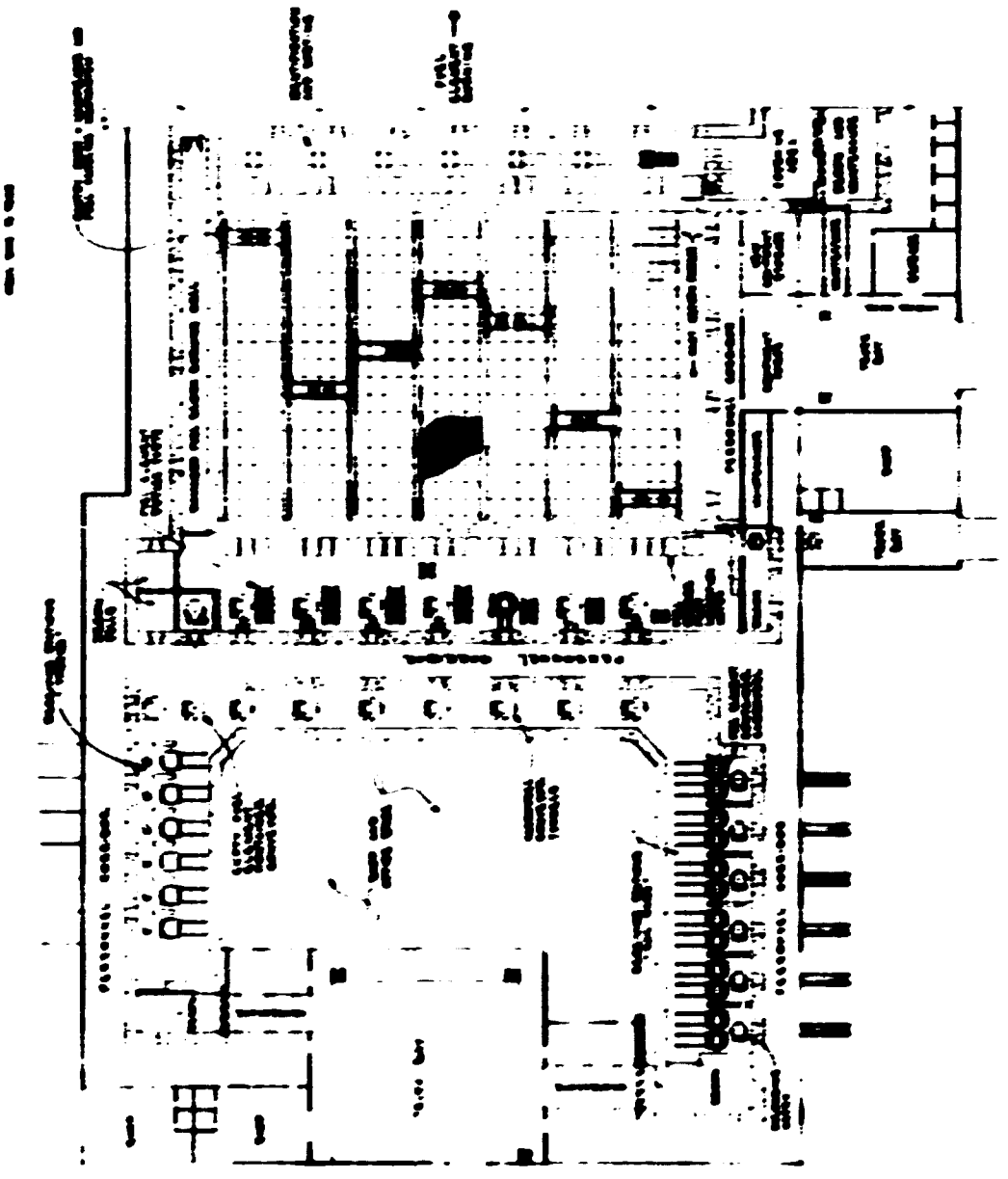

Fig. 6.6. Plan View of the Receiving, Handling, Storing, and Sorting Areas of an HTGR Reprocessing Plant.

that can be realistically operated (i.e., one burner operates on the IM elements, the other on 23R and 25R elements).

With two shipping casks per reactor (20 total) the cask fleet can move one annual discharge per month. Again, the shipping fleet will be operating ten months per year.

6.3.3 Modular Plant — J. W. Snider and D. C. Watkin

When one considers the uncertainties in trying to build a reprocessing-refabrication plant that will be of the exact size required at full capacity, a modular plant appears attractive. While the ultimate cost of this plant will be higher than the initially built full-capacity plant, it aids with cask flow, allows for adjustment of changes in the reactor growth curve, allows for improved technology as modules are added later, and can accommodate ratchetting regulations at less cost.

Since the storage area connects with the head-end systems in a reprocessing plant, both the storage and head-end portion of the plant must be modular. One such concept is shown in Fig. 6.7. A maintenance and decontamination cell is located at the intersection of a "tee." One leg of the "tee" serves the crusher, one leg serves the primary burners, and the third leg serves the secondary burning and dissolution equipment. That portion shown by solid lines would be built first and would accommodate 10 to 15 reactors. That portion represented by dotted lines would be for future expansion. This concept would allow for incremental expansion while allowing fuel reprocessing within the plant to continue without interruptions until construction is completed. At that time the removable walls that separate the old portion of the plant from the newly constructed portion would be removed. This last step of removing the shielding and containment walls may, however, prove to be a formidable problem. One approach would be to construct the walls of solid shielding blocks in such a way as to afford adequate shielding, but also allow the blocks to be removed without structurally affecting the ceiling, floor, or walls to which they interface. This work could be done using direct maintenance techniques. However, the inner liner, which served as containment for the old facility, would probably need to be remotely removed by cutting into small pieces, which will be disposed of as solid wastes.

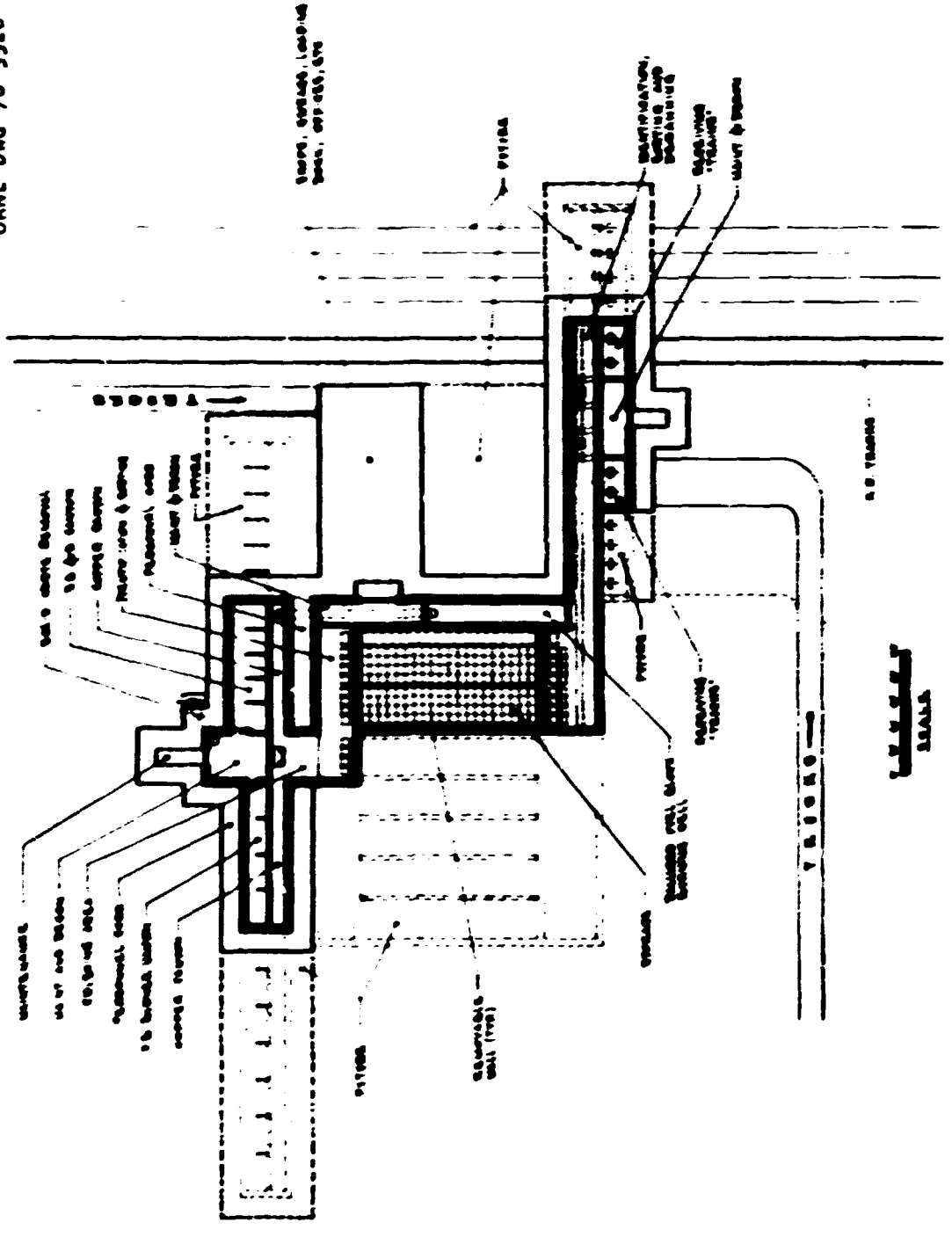

Fig. 6.7. Plan View of a Proposed Modular HTGR Reprocessing Plant.

6.3.4 Spent Fuel Element Storage Capacity – J. W. Snider

When the steps between a seasonal reactor discharge and the reload of that reactor one year later are considered, it becomes apparent that to meet this schedule and utilize the recycle elements with a one-year turnaround time the shipping, reprocessing, and refabrication capacity of the plant will need to be 25-40% greater than that required by using 300 operating days to determine capacity. This comes from the following assumptions:

1. Spent fuel shipments from the reactor cannot commence for three months following reactor shutdown.

2. Recycle elements should be on site at the reactor one month before reactor shutdown.

3. Fuel recovered from spent fuel elements entering head-end processing requires three months for reprocessing, refabrication, and shipping.

Thus, the last of a seasonal reactor discharge must enter head-end operations within five months from the beginning of shipment. The more imbalance between the seasonal discharges, the more excess capacity the system must have. One can avoid overcapacity design of the system by allowing a portion of the recycle fuel to operate on a two-year turnaround time.

The amount of spent fuel storage capacity shown in Figs. 6.6 and 6.7 represents about 50% of the annual amount to be reprocessed by the plant. If the plant is designed at less than 50% storage capacity it may run into situations in which the head-end campaigns, less than annual, will be shorter than desirable, because of the unavailability of fuel to reprocess.

6.3.5 Reflector Block Handling – J. W. Snider

The reflector blocks may amount to 20 to 30% of the number of spent fuel elements per reactor discharge. If they are to be handled at the reprocessing plant the shipping fleet needs to be increased over that discussed above. However, if a separate cask is designed for the reflector blocks and if it can also handle the recycle element shipments,

then the spent fuel shipping casks can operate between only two stops, one at the reactor for spent fuel loading, and one at the reprocessing plant for unloading. This reflector-recycle block cask will require less shielding than the spent fuel element shipping cask, with a saving in shipping charges.

6.4 CHARACTERIZATION OF EFFLUENTS FROM A COMMERCIAL HTGR FUEL REFABRICATION PLANT (WORK UNIT 3102) — M. S. Judd

The types and quantities of chemical and radioactive effluents that would be released from an assumed commercial-scale fuel refabrication facility that would accommodate a 50,000 MW(e) HTGR economy have been determined.[3] The objectives were primarily to establish the types and amounts of effluents that would derive from such a plant, and secondly to define those process areas where confirmatory research and development are needed. The assumed processes have all been shown to be technically feasible and in most cases have been developed to the stage where scale-up to full-size equipment is the next logical stage of development.

The assumptions of reject rates and effluent compositions are all based on currently available data and conservative engineering extrapolations or estimates. The data are presented in such a fashion that they can be easily scaled to a different throughput or production rate. The releases of radioactive and toxic materials to the environment are minimal, but they are not negligible. Properly scaled, this effluent information could be coupled with similar information from the required adjacent HTGR Fuel Reprocessing Plant to provide source terms for an assessment of the effects of such a plant on the environment.

This study identified the need for confirmatory research and development in the scrap recovery and waste treatment areas. Currently, a development program (Work Unit 2109) is fulfilling these development needs.

6.5 SURVEY OF SAFEGUARDS PROBLEMS ASSOCIATED WITH THE HTGR FUEL CYCLE (WORK UNIT 3103) — M. L. Tobias

The activity under this heading has two parts. First, an internal document has been prepared bearing on the above subject and will eventually

be issued as a final report.[4] Second, the members of the Thorium Utilization Program have been kept informed of safeguards-related matters on a regular basis through the monthly program reports of the Thorium Utilization Program. The information provided consists of the following:

1. notices of the issuance of regulatory guides that are relevant to safeguards planning and design;
2. notices of changes to Title 10 of the *Code of Federal Regulations*;
3. indications of policy trends in this field by reporting of public statements by responsible officials;
4. reporting of technical developments obtained at scientific meetings, from technical journals, and from topical reports issued by investigators at such centers as Brookhaven National Laboratory (Technical Support Organization) and Los Alamos Scientific Laboratory;
5. reporting of occasionable notable events in this field, such as the investigation of alleged irregularities at the Kerr-McGee plant in Oklahoma.

Several conclusions were reached after an examination of the issues relevant to commercial fuel recycle plants. A principal conclusion is that the most immediate concern should be for physical security of the plant and only secondarily on material accountability procedures. The latter are basically passive and nonpreventive; they detect events only after they occur. Further, they can never be made tamper-proof or perfectly accurate, so both false alarms and false assurances are possible. Finally, they cannot prevent acts of sabotage or violence. (These remarks are not intended to deny the necessity for accountability methods; they fulfill the essential function of verification of physical security procedures. Extensive research, moreover, is under way to reduce the time lag mentioned between the diversion or theft of nuclear material and the detection thereof.) Physical security procedures, on the other hand, provide the preventive function both passively and aggressively. The latter is the chief drawback, because excessive activity in this respect — the multiplication of guards, searches, and surveillance — can become not only expensive but stultifying to the main business of the plant, which is recycling HTGR fuel.

The principal potential threats against the HTGR plant were judged to be the following:

1. sabotage and/or destructive action by commandos;
2. armed theft by commandos;
3. employee sabotage;
4. theft of special nuclear material by employees in amounts too small to be detected by accountability procedures;
5. thefts large enought to be detected by accountability procedures.

It was concluded that present regulatory commission requirements were sufficient to reduce plant vulnerability to thefts of the types represented by 4 and 5 to the point where would-be thieves would look elsewhere. Most probably, diversion would be attempted in the transportation process. Likewise, physical security measures expressed and implied by the regulations and guides should be adequate against individual intruders but not against trained armed groups. Some of the techniques specifically useful in prevention of acts of theft or sabotage by employees are:

1. preemployment screening for previous job history and mental instability;
2. employee relations procedures:
   a. cooperative implementation of work discipline procedures,
   b. care in selection of security staff to avoid thrill seekers and paranoids,
   c. the employment of professional mental health practitioners for employee counseling,
   d. management training in supervisory skills, particularly those of an interpersonal nature,
   e. recognition that excessive security measures will produce an oppressive atmosphere detrimental to proper plant operation;
3. surveillance procedures and technique:
   a. polygraphing *not* recommended,
   b. closed-circuit television openly used,
   c. personal searches to be used with restraint,
   d. badge screening,
   e. portal monitors (metal and SNM detectors are effective, but at present high-explosive detectors are impractical);

4. passive protection methods:
   a. complete clothing change,
   b. voluntary self-administered health physics checks;
5. surveillance and inspection of the effectiveness of the security system by feigned illegal acts (so-called "black-hat" testing).

The actions of armed groups bent on theft or destruction can be prevented, in theory, by an adequately equipped Federal guard force of military character. The use of such forces raises a large number of legal and social questions and is now under examination by the Nuclear Regulatory Commission.[5] For the purposes of the fuel cycle plant, the following approaches were recommended in the present study:

1. the use of an effective civilian guard force, which implements the intent of present regulatory guides and the CFR;
2. the maintenance of confidentiality not only concerning actual safeguards plans (this is now practiced), but also with respect to the details of plant operation and the actual location of vital facilities;
3. a careful examination of plant vulnerability and safety procedures in terms of deliberate, malicious attempts to cause damage; particular aspects to be studied are:
   a. the potential of materials already on site for destructive use,
   b. the possibility that plant processes can be distorted or altered to cause fire,
   c. the consequences of disruption of plant utilities,
   d. the procedures to be followed in the event of an attack.

At present, the safeguards study work is confined mainly to keeping up with developments in the field. Should this study be resumed on a more substantial scale, we recommend that:

1. appropriate pilot plant facilities connected with the Thorium Utilization Program be used as practical testing grounds for physical protection methods,
2. the personnel assigned should gain realistic experience by being made ex-officio members of existing plant protection committees,

3. permission for access to actual licensee safeguards plans be obtained from the Nuclear Regulatory Commission, such access to be handled on a classified basis.

6.6 ANALYSIS OF THE ENVIRONMENTAL IMPACT OF ^{14}C RELEASES FROM AN HTGR FUEL REPROCESSING PLANT (WORK UNIT 3103) — S. V. Kaye

The work in this activity has been divided into two parts: local environmental impacts of the release of ^{14}C from a model HTGR fuel reprocessing facility, and the long-term global radiological implications of such releases. Initially, priority has been given to the former aspect of the problem, but a foundation also has been laid for the latter. The assessment of local impacts has included the computation of new factors for computing the dose rates to various organs of man, the application of existing methodology to predict the atmospheric transport of ^{14}C, the development of a carbon assimilation and growth prediction model that is applicable to various types of forage and food crops, and the estimation of dose to local residents and populations and to a maximally exposed individual.

Preparation for the eventual assessment of long-term global impacts has consisted of a review of literature related to levels of ^{12}C and ^{14}C now present in the various world reservoirs, transfer rates between reservoirs, and production and decay rates of various types of biota in the sea and on land and the area extent of each type. On the basis of such information, computer-implemented models can simulate the global cycling of natural and man-made carbon, and scenarios of exposure of populations to ^{14}C can be studied. Several such models have been reviewed, all of which are hampered by the lack of complete data sets and want of a coordinated approach to compiling data from all available sources.

A thorough investigation of the cycling of ^{14}C from nuclear testing is the appropriate course to follow to assess global cycling of ^{14}C released from nuclear facilities. From available estimates of carbon pool sizes and production rates of the various terrestrial biosphere components and specific activities of these compounds, the amounts of natural and excess ^{14}C present in terrestrial biota were calculated.

The resulting estimates are somewhat higher than corresponding values reported in the literature and suggest that existing models of the global carbon cycle might assign too large a fraction of the total budget to the deep ocean.

The plant growth Carbon Assimilation Model (CAM) was developed to help study the dynamics of carbon uptake and retention in plants, and particularly the eventual specific activity of ^{14}C in the tissue of plants exposed to episodic excursions of high concentration of ^{14}C in the air near the reprocessing facility. Such episodes occur in the presence of meteorological wind-speed and stability-class combinations that permit the plume to reach the ground before it has traveled far from the stack. Three cases have been included in the model's implementation, which are believed to represent minimum, maximum, and average concentrations.

The starting point of the local environmental assessment[6] was an assumed annual release, at a uniform rate, of 5000 Ci ^{14}C to the atmosphere as carbon dioxide. While the assessment is generic with respect to hypotheses concerning distributions of population and sites of food production in the area, meteorological data specific to the Oak Ridge area have been employed in the prediction of atmospheric dispersion of the release and the resulting ground-level concentrations. Calculations were performed for 90- and 305-m (300- and 1000-ft) stacks.

Dose estimates were computed for:

1. a hypothetical maximally exposed individual or "fence-post accident man,"
2. an average off-site resident within 50 miles of the facility,
3. a population of 10^6 individuals uniformly distributed over the same area.

The dose estimates are believed to tend toward conservatism. They incorporate a number of uncertainties, which are primarily associated with assumptions made in the atmospheric dispersion calculation, and they are believed to be quite sensitive to variations in the meteorology. Moreover, the degree of plume rise due to momentum, which strongly affects the fence-post dose rate, depends on stack parameters other than

height (viz., the ejection velocity and the internal diameter of the stack). Calculations to bound the uncertainties and to analyze the sensitivity of the computed doses to the meteorology and other parameters are now under way.

6.7 REFERENCES

1. W. E. Thomas, *Preliminary Development of the Capability to Evaluate Economics of Process Options in Commercial HTGR Fuel Recycle*, ORNL/TM-5125 (in preparation).
2. J. W. Snider, D. C. Watkin, and H. Barnert-Weimer, *An Evaluation of HTGR Primary Burning*, ORNL-TM-4520 (November 1974).
3. M. S. Judd, R. A. Bradley, and A. R. Olsen, *Characterization of Effluents from a High-Temperature Gas-Cooled Reactor Fuel Refabrication Plant*, ORNL-TM-5059 (December 1975).
4. M. L. Tobias, *Safeguards for a Commercial HTGR Fuel Recycle Plant*, GCR: 75-31 (August, 1975), unpublished.
5. "Security Agency Study — Announcement and Request for Comment," *Fed. Reg.* 40(176) (Sept. 10, 1975).
6. S. V. Kaye et al., *Progress Report on Evaluation of Potential Impact of ^{14}C Releases from an HTGR Fuel Reprocessing Facility*, ORNL-TM report in preparation.

7. CONCEPTUAL DESIGN OF A COMMERCIAL RECYCLE PLANT (SUBTASK 320)

J. D. Sease

7.1 INTRODUCTION

A major part of the current plans for developing HTGR recycle technology is the design and construction of an ERDA-supported HTGR Recycle Demonstration Facility (HRDF). It will probably be built in the late 1980's and will provide interim recycle production capacity for the HTGR industry. The ultimate size and schedule of this plant depends upon the HTGR reactor build schedule. Because of the uncertainty of the HTGR sales, it will probably be advantageous to design the HRDF as modular production units to accommodate a wide range of reactor build schedules. The anticipated ultimate size of the HRDF will probably be a plant capable of reprocessing 20,000 spent fuel elements per year and refabricating 10,000 recycle fuel elements per year.

The objective of this subtask is to assist in the conceptual design of the HRDF. The conceptual design will provide an early appreciation of the problems involved in providing such a facility and will provide a reference to guide the supporting development programs.

The objective of the initial phase of this subtask was to help define a modular plant configuration by a series of preconceptual plant layout studies of different plant sizes. This subtask was not defined until late in the report period and was provided with only modest funding. The limited time and funding restricted the work during this report period to a preconceptual layout study of a selected single plant size of the HRDF.

7.2 20/10 HRDF PRECONCEPTUAL DESIGN STUDY — C. C. Haws, L. C. Hensley, W. H. Pechin, F. E. Harrington, A. R. Olsen, J. E. Van Cleve, T. F. Scanlan, K. H. Lin, and M. S. Judd

The plant capacity chosen for the first design of the study is reprocessing 20,000 spent fuel elements per year and refabricating 10,000 recycle fuel elements per year (i.e., 20/10). This plant size was selected because this was the scale proposed in a draft of an

BLANK PAGE

alternate Fuel Recycle Development Program plan prepared by ERDA in the spring of 1975. Similar studies might be done successively in the future on 10/5 and 5/2.5 sized plants, so that a modular approach to the construction of an HRDF could be evaluated.

The design study of this 20/10 plant was limited in scope and was based on readily available process engineering data obtained in the preconceptual design of the 50/20 TARGET Recycle Facility[1] and the conceptual designs of the reprocessing and refabrication pilot plants at the Idaho Chemical Processing Plant[2] and at ORNL.[3]

The design study comprised the following steps:

1. generation of a design philosophy and defined terminology,
2. development of process flowsheets for each major processing area,
3. determination of space requirements for each major processing area,
4. determination of proximity relationships between and within process areas and support areas,
5. preparation of an initial facility layout using a systematic layout procedure to determine the most efficient layout, and
6. review and revision of the initial layout and each succeeding revised layout until a mutually acceptable layout was derived.

The design philosophy was prepared to be generally applicable to any HTGR recycle plant. The emphasis of the design philosophy was to define philosophy items that could have a significant impact on the layout of the HRDF. The major areas in the design philosophy are isolation, maintenance, operation, flow of material, waste handling, and utilities. Because of the many and sometimes confusing terms used in HTGR recycle technology, a document is being prepared to define terminology for the HRDF studies. The major headings of this document are fuel element identification, scrap, waste, waste categories, contamination categories, process stream identification, maintenance categories, intermediate process products, and abbreviations.

Before a facility layout could be prepared, process flowsheets for each major processing area were needed. Figure 7.1 illustrates the HRDF processing steps for which detailed flowsheets were prepared. These flowsheets were then used to determine space requirements and the interfaces between processing areas.

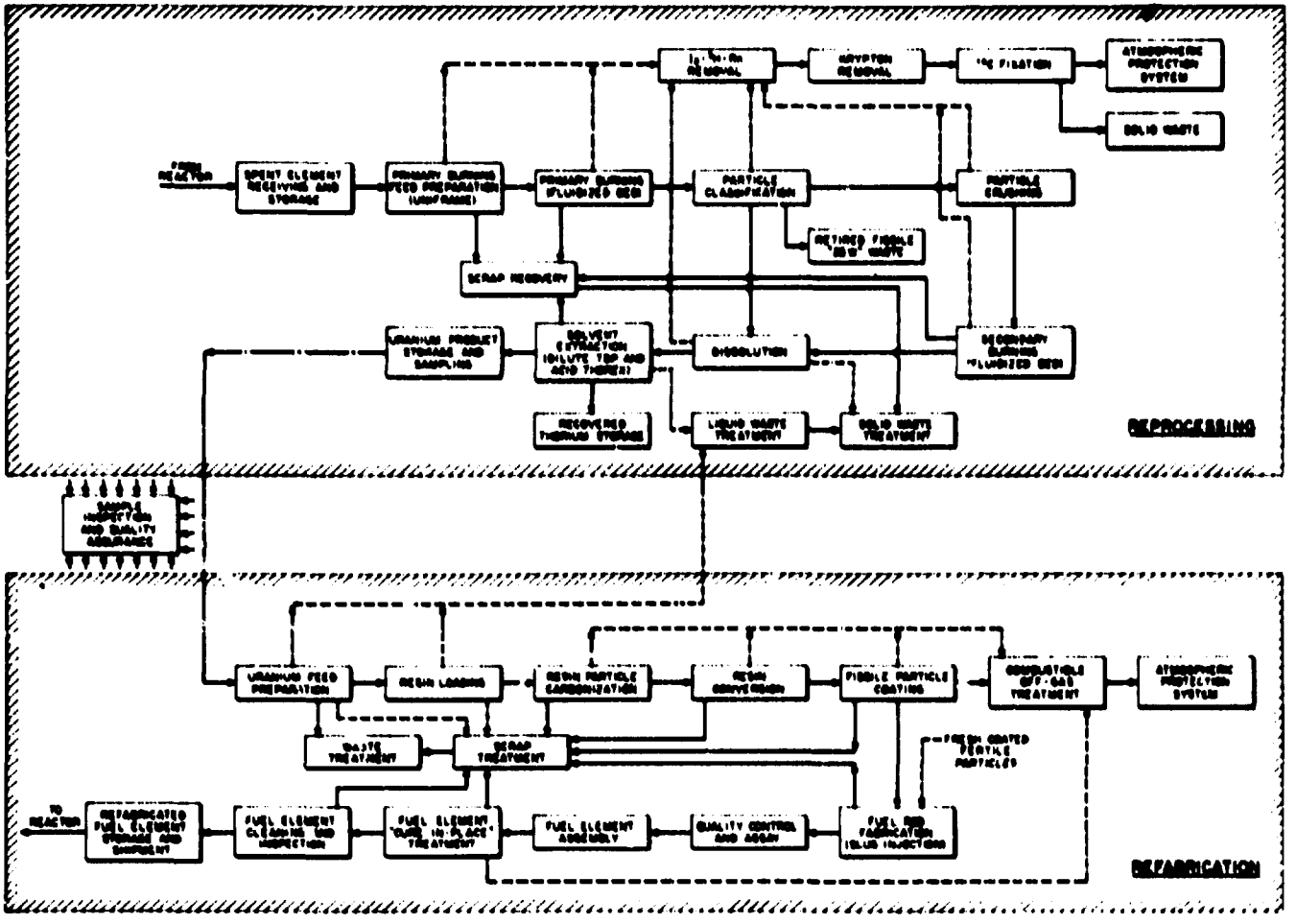

Fig. 7.1. Preliminary HRDF Process Outline.

The preconceptual block layout of the 20/10 HRDF is shown in Fig. 7.2. This layout, which can only be considered very preliminary to the conceptual design of an HRDF, does provide an approximation to overall size and complexity of such a facility. The facility is estimated to contain some 46,000 m^2 (500,000 ft^2) of floor space for process operation and utility services. In the facility, the interfacing and interrelationships among process operations, contamination control, and maintenance philosophy are very complex. A more detailed report of this design study is being prepared.

7.3 REFERENCES

1. General Atomic Company, *Conceptual Design Summary and Design Qualifications for HTGR Recycle Plant* (Draft), GA-A13365, Vol. I, pp. 1–9 (March 1975).
2. Ralph M. Parsons Company, *Conceptual Design Report, HTGR Fuel Reprocessing Facility,* Vols. I, II, and III, USERDA, Idaho Operations Office, Idaho Falls, Idaho, February 1975.
3. *Conceptual Design Report for the HTGR Fuel Refabrication Pilot Plant,* GCR: 74-30, Vols. II and III, May 1, 1975, unpublished; Chap. 4 of this report is a summary of it.

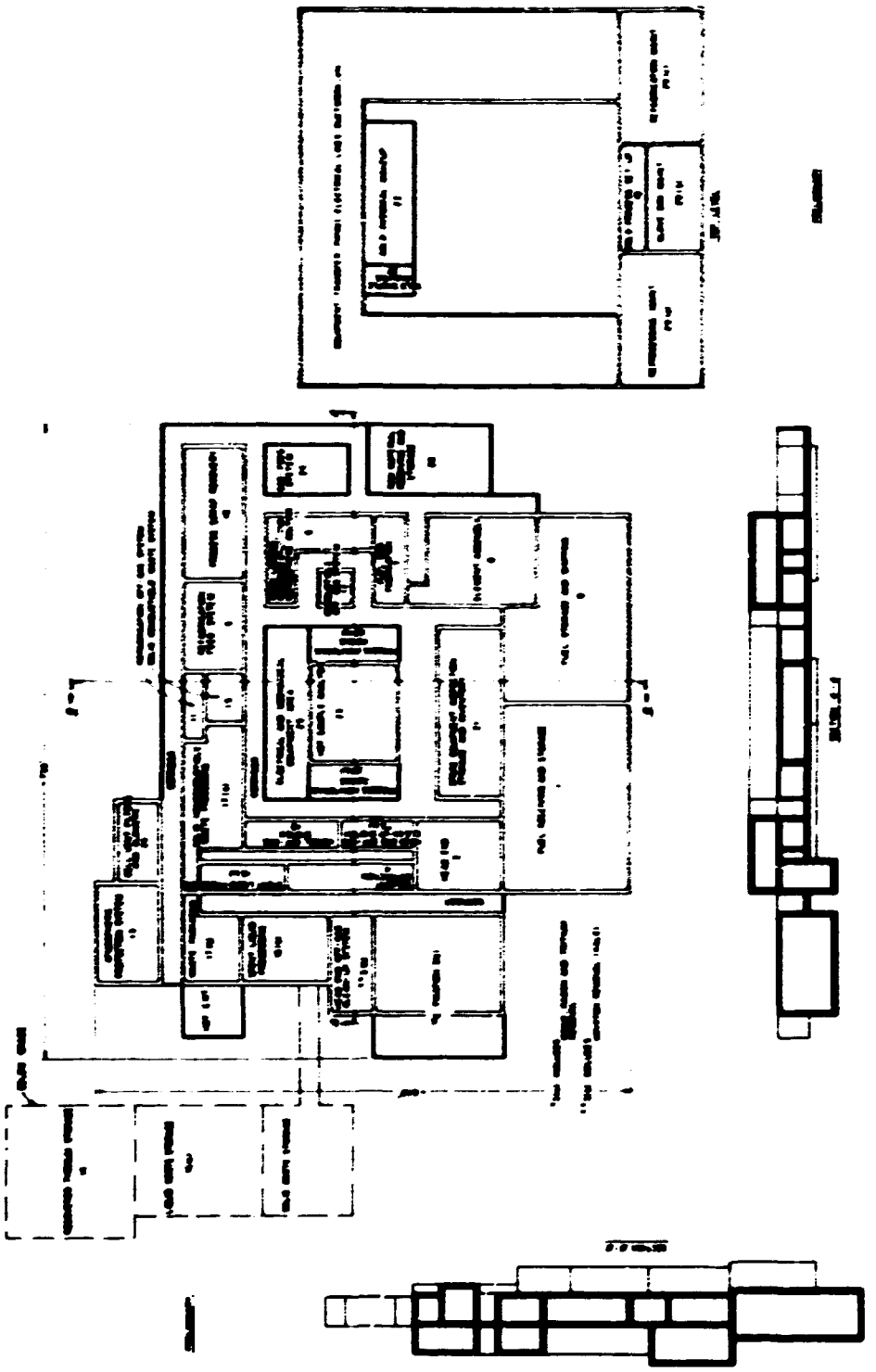

Fig. 7.2. Preconceptual Block Layout of a 20/10 HRDF. Overall dimensions of main floor are about 195 by 220 m (640 by 730 ft).

GAS-COOLED REACTOR PROGRAMS

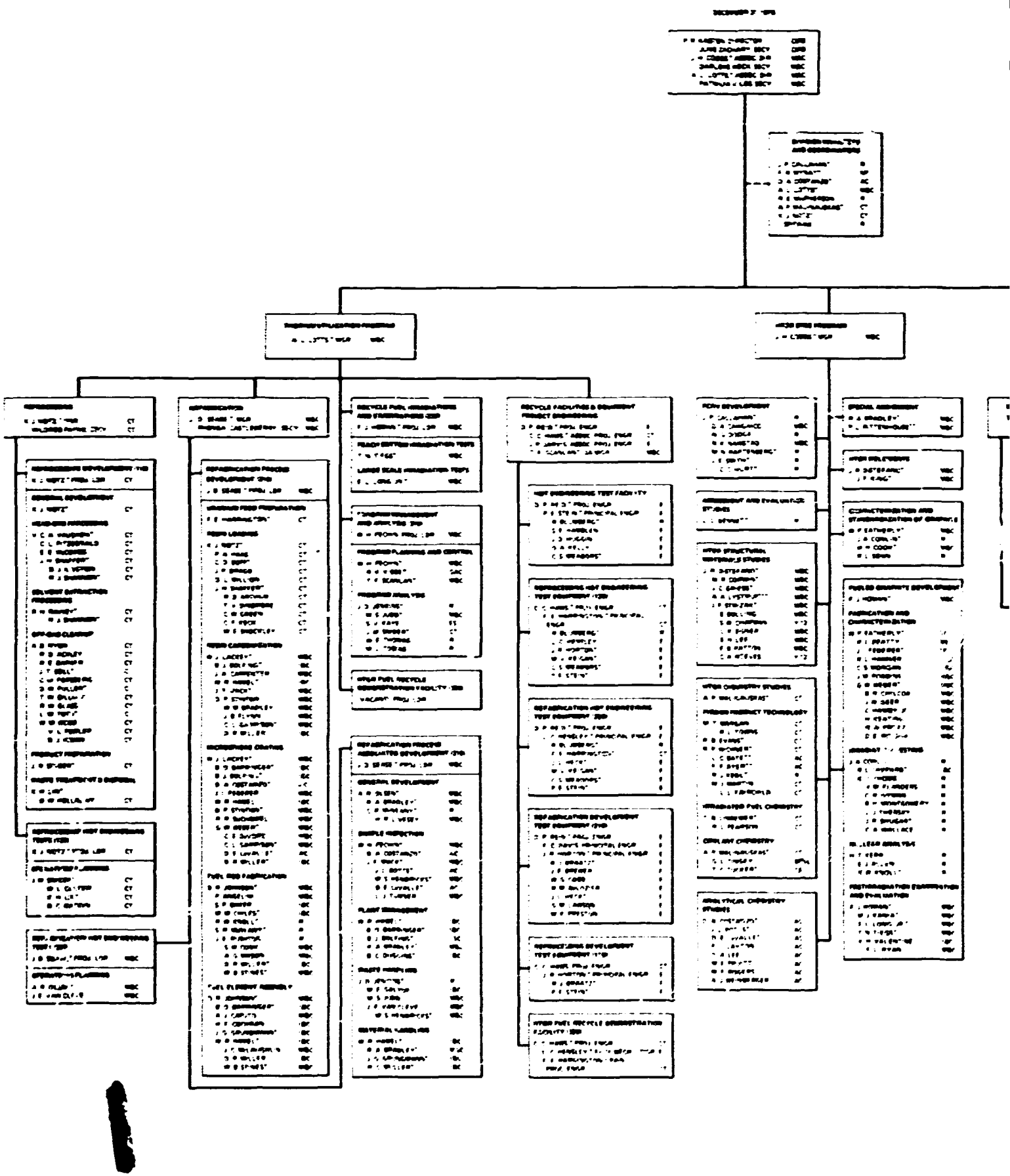

BLANK PAGE

GAS-COOLED REACTOR PROGRAMS

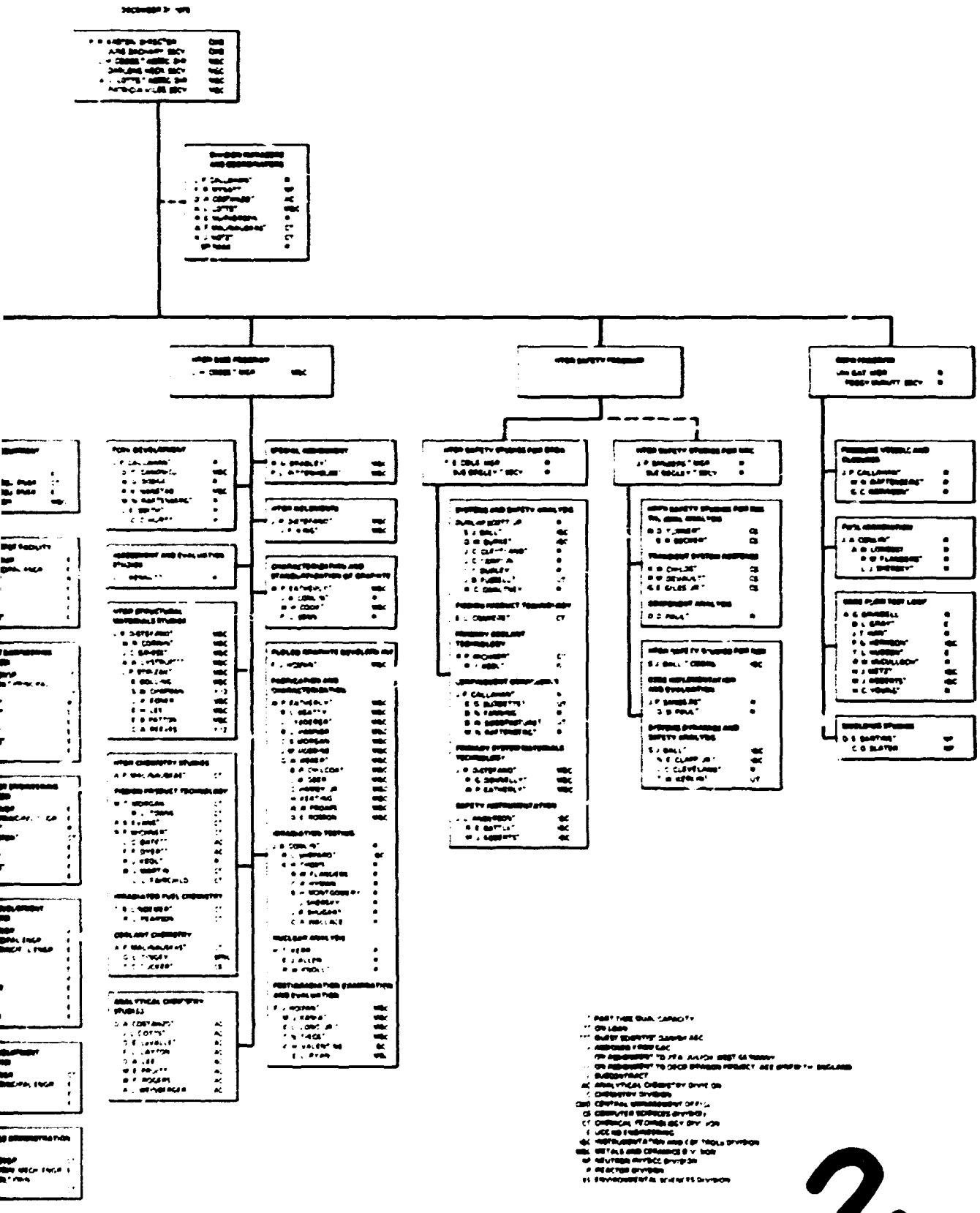

2